FLUID-STRUCTURE INTERACTION IN CASE OF WATERHAMMER WITH CAVITATION

Proefschrift

ter verkrijging van de graad van doctor aan de
Technische Universiteit Delft, op gezag van de
Rector Magnificus, prof. drs. P.A. Schenck, in
het openbaar te verdedigen ten overstaan van een
commissie aangewezen door het College van Dekanen
op dinsdag 29 juni 1993 te 16.00 uur

door

Arris Sieno Tijsseling
geboren te Bellingwolde
wiskundig ingenieur

1993

Dit proefschrift is goedgekeurd door de promotor: prof. dr. ir. J.A. Battjes.
Toegevoegd promotor: dr. ir. H.L. Fontijn.

Front cover: Joukowsky's visualization of pressure wave propagation, tube deformation and hoop stress [Joukowsky 1898, Figure 3].

This thesis is also published in the series 'Communications on Hydraulic and Geotechnical Engineering' of the Faculty of Civil Engineering as Report No. 93-6, ISSN 0169-6548.

Summary

The transient behaviour of liquid-filled pipe systems is studied. The time scale is acoustic. Pressure waves in the liquid, and axial, lateral and torsional stress waves in the pipes, are the dominant phenomena. The phenomena in the liquid (*waterhammer*) and the phenomena in the pipe system (*structural dynamics*) influence each other (*fluid-structure interaction*) if significant radial and axial pipe motions occur. When, in addition, the dynamic pressure drops to the vapour pressure, vapour bubbles will form in the liquid (*cavitation*). The major new element of the present work is in the simultaneous occurrence of fluid-structure interaction (FSI) and cavitation, which is investigated both theoretically and experimentally.

An extensive review of literature on the subject is given. One-dimensional basic equations are obtained by integration of general three-dimensional equations for fluid dynamics and structural linear elasticity. Three FSI-mechanisms (*junction-, Poisson-* and *friction-coupling*) are taken into account. The governing equations, formulated as a hyperbolic set of fourteen first-order partial differential equations, are solved by the method of characteristics. Vaporous cavitation is numerically simulated by the relatively simple concentrated cavity model.

The cavitation model, without the effects of FSI, is validated against experimental data of Simpson [1986], whereas the FSI-model, without the effects of cavitation, is validated against experiments of Vardy and Fan [1989, 1993]. Vardy and Fan's test rig (laboratory scale) has also been used for the purpose of the present investigation. Experiments, in which the combination of FSI and cavitation is evident, were performed with a straight-pipe system and with a system consisting of two straight pipes connected by a rigid 90-degrees elbow. The agreement found between theoretical and experimental results justifies the application of the present numerical model to larger pipe systems than those used in the laboratory tests.

Samenvatting

Er is onderzoek verricht naar het kortstondige dynamische gedrag van leidingsystemen gevuld met vloeistof. De tijdschaal is akoestisch. Drukgolven in de vloeistof en spanningsgolven (longitudinaal, transversaal en torsie) in de leidingen, bepalen de fysische verschijnselen. De verschijnselen in de vloeistof (*waterslag*) en in het leidingsysteem (*dynamica van constructies*) beïnvloeden elkaar (*vloeistof-leiding interactie*) ten gevolge van de radiale en longitudinale bewegingen van de leidingen. Bovendien treedt dampbelvorming (*cavitatie*) op wanneer de dynamische drukken in de vloeistof de dampspanning bereiken. Het nieuwe element in het uitgevoerde onderzoek betreft het gelijktijdig optreden van vloeistof-leiding interactie (VLI) en cavitatie, zowel in fysisch experiment als in numerieke simulatie.

De resultaten van een uitgebreid literatuuronderzoek zijn gerapporteerd. Eendimensionale basisvergelijkingen worden verkregen na integratie van de algemene driedimensionale vergelijkingen uit de vloeistofdynamica en de lineaire elasticiteitstheorie. De drie VLI-mechanismes (*junctie-, Poisson-* en *wrijvingskoppeling*) zijn verdisconteerd. De basisvergelijkingen, geformuleerd als een hyperbolisch systeem van veertien eerste-orde partiële differentiaalvergelijkingen, worden opgelost met de karakteristiekenmethode. Dampcavitatie is numeriek gesimuleerd met het, relatief eenvoudige, geconcentreerde caviteiten model.

Het cavitatiemodel, zonder VLI-effecten, is gevalideerd aan de hand van experimentele resultaten van Simpson [1986], terwijl het VLI-model, zonder de effecten van cavitatie, is gevalideerd met experimentele resultaten van Vardy en Fan [1989, 1993]. Vardy en Fan's proefopstelling (op laboratoriumschaal) is ook gebruikt met betrekking tot het huidige onderzoek. Experimenten, waarin de gevolgen van zowel VLI als cavitatie duidelijk zichtbaar zijn, zijn uitgevoerd met een systeem bestaand uit een enkele rechte buis en met een systeem bestaand uit twee rechte buizen die onder een hoek van negentig graden verbonden zijn door een stijf bochtstuk. De goede overeenkomst tussen theoretische en experimentele resultaten rechtvaardigt de toepassing van het ontwikkelde numerieke model op grotere leidingsystemen dan die in het beschreven laboratoriumexperiment.

Acknowledgements

The author thanks:

Prof. J.A. Battjes and Dr. H.L. Fontijn of Delft University of Technology for critically reading the manuscript, the valuable suggestions for improvement and the encouraging support during the entire project;

C.S.W. Lavooij, M.Sc., initiator of the FLUSTRIN project at Delft Hydraulics, for his friendship, his enthusiasm and the many discussions on a wide variety of subjects;

Prof. A.E. Vardy and Dr. D. Fan of the University of Dundee for their hospitality during my stays in Dundee in 1989 and 1990, the fruitful co-operation and the discussions on waterhammer and related affairs;

Mr. E.W. Kuperus of the University of Dundee for the technical assistance with the experiments, for his patience and for his precision;

Prof. D.C. Wiggert of Michigan State University for sharing his knowledge and experience with us in the beginning of the FLUSTRIN project;

Dr. A.R. Simpson of the University of Adelaide for providing the experimental results presented in section 6.1;

Dr. A. Anderson of the University of Newcastle upon Tyne for providing valuable information on the early history of waterhammer;

Dr. A.G.T.J. Heinsbroek and A.C.H. Kruisbrink, M.Sc., of Delft Hydraulics for their keen interest in my work and the discussions on fluid-structure interaction;

Mr. P. van der Salm for drawing figures;

all my colleagues at Delft University, in particular P. Blom, X.-Y. Jin, E.J. Langendoen and P.J. de Wit, who have contributed to this study in various ways;

all my (former) colleagues at Delft Hydraulics for their advices and friendship in the past six years.

The author is grateful to:

Delft Hydraulics, Industrial Technology Division, for financially supporting the project, the facilities made available and the library services;

Delft University of Technology and the University of Dundee, Departments of Civil Engineering, for giving me the opportunity to carry out the research the results of which are recorded in the present report.

Table of contents

Nomenclature

A	cross-sectional area
$\mathbf{A}$	matrix of coefficients
$\mathbf{B}$	matrix of coefficients
c	wave propagation speed (celerity) (classical); damping coefficient
$\tilde{c}$	wave propagation speed (present study)
c_0	wave propagation speed in unconfined fluid
c_1	wave propagation speed in highly elastic tube
c_l	wave propagation speed of sinusoidal lateral wave
D	inner diameter
E	Young's modulus of elasticity
e	pipe wall thickness (French: épaisseur)
F	body-force density
f	Darcy-Weisbach friction coefficient
G	shear modulus; Poisson coupling factor
g	gravitational acceleration
H	cross-sectional averaged pressure head
h	elevation
I	second moment of cross-sectional area
J	polar second moment of cross-sectional area
K	liquid bulk modulus
k	stiffness coefficient
L	pipe length
M	bending moment
$\mathbf{M}$	junction coupling matrix
m	mass
N	number of elements
n	unit-normal
P	cross-sectional averaged pressure
p	pressure
Q	lateral shear force (German: Querkraft)

q right-hand side in compatibility equations

R inner radius

r radial co-ordinate

$\mathbf{r}$ right-hand-side vector

$\mathbf{S}$ transformation matrix

T period of time; time scale; surface traction

$\mathbf{T}$ transformation matrix

t time; component of matrix $\mathbf{T}$

$\mathbf{t}$ eigenvector

u pipe displacement

$\dot{u}$ pipe velocity

$\ddot{u}$ pipe acceleration

V cross-sectional averaged fluid velocity; rod velocity

$\mathcal{V}$ cavity volume

v fluid velocity

$\mathbf{v}$ transformed vector of unknowns

x lateral co-ordinate

Y admittance

y lateral co-ordinate

$\mathbf{y}$ vector of unknowns

z axial co-ordinate

α void fraction; coefficient in compatibility equations

β coefficient in compatibility equations

γ elevation angle of pipe; coefficient in compatibility equations

Δ difference; mesh-spacing; discontinuity; jump; change

δ coefficient in compatibility equations

ε strain

θ rotation of pipe; parameter in numerical integration

$\dot{\theta}$ rotational velocity of pipe

κ bulk viscosity

κ^2 shear coefficient

Λ	diagonal matrix of eigenvalues
λ	wavelength; characteristic root; eigenvalue
μ	dynamic viscosity
ν	Poisson's ratio
ρ	mass density
σ	normal stress (component)
τ	shear stress (component); given function of time
τ_0	shear stress between liquid and pipe wall
ϕ	circumferential co-ordinate
φ	function defining boundary condition
ψ	correction factor in formula for pressure wave speed

Subscripts

abs	absolute
b	bending
c	closure of valve
cav	cavity
cs	column separation
F	fluid
f	fluid
g	gyration
in	inner; internal
jc	junction coupling
l	liquid
out	outer; external
p	pipe
r	radial direction; rod
rel	relative
res	reservoir
s	shear
t	tube; pipe

tor	torsion
v	vapour; valve
x	lateral direction
y	lateral direction
z	axial direction
ϕ	circumferential direction; hoop
0	initial value

Superscript

T	transposed
*	adjusted value; residual value

Dots and overlines

$\cdot$	first time-derivative
$\cdot\cdot$	second time-derivative
$\bar{}$	cross-sectional averaged value
=	cross-sectional averaged value (alternative)

1. INTRODUCTION

Fluid-structure interaction is the general term used for physical phenomena where moving boundaries between fluid and solid play an important role. The moving boundaries cause a dynamic coupling which makes a simultaneous treatment of fluid and structure necessary when modelling the phenomena. In the present study fluid-structure interaction refers to the dynamic coupling between a pipe system and its contained liquid. The liquid is allowed to vaporize so that liquid-vapour-pipe interactions may take place. Key words are: waterhammer, cavitation, structural dynamics and fluid-structure interaction (FSI). These are explained in section 1.1. In section 1.2 the present investigation is placed in its local historical context; a survey is given of previous research in Delft. (A more general review of literature is given in chapter 2.) Section 1.3 describes the objectives of the present work and gives an outline of the report.

1.1. Basic concepts

The subjects waterhammer, cavitation, structural dynamics and fluid-structure interaction are introduced in the next subsections.

1.1.1. *Waterhammer*

Waterhammer, also referred to as *pressure surges* or *hydraulic transients*, is a spectacular form of unsteady flow in liquid-filled pipe systems. It is generated by abrupt changes in the steady flow conditions. These changes are mostly due to the rapid closing or opening of valves, and to the stopping or starting of pumps. Other causes of waterhammer are load rejection of turbines, seismic excitation and pipe rupture. Waterhammer involves large transient pressure variations which may damage the pipe system and its components. In order to prevent damage, waterhammer can be suppressed and controlled by devices like: surge tanks, air chambers, flexible hoses, pump flywheels, relief valves and rupture disks. In practice waterhammer analyses are carried out in order to judge whether the quite expensive devices are necessary and if so, what their dimensions should be. Predicted maximum

pressures prescribe the required strength of the pipe work.

1.1.2. *Cavitation*

Waterhammer not only leads to high pressures but also to low pressures. Low pressures involve the danger of pipe collapse, especially in case of buried pipelines. When the pressure comes below a certain level, cavitation occurs. Distinction should be made between gaseous and vaporous cavitation. *Gaseous cavitation* occurs when the pressure falls below the saturation pressure of the gas, so that it comes out of solution. This is a relatively slow process compared to vaporous cavitation. *Vaporous cavitation* occurs when the pressure drops to the vapour pressure. Vapour cavities will form in the liquid. When the vapour cavities appear as tiny bubbles dispersed throughout the liquid along great lengths of pipe, it will be referred to as *distributed cavitation*. When the vapour cavities coalesce and form one local bubble occupying a large part of pipe cross-section, it will be referred to as *column separation*. Column separations generally occur near specific points in a pipe system such as valves, pumps, bends and high points. Column separations occasionally occur in pipe intermediate points when two low pressure waves meet. The collapse of column separations is usually attended with almost instantaneous pressure rises. These may be avoided by positioning air-inlet valves at critical points in the pipe system. In general the policy is to prevent cavitation.

1.1.3. *Structural dynamics*

Steady-flow and waterhammer analyses provide information on the liquid behaviour under operational conditions. Static pipe stress and structural dynamics analyses give insight in the corresponding behaviour of the pipe system. Where the liquid-analysis yields extreme pressures, the structural analysis provides dynamic stresses, reaction forces and resonance frequencies. It is not unusual to perform an *uncoupled calculation*. Pressure histories, resulting from a waterhammer analysis, are used as the dynamic loadings in a structural dynamics analysis. The calculation is called uncoupled since the predicted structural response does not influence the liquid pressures. This procedure is doubtful since pipe motion can significantly affect dynamic pressures. Fluid-structure interaction should therefore be considered.

1.1.4. *Fluid-structure interaction*

In conventional waterhammer analyses pipe elasticity is incorporated in the propagation speed of the pressure waves. Pipe inertia and pipe motion are not taken into account. This is acceptable for rigidly anchored pipe systems. For less restrained systems fluid-structure interaction may become of importance. In that case the dynamic behaviour of liquid and pipe system should be treated simultaneously.

Three liquid-pipe interaction mechanisms can be distinguished: friction coupling, Poisson coupling and junction coupling. *Friction coupling* represents the mutual friction between liquid and pipe. The more important *Poisson coupling* relates the pressures in the liquid to the axial stresses in the pipe through the radial contraction or expansion of the pipe wall. It is named after Poisson in connection with his contraction coefficient ν, and it is associated with the *breathing* or *hoop mode* of the pipe. Poisson coupling leads to *precursor waves*. These are stress-wave induced disturbances in the liquid which travel faster than, and hence in front of, the classical waterhammer waves. Where friction and Poisson coupling act along the entire pipe, *junction coupling* acts at specific points in a pipe system such as unrestrained valves, bends and tees. A standard example is the moving elbow, which induces pressure waves in the liquid through a combined pumping (compressing) and storage (decompressing) action. An illustrative explanation of Poisson and junction coupling can be found in [Tijsseling & Lavooij 1990].

The main effects of fluid-structure interaction are problem dependent. When compared to predictions of conventional analyses, predictions including fluid-structure interaction may lead to: higher or lower extreme pressures and stresses, changes in the natural frequencies of the system, and more damping and dispersion in the pressure and stress histories.

In practice pipe systems are never entirely rigid. Too rigid systems may experience extremely high stresses due to temperature effects. The problem is to judge when fluid-structure interaction is of importance. In [Lavooij & Tijsseling 1991] a provisional guideline is proposed in order to answer this question. The guideline is based on characteristic time scales of the system under consideration. It says that fluid-structure interaction is important when the time scale of the pipe system is 1) smaller than the time scale of the liquid and 2) larger than the time scale of the excitation. The eigenperiods of the pipe system, the main periods of the waterhammer waves and, for instance, the effective closure time of a valve,

provide the relevant time scales.

Calculations with fluid-structure interaction are necessary in situations with high safety requirements, mostly encountered in nuclear and chemical industry. They may also be useful in post-accident analyses [Wang et al. 1989; Obradović 1990b].

1.2. Previous research in Delft

Delft has a rich history with respect to the subjects introduced in the foregoing section. Here Delft stands for Delft University of Technology and Delft Hydraulics (formerly Delft Hydraulics Laboratory). A survey is given of work that is related to the present study. The realization of the present project as a co-operation between Delft University and Delft Hydraulics is shortly described. A more comprehensive literature review is given in chapter 2.

1.2.1. *Waterhammer*

The Industrial Technology Division of Delft Hydraulics has almost thirty years of experience in the area of waterhammer. The research started in the mid sixties [Vreugdenhil 1964] and developments kept pace with the increasing power of computer facilities. The results of experimental and theoretical work have been published in [Manuel 1968; Manuel et al. 1968; Nuhoff et al. 1969; Wijdieks 1972, 1974, 1978, 1983; Provoost 1978].

In the Laboratory of Fluid Mechanics of the Department of Civil Engineering of the Delft University of Technology, quite recently, experiments were performed on hydraulic rams. Hydraulic rams are self-operating pumps which harness the waterhammer phenomenon. The work has been reported in [Tacke 1988; Tacke & Verspuy 1989; Verspuy & Tijsseling 1993].

1.2.2. *Cavitation*

The research on cavitation due to waterhammer started in the mid sixties as well. Ten years of close co-operation between Delft Hydraulics and the Delft University of Technology has led to many valuable results.

Siemons used a *separated flow model*[1] in a theoretical treatment of cavitation [Siemons 1966, 1967]. Dijkman extended this model by taking into account the effects of dissolved gas [Dijkman 1968; Dijkman & Vreugdenhil 1969]. Kalkwijk and Kranenburg developed their *bubble flow model*[1] and compared the results with experimental data obtained in a PVC pipeline with length 200 m and diameter 0.08 m [Kalkwijk & Kranenburg 1971, 1973]. The separated flow model and the bubble flow model are compared in [De Vries et al. 1971; Kalkwijk et al. 1972]. At Delft Hydraulics experiments were performed in a steel pipeline, with length 1450 m and diameter 0.10 m, in order to examine distributed cavitation. The experimental results are compared with predictions of the separated flow model and the bubble flow model in [Vreugdenhil et al. 1972; Kloosterman et al. 1973]. De Vries simulated the experiments by applying the *concentrated cavity model*[1] to distributed cavitation regions [De Vries 1972, 1973, 1974]. Safwat did also experiments at Delft Hydraulics [Safwat 1972abcd]. He investigated column separations in a plexiglass pipeline with optionally a high section with or without condenser. The pipeline had a diameter of 0.09 m and lengths varied between 40 m and 58 m. Column separations were modelled at two fixed points, distributed cavitation was modelled in a primitive way [Safwat & de Kluyver 1972; Safwat & van den Polder 1973a]. Kranenburg did an extensive study on the effects of free and dissolved gas on transient cavitation [Kranenburg 1972, 1974ab].

A review of cavitation research in Delft can be found in [De Vries 1975]. Provoost reviews the three developed cavitation models in [Provoost 1976] and compares the results with the field measurements reported in [Provoost 1975]. Some numerical aspects of the concentrated cavity model are dealt with in [Provoost & Wylie 1981].

In the second half of the seventies the research in Delft concentrated on cavitation susceptibility and cavitation on valves [Oldenziel 1975, 1976, 1979, 1982ab; Oldenziel & Teijema 1976].

1.2.3. *Fluid-structure interaction (FSI)*

At Delft University Kuiken performed a comprehensive theoretical study on FSI in straight tubes [Kuiken 1984abcd, 1986, 1988]. Dieterman investigated theoretically and

---

[1] see section 2.2

experimentally FSI effects in water towers [Dieterman 1988].

At Delft Hydraulics the research on FSI started in 1984 with the work of Van der Weijde [Van der Weijde 1984, 1985ab, 1986]. He did experiments in a 0.05 m diameter PVC pipeline containing a 24 m long U-shaped test section. An adjustable spring was used to vary the stiffness of the system. For less stiff systems he found considerable discrepancies between the experimental results and predictions obtained with conventional waterhammer theory. For this reason Delft Hydraulics decided to study FSI more thoroughly. A project was set up in co-operation with and sponsored by participants from industry, public authorities and consulting engineers' offices [FLUSTRIN 1986]. The project, named FLUSTRIN, got the EUREKA status[2] in 1988 and was therefore subsidized by the European Community as well [EUREKA 1988]. One of the aims of the project is to make available to users in practice the advanced FSI-knowledge which is already present at universities.

The FLUSTRIN project was divided in three phases. Phase 1 included the following items: survey of literature, derivation of governing equations, inventory of field cases, definition of benchmark problems, testing of various numerical methods, development of pilot program, assessment of the relative importance of interaction mechanisms. The help of professor Wiggert of Michigan State University, USA, in this stage of the project was highly appreciated. Results of phase 1 have been reported and published in [Lavooij 1986; Lavooij & Tijsseling 1988, 1989, 1991; Lavooij 1990; Tijsseling & Lavooij 1990; Heinsbroek et al. 1991; Heinsbroek & Tijsseling 1993]. Phase 2 consisted of the development of a user-friendly computer code for the calculation of FSI effects in unbranched pipe systems [FLUSTRIN 1990]. In phase 3 the computer code was validated against experimental results obtained in a larger than usual FSI test circuit: length 76 m, diameter 0.10 m, 6 elbows [Heinsbroek & Kruisbrink 1991, 1993; Kruisbrink & Heinsbroek 1992ab; Heinsbroek 1993].

1.2.4. *Fluid-structure interaction and cavitation (present study)*

During a three-days course on FSI given by Hatfield, Wiggert and Zielke [Hatfield et al. 1987] and attended by the author, it became clear that the collapse of column separations in combination with FSI is an important and still unexplored field, which deserves to be studied.

---

[2] EUREKA project 274

Due to the complexity and novelty of the subject, several years of basic research were expected to be needed in order to get satisfactory results. Therefore Delft Hydraulics approached Delft University of Technology to come to a co-operation once more. As a result the author has been able to work for a period of four years on the present subject, which may be seen as an extension of the FLUSTRIN work. The final results are presented in the report at issue. Earlier publications are [Tijsseling & Lavooij 1989; Tijsseling & Fan 1991ab, 1992; Fan & Tijsseling 1992].

1.3. Objectives and preview of study

In case of severe waterhammer it is not unlikely that cavitation and pipe motion occur together. The collapse of large vapour cavities or column separations leads to pressure waves with steep wave fronts. These waves excite the pipe system and, since their fronts are steep, the time scale of excitation is very small. Then, according to the guideline described in subsection 1.1.4, fluid-structure interaction (FSI) becomes of importance, provided the characteristic time scale of the structure is smaller than that of the fluid.

The **objective** of the present study is to model mathematically the combination of FSI and cavitation. The model should be suitable to be implemented in existing waterhammer and/or structural dynamics computer codes. Furthermore the model should be validated against experimental results in which the combination of FSI and cavitation is evident.

The mathematical model presented herein combines the FSI work of Wiggert[3] et al. with the Delft cavitation-work reviewed in subsection 1.2.2. The model is one-dimensional; it is based on conventional waterhammer and beam theories. The three interaction mechanisms, friction, Poisson and junction coupling, are taken into account. Cavitation is simulated with the concentrated cavity model. The numerical approach is the method of characteristics (MOC).

The experimental apparatus used is that of Vardy and Fan of the University of Dundee, UK. It consists of an isolated part of a pipe system, closed at the ends and suspended by wires. The system is filled with pressurized water. Transients are generated by striking one of the closed ends with a steel rod, as shown in figure 1.1. This report includes results for

[3] see subsection 2.3.5

a straight pipe and for a system with one elbow.

A review of literature is given in the next chapter. Emphasis is placed upon FSI in the time domain. The basic equations are derived in chapter 3, the underlying assumptions are given. Initial and boundary conditions complete the mathematical model. The MOC approach is worked out in chapter 4, together with the concentrated cavity model. In chapter 5 the experiments are described, the results of which are compared with theoretical predictions in chapter 6. Chapter 7 finishes the study with a review and conclusions.

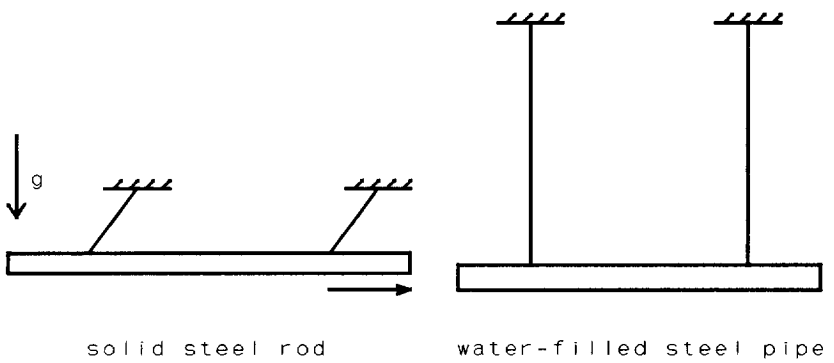

Figure 1.1. Sketch of Dundee experimental apparatus.

2. REVIEW OF LITERATURE

In this chapter literature referring to the subjects waterhammer, cavitation and fluid-structure interaction (FSI) is reviewed. In section 1.2 this was already done for work carried out in Delft; here the review is world-wide. Waterhammer and cavitation are discussed shortly, most attention is directed to FSI in the time domain. Literature dealing with both FSI and cavitation is treated separately.

2.1. Waterhammer

The first work with respect to waterhammer is attributed to Ménabréa [1858, 1862]. Although several other publications were brought out in the second half of the 19th century, the present waterhammer theory is based on the classic investigations of Joukowsky [1898] and Allievi [1903]. Joukowsky conducted extensive measurements in the Moscow water distribution system. In his theoretical treatment he derived the formula that bears his name

$$\Delta P = \rho_f c_f \Delta V \tag{2.1}$$

This formula was also derived by Frizell [1898] and earlier by Rankine [1870]. It relates pressure changes ΔP to velocity changes ΔV by the constant factor $\rho_f c_f$, with ρ_f the mass density of the fluid and c_f the velocity of sound in the fluid. Joukowsky used the sound velocity according to Korteweg [1878], which takes into account both the compressibility of the fluid and the elasticity of the pipe walls. Allievi gives an excellent mathematical treatment of the waterhammer equations in [Allievi 1913]. His way of solution has been in use until the more practical *graphical method* was developed. This method is connected with the names of Schnyder [1929] and Bergeron [1935], although there were a few predecessors. With the introduction of digital computers in the early sixties, waterhammer calculations evolve to their present form. The method of characteristics (MOC) becomes the standard numerical approach. All fundamentals can be found in the classic textbook of Streeter and Wylie [1967]. Other good textbooks on the subject are those of Bergeron [1950], Gandenberger [1950], Rich [1951], Parmakian [1955], Zielke [1974], Jaeger [1977], Fox

[1977, 1989], Wylie & Streeter [1978a, 1993], Watters [1979], Chaudhry [1979], Chaudhry & Yevjevich [1981], Tullis [1989] and De Almeida & Koelle [1992]. Historical reviews are given by Paynter [1961], Wood [1970], Martin [1973], Anderson [1976] and Thorley [1976]. Jaeger [1977] is very precise in his footnotes, where he refers to the original researchers and their work.

2.2. Cavitation

Cavitation is a broad field of research. This study is confined to the macroscopic aspects of transient vaporous cavitation. For information on the physical phenomena on a microscopic scale, cavitation erosion and advanced cavitation theory, good textbooks are available like [Knapp et al. 1970; Hammitt 1980; Young 1989]. Valuable information may also be obtained from Arndt's [1981] review. An excellent review of literature on cavitation due to waterhammer is given by Simpson in his dissertation [Simpson 1986]. De Almeida [1987] reviews the various models that are in use to simulate transient cavitation.

Thorley [1976] attributes the first work on vapour cavities and column separations to Hogg & Traill [1926] and Langevin [1928]. Simpson [1986] starts his review in the 1930s with contributions of Billings et al. [1933], Angus [1935, 1937ab], LeConte [1937], Knapp [1937ab, 1939] and Bergeron [1939]. His survey goes to the mid eighties and includes the Delft work described in subsection 1.2.2. The early investigations concern the occurrence of column separations at specific points in a pipe system; the danger of high pressures following cavity collapse is recognized. Column separations can be adequately modelled in a simple manner [Bergeron 1950; Streeter & Wylie 1967]. For a physically correct representation of distributed cavitation more complicated models are needed. The three models already mentioned in subsection 1.2.2 are basic.

The *separated flow model* [Baltzer 1967, Siemons 1967] assumes the cavities to coalesce at the upper part of a pipe, forming one thin layer of vapour and/or gas. Regions of cavitating fluid are then treated as open-channel flows. Problems encountered in this kind of modelling are the appearance of gravity waves and the numerical treatment of the moving boundaries between cavitating and non-cavitating regions. Furthermore, the model is physically incorrect for vertical pipes. The *bubble flow model* [Kalkwijk & Kranenburg 1971, 1973] is a physically more realistic representation of distributed cavitation. It assumes the

cavities to be dispersed throughout the liquid and treats cavitating regions as one-dimensional two-phase flows [Wallis 1969]. Difficulties in this way of modelling are pressure-dependent wave propagation, the formation of shock waves and numerical instabilities. Column separations must be treated separately. The *concentrated cavity model*, also referred to as *discrete* or *lumped cavity model*, treats distributed cavitation regions and column separations mathematically in the same way. Cavities are allowed to form only at a fixed number of locations along the pipe. Pure liquid is assumed to exist between these locations. The great disadvantage of this method is in the occurrence of spurious oscillations and unrealistic pressure spikes.[1]

Simpson [1986] discusses the literature dealing with the various models. In the remaining of this section the focus is on the concentrated cavity model, since this is the model used in the present study. After a short historical review, the most recent literature dealing with the model is summarized, which may be regarded as an addition to Simpson's [1986] review.

The concentrated *vapour* cavity model was formulated by Thibessard [1961], Streeter [1969] and Tanahashi & Kasahara [1969]. However, these investigators did not apply the model to regions of distributed cavitation. This was done by De Vries [1972] when he simulated the experiments mentioned in subsection 1.2.2. He is the first who reports on numerical oscillations induced by the simulated nullification of a region of distributed cavitation. To suppress these oscillations he adds small amounts of free gas to the discrete cavities. In fact he then uses the concentrated (discrete, lumped) *free gas* cavity model developed by Brown [1968]. This model, later on used by Enever [1972], Tullis et al. [1976], Ewing [1980] and Suda [1990], allows for the presence of free gas in the liquid. Ewing [1980] also discusses various damping mechanisms in liquid-gas mixtures. Thorough treatises of both the vapour and the free gas concentrated cavity models are given by Wylie [1984] and Zielke & Perko [1985].

The concentrated cavity model is widely used because of its simplicity, its general applicability and the fact that it fits in with the method of characteristics (MOC) approach employed in standard waterhammer calculations. Its validity follows from the comparison of its predictions with results of laboratory and field tests. Provoost [1976] validates the model against both laboratory experiments and field measurements. The latter concern a 27.9 km

[1] see subsection 4.5.3

long pipeline with a diameter of 1.8 m. Sharp [1977] presents field measurements in a 12.3 km long, 0.25 m diameter, pipeline. In his calculation he allows cavities to form at not more than six locations. Nevertheless he obtains reasonable results. Kot & Youngdahl [1978ab] give a clear explanation of the concentrated cavity model and use experiments in a 9.15 m long closed tube for validation. Aga et al. [1980] apply the model to oil flow in a 250 m long, 0.09 m diameter, test rig. Gottlieb et al. [1981] and Graze & Horlacher [1983] investigate maximum pressures due to the collapse of column separations in various pipe configurations. They use discrete cavities in their simulations. Evans & Sage [1983] have confidence in the model and use it for the waterhammer analysis of a practical situation. Carmona et al. [1987] conducted extensive measurements in a laboratory set-up resembling that of [Provoost 1976] and showed numerical results as well. Golia & Greco [1990] find excellent agreement between computations and experimental data provided by Martin [1983]. Barbero & Ciaponi [1991] report on 23 experiments performed in a nearly 500 m long, 0.11 m diameter, test circuit. In their calculations they examine the influence of initial free gas and gas release. Anderson et al. [1991ab] discuss several aspects of the concentrated cavity model and show results of laboratory measurements for three levels of cavitation severity. Wang & Locher [1991] find surprisingly good agreement between simulations and field data obtained in a 47 km long cross-country pipeline with a diameter of 0.84 m.

From all the validation tests quoted it may be concluded that, despite its simplicity, the concentrated cavity model reproduces the essential features of transient cavitation. The versatility of the model is demonstrated by the variety of pipe systems used in the tests. The common belief that the model yields conservative results is contradicted by the findings of Wang & Locher [1991]. The major deficiency of the model is the appearance of non-physical oscillations in the results. These are highlighted in a paper by Wylie & Streeter [1978b]. Papers by Provoost & Wylie [1981] and Simpson & Wylie [1985] deal with the reduction and the generation, respectively, of numerical oscillations and unrealistic pressure spikes.

The latest developments aiming at physically better models are due to Streeter [1983] and Simpson [1986]. Streeter's consolidation method treats distributed cavitation regions in sloping pipes as areas of constant pressure moving under the influence of gravity and friction forces. Column separations are allowed to form at specific locations of the pipe system. Simpson's work [Simpson 1986; Simpson & Wylie 1989, 1991; Bergant & Simpson 1992] is based on that of Streeter. However, his *interface model* allows column separations to form

at any point in a pipe system whenever two low pressure waves meet. In his dissertation [Simpson 1986] he compares predictions of both the interface model and the concentrated cavity model with experimental data obtained in a 36 m long upward sloping pipe of 0.02 m diameter. Although the interface model gives reliable results, it is too complicated for general use.

2.3. Fluid-structure interaction (FSI)

2.3.1. *Early developments*

In the 19th century the studies of standing waves in musical instruments and pulsatile flows in blood vessels asked for an accurate determination of the velocity of sound in fluids. The sound velocity in unconfined fluids was and is known to be

$$c_0 = \sqrt{\frac{K}{\rho_f}} \tag{2.2}$$

where K is the bulk modulus of the fluid. For liquids contained in a tube the sound velocity was found to be much lower. Von Helmholtz [1848] correctly attributes this effect to the elasticity of the tube walls. For *in*compressible fluids in elastic tubes, like rubber hoses and blood vessels, Young [1808], Weber [1866], Résal [1876] and Moens [1878] came to the formula

$$c_1 = \sqrt{\frac{Ee}{\rho_f D}} \tag{2.3}$$

where E is Young's modulus of the wall material, e is the wall thickness and D is the internal tube diameter. For compressible fluids in elastic tubes Korteweg [1878] derived

$$\frac{1}{c_f^2} = \frac{1}{c_0^2} + \frac{1}{c_1^2} \tag{2.4}$$

which is equivalent with

$$c_f = \sqrt{\frac{K}{\rho_f}\left(1 + \psi \frac{DK}{eE}\right)^{-1}} \tag{2.5}$$

where the coefficient $\psi = 1$. The coefficient ψ is explained in subsection 2.3.3.

Formula (2.5) gives the pressure wave speed c_f used in standard waterhammer calculations. For compressible fluids in inelastic tubes, $E >> K$, c_f equals c_0, whereas for incompressible fluids in elastic tubes, $K >> E$, c_f equals c_1.

In deriving formula (2.5) Korteweg [1878] considers the tube as a series of massless rings expanding and contracting in accordance with the internal fluid pressure, P. The hoop stress, σ_ϕ, and the radial displacement, u_r, of a ring are given by

$$\sigma_\phi = \frac{R}{e} P \tag{2.6}$$

$$u_r = \frac{R^2}{eE} P \tag{2.7}$$

respectively, where R is the inner radius of the tube. The tube walls follow the liquid, there is no question of fluid-structure *interaction*. Axial stresses in the tube wall, σ_z, and tube wall inertia are neglected:

$$\sigma_z = 0 \tag{2.8}$$

$$\rho_t = 0 \tag{2.9}$$

with ρ_t the mass density of the tube wall material.

Korteweg [1878] indicates that his theory is valid for long[2] wavelengths. He points out that Poisson's ratio effects[3] occur when the axial stresses in the tube wall are not neglected. When, in addition, *axial* tube wall inertia is taken into account, axial stress waves will propagate along the tube. Korteweg, however, investigates the influence of *radial* inertia. He shows that for short wavelengths the radial inertia of both fluid and tube wall becomes of importance, thereby leading to wave speeds varying with the wavelength. Gromeka [1883], quoted by Joukowsky [1898], takes pipe wall inertia into account when he considers *in*compressible liquids in elastic tubes. He gives a bi-quadratic equation from which two wave speeds follow: one for the pressure waves in the fluid and one for the axial stress waves in the tube wall. Lamb [1898] is very complete in his treatment of the combined axial and radial vibrations of a fluid-filled tube. Poisson coupling[3] is included in his work. He distinguishes three classes of vibrations, viz. 1) the pressure waves in the fluid as modified by the yielding of the tube, 2) the axial vibrations of the tube wall as modified (very slightly) by the presence of the fluid, and 3) the radial vibrations of the system. Lamb derives a dispersion equation which relates phase velocities to wavelengths. For long wavelengths the pressure waves and the axial stress waves are predominant, with the propagation speeds close to c_f and c_t, respectively, where

$$c_t = \sqrt{\frac{E}{\rho_t}} \tag{2.10}$$

and c_f is given by (2.5). The radial vibrations are important only for short wavelengths.

Boulanger [1913] gives an extensive survey of the developments in the 19th century.

2.3.2. *Wave propagation modes*

Lamb's [1898] work has been extended by numerous researchers dealing with the problem of wave propagation in fluid-filled cylinders. The general approach is to apply Fourier

---

[2] with respect to pipe diameter

[3] see subsection 1.1.4 for Poisson coupling

analysis to the basic equations. A dispersion equation is then derived, from which the natural modes of wave propagation follow.

Skalak [1956] presents an excellent piece of work which can be seen as the theoretical basis underlying the present study. He extends Lamb's [1898] work by including in his axially symmetric tube model bending stiffness and rotatory inertia. From his dispersion equation he finds an infinite number of wave propagation modes. Only the two lowest modes have a finite phase velocity as the wavelength approaches infinity and the frequency approaches zero. The lowest mode corresponds to the pressure waves in the fluid, the second lowest to the axial stress waves in the tube wall. The phenomenon of *precursor waves*[4] is described with the aid of clear pictures. Simplified equations are given which permit precursor-type solutions without dispersion effects. These are the equations used in the present study (see subsection 3.1.2).

Lin & Morgan [1956ab] delivered work similar to Skalak's. Beside bending stiffness and rotatory inertia, they take into account transverse shear deformation in their tube model. These matters are of importance only in the high frequency range.

Herrmann & Mirsky [1956] consider an empty tube and find basic equations that slightly differ from those of Lin & Morgan [1956a]. They survey the various models that are in use for axially symmetric motions of thin-walled cylinders. Equations governing the non-axially symmetric motion of cylinders are given in [Mirsky & Herrmann 1957], whereas in [Mirsky & Herrmann 1958] thick-walled cylinders are considered.

Spillers [1965] and Tang [1965] apply the method of characteristics to, respectively, Herrmann & Mirsky's and Lin & Morgan's equations.

King & Frederick [1968] use Lin & Morgan's equations in a completion of Skalak's work. By applying a Hankel transformation to the two-dimensional fluid equations, they obtain an infinite system of one-dimensional wave equations for the fluid. A finite set from this system, along with three one-dimensional wave equations for the tube, is transformed into ordinary differential equations by means of the method of characteristics. Finally, a numerical integration procedure leads to the early-time waterhammer response solutions which the authors were looking for.

Thorley [1969] follows Skalak's approach, but neglects transverse shear deformation,

---

[4] see subsection 1.1.4 for precursor waves

rotatory inertia and, partly, bending stiffness. He performed physical experiments in steel, aluminium alloy, and polythene pipes of 0.05 m diameter and 0.005 m wall thickness. Thorley is the first who actually observes *precursor waves*.

DeArmond & Rouleau [1972] extend Lin & Morgan's work by considering a viscous liquid in an elastic tube. They concentrate on the two lowest modes of wave propagation. Rubinow & Keller [1978] study, for infinitely many modes, a viscous liquid in a visco-elastic tube. Kuiken [1984abcd] comes with the most complete model, encompassing viscous liquids or gases, orthotropic visco-elastic tubes, pre-stressed and surrounded by other materials, and thermodynamic effects. Möser et al. [1986] investigate those modes that produce audible sound. They present results of accurate measurements.

The advanced study of wave propagation in fluid-filled tubes is nowadays still of importance, in particular with respect to pulsatile flows in mammalian arteries. For the description of pressure waves in pipe systems one- or two-mode solutions are sufficient. One-mode solutions are found with classical waterhammer theory, two-mode solutions are calculated in the present study. The latter are extensively treated in the literature discussed in this subsection, where the tubes were assumed to be thin-walled.

2.3.3. *Wave propagation speeds*

Halliwell [1963] gives, within the context of classical waterhammer theory, formulae for the pressure wave speed in both thin- and thick-walled pipes. He also discusses the disparity in wave speed formulae found in textbooks. This disparity is due to the way pipe support conditions are taken into account. In theoretical analyses three support conditions are standard: 1) pipe anchored with expansion joints throughout, 2) pipe anchored throughout against axial motion, and 3) pipe anchored at its upstream end only. The correction factor ψ in the wave speed formula (2.5) accounts for the different support conditions. Support condition 1) corresponds to the situation described by Korteweg [1878], in which the axial stresses are neglected ($\psi = 1$). In condition 2) the axial displacements are neglected, leading to $\psi = 1 - \nu^2$. In condition 3) the axial stress in the pipe wall is assumed to be proportional to the fluid pressure acting on a closed valve downstream, giving $\psi = 1 - \nu/2$. Correct treatises of the subject can be found in [Wylie & Streeter 1978a] and [Schwarz 1978]. In deriving the values of ψ pipe wall inertia is neglected, so that quasi-static conditions prevail.

The support conditions 1) and 3) allow for axial pipe motion. For these cases it has been assumed that the axial stress in the entire pipe is permanently equal to its value at the anchors or to its value at the valve. The more thorough treatise, presented in the report at issue[5], considers axial stress waves in the pipe wall by taking into account axial pipe wall inertia [Stuckenbruck et al. 1985]. This approach leads to a unique wave speed for a single pipe supported at its ends, which is physically correct since the wave speed should not depend on the end conditions: a disturbance generated at the middle of the pipe, and travelling at finite speed, does not "know" in advance which situation it will meet at the pipe ends. In this respect it is noted that ignoring axial pipe wall inertia leads to axial stress waves theoretically travelling at infinitely high velocity, so that the end conditions are permanently "felt" along the entire pipe.

2.3.4. *Junction coupling*

In classical waterhammer theory the only influence of the pipe support conditions is in the correction factor ψ in the pressure wave speed (2.5). When the support conditions allow for pipe motion, fluid-structure interaction may occur. The most important interaction mechanism is junction coupling[6]. In general a pipe system consists of straight sections of pipe, connected by elbows, tees and diameter changes, and terminated by reservoirs, pumps and valves. Here the connecting and terminal points are referred to as *junctions*. Other hydraulic equipment than those mentioned above may also be located at junctions. When a junction has the possibility to move in the axial pipe direction, which is the direction of the pressure waves, mutual forces between fluid and pipe system may cause a dynamic interaction, which is known as *junction coupling*.

Regetz [1960] investigates pressure and velocity fluctuations in a straight pipe filled with rocket fuel. His experimental apparatus allows for axial pipe motion. Pipe velocities recorded at the unrestrained pipe end are incorporated in a standard waterhammer analysis in the frequency domain. It is shown that pipe motion has a definite effect on the fluid behaviour.

Blade et al. [1962] extend Regetz's work; a flexibly supported elbow is included in the

---

[5] see subsection 4.2.3

[6] see subsection 1.1.4 for junction coupling

pipe system. Axial pipe motion is simulated by means of a spring-mass system. Junction coupling is modelled by relating pressures and velocities in the fluid to stresses and velocities in the pipe according to the local force equilibrium and continuity; the same approach is followed in the present study.

D'Souza & Oldenburger [1964] let pressure waves in the fluid interact with stress waves in the pipe wall by way of junction coupling at an unrestrained pipe end. They utilize Laplace transformations in a frequency response analysis of their basic equations. Excellent agreement is found between theory and experiments conducted in a straight pipe filled with hydraulic oil.

Holmboe & Rouleau [1967] had problems with unwanted FSI-effects in their experimental apparatus and decided to embed their spiral tube in concrete.

Swaffield [1968-1969] examined the influence of elbows on passing pressure waves by means of a comprehensive series of tests. The influence of pipe restraint was part of his work. Unfortunately, his results are invalidated by the fact that some supports in his experiments were not sufficiently rigid [Wilkinson 1980, p. 197].

Davidson & Smith [1969] model curved pipes in a Timoshenko-beam-like manner including liquid-pipe interaction. The model is validated against results of frequency response tests in an oil-filled single-elbow pipe system. The work is extended to non-plane multi-elbow configurations by Davidson & Samsury [1972].

Wood [1968, 1969] gives a clear explanation of junction coupling in terms of moving hydraulic discontinuities. He presents a time-domain analysis in which the structure is represented by a spring-mass system where the fluid pressure is the driving force. His experimental apparatus consists of a rigidly supported straight pipe terminated by a spring-mass device. In [Wood 1968] the liquid is subjected to periodic disturbances, whereas in [Wood 1969] the system is excited by rapid valve-closure. In the latter it is shown that pressure rises may significantly exceed Joukowsky's value (2.1), when axial pipe motion occurs. An interesting parameter variation study is given which links up with the guideline described in section 1.1.4. In [Wood & Chao 1971] the work is extended with elbows and branches. A valuable series of tests was carried out on 30, 60, 90, 120 and 150 degrees mitre bends and on a 90 - 90 degrees T-junction. No attempt was made to model the structure; measured junction velocities were used as input to the analysis. It is shown that rigidly supported junctions have a negligible influence on pressure waves, whereas unrestrained

junctions affect them considerably. Jones & Wood [1972] give an analytically derived expression for the junction coupling induced pressure oscillations around Joukowsky's value in case of rapid valve-closure downstream in a single pipe. The pipe is conceived of as a spring-mass system. Results are compared with measurements in an unrestrained vertical pipe.

Ellis [1980] considers junction coupling at a check-valve, a T-branch and a 90 degrees bend in an analysis of a practical system. Pressure waves and axial stress waves are modelled; flexural motion is accounted for by a spring-mass system. The method of characteristics is employed to solve the basic equations.

2.3.5. *Junction and Poisson coupling*

In the work reviewed in the previous subsection the influence of axial junction motion on pressure waves was investigated. The axial pipe motion was represented by measured data or by a simple spring-mass system. Only D'Souza & Oldenburger [1964] and Ellis [1980] model axial stress waves in the pipe wall. However, they did not account for *Poisson coupling*, i.e. the FSI-mechanism that relates internal fluid pressures to pipe wall axial stresses. The work of researchers including this mechanism in their model is discussed in this subsection. In fact they utilize the two-modes model introduced in subsection 2.3.2.

Bürmann [1974ab, 1975, 1980b] gives a rigorous mathematical treatment of axial wave propagation in liquid-filled co-axial cylinders, including Poisson coupling. The basic equations are solved by the method of characteristics (MOC). Non-axial effects are studied in [Bürmann et al. 1979, 1983, 1987c]. Bürmann [1980a, 1983] compares the responses of three different tube models to waterhammer induced by the rapid closure of a rigidly supported valve. The three tube models correspond to the shell and membrane theories such as given by Herrmann & Mirsky [1956], and to the simple one employed in classical waterhammer theory. Bürmann concludes that shell theory is necessary for very short pipes and for obtaining accurate solutions in the vicinity of very steep wave fronts. The membrane theory in combination with extended waterhammer equations allows for precursor waves and is sufficient for most practical purposes. The classical waterhammer theory fails to predict pipe motion. A four-equation model is proposed to describe the coupled axial motion of pipe and liquid [Thielen & Bürmann 1980; Bürmann et al. 1980]. In principle this is the

simplified model of Skalak [1956]. Bürmann, and his group, carried out an impressive series of field measurements in order to validate the theoretical work. In [Bürmann 1979; Bürmann & Thielen 1988] measurements are presented on the filling pipe of a subterranean salt cavern. The salt cavern is used for oil storage and the filling pipe, which is vertically placed within a second pipe, has a length of more than 1 km. The pipe is minimally restrained and shows motion in axial and lateral direction when it is excited by waterhammer due to pump stop. In [Bürmann et al. 1985, 1986b, 1987a] the pipe bridge of a water main across the river Neckar is studied. Coupled motion of liquid and pipe is generated by rapid valve opening. At one end the pipe was lifted from its support to enhance axial motion. In [Bürmann et al. 1986a, 1987b] a loading line, used for liquid transport between storage tanks and ships, is subject of investigation. A most detailed description of the measurements and the corresponding simulations is given for all three cases. It is encouraging to see that satisfactory agreement is found between theory and field data, although in the simulations measured data was used as input.

Walker & Phillips [1977] present a theoretical study on the propagation of short duration pressure pulses in a straight elastic pipe, including Poisson and junction coupling. Radial fluid and pipe inertia is taken into account, leading to a six-equation model. The equations are solved by the MOC, but the procedure is not described in detail. In this respect some doubt may exist about the distinction between numerical and physical dispersion, not discussed by the authors. For the case that pressure and axial stress waves travel at the same velocity, an analytical solution is given. Valentin, Phillips & Walker [1979] present an eight-equation model for a liquid-filled curved pipe. Poisson coupling is included, but radial inertia is neglected. A dispersion equation is derived and elbow reflection and transmission coefficients are calculated.

Williams [1977] presents valuable experimental results obtained in steel, ABS and PVC pipes. The effect of pipe motion, brought about by axial stress waves, is clearly visible in the recorded pressures. The observed damping of pressures is attributed to FSI. Flexural pipe motion and interaction at bends are discussed. Williams' correct mathematical analysis is in terms of jump conditions across wave fronts.

Krause et al. [1977] studied the propagation of axial stress and pressure pulses in water-filled aluminium and acrylic plastic tubes. Their experimental apparatus consists of a closed tube supported partly by strings and partly by blocks. Short duration pulses are generated by

firing steel spheres onto the tube ends. Measured wave propagation speeds are in good agreement with those predicted by Skalak's [1956] simplified model. The work is extended, both experimentally and theoretically, by Barez et al. [1979]. The experiments are executed on a tube supported by blocks and filled with various liquids, initially either at rest or flowing. Skalak's simplified theory is extended with radial tube inertia and a visco-elastic Young's modulus, yielding a six-equation model similar to that of Walker & Phillips [1977]. A Laplace transformation gives solutions which are inverted numerically. The computed propagation of single pulses is in good agreement with the observed ones. Adachi et al. [1991] apply the same solution technique to the full shell equations and compare the results of classical, uncoupled and coupled calculations. They come to the same conclusion as Bürmann [1980a, 1983]: shell theory is only necessary for very short pipes and for accurate solutions close to wave fronts. Uncoupled calculations lead to erroneous results.

Schwarz [1978] performed an extensive numerical study on coupled axial liquid and pipe motion in a single straight pipe. His approach is similar to that of Walker and Phillips [1977]. He starts with a six-equation model and solves it with the MOC. By neglecting the relatively unimportant radial inertia terms he comes to a four-equation model, which is subsequently solved by a finite-difference method. Calculations with Poisson and junction coupling are compared with calculations without coupling.

Wilkinson [1978] presents a complete work formulated in the frequency domain. In addition to pressure and axial stress waves, he considers flexural and torsional stress waves, which results in a fourteen-equation model. The flexural waves are in two directions, so that five wave families are distinguished. The wave families are coupled at the various junctions described by the author. Poisson coupling is not included in the model, but this may be done by incorporating the work of Wiggert et al. [1987b] or Kuiken [1988]. In [Wilkinson 1980] the problem is formulated in the time domain. Reflection and transmission coefficients for various moving junctions are given. In [Wilkinson & Curtis 1980] a most detailed analysis of the impact of a liquid column with the closed end of a straight pipe is given and validated against experimental results. Poisson coupling and plasticity are part of the work. Solutions are found by tracing wave fronts and applying jump conditions as Williams [1977] did. Since one incident wave leads to two reflected waves, the method is quite laborious. Edwards & Please [1988] propose an original alternative method to overcome this problem.

The researchers Wiggert (fluid mechanics) and Hatfield (structural mechanics) at Michigan

State University joined their knowledge in order to tackle the problem of FSI in liquid-filled pipe systems. Together with Otwell, Lesmez, Budny and Stuckenbruck, they have been working on the subject for more than ten years. Many valuable publications were the result. Their work was in both frequency and time domain. Two different approaches were followed, the *component-synthesis method* and the *MOC method*. These terms refer to the numerical treatment of the structure. The former method is associated with natural modes of vibration, whereas the latter corresponds to wave propagations. Experimental validation tests completed the investigations. The present work is based on the findings of Wiggert and his team. In [Hatfield et al. 1982a] the component-synthesis method is introduced for application in the frequency domain. In this method the structural motion is represented by a limited number of natural modes of vibration, which are determined with a commercially available finite-element computer code. Fluid-structure interaction is introduced by means of junction coupling. The method was validated against the experiment of Blade et al. [1962], and, in [Hatfield et al. 1982b or 1983], against the experiments of Davidson & Smith [1969] and Davidson & Samsury [1972]. In principle, time-domain solutions can be obtained from frequency-domain solutions by means of inverse Fourier transformations. In practice, however, this approach may lead to serious difficulties. In particular, when the transient response to impact loads is studied, the approach is impractical. Hatfield & Wiggert [1983] came to that conclusion. As a result they developed a time-domain implementation of the component-synthesis method, in which the standard waterhammer procedure is coupled to a modal representation of the structural motion [Wiggert & Hatfield 1983]. Poisson coupling is not included in this work, which is an extension of [Otwell 1982]. In [Wiggert et al. 1983] the previous investigations are summarized and laboratory tests are presented in which the pressures, as a consequence of elbow motion, exceed Joukowsky's prediction (2.1). The tests, performed with copper pipes of 0.025 m diameter, are successfully simulated in [Otwell 1984; Wiggert et al. 1985a]. A four-equation model, including Poisson coupling, was employed for axial motion; lumped stiffness accounted for flexural motion. The MOC method was applied to get numerical solutions. In [Wiggert et al. 1985b, 1986, 1987a] a fourteen-equation model describing the axial, flexural and torsional motions of a liquid-filled pipe system is solved by means of the MOC method. This approach is adopted in the present study; it is worked out in the chapters 3 and 4. The fourteen-equation model is treated in the frequency domain by Wiggert et al. [1987b] in a way similar to that of Wilkinson [1978],

on the understanding, however, that Poisson coupling is taken into account. The numerical results are validated against the experimental data of Davidson & Smith [1969], and against new experimental data on a U-bend [Lesmez 1989; Lesmez et al. 1990]. In [Wiggert 1986] a brief review of literature is given. The frequency response of a straight pipe to seismic ground motion is examined by Hatfield & Wiggert [1987, 1990]. Stuckenbruck & Wiggert [1987] study the axial motion of highly flexible tubes with Poisson's ratios nearly equal to 0.5. Structural damping, which is of less importance for the early-time solutions calculated in the present study, is investigated theoretically and experimentally in [Budny 1988; Budny et al. 1989, 1990, 1991].

Structural damping and associated energy losses are also subject of investigation in [Jelev 1989]. Kojima et al. [1986] study a straight pipe, using a four-equation model with Poisson coupling from fluid to pipe. Experimental data on an oil-filled pipe are provided.

Vardy and Fan, at the University of Dundee, started research on fluid-structure interaction in 1984. The main contribution to the development of FSI-knowledge is in their accurate measurements of axial and flexural wave propagations in isolated parts of a pipe system. In their theoretical work they follow Wiggert et al. [1987a]. First experimental results are presented in [Vardy & Fan 1986], where these are compared with predictions from Wilkinson's theories [Wilkinson 1980; Wilkinson & Curtis 1980]. Comparison with results from Wiggert's approach follow in [Vardy & Fan 1987], together with some theoretical considerations. In [Fan 1989; Vardy & Fan 1989] experiments in a straight pipe are described. Excellent agreement is found between theory and experiment for both axial and flexural wave propagations. Pipe systems with an elbow, a T-piece and a combination of both, will be dealt with in a forthcoming paper [Vardy & Fan 1993]. The present work is an extension of that of Vardy and Fan in the sense that cavitation is included. In co-operation with Vardy and Fan experiments were performed with the test rig at the University of Dundee. The experimental apparatus is described in detail in section 5.2.

The FSI-work carried out in Delft[7] is strongly based upon Wiggert and Hatfield's investigations. Lavooij & Tijsseling [1991] apply two techniques to solve the basic equations in the time domain: the *MOC-FEM procedure* and the *MOC procedure*. The MOC-FEM procedure, which includes Poisson coupling, corresponds to the component-synthesis method

[7] see subsection 1.2.3

of Wiggert & Hatfield [1983], the MOC procedure to the approach in [Wiggert et al. 1985b]. Laboratory tests on a scale larger than usual were conducted in order to validate the developed computer code [Kruisbrink & Heinsbroek 1992]. Kruisbrink [1990] attributes the observed damping of pressures in tests with relief valves to FSI effects, and verifies this assertion through simulations with the FSI computer-code of Lavooij & Tijsseling [1989].

Obradović [1990abc] uses the MOC method of Wiggert et al. [1987a] in solving a fourteen-equation model. In [Obradović 1990b] an accident is simulated.

The FSI computer code of Bettinali et al. [1991] is based on a solution technique similar to the MOC-FEM procedure of Lavooij & Tijsseling [1989], although the Poisson coupling is modelled in a different way. Some numerical results with respect to a simple single pipe system subjected to seismic excitation are shown.

De Almeida & Koelle [1992, pp. 60-61] show work of Vasconcelos [1991] on a reservoir-pipe-valve system, in which classical waterhammer predictions are compared with results calculated with Poisson and friction coupling.

2.3.6. *FSI-analysis by coupling or extending existing software*

The literature dealt with in the preceding subsection is closely related to the present work. Fluid and structure are modelled one-dimensionally, junction and Poisson coupling are taken into account. Some other literature is reviewed here. In contrast to the previous subsection, where most of the contributions came from universities, here work is discussed that comes from the practice of, in particular, nuclear power stations. The general approach is to use existing computer codes based on the finite element method (FEM) to model the pipe system. Waterhammer loads are calculated by means of existing computer codes as well. FSI is simulated by coupling the fluid and structural codes. At this point it is worthwhile to cite Belytschko et al. [1986, p. 249]: "Although the marriage of such fluid and structural analyses programs for the purpose of conducting fully coupled fluid-structure computations of the waterhammer response are possible in principle, the awkwardness and large size of such couples makes them quite unattractive. Furthermore, the amount of computer time which would be required to run such coupled analyses would be quite exorbitant, for in addition to the large number of computations, the system would have to cope with the problem of transferring in and out of fast core the structural and fluid analysis programs for each time step."

Data transfer is one of the difficulties when coupling existing software. In many cases human interference is necessary, in other cases special software has to be developed [Ware & Williamson 1982]. For *uncoupled calculations*[8] data transfer is one-way traffic, from fluid to structure. The fluid calculation precedes the structural calculation. Typical examples are given by Meder & Nguyen-Tuong [1984], Bühl [1987] and Hankinson & Van Duyne [1987]. When FSI is taken into account, fluid and structural calculation must run simultaneously, with data transfer and possible iterations each time step. In the following a selection of relevant time-domain literature is given.

FSI experiments performed at Stanford Research Institute (SRI) under contract to Argonne National Laboratory (ANL) were simulated by several investigators using different mathematical models and solution procedures. The experimental apparatus comprised one water-filled nickel test pipe of 1.5 m length, 0.07 m diameter and 0.0017 m wall thickness, or two of these pipes connected by a rigid elbow. Pipe ends and elbow were rigidly fixed to the ground. At one of the closed ends a pressure pulse of 3 ms duration and 0.2 ms rise time was generated by means of an explosion, representing a hypothetical core disruptive accident or a liquid sodium-water reaction in a nuclear plant. The pressure pulse reached values up to 16 MPa, causing local plastic wall deformation in the nickel pipe, which was extensively instrumented with pressure transducers and strain gauges.

A-Moneim & Chang [1978, 1979] simulate both the straight pipe and one-elbow experiment, using a two-dimensional computer code allowing for fluid-structure coupling. The fluid equations are solved by a finite-difference method, the pipe equations by the FEM with axially-symmetric thin-shell elements. Precursor effects, predicted for both fluid and pipe wall, were observed in the pipe wall only. Romander et al. [1980], Youngdahl et al. [1980], Wiedermann [1982] and Kulak [1982, 1985] simulate the straight-pipe experiment. Romander et al. [1980] use for the pipe a two-dimensional model similar to that of A-Moneim & Chang, but solve the fluid equations by the FEM. Youngdahl et al. [1980] extend a conventional one-dimensional MOC waterhammer code with a simple ring-hoop deformation model for the pipe. Wiedermann [1982] employs a similar quasi-static interaction model. Numerical dispersion is presented as physical dispersion (opinion of present author). Kulak [1982, 1985] utilizes a FEM code with three-dimensional elements for both fluid and

[8] see subsection 1.1.3

pipe. It is noted that all the quoted investigators used a measured pressure pulse as input to their calculations and that junction coupling was not involved. Their work focused on plastic wall deformation and/or Poisson coupling.

Junction coupling, and not Poisson coupling, was taken into account by Giesecke [1981], Kellner & Schönfelder [1982] and Kellner et al. [1983]. Giesecke applies the standard MOC to the one-dimensional fluid equations and uses beam elements to model the pipes within the FEM. He validates his results against the, not entirely reliable[9], measurements of Swaffield [1968-1969]. Kellner & Schönfelder [1982] couple a fluid and a structural computer code and show that neglecting FSI may lead to unrealistic predictions. In [Kellner et al. 1983] convincing validation tests are presented for three pipe systems: a system with one elbow, a system with one branch and a three-dimensional system with four elbows. The length of the latter system was 13.4 m, pipe diameters were 0.10 m.

Structural engineers determine the dynamic behaviour of pipe systems with the aid of general-purpose FEM computer codes. For them, it is attractive to solve the fluid equations with the same FEM code as well, especially when FSI has to be taken into account. In principle this is possible. For example, Bach & Spangenberg [1990] apply the FEM to the classical waterhammer equations. Romander et al. [1980] and Kulak [1985], already mentioned before, solved the fluid equations by means of the FEM as well. Their models were two- and three-dimensional, respectively, and junction coupling was neglected. Investigators applying the FEM to one-dimensional fluid models are considered next.

Howlett [1971] models the liquid contained within a pipe system by means of beams without bending stiffness. Schwirian & Karabin [1981ab], Schwirian [1982, 1984], Axisa & Gibert [1982], Everstine [1984] and Belytschko et al. [1986] follow the same approach and include elbows, tees and area changes in their work. The pipe system is modelled by beam elements, junction coupling is included, Poisson coupling is not. Schwirian [1982, 1984], additionally, presents a multi-dimensional fluid element with Poisson coupling incorporated. Axisa & Gibert [1982] give a thorough mathematical treatment of their method. Everstine [1984] compares predictions of a one-dimensional fluid and pipe model with those of a three-dimensional model (like Kulak's [1982, 1985]) and with the experimental results of Davidson & Smith [1969]. Belytschko et al. [1986] introduce silent boundaries in order to analyse

---

[9] see subsection 2.3.4

small portions of complex pipe systems. Thomas [1991] gives a one-dimensional FEM treatise of fluid and structure in which the interaction is formulated in terms of local sources [Gibert et al. 1978]. Just as Axisa & Gibert [1982] and Everstine [1984], he derives a symmetric coefficient matrix by taking the displacement or velocity potential, rather than the pressure, as the fundamental fluid-unknown. It is interesting to note that within the context of an FEM-formulation of waterhammer, Joukowsky's formula (2.1) is regarded as a dashpot-equation.

In Germany an impressive research program with respect to the safety of nuclear power stations started in the mid seventies. The program was carried out by the Karlsruhe Nuclear Research Center (KfK - Kernforschungszentrum Karlsruhe) on behalf of the German government. The general objective of the program was the experimental validation of calculation tools and procedures. For this purpose a full scale test facility was available, the superheated steam reactor (HDR - Heißdampfreaktor) in Kahl near Frankfurt, a former 100 MW nuclear plant. The experimental work was exclusively performed by KfK, whereas the computations were done by several specialized institutions. Comparison and certification of software was part of the program. Pipe systems, empty and filled, straight and curved, branched and unbranched, were extensively investigated for static and dynamic, periodic and transient, elastic and plastic, as well as failure and crack behaviour. Results have been presented on all the SMiRT (Structural Mechanics in Reactor Technology) conferences since 1977.

One test configuration, defined as a German Standard Problem, is of particular interest here. It comprises a three-dimensional pipe system of 20 m length, 0.40 m diameter and 0.02 m wall thickness, including four elbows. The system is filled with subcooled water of 7-9 MPa pressure and about 500 K temperature. In one of the tests, transients are generated by a check-valve closure due to a simulated pipe break. Some publications dealing with this specific test are considered now. Bietenbeck et al. [1985] simulate an earlier version of the above-mentioned experiment. In an uncoupled calculation, measured pressure histories are used as input to a FEM code in which beam elements represent the pipe system. Müller [1986, 1987a] performs uncoupled calculations as well. Predicted pressure histories, obtained from a one-dimensional two-phase flow computer-code based on the MOC, are used as input to a FEM code similar to that of Bietenbeck et al. In [Müller 1987b] FSI effects are taken into account. Results of coupled and uncoupled analyses are compared, but not validated

against experimental data. The underlying calculation procedure is described by Grillenberger [1985], who demonstrates the significance of FSI in a simple reservoir-pipe-valve system. Firnhaber & Müller [1987] evaluate the pipe responses computed by eleven German engineering firms. The firms were provided with measured pressures, whilst the measured structural response was kept secret. The results of their uncoupled calculations showed differences which are mainly due to the used structural code, the way the measured pressures were incorporated, and the insight of the analyst. Kussmaul et al. [1989] perform an uncoupled calculation with measured data as input. Membrane-type pipe elements were used in a standard FEM code. Plasticity was taken into account since, after a certain period of time, local plastification occurred in the experiment as a consequence of pressure peaks with observed magnitudes up to 31 MPa. It is noted that measured pressures contain the influences of FSI in case this is of importance. By using these measured pressures in the simulations, FSI effects are tacitly introduced. In [Malcher & Steinhilber 1991] a review is given of the seismic tests conducted at the HDR test facility. It is reported that 25 institutions contributed to the project with analytical work.

2.3.7. *Another mechanism of fluid-structure interaction*

For the sake of completeness mention must be made of another mechanism of fluid-structure interaction in liquid-filled pipes. This mechanism has nothing to do with hydraulic transients. It concerns dynamic instabilities which lead to violent flexural vibrations of liquid-conveying pipes. The phenomenon occurs when the steady flow velocity reaches a certain limit, the critical velocity, at which the system looses stability by either buckling or flutter. "In general, the critical flow velocity is very high and is of no great concern in practice" [Jendrzejczyk & Chen 1984, p. 145]. Fluid-structure interaction is induced by the fluid centrifugal force and the fluid Coriolis force. The system response is highly dependent on the pipe support conditions. Some relevant literature on the subject is [Housner 1952; Gregory & Païdoussis 1966; Païdoussis & Issid 1974; Païdoussis & Laithier 1976; Jendrzejczyk & Chen 1984, 1985]. A historical review is given by Païdoussis & Issid [1974].

2.4. Fluid-structure interaction (FSI) and cavitation

The purpose of the present work is to study, both theoretically and experimentally, the simultaneous occurrence of FSI and cavitation. In this section, literature dealing with both FSI and cavitation is considered in order to see to which extent the present investigation is innovative.

A-Moneim & Chang [1978, 1979] report the occurrence of cavitation in the SRI experiment described in subsection 2.3.6. They account for this phenomenon by taking a simple pressure cut-off level in their model. Youngdahl et al. [1980] and Wiedermann [1982] apply the concentrated cavity model in simulating the SRI experiment. FSI is taken into account only when the pipe is plastically deforming. Kot et al. [1980, 1981] analyse cavitation in combination with junction coupling. A thin spherical end cap interacts with the pressure waves in a liquid-filled pipe. The pressure waves are described by classical waterhammer theory in combination with the concentrated cavity model; the end cap is modelled as a thin shell within the FEM. Experimental validation is not given. Giesecke [1981] mentions the concentrated cavity model but does not show any results. Axisa & Gibert [1982] and Schwirian [1982, 1984] employ the same model within the context of the FEM; gaps are allowed to form between the axial beam elements simulating the liquid. They compare numerical results obtained with and without cavitation. Van der Weijde [1985b] shows results of experiments with FSI and cavitation. All his calculations were without FSI.

In the HDR experiment described in subsection 2.3.6 subcooled water of 7-9 MPa pressure and 500 K temperature was used. When depressurizing the water, cavitation will occur, i.e. a steam-water mixture will form. Müller [1987b] simulates this phenomenon with the aid of a two-phase flow computer-code including thermodynamic effects. He couples the code to a structural FEM code thereby including FSI, although it is not exactly clear to the present author which coupling mechanisms he takes into account. Müller states that FSI is unimportant as long as the two-phase conditions prevail, since all the elasticity is then in the fluid. The present author agrees with this point of view so far as Poisson coupling is aimed at, but disagrees when junction coupling is meant. Müller does not compare his computed results with the available experimental data of [Müller 1986, 1987a].

Bettinali et al. [1991] use the concentrated cavity model in their FSI computer-code. Results of one numerical test case are presented.

Although there have been interesting developments in the past fifteen years, literature comprehensively dealing with the combination of junction coupling, Poisson coupling and cavitation does not exist. Nevertheless, computational tools are available which have the potential to handle these phenomena. "However, experimental data which would permit the simultaneous verification of fluid and structural response calculation currently do not exist" [Kot et al. 1981, p. 350]. Today this still is the case, except for the measurements documented in the present report.

2.5. Review and conclusions

The history of the research on pressure waves in fluid-filled pipe systems is surveyed. Important developments are the waterhammer investigations of Joukowsky and Allievi around 1900, the recognition of column separations in the 1930s, and the recognition of FSI effects in the 1960s. Nowadays powerful computer codes exist which are, in principle, able to simulate waterhammer, cavitation and FSI phenomena.

In the present study, two adequate and validated numerical models are combined and adapted in order to simulate the simultaneous occurrence of cavitation and FSI. Cavitation is modelled by the concentrated cavity model, FSI by models developed by Wiggert and his team. The combination of these models is new. The numerical results are compared with unique experimental data obtained in closed pipe systems.

3. MATHEMATICAL MODEL

A one-dimensional mathematical model is presented which describes the transient behaviour of liquid-filled pipes. The model is based on conventional waterhammer and beam theories. Fluid-structure interaction, cavitation and column separation are taken into account. Pipes are connected at junctions. The governing equations for single straight pipes are derived in section 3.1 by integration of three-dimensional basic equations. Steady-state initial conditions are given in section 3.2. Junctions are treated as boundary conditions for the adjacent pipes in section 3.3.

3.1. Governing equations

The 14-equation model, already mentioned in subsection 2.3.5, is deduced from general equations for fluid and structure. The fourteen first-order partial differential equations are divided into four independent groups. Three groups of four equations represent axial and - for two directions - lateral motion. One group of two equations accounts for torsional motion. The four groups may be coupled at junctions like diameter-change and elbow, such as described in the subsections 3.3.5 and 3.3.6.

The axial motion of liquid and pipe is coupled as a result of Poisson's ratio effects[1]. Extended waterhammer equations for the liquid and extended axial beam equations for the pipe allow for the Poisson coupling. Radial fluid and pipe inertia is neglected, so that the radial motion is quasi-static; hoop stress and radial displacement follow instantaneously the fluid pressure and axial pipe stress. The lateral motion of the pipe is governed by Timoshenko beam equations in which the mass of the liquid is incorporated. Fluid-structure interaction is not involved. Torsional pipe motion is modelled without interaction as well. Cavitation is treated separately in subsection 3.1.5.

The main assumptions underlying the governing equations are summarized next.

---

[1] see subsection 1.1.4

3.1.1. *Assumptions*

The theory developed is valid for straight, slender, thick-walled and prismatic pipes of circular cross-section. The pipes are surrounded by a non-viscous fluid of constant pressure, so that they are not restrained in their motion. The pipe wall material is homogeneous, isotropic, linearly elastic and subjected to small deformations. The resistance to radial motion by inertia, bending stiffness and shear deformation is ignored. The contained liquid is Newtonian with homogeneous, isotropic and linearly elastic properties. Isothermal conditions prevail. Structural and liquid damping mechanisms are disregarded, except for the friction between liquid and pipe wall, which is modelled quasi-stationary. For torsional motion liquid and pipe are allowed to slip.

The model is one-dimensional, there is one spatial co-ordinate along the central axis of the pipe. This approach is valid for long wavelengths or low frequencies (long wavelength approximation, $\lambda >> D$).

The liquid and pipe velocities are considered to be much less than the wave velocities, so that convective terms may be neglected (acoustic approximation, $c_f >> V$ and $c_t >> \dot{u}_z$).

Axial, lateral and torsional pipe motions do not interact along the pipe length, only at pipe junctions such as treated in section 3.3. The interaction between (incompressible) liquid flow and lateral pipe motion, such as described in subsection 2.3.7, is not taken into account, neither is the influence of lateral pipe deformation on a (compressible) liquid, such as observed in a closed pipe by Budny [1988, Appendix A].

The cavitation model is suitable for transient vaporous cavitation. It is based on the strong physical constraint that the pressure equals the vapour pressure as long as vapour bubbles exist in the liquid.

The derived equations are linear, except for the relatively unimportant friction terms. However, non-linear boundary conditions and the occurrence of cavitation may invalidate this assertion.

3.1.2. *Axial and radial motion*

The axial or longitudinal motion of an axially symmetric liquid-filled pipe is discussed. Pipe and liquid interact via the coupled radial motion. The basic equations were already given by

Lamb[2] [1898]. A four-equation model is attained that permits two-modes[3] solutions.

Liquid

In deriving the basic equations for the liquid, the approach of D'Souza & Oldenburger [1964], Kuiken [1986] and Budny [1988] is followed. Starting-point are the two-dimensional continuity and Navier-Stokes equations expressed in the cylindrical co-ordinates z (axial) and r (radial) [e.g. Bird et al. 1960, Mase 1970]. The circumferential co-ordinate (ϕ) is omitted in view of the axial symmetry. The equations read

Continuity equation

$$\frac{\partial \rho_f}{\partial t} + v_z \frac{\partial \rho_f}{\partial z} + v_r \frac{\partial \rho_f}{\partial r} + \rho_f \frac{\partial v_z}{\partial z} + \frac{\rho_f}{r} \frac{\partial}{\partial r}(r v_r) = 0 \tag{3.1}$$

Equation of motion in axial direction

$$\begin{aligned} &\rho_f \frac{\partial v_z}{\partial t} + \rho_f v_z \frac{\partial v_z}{\partial z} + \rho_f v_r \frac{\partial v_z}{\partial r} + \frac{\partial p}{\partial z} = F_z + \\ &+ (\kappa + \tfrac{1}{3}\mu) \frac{\partial}{\partial z} \{ \frac{\partial v_z}{\partial z} + \frac{1}{r} \frac{\partial (r v_r)}{\partial r} \} + \mu \{ \frac{1}{r} \frac{\partial}{\partial r} (r \frac{\partial v_z}{\partial r}) + \frac{\partial^2 v_z}{\partial z^2} \} \end{aligned} \tag{3.2}$$

Equation of motion in radial direction

$$\begin{aligned} &\rho_f \frac{\partial v_r}{\partial t} + \rho_f v_z \frac{\partial v_r}{\partial z} + \rho_f v_r \frac{\partial v_r}{\partial r} + \frac{\partial p}{\partial r} = F_r + \\ &+ (\kappa + \tfrac{1}{3}\mu) \frac{\partial}{\partial r} \{ \frac{\partial v_z}{\partial z} + \frac{1}{r} \frac{\partial (r v_r)}{\partial r} \} + \mu \{ \frac{1}{r} \frac{\partial}{\partial r} (r \frac{\partial v_r}{\partial r}) - \frac{v_r}{r^2} + \frac{\partial^2 v_r}{\partial z^2} \} \end{aligned} \tag{3.3}$$

with v_z and v_r the axial and radial velocities, ρ_f the mass density of the liquid, p the pressure, F_z and F_r the axial and radial body-force densities for the liquid, κ and μ the bulk and the dynamic viscosity, and t the time. Equation (3.1) represents conservation of mass; equations (3.2) and (3.3) are the linear momentum balances in axial and radial direction, respectively,

---

[2] see also subsection 2.3.1

[3] see also subsection 2.3.2

in which equation (3.1) has been substituted. The variables ρ_f, v_z, v_r and p are functions of z, r and t. The equation of state relates the density, regarded as a function of pressure and temperature, to the pressure

Equation of state

$$\frac{\partial \rho_f}{\partial p} = \frac{\rho_f}{K} \tag{3.4}$$

in which the bulk modulus K is a function of pressure and temperature. For a liquid under isothermal conditions K and ρ_f, on the right-hand side of equation (3.4), are approximated by constant values, yielding a linear relation between density and pressure. By replacing the derivatives of ρ_f in the continuity equation (3.1) by derivatives of p, the variable ρ_f is eliminated in favour of a constant ρ_f. This procedure is valid if $p << K$. The right-hand side of equation (3.4) equals $1/c_0^2$, where c_0 is the isothermal velocity of sound in an unconfined liquid, as given by equation (2.2). In general c_0 is much greater than v_z and v_r, so that the convective terms, i.e. the second and third terms on the left-hand sides of equations (3.1)-(3.3), may be neglected (see [D'Souza & Oldenburger 1964, Appendix 2]). The only important viscosity term is $\frac{1}{r}\frac{\partial}{\partial r}(r\frac{\partial v_z}{\partial r})$ (see [D'Souza & Oldenburger 1964, Appendix 2; Kuiken 1986; Budny 1988]). The axial body force is due to gravity, $F_z = \rho_f g \sin\gamma$, in which γ denotes the angle of inclination of the pipe with the horizontal. Radial body forces due to gravity are omitted in view of the axial symmetry: $F_r = 0$. With the foregoing assumptions the basic equations (3.1)-(3.3) simplify to

Continuity equation

$$\frac{1}{K}\frac{\partial p}{\partial t} + \frac{\partial v_z}{\partial z} + \frac{1}{r}\frac{\partial}{\partial r}(r v_r) = 0 \tag{3.5}$$

Equation of motion in axial direction

$$\rho_f \frac{\partial v_z}{\partial t} + \frac{\partial p}{\partial z} = \rho_f g \sin\gamma + \frac{\mu}{r}\frac{\partial}{\partial r}(r\frac{\partial v_z}{\partial r}) \tag{3.6}$$

Equation of motion in radial direction

$$\rho_f \frac{\partial v_r}{\partial t} + \frac{\partial p}{\partial r} = 0 \tag{3.7}$$

Note that, although the density in the above equations is constant, liquid compressibility still exists. It is in the first term of the continuity equation (3.5).

To come to a one-dimensional formulation, in accordance with classical waterhammer theory, the equations (3.5) and (3.6) are multiplied by $2\pi r$, integrated with respect to r from 0 to R, and divided by πR^2. The result is

Continuity equation

$$\frac{1}{K}\frac{\partial P}{\partial t} + \frac{\partial V}{\partial z} + \frac{2}{R} v_r|_{r=R} = 0 \tag{3.8}$$

Equation of motion in axial direction

$$\rho_f \frac{\partial V}{\partial t} + \frac{\partial P}{\partial z} = \rho_f g \sin\gamma + \mu \frac{2}{R} \frac{\partial v_z}{\partial r}|_{r=R} \tag{3.9}$$

in which

$$V = \frac{1}{\pi R^2} \int_0^R 2\pi r\, v_z \, dr \tag{3.10}$$

$$P = \frac{1}{\pi R^2} \int_0^R 2\pi r\, p \, dr \tag{3.11}$$

are the cross-sectionally averaged axial velocity and pressure, respectively. The last term in equation (3.9) represents the shear stress, τ_0, between liquid and pipe wall. For a Newtonian fluid this shear stress is equal to

$$\tau_0 = -\mu \frac{\partial v_z}{\partial r}|_{r=R} \tag{3.12}$$

Substitution of (3.12) in (3.9) yields

Equation of motion in axial direction

$$\rho_f \frac{\partial V}{\partial t} + \frac{\partial P}{\partial z} = \rho_f g \sin\gamma - \frac{2}{R}\tau_0 \tag{3.13}$$

The radial equation of motion (3.7) is multiplied by $2\pi r^2$, integrated with respect to r from 0 to R, and divided by $2\pi R^2$. The result is

Equation of motion in radial direction

$$\frac{1}{2}\rho_f R \frac{\partial v_r}{\partial t}\Big|_{r=R} + p\Big|_{r=R} - P = 0 \tag{3.14}$$

In deriving this equation it has been assumed that $rv_r = Rv_r|_{r=R}$, which is in accordance with the continuity equation (3.5) if compressibility is disregarded and axial inflow is concentrated at the central axis by means of a point source (singularity). Walker and Phillips [1977] find the same equation by using asymptotic expansions.

Pipe

In deriving the axial equations for the pipe, the approach of Lin & Morgan [1956a] and Herrmann & Mirsky [1956] is followed. Starting-point are the two-dimensional equations of motion formulated in cylindrical co-ordinates z (axial) and r (radial) [e.g. Kolsky 1953, Mase 1970]. The circumferential co-ordinate (ϕ) is omitted in view of the axial symmetry. Circumferential pipe motion is treated in subsection 3.1.4.

Equation of motion in axial direction

$$\rho_t \frac{\partial \dot{u}_z}{\partial t} + \rho_t \dot{u}_z \frac{\partial \dot{u}_z}{\partial z} + \rho_t \dot{u}_r \frac{\partial \dot{u}_z}{\partial r} = \frac{\partial \sigma_z}{\partial z} + \frac{1}{r}\frac{\partial (r\tau_{zr})}{\partial r} + F_z \tag{3.15}$$

Equation of motion in radial direction

$$\rho_t \frac{\partial \dot{u}_r}{\partial t} + \rho_t \dot{u}_z \frac{\partial \dot{u}_r}{\partial z} + \rho_t \dot{u}_r \frac{\partial \dot{u}_r}{\partial r} = \frac{1}{r}\frac{\partial (r\sigma_r)}{\partial r} + \frac{\partial \tau_{rz}}{\partial z} - \frac{\sigma_\phi}{r} + F_r \tag{3.16}$$

with $\dot{u}_z$ and $\dot{u}_r$ the axial and radial velocities, ρ_t the mass density of the pipe wall material, σ_z and σ_r the axial and radial stresses, σ_ϕ the hoop stress, τ_{zr} and τ_{rz} the shear stresses, F_z and F_r the axial and radial body-force densities for the pipe, and t the time. Equations (3.15) and (3.16) are the linear momentum balances in axial and radial direction. The effects of bending stiffness, rotatory inertia and transverse shear deformation are omitted in the long wavelength approximation, see subsection 2.3.2, so that the moment-of-momentum balance needs not to be considered here. The variables $\dot{u}_z$, $\dot{u}_r$, σ_z, σ_r, σ_ϕ and $\tau_{zr} = \tau_{rz}$ are functions of z, r and t. The density ρ_t is constant. The convective terms, i.e. the second and third terms on the left-hand sides of equations (3.15) and (3.16), are neglected because the deformations are assumed to be small and/or because the acoustic approximation is made, just as in the liquid equations. The axial body force is due to gravity, $F_z = \rho_t g \sin\gamma$, radial body forces are not taken into account: $F_r = 0$. The equations (3.15) and (3.16) become

Equation of motion in axial direction

$$\rho_t \frac{\partial \dot{u}_z}{\partial t} = \frac{\partial \sigma_z}{\partial z} + \frac{1}{r}\frac{\partial (r\tau_{zr})}{\partial r} + \rho_t g \sin\gamma \tag{3.17}$$

Equation of motion in radial direction

$$\rho_t \frac{\partial \dot{u}_r}{\partial t} = \frac{1}{r}\frac{\partial (r\sigma_r)}{\partial r} + \frac{\partial \tau_{rz}}{\partial z} - \frac{\sigma_\phi}{r} \tag{3.18}$$

See figures 3.1 and 3.2 for definition sketches.

To arrive at a one-dimensional formulation, the above equations are multiplied by $2\pi r$, integrated with respect to r from R to $R+e$, and divided by $2\pi(R+\frac{1}{2}e)e$, with e the thickness of the pipe wall. The axially symmetric shear force, $\int_R^{R+e} 2\pi r\, \tau_{rz}\, dr$, appearing in the right-hand side of the integrated equation (3.18), is omitted in the long-wavelength approximation, so that the result is

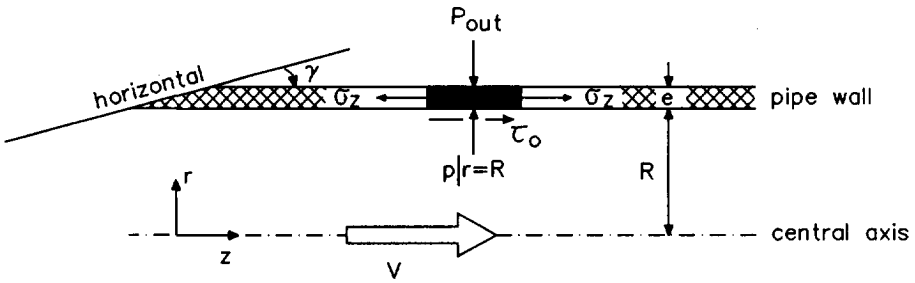

Figure 3.1. Definition sketch, side view (z-r plane): stresses acting on pipe wall.

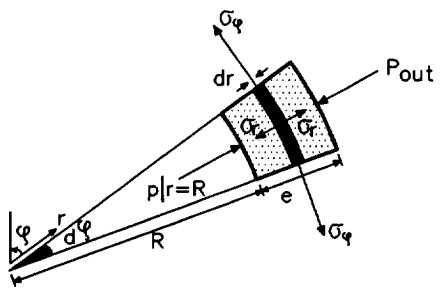

Figure 3.2. Definition sketch, cross-sectional view (r-ϕ plane): normal stresses acting on element of pipe wall.

Equation of motion in axial direction

$$\rho_t \frac{\partial \overline{u_z}}{\partial t} = \frac{\partial \overline{\sigma_z}}{\partial z} + \frac{R+e}{(R+\frac{1}{2}e)\,e}\,\tau_{zr}\big|_{r=R+e} - \frac{R}{(R+\frac{1}{2}e)\,e}\,\tau_{zr}\big|_{r=R} + \rho_t g \sin\gamma \quad (3.19)$$

Equation of motion in radial direction

$$\rho_t \frac{\partial \overline{u_r}}{\partial t} = \frac{R+e}{(R+\frac{1}{2}e)\,e}\,\sigma_r\big|_{r=R+e} - \frac{R}{(R+\frac{1}{2}e)\,e}\,\sigma_r\big|_{r=R} - \frac{1}{R+\frac{1}{2}e}\,\overline{\sigma_\phi} \quad (3.20)$$

in which

$$\overline{\dot{u}_z} = \frac{1}{2\pi(R+\frac{1}{2}e)e} \int_R^{R+e} 2\pi r\, \dot{u}_z \, dr \tag{3.21}$$

$$\overline{\dot{u}_r} = \frac{1}{2\pi(R+\frac{1}{2}e)e} \int_R^{R+e} 2\pi r\, \dot{u}_r \, dr \tag{3.22}$$

$$\overline{\sigma_z} = \frac{1}{2\pi(R+\frac{1}{2}e)e} \int_R^{R+e} 2\pi r\, \sigma_z \, dr \tag{3.23}$$

$$\overline{\sigma_\phi} = \frac{1}{e} \int_R^{R+e} \sigma_\phi \, dr \tag{3.24}$$

are averaged values of $\dot{u}_z$, $\dot{u}_r$, σ_z and σ_ϕ.

The equations of motion relate axial velocities to axial stresses (3.19) and radial velocities to hoop stresses (3.20). Stress-displacement relations will complete the mathematical model. Stress-*strain* relations are provided by the generalized Hooke's law. For a three-dimensional isotropic solid the normal strains ε_z, ε_ϕ and ε_r depend linearly on the normal stresses σ_z, σ_ϕ and σ_r,

$$\varepsilon_z = \frac{1}{E}\{\sigma_z - \nu(\sigma_\phi + \sigma_r)\} \tag{3.25}$$

$$\varepsilon_\phi = \frac{1}{E}\{\sigma_\phi - \nu(\sigma_z + \sigma_r)\} \tag{3.26}$$

$$\varepsilon_r = \frac{1}{E}\{\sigma_r - \nu(\sigma_z + \sigma_\phi)\} \tag{3.27}$$

or, when inverted,

$$\sigma_z = \frac{E}{(1+\nu)(1-2\nu)} \{ (1-\nu)\varepsilon_z + \nu(\varepsilon_\phi + \varepsilon_r) \} \tag{3.28}$$

$$\sigma_\phi = \frac{E}{(1+\nu)(1-2\nu)} \{ (1-\nu)\varepsilon_\phi + \nu(\varepsilon_z + \varepsilon_r) \} \tag{3.29}$$

$$\sigma_r = \frac{E}{(1+\nu)(1-2\nu)} \{ (1-\nu)\varepsilon_r + \nu(\varepsilon_z + \varepsilon_\phi) \} \tag{3.30}$$

which is equivalent with

$$\sigma_z = \frac{E}{1-\nu^2}(\varepsilon_z + \nu\varepsilon_\phi) + \frac{\nu}{1-\nu}\sigma_r \tag{3.31}$$

$$\sigma_\phi = \frac{E}{1-\nu^2}(\varepsilon_\phi + \nu\varepsilon_z) + \frac{\nu}{1-\nu}\sigma_r \tag{3.32}$$

$$\sigma_r = E\varepsilon_r + \nu(\sigma_z + \sigma_\phi) \tag{3.33}$$

where E is Young's modulus of elasticity and ν is Poisson's ratio.

The strain-displacement relations are

$$\varepsilon_z = \frac{\partial u_z}{\partial z} \tag{3.34}$$

$$\varepsilon_\phi = \frac{u_r}{r} \tag{3.35}$$

$$\varepsilon_r = \frac{\partial u_r}{\partial r} \tag{3.36}$$

The axial stress σ_z is expressed in displacements after substitution of (3.34)-(3.36) in (3.28),

Axial stress-displacement relation

$$\sigma_z = \frac{E}{(1+\nu)(1-2\nu)} \left\{ (1-\nu) \frac{\partial u_z}{\partial z} + \nu \frac{1}{r} \frac{\partial (r u_r)}{\partial r} \right\} \tag{3.37}$$

Differentiation with respect to t, multiplication by $2\pi r$, integration with respect to r from R to $R+e$, and division by $2\pi(R+\frac{1}{2}e)e$ leads to

Axial stress-velocity relation

$$\frac{\partial \overline{\sigma_z}}{\partial t} = \frac{E}{(1+\nu)(1-2\nu)} \left\{ (1-\nu) \frac{\partial \overline{u_z}}{\partial z} + \nu \frac{R+e}{(R+\frac{1}{2}e)e} \dot{u}_r|_{r=R+e} - \nu \frac{R}{(R+\frac{1}{2}e)e} \dot{u}_r|_{r=R} \right\} \tag{3.38}$$

Unfortunately, this equation is not appropriate for the present investigation, as will become clear in the next paragraph. An alternative, and more suitable, equation is found by substituting the axial strain (3.34) in equation (3.25), yielding

Axial stress-displacement relation

$$\sigma_z = E \frac{\partial u_z}{\partial z} + \nu \sigma_\phi + \nu \sigma_r \tag{3.39}$$

and, applying the transformation between (3.37) and (3.38),

Axial stress-velocity relation

$$\frac{\partial \overline{\sigma_z}}{\partial t} = E \frac{\partial \overline{u_z}}{\partial z} + \nu \frac{\partial \overline{\overline{\sigma_\phi}}}{\partial t} + \nu \frac{\partial \overline{\sigma_r}}{\partial t} \tag{3.40}$$

in which

$$\overline{\overline{\sigma_\phi}} = \frac{1}{2\pi(R+\frac{1}{2}e)e} \int_R^{R+e} 2\pi r \sigma_\phi \, dr \tag{3.41}$$

$$\overline{\sigma_r} = \frac{1}{2\pi(R+\frac{1}{2}e)\,e} \int_R^{R+e} 2\pi r\,\sigma_r\,dr \tag{3.42}$$

Liquid-pipe coupling

The liquid and pipe equations are coupled by means of boundary conditions representing the contact between liquid and pipe wall on the interface at $r = R$. Outside the pipe a constant pressure, P_{out}, is assumed to exist. The interface conditions are

$$\tau_{zr}|_{r=R} = -\tau_0 \qquad \tau_{zr}|_{r=R+e} = 0 \tag{3.43}$$

$$\sigma_r|_{r=R} = -p|_{r=R} \qquad \sigma_r|_{r=R+e} = -P_{out} \tag{3.44}$$

$$\dot{u}_r|_{r=R} = v_r|_{r=R} \qquad \dot{u}_r|_{r=R+e} = (v_r)_{out} \tag{3.45}$$

where $(v_r)_{out}$ is the radial velocity of the external fluid, mostly air, but in some cases liquid [Bürmann 1975]. Buried pipes are not considered here.

The dynamic conditions (3.43) and (3.44) give, respectively, the shear stresses and fluid pressures acting on the pipe wall. The kinematic conditions (3.45) prescribe the adherence of solid and fluid. Except for its constant pressure, P_{out}, the fluid outside the pipe is not modelled, so that $(v_r)_{out}$ is not known. For this reason, and because the liquid inside the pipe will not be modelled two-dimensionally, the relations (3.45) do not provide suitable boundary conditions for the pipe equations. Therefore, equation (3.38) has been replaced by equation (3.40), which is appropriate for the one-dimensional approach in the present study.

The conditions (3.43) and (3.44) are substituted in the equations of axial (3.19) and radial (3.20) pipe motion. The condition (3.45), at $r = R$, is substituted in the liquid equations (3.8) and (3.14). After the substitutions and a rearrangement of terms, eight basic equations remain for the eight variables P, V, σ_z, $\overline{u_z}$, σ_ϕ, u_r, σ_r and $p|_{r=R}$. The eight equations stem from, successively, the equations (3.13), (3.8), (3.19), (3.40), (3.14), (3.20), (3.26)+(3.35) and (3.27)+(3.36).

Liquid, axial

$$\frac{\partial V}{\partial t} + \frac{1}{\rho_f}\frac{\partial P}{\partial z} = -\frac{2}{\rho_f R}\tau_0 + g\sin\gamma \tag{3.46}$$

$$\frac{\partial V}{\partial z} + \frac{1}{K}\frac{\partial P}{\partial t} + \frac{2}{R}\dot{u}_r|_{r=R} = 0 \tag{3.47}$$

Pipe, axial

$$\frac{\partial \overline{\dot{u}_z}}{\partial t} - \frac{1}{\rho_t}\frac{\partial \overline{\sigma_z}}{\partial z} = \frac{R}{\rho_t (R + \frac{1}{2}e)\, e}\tau_0 + g\sin\gamma \tag{3.48}$$

$$\frac{\partial \overline{\dot{u}_z}}{\partial z} - \frac{1}{E}\frac{\partial \overline{\sigma_z}}{\partial t} + \frac{\nu}{E}\frac{\partial}{\partial t}\{\overline{\overline{\sigma_\phi}} + \overline{\sigma_r}\} = 0 \tag{3.49}$$

Liquid, radial

$$p|_{r=R} = P - \tfrac{1}{2}\rho_f R\frac{\partial \dot{u}_r}{\partial t}|_{r=R} \tag{3.50}$$

Pipe, radial

$$\rho_t \frac{\partial \overline{\dot{u}_r}}{\partial t} = -\frac{R+e}{(R+\frac{1}{2}e)\, e}P_{out} + \frac{R}{(R+\frac{1}{2}e)\, e}p|_{r=R} - \frac{1}{R+\frac{1}{2}e}\overline{\sigma_\phi} \tag{3.51}$$

$$u_r = \frac{r}{E}\{\sigma_\phi - \nu(\sigma_z + \sigma_r)\} \tag{3.52}$$

$$\frac{\partial u_r}{\partial r} = \frac{1}{E}\{\sigma_r - \nu(\sigma_z + \sigma_\phi)\} \tag{3.53}$$

Substitution of expression (3.50) in (3.51) gives

Equation of motion in radial direction

$$\rho_t (R + \tfrac{1}{2}e)\, e \frac{\partial \overline{\dot{u}_r}}{\partial t} + \tfrac{1}{2}\rho_f R^2 \frac{\partial \dot{u}_r}{\partial t}\Big|_{r=R} = RP - (R+e)\, P_{out} - e\,\overline{\sigma_\phi} \tag{3.54}$$

Substitution of expression (3.52) in (3.47) gives

Continuity equation

$$\frac{\partial V}{\partial z} + \frac{1}{K}\frac{\partial P}{\partial t} + \frac{2}{E}\frac{\partial}{\partial t}\{\sigma_\phi|_{r=R} - \nu\,\sigma_z|_{r=R} - \nu\,\sigma_r|_{r=R}\} = 0 \tag{3.55}$$

Four-equation model

For long wavelengths the acceleration in radial direction is negligible, so that the radial inertia terms in equation (3.54) can be left out [Skalak 1956; Lin & Morgan 1956ab; Meißner 1978; Schwarz 1978; Barez et al. 1979; Bürmann 1980a]. A quasi-static relation between the hoop stress and the internal pressure is the result,

$$\overline{\sigma_\phi} = \frac{R}{e}P - \frac{R+e}{e}P_{out} \tag{3.56}$$

Neglecting radial liquid inertia means that p equals P, the pressure is constant across the cross section of the pipe.

Equation (3.56) is confirmed in appendix A, equation (A.7), where the quasi-static stress distribution in a pressurized ring is given. Furthermore, from the equations (A.10) and (A.6), it follows that,

$$\frac{\partial}{\partial t}\{\overline{\overline{\sigma_\phi}} + \overline{\sigma_r}\} = \frac{R}{e}\frac{1}{1+\frac{1}{2}\frac{e}{R}}\frac{\partial P}{\partial t} \tag{3.57}$$

and

$$\frac{\partial}{\partial t}\{\sigma_\phi|_{r=R}\} = \left(\frac{R}{e} + \frac{1+\frac{e}{R}}{2+\frac{e}{R}}\right)\frac{\partial P}{\partial t} \tag{3.58}$$

Equation (3.57) is substituted in (3.49), and equation (3.58), together with $\sigma_r|_{r=R} = -P$,

is substituted in (3.55). The r-dependency of ε_z, and hence σ_z, is considered to be small, which means that the pipe cross-section remains almost plane when it stretches axially. The quantity $\sigma_z|_{r=R}$ in equation (3.55) then can be replaced by $\overline{\sigma_z}$. Note that $\sigma_\phi + \sigma_r$, as introduced by an internal pressure P, is a function of z and t only (see appendix A), so that according to equation (3.39) the hoop and radial stresses do not introduce r-dependency in σ_z. Four basic equations remain, (3.46), (3.55), (3.48), (3.49), for the four unknowns P, V, $\overline{\sigma_z}$ and $\overline{u_z}$,

Liquid, axial

$$\frac{\partial V}{\partial t} + \frac{1}{\rho_f}\frac{\partial P}{\partial z} = -\frac{2}{\rho_f R}\tau_0 + g\sin\gamma \tag{3.59}$$

$$\frac{\partial V}{\partial z} + \left\{\frac{1}{K} + \frac{2}{E}\left(\frac{R}{e} + \frac{1+\frac{e}{R}}{2+\frac{e}{R}} + \nu\right)\right\}\frac{\partial P}{\partial t} - \frac{2\nu}{E}\frac{\partial \overline{\sigma_z}}{\partial t} = 0 \tag{3.60}$$

Pipe, axial

$$\frac{\partial \overline{u_z}}{\partial t} - \frac{1}{\rho_t}\frac{\partial \overline{\sigma_z}}{\partial z} = \frac{1}{\rho_t\left(1+\frac{1}{2}\frac{e}{R}\right)e}\tau_0 + g\sin\gamma \tag{3.61}$$

$$\frac{\partial \overline{u_z}}{\partial z} - \frac{1}{E}\frac{\partial \overline{\sigma_z}}{\partial t} + \frac{\nu R}{E e}\frac{1}{1+\frac{1}{2}\frac{e}{R}}\frac{\partial P}{\partial t} = 0 \tag{3.62}$$

The assumption that the pipe is thin-walled, $e << R$, will be made in chapter 4, where the *four-equation model* (3.59)-(3.62) is solved numerically.

Friction

Where Kuiken [1986] and Budny [1988] proceed with frequency-dependent friction[4]

[4] see [Zielke 1968; Trikha 1975; Vardy & Hwang 1991; Eichinger & Lein 1992] for frequency-dependent friction

formulations, here the standard waterhammer approach is adopted [Wylie & Streeter 1978a, p. 18]. The shear stress τ_0 is assumed to be the same as if the flow were steady. So, in terms of the *Darcy-Weisbach friction factor f*,

$$\tau_0 = \rho_f f \frac{V_{rel} | V_{rel} |}{8} \tag{3.63}$$

where V_{rel} is the one-dimensional relative velocity $V - \overline{u_z}$ between liquid and pipe wall. Expression (3.63) is obtained from the Darcy-Weisbach [Darcy 1857; Weisbach 1855] relation $\Delta P = f \rho_f (L/D) (V^2/2)$ and the steady-state force balance $\Delta P (\pi D^2)/4 = \tau_0 \pi D L$ by eliminating ΔP. The pressure difference ΔP exists over a horizontal pipe section of length L and diameter D. The friction factor f is generally estimated with aid of the so-called *Moody diagram* [Moody 1944]. Equation (3.63) is important for the determination of the stationary initial conditions. An initial pressure gradient influences the dynamic pressures. When this phenomenon becomes dominant it is referred to as *line packing*. Equation (3.63) is a poor friction model for the strongly dynamic problems treated herein. Fortunately, the effects of friction are negligible in the beginning of a transient event. This is due to the small time scales involved.

3.1.3. *Lateral motion*

The lateral (or flexural, or transverse) motion of a liquid-filled pipe is assumed to be independent of the axial, radial and torsional motions discussed in the previous and next subsections. The only influence of the liquid on the lateral motion is in its inertia. Four equations are attained corresponding to the *Timoshenko beam theory* [Bresse 1859; Timoshenko 1921, 1922].

Pipe

In deriving the lateral equations, the approach of Cowper [1966] is followed. Starting-point are the three-dimensional equations of motion for an empty pipe, formulated in rectangular co-ordinates z (axial), x (lateral, horizontal) and y (lateral, normal to z and x); see figures 3.3 and 3.4. The z-axis is the central line of the pipe, so that

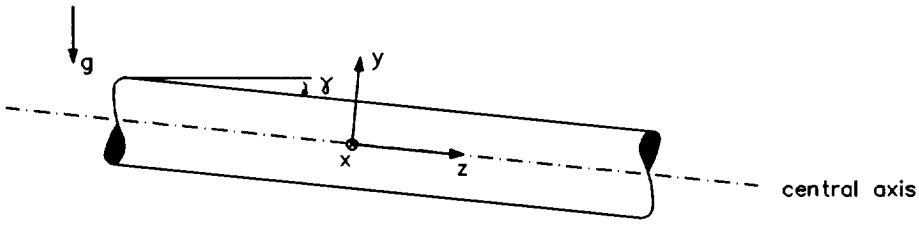

Figure 3.3. Definition sketch, side view (z-y plane): co-ordinates.

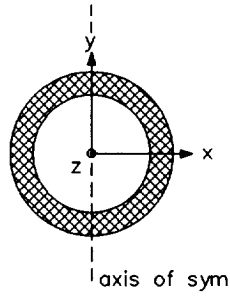

Figure 3.4. Definition sketch, cross-sectional view (y-x plane): co-ordinates.

$$\int\int x\,dxdy = \int\int y\,dxdy = 0 \tag{3.64}$$

where the integration is over the cross-sectional pipe area. In contrast to the subsections 3.1.2 and 3.1.4, where axially symmetric problems are considered, here symmetry about the plane of deflection is assumed. For deflections in the z-y plane, the equations of motion are

Equation of motion in axial direction

$$\rho_t \frac{\partial \dot{u}_z}{\partial t} + \rho_t \dot{u}_x \frac{\partial \dot{u}_z}{\partial x} + \rho_t \dot{u}_y \frac{\partial \dot{u}_z}{\partial y} + \rho_t \dot{u}_z \frac{\partial \dot{u}_z}{\partial z} = \frac{\partial \tau_{zx}}{\partial x} + \frac{\partial \tau_{zy}}{\partial y} + \frac{\partial \sigma_z}{\partial z} + F_z \tag{3.65}$$

Equation of motion in lateral direction

$$\rho_t \frac{\partial \dot{u}_y}{\partial t} + \rho_t \dot{u}_x \frac{\partial \dot{u}_y}{\partial x} + \rho_t \dot{u}_y \frac{\partial \dot{u}_y}{\partial y} + \rho_t \dot{u}_z \frac{\partial \dot{u}_y}{\partial z} = \frac{\partial \tau_{yx}}{\partial x} + \frac{\partial \sigma_y}{\partial y} + \frac{\partial \tau_{yz}}{\partial z} + F_y \tag{3.66}$$

with $\dot{u}_z$, $\dot{u}_y$ and $\dot{u}_x$ the axial and lateral velocities of the pipe, ρ_t the mass density, σ_z and σ_y the axial and lateral stresses, τ_{zx}, τ_{zy}, τ_{yx} and τ_{yz} the shear stresses, F_z and F_y the axial and lateral body-force densities, and t the time. Equations (3.65) and (3.66) represent the linear momentum balances in the axial and the lateral direction, respectively. The influence of the axial stress $\overline{\sigma_z}$ on the lateral motion, which is predominant in strings and cables, is neglected [Clough & Penzien 1975, pp. 296-297], just as the effects of flow-induced centrifugal and Coriolis forces [Païdoussis & Laithier 1976]. The variables $\dot{u}_z$, $\dot{u}_y$, $\dot{u}_x$, σ_z, σ_y, τ_{zx}, $\tau_{zy} = \tau_{yz}$ and τ_{yx} are functions of z, y, x and t. The density ρ_t is constant. The convective terms, i.e. the last three terms on the left-hand sides of equations (3.65) and (3.66), are omitted because the deformations are small and the acoustic approximation is valid. The body forces are due to gravity, $F_z = \rho_t g \sin\gamma$ and $F_y = -\rho_t g \cos\gamma$. The equations (3.65) and (3.66) now become

Equation of motion in axial direction

$$\rho_t \frac{\partial \dot{u}_z}{\partial t} = \frac{\partial \tau_{zx}}{\partial x} + \frac{\partial \tau_{zy}}{\partial y} + \frac{\partial \sigma_z}{\partial z} + \rho_t g \sin\gamma \tag{3.67}$$

Equation of motion in lateral direction

$$\rho_t \frac{\partial \dot{u}_y}{\partial t} = \frac{\partial \tau_{yx}}{\partial x} + \frac{\partial \sigma_y}{\partial y} + \frac{\partial \tau_{yz}}{\partial z} - \rho_t g \cos\gamma \tag{3.68}$$

To come to a one-dimensional formulation, equation (3.67), multiplied by y, and equation (3.68) are integrated over the pipe wall cross-section. The result is

Equation of rotation about the x-axis

$$\rho_t I_t \frac{\partial \dot{\overline{\theta}}_x}{\partial t} = \int\int y \left(\frac{\partial \tau_{zx}}{\partial x} + \frac{\partial \tau_{zy}}{\partial y}\right) dx\,dy - \frac{\partial M_x}{\partial z} \tag{3.69}$$

Equation of motion in lateral direction

$$\rho_t A_t \frac{\partial \overline{\dot{u}_y}}{\partial t} = \int\int \left(\frac{\partial \tau_{yx}}{\partial x} + \frac{\partial \sigma_y}{\partial y}\right) \mathrm{d}x\mathrm{d}y - \frac{\partial Q_y}{\partial z} - \rho_t A_t g \cos\gamma \tag{3.70}$$

in which

$$\overline{\dot{\theta}_x} = \frac{1}{I_t} \int\int y \dot{u}_z \, \mathrm{d}x\mathrm{d}y \tag{3.71}$$

$$\overline{\dot{u}_y} = \frac{1}{A_t} \int\int \dot{u}_y \, \mathrm{d}x\mathrm{d}y \tag{3.72}$$

$$M_x = -\int\int y \sigma_z \, \mathrm{d}x\mathrm{d}y \tag{3.73}$$

$$Q_y = -\int\int \tau_{yz} \, \mathrm{d}x\mathrm{d}y \tag{3.74}$$

where

$$A_t = \int\int \mathrm{d}x\mathrm{d}y = 2\pi (R + \tfrac{1}{2}e) e \tag{3.75}$$

$$I_t = \int\int y^2 \, \mathrm{d}x\mathrm{d}y = \tfrac{1}{4}\pi \{(R+e)^4 - R^4\} \tag{3.76}$$

are the area and the second moment, about the x-axis, of the pipe cross-section. The expressions (3.71) and (3.72) give averaged values of the velocities of the angle of rotation of the pipe cross-section about the x-axis, and the y-deflection of the pipe, respectively. In the equations (3.73) and (3.74), where the (unconventional) sign convention of figure 3.5 has been adopted, the bending moment M_x and the lateral shear force Q_y are defined.

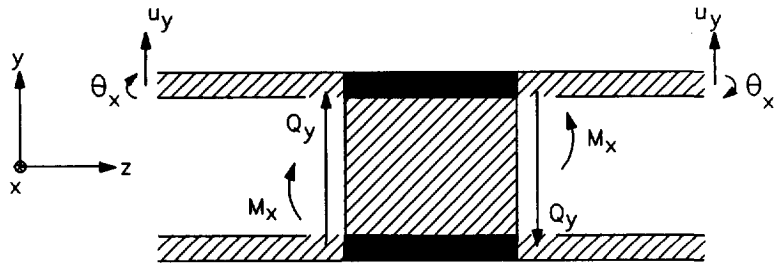

Figure 3.5. Definition sketch: generalized forces and displacements, positive directions.

The integrals in the equations (3.69) and (3.70), applying integration by parts and the divergence theorem of Gauss, are found to be

$$\begin{aligned} \int\int y\left(\frac{\partial \tau_{zx}}{\partial x} + \frac{\partial \tau_{zy}}{\partial y}\right) dx dy &= \int\int \left\{\frac{\partial (y\tau_{zx})}{\partial x} + \frac{\partial (y\tau_{zy})}{\partial y} - \tau_{zy}\right\} dx dy = \\ &= \oint y\,(\tau_{zx} n_x + \tau_{zy} n_y)\, ds - \int\int \tau_{yz}\, dx dy = \oint y T_z\, ds + Q_y = Q_y \end{aligned} \tag{3.77}$$

$$\int\int \left(\frac{\partial \tau_{yx}}{\partial x} + \frac{\partial \sigma_y}{\partial y}\right) dx dy = \oint (\tau_{yx} n_x + \sigma_y n_y)\, ds = \oint T_y\, ds = 0 \tag{3.78}$$

where n_x and n_y are the components of the unit-normal to the pipe wall surfaces and ds is a line element on those surfaces. The surface tractions T_z and T_y are due to a constant shear force τ_0, and axially symmetric pressures P and P_{out}, respectively; see subsection 3.1.2. The corresponding integrals vanish, because of symmetry in the integrands.

The equations of motion relate rotational velocities to bending moments (3.69) and lateral velocities to transverse shear forces (3.70). The following stress-displacement relations complete the mathematical model,

Axial normal stress-displacement relation

$$E\frac{\partial u_z}{\partial z} = \sigma_z - \nu(\sigma_x + \sigma_y) \tag{3.79}$$

Lateral shear stress-displacement relation

$$\frac{\partial u_y}{\partial z} + \frac{\partial u_z}{\partial y} = \frac{\tau_{yz}}{G} \tag{3.80}$$

in which $G = \frac{1}{2}E/(1+\nu)$ is the shear modulus. The displacements u_y and u_z are expressed as their averaged values $\overline{u_y}$ and $\overline{u_z} + y\overline{\theta_x}$ plus local deviations u_y^* and u_z^*,

$$u_y = \overline{u_y} + u_y^* \quad \text{and} \quad u_z = \overline{u_z} + y\overline{\theta_x} + u_z^* \tag{3.81}$$

with

$$\overline{u_y} = \frac{1}{A_t}\int\int u_y \,\mathrm{d}x\mathrm{d}y \;,\; \overline{u_z} = \frac{1}{A_t}\int\int u_z \,\mathrm{d}x\mathrm{d}y \quad \text{and} \quad \overline{\theta_x} = \frac{1}{I_t}\int\int y u_z \,\mathrm{d}x\mathrm{d}y \tag{3.82}$$

The pipe cross-section does not remain plane when it deforms, the residual displacement u_z^* represents its warping. With (3.64) and (3.82) it follows from (3.81) that

$$\int\int u_y^* \,\mathrm{d}x\mathrm{d}y = \int\int u_z^* \,\mathrm{d}x\mathrm{d}y = \int\int y u_z^* \,\mathrm{d}x\mathrm{d}y = 0 \tag{3.83}$$

Substitution of (3.81) in (3.79) and (3.80) yields

$$E\frac{\partial \overline{u_z}}{\partial z} + yE\frac{\partial \overline{\theta_x}}{\partial z} = \sigma_z - \nu(\sigma_x + \sigma_y) - E\frac{\partial u_z^*}{\partial z} \quad \text{and} \quad \frac{\partial \overline{u_y}}{\partial z} + \overline{\theta_x} = \frac{\tau_{yz}}{G} - \frac{\partial u_y^*}{\partial z} - \frac{\partial u_z^*}{\partial y} \tag{3.84}$$

To arrive at a one-dimensional formulation, the first equation (3.84), multiplied by y, and the second equation (3.84), divided by A_t, are integrated over the pipe wall cross-section. Using (3.64), (3.73)-(3.76) and (3.83), the result is

Bending moment-rotation relation

$$EI_t\frac{\partial \overline{\theta_x}}{\partial z} = -M_x - \nu\int\int y(\sigma_x + \sigma_y)\,\mathrm{d}x\mathrm{d}y \tag{3.85}$$

Lateral shear force-displacement relation

$$\frac{\partial \overline{u_y}}{\partial z} + \overline{\theta_x} = \frac{1}{A_t G} \int\int \left(\tau_{yz} - G \frac{\partial u_z^*}{\partial y} \right) dx dy \tag{3.86}$$

The integral in equation (3.85) is neglected, since the lateral stresses σ_x and σ_y, which are symmetric with respect to the *z*-*y* plane, are considered to be small as compared with the axial stress σ_z. The integral in equation (3.86) is evaluated by approximating τ_{yz} and u_z^*. Analytical solutions, available for the case that Q_y is constant or linearly varying with *z*, are substituted for τ_{yz} and u_z^* [Cowper 1966]. The integral in (3.86) is then calculated as

$$\int\int \left(\tau_{yz} - G \frac{\partial u_z^*}{\partial y} \right) dx dy = - \frac{Q_y}{\kappa^2} \tag{3.87}$$

where κ^2 is the *shear coefficient*. For a thick-walled pipe Cowper [1966] finds

$$\kappa^2 = \frac{6(1+\nu)(1+m^2)^2}{(7+6\nu)(1+m^2)^2 + (20+12\nu)m^2} \tag{3.88}$$

with $m = 1/(1+\frac{e}{R})$. For a thin-walled pipe m tends to 1, in which case

$$\kappa^2 = \frac{2(1+\nu)}{4+3\nu} \tag{3.89}$$

The expressions (3.88) and (3.89) are valid for long wavelengths and low frequencies, since they are based on a quasi-static shear-stress distribution. For short wavelengths κ^2 becomes frequency dependent. Hutchinson and El-Azhari [1986] verified Cowper's shear coefficients (3.88), (3.89) by comparing them with κ^2-values resulting from a three-dimensional analysis of the free vibrations of a hollow cylinder.

Liquid

With respect to its lateral motion, the liquid is regarded as a rigid column moving together with the pipe. To account for this effect, the inertia term on the left-hand side of the lateral

equation of motion (3.70) is modified. The mass per unit length of the liquid is added to that of the pipe: $\rho_t A_t$ is replaced by $\rho_t A_t + \rho_f A_f$, where $A_f = \pi R^2$ is the cross-sectional discharge area.

Many investigators, like Païdoussis & Laithier [1976], Wiggert et al. [1986, 1987ab], Lavooij [1986], Vardy & Fan [1989], Obradović [1990abc], let, incorrectly, the liquid contribute to the rotatory inertia of the liquid-filled pipe. They replace $\rho_t I_t$ in the rotational equation of motion (3.69) by $\rho_t I_t + \rho_f I_f$, where $I_f = \frac{1}{4}\pi R^4$ is the second moment about the x-axis of the cross-sectional discharge area. However, the rotation about the x-axis of a cross section of the pipe wall does not introduce a rotation of the corresponding cross section of the liquid. Due to the small pipe deformations, the rotational motion of the pipe wall is nearly axial. The associated liquid motion is confined to the boundary layer near the pipe wall; it is of less importance and can be accounted for only by a proper friction model.

Four basic equations

The four basic equations governing the four unknowns $\overline{\dot{\theta}_x}$, M_x, $\overline{u_y}$ and Q_y are given by (3.69)+(3.77), (3.85) differentiated with respect to time, (3.70)+(3.78) and (3.86)+(3.87) differentiated with respect to time,

$$\frac{\partial \overline{\dot{\theta}_x}}{\partial t} + \frac{1}{\rho_t I_t}\frac{\partial M_x}{\partial z} = \frac{1}{\rho_t I_t} Q_y \tag{3.90}$$

$$\frac{\partial \overline{\dot{\theta}_x}}{\partial z} + \frac{1}{EI_t}\frac{\partial M_x}{\partial t} = 0 \tag{3.91}$$

$$\frac{\partial \overline{\dot{u}_y}}{\partial t} + \frac{1}{\rho_t A_t + \rho_f A_f}\frac{\partial Q_y}{\partial z} = -g\cos\gamma \tag{3.92}$$

$$\frac{\partial \overline{u_y}}{\partial z} + \frac{1}{\kappa^2 G A_t}\frac{\partial Q_y}{\partial t} = -\overline{\theta_x} \tag{3.93}$$

For deflections in the z-x plane the same equations are found with y replaced by x and, due to the sign convention of figure 3.5, with opposite signs in the M and $\bar{\theta}$ terms and definitions. Since the x-direction is horizontal the gravity term in (3.92) vanishes.

3.1.4. *Torsional motion*

The torsional (or circumferential, or tangential) motion of the pipe wall is assumed to be unaffected by the liquid. Circumferential liquid motion and circumferential liquid-pipe friction are disregarded. The basic equations for the motion of the pipe wall can be found in [Timoshenko & Goodier 1970, pp. 341-344], where the axial and radial displacements are zero and the circumferential motion is axially symmetric. Pipe cross-sections remain plane, but radii of cross section may distort. The two-dimensional equation of motion, without convective terms and body forces, in cylindrical co-ordinates z and r, reads

Equation of motion in circumferential direction

$$\rho_t \frac{\partial \dot{u}_\phi}{\partial t} = \frac{\partial \tau_{\phi z}}{\partial z} + \frac{\partial \tau_{\phi r}}{\partial r} + 2\frac{\tau_{\phi r}}{r} \tag{3.94}$$

where the circumferential co-ordinate (ϕ) has been omitted in view of the axial symmetry. The circumferential velocity $\dot{u}_\phi$ and the shear stresses $\tau_{\phi z}$ and $\tau_{\phi r}$ are functions of z, r and t, the density ρ_t is constant. The shear stresses are related to the circumferential displacement u_ϕ by

Circumferential shear stress-displacement relations

$$\tau_{\phi z} = G\frac{\partial u_\phi}{\partial z} \tag{3.95}$$

$$\tau_{\phi r} = G r \frac{\partial}{\partial r}\left(\frac{u_\phi}{r}\right) \tag{3.96}$$

For a prismatic pipe of circular cross-section the assumption is justified that u_ϕ varies linearly with r,

$$u_\phi = r\,\theta_z(z,t) \tag{3.97}$$

where θ_z is the angle of rotation about the z-axis. Now the radii of cross section remain straight and $\tau_{\phi r}$ vanishes. To arrive at a one-dimensional formulation, the remaining equations (3.94) and (3.95) are multiplied by $2\pi r^2$, integrated with respect to r from R to $R+e$ and divided by J_t. With (3.95) differentiated with respect to time, the result is

Equation of motion in circumferential direction

$$\frac{\partial \dot{\theta}_z}{\partial t} - \frac{1}{\rho_t J_t}\frac{\partial M_z}{\partial z} = 0 \tag{3.98}$$

Torsional moment-rotation relation

$$\frac{\partial \dot{\theta}_z}{\partial z} - \frac{1}{G J_t}\frac{\partial M_z}{\partial t} = 0 \tag{3.99}$$

in which the torsional moment M_z, the torsional angular velocity $\dot{\theta}_z$ and the polar second moment of the pipe cross-section J_t, are defined as

$$\dot{\theta}_z = \frac{\partial \theta_z}{\partial t} \tag{3.100}$$

$$M_z = \int_R^{R+e} 2\pi r^2\,\tau_{\phi z}\,\mathrm{d}r \tag{3.101}$$

$$J_t = \int_R^{R+e} 2\pi r^3\,\mathrm{d}r = \tfrac{1}{2}\pi\{(R+e)^4 - R^4\} \tag{3.102}$$

The two equations (3.98) and (3.99), describing torsional motion, are not used in the present work where only plane pipe systems are considered.

3.1.5. *Cavitation*

The cavitation model is based on the strong physical constraint that the absolute fluid pressure equals vapour pressure,

$$P = P_v \tag{3.103}$$

as long as vaporous cavities exist in the liquid. The vapour pressure P_v is a function of the temperature, as shown for water in figure 3.6. Equation (3.103) is valid if free gas is absent and gas release does not occur. Cavitation starts at the instant the liquid pressure reaches the vapour pressure; it ends when all cavities have vanished. The ending has to be inferred from the void fraction α, which is the ratio of the vapour volume to the total volume,

$$\alpha = \frac{V_v}{V_l + V_v} \tag{3.104}$$

where V_v and V_l are the vapour and liquid volumes per unit length of pipe. *Column separations* are identified by void fractions close to unity, whereas *distributed cavitation* is identified by void fractions which are small with respect to unity. Column separations occur locally and are therefore treated as boundary conditions in subsection 3.3.7. Distributed cavitation occurs along great lengths of pipe and is considered here.

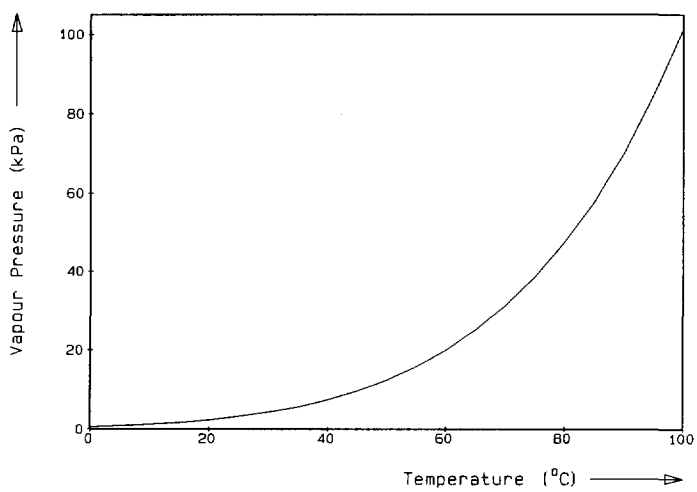

Figure 3.6. Vapour pressure of water versus temperature from melting point to atmospheric boiling point. Source: [Lide 1991, p. 6-13].

The liquid equations presented in subsection 3.1.2 are not valid in regions of cavitating flow. A simple one-dimensional two-phase flow model describing these regions is given now. The model, developed by Kalkwijk & Kranenburg [1971], Kranenburg [1972, 1974ab] and extended by Wylie & Streeter [1978b], Streeter [1983] and Simpson [1986], is based on equation (3.103). When vapour cavities exist in the liquid, all the fluid's elasticity is in the vapour and the elasticity of liquid and pipe wall may be ignored in the fluid equations. Fluid-structure *interaction* through Poisson coupling is not of importance[5]; the interface condition (3.45), at $r = R$, does not hold any more. The continuity equation then reduces to

Two-phase continuity equation

$$\frac{\partial \alpha}{\partial t} + V\frac{\partial \alpha}{\partial z} = \frac{\partial V}{\partial z} \tag{3.105}$$

where V is the average velocity of the liquid-vapour mixture [Simpson 1986, pp. 50-52]. The convective term, i.e. the second term on the left-hand side, may not be neglected here, since the pressure wave speed can be very low in a liquid-vapour mixture and, consequently, the acoustic approximation does not hold. Equation (3.105) simply states that the void fraction follows the velocity gradient. It is the equivalent of the liquid continuity equation (3.47), with P constant and the convective term added, allowing for tearing voids in the liquid. The two-phase equivalent of the liquid equation of motion (3.46) is

Two-phase equation of motion

$$\frac{\partial V}{\partial t} + V\frac{\partial V}{\partial z} = -\frac{2}{\rho_f R}\tau_0 + g\sin\gamma \tag{3.106}$$

with τ_0 defined by (3.63) [Simpson 1986, pp. 53-54]. Equation (3.106) states that the fluid motion in a region of distributed cavitation is governed by wall friction and gravity.

The three variables P, V and α obey the three equations (3.103), (3.105) and (3.106). Although an analytical solution of these equations can easily be found, the problem with this

---

[5] Fluid-structure interaction may be important when the nullification of distributed cavitation regions is accompanied with shock waves [Kranenburg 1974a, pp. 101, 107]

model is to keep track of the moving boundaries between the waterhammer regions ruled by equations (3.46)-(3.47) and the cavitating regions ruled by the equations (3.103), (3.105) and (3.106). The difficulties associated with the moving boundaries, or *interfaces*, concern pressure-dependent wave propagation, shock waves and the occurrence of intermediate column separations. Although Simpson [Simpson 1986; Bergant & Simpson 1992] finds reliable solutions with his *interface model*, in the present work a simpler, numerical, approach has been adopted. This approach is worked out in section 4.5.

Note

The fluid mass per unit length, $\rho_f A_f$, in the lateral equation (3.92) is assumed not to be affected by distributed cavitation, because the void fractions generally are small.

3.2. Initial conditions

The liquid-filled pipe system is assumed to be in equilibrium (steady state) before a transient event starts. The initial values of the basic variables, these are generalized forces and velocities, and of the structural displacements, are derived from the one-dimensional equations of section 3.1 omitting the non-stationary terms. The basic equations are non-linear due to the friction term (3.63) and due to the cavitation model of subsection 3.1.5. The particular (static or stationary) and homogeneous (dynamic) solutions of the differential equations are therefore not allowed to be superposed. Superposition of solutions is allowed only for the special case that cavitation does not occur and friction is statically and/or dynamically negligible.

3.2.1. *Single pipe*

Initial values for axial motion

The steady state pertaining to the four-equation model (3.59)-(3.62) follows from the

stationary equations

$$\frac{\partial P}{\partial z} = -\frac{2}{R}\tau_0 + \rho_f g \sin\gamma \tag{3.107}$$

$$\frac{\partial V}{\partial z} = 0 \tag{3.108}$$

$$\frac{\partial \overline{\sigma_z}}{\partial z} = -\frac{1}{(1+\frac{1}{2}\frac{e}{R})e}\tau_0 - \rho_t g \sin\gamma \tag{3.109}$$

$$\frac{\partial \overline{u_z}}{\partial z} = 0 \tag{3.110}$$

so that

$$P = P(0,0) - \{\frac{2}{R}\tau_0 - \rho_f g \sin\gamma\}\, z \tag{3.111}$$

$$V = V(0,0) \tag{3.112}$$

$$\overline{\sigma_z} = \overline{\sigma_z}(0,0) - \{\frac{1}{(1+\frac{1}{2}\frac{e}{R})e}\tau_0 + \rho_t g \sin\gamma\}\, z \tag{3.113}$$

$$\overline{u_z} = \overline{u_z}(0,0) \tag{3.114}$$

The constants of integration, $P(0,0)$, $V(0,0)$, $\overline{\sigma_z}(0,0)$ and $\overline{u_z}(0,0)$, are obtained from two boundary conditions at each pipe end. These boundary conditions may exhibit coupling between the liquid and pipe variables. The axial displacement follows from the integrated equation (3.39),

$$\frac{\partial \overline{u_z}}{\partial z} = \frac{1}{E}\overline{\sigma_z} - \frac{\nu}{E}(\overline{\overline{\sigma_\phi}} + \overline{\sigma_r}) \tag{3.115}$$

With $\overline{\overline{\sigma_\phi}} + \overline{\sigma_r}$ according to equation (A.10) and the axial steady-state (3.111)-(3.114), the result is

$$\overline{u_z} = \overline{u_z}(0,0) + \frac{z}{E}\{\overline{\sigma_z}(0,0) - \nu\frac{R}{e}\frac{1}{1+\frac{1}{2}\frac{e}{R}}(P(0,0) - (1+\frac{e}{R})^2 P_{out})\} + \\ - \frac{z^2}{2E}\{\frac{1-2\nu}{(1+\frac{1}{2}\frac{e}{R})e}\tau_0 + (\rho_t + \nu\frac{R}{e}\frac{1}{1+\frac{1}{2}\frac{e}{R}}\rho_f)\, g\sin\gamma\} \tag{3.116}$$

where the constant $\overline{u_z}(0,0)$ defines the zero level.

Initial values for lateral motion

The steady state pertaining to the four lateral equations (3.90)-(3.93) follows from the static equations

$$\frac{\partial M_x}{\partial z} = Q_y \tag{3.117}$$

$$\frac{\partial \overline{\dot{\theta}_x}}{\partial z} = 0 \tag{3.118}$$

$$\frac{\partial Q_y}{\partial z} = -(\rho_t A_t + \rho_f A_f)\, g\cos\gamma \tag{3.119}$$

$$\frac{\partial \overline{u_y}}{\partial z} = -\overline{\dot{\theta}_x} \tag{3.120}$$

so that

$$M_x = M_x(0,0) + Q_y(0,0)\, z - \tfrac{1}{2}\rho_t A_t g\cos\gamma\, z^2 \tag{3.121}$$

$$\overline{\dot{\theta}_x} = \overline{\dot{\theta}_x}(0,0) \tag{3.122}$$

$$Q_y = Q_y(0,0) - (\rho_t A_t + \rho_f A_f)\, g\cos\gamma\, z \tag{3.123}$$

$$\overline{u_y} = \overline{u_y}(0,0) - \overline{\dot{\theta}_x}(0,0)\, z \tag{3.124}$$

The constants of integration, $M_x(0,0)$, $\overline{\dot{\theta}_x}(0,0)$, $Q_y(0,0)$ and $\overline{u_y}(0,0)$, are obtained from

two boundary conditions at each pipe end. The rotation due to bending and the lateral displacement follow from the equations (3.85)-(3.87) and the lateral steady-state (3.121)-(3.124),

$$\overline{\theta_x} = \overline{\theta_x}(0,0) - \frac{z}{EI_t} M_x(0,0) - \frac{z^2}{2EI_t} Q_y(0,0) + \frac{z^3}{6EI_t} (\rho_t A_t + \rho_f A_f) g \cos\gamma \quad (3.125)$$

$$\overline{u_y} = \overline{u_y}(0,0) - z\{\overline{\theta_x}(0,0) + \frac{Q_y(0,0)}{\kappa^2 A_t G}\} + \frac{z^2}{2}\{\frac{M_x(0,0)}{EI_t} + \frac{\rho_t A_t + \rho_f A_f}{\kappa^2 A_t G} g\cos\gamma\} + \\ + \frac{z^3}{6EI_t} Q_y(0,0) - \frac{z^4}{24EI_t} (\rho_t A_t + \rho_f A_f) g\cos\gamma \quad (3.126)$$

where the constants $\overline{\theta_x}(0,0)$ and $\overline{u_y}(0,0)$ define the zero level.

Initial values for torsional motion

The steady state pertaining to the two torsional equations (3.98)-(3.99), combined with (3.100), follows from the static equations

$$\frac{\partial M_z}{\partial z} = 0 \quad (3.127)$$

$$\frac{\partial \dot{\theta}_z}{\partial z} = 0 \quad (3.128)$$

$$\frac{\partial \theta_z}{\partial z} = \frac{1}{GJ_t} M_z \quad (3.129)$$

so that

$$M_z = M_z(0,0) \quad (3.130)$$

$$\dot{\theta}_z = \dot{\theta}_z(0,0) \quad (3.131)$$

$$\theta_z = \theta_z(0,0) + \frac{z}{GJ_t} M_z(0,0) \quad (3.132)$$

The constants of integration, $M_z(0,0)$, $\dot{\theta}_z(0,0)$ and $\theta_z(0,0)$, are obtained from three boundary conditions at the pipe ends.

3.2.2. *Multi-pipe system*

In multi-pipe systems the single pipes are connected at *junctions*. Junction coupling relates the constants of integration of the adjacent pipes. In this way the axial, lateral and torsional equations may be fully coupled. Due to the friction terms, which are dominant in the steady state, and due to boundary conditions like pumps and valves, the coupling equations are non-linear. Minor losses should be included as well [Idelchik 1986; Miller 1990]. Numerical techniques, shortly described in section 4.6, are generally used to find the steady state in a multi-pipe system and its connected hydraulic machinery.

3.3. Boundary conditions

The single straight pipes considered in the previous two sections are connected at *junctions* and terminated at *ends*. Both junctions and ends are mathematically treated as boundary conditions. When the boundary conditions couple the liquid and pipe variables, this is, within the context of fluid-structure interaction, called *junction coupling*. Transients are generated by time-varying boundary conditions.

In one-dimensional pipe systems, being systems where the pipes are in a direct line, the axial, lateral and torsional equations are not coupled through the boundary conditions. In two-dimensional pipe systems, being systems where the pipes are in one plane, the axial and lateral motions within the plane are coupled through unrestrained junctions. Torsional motion and lateral motion out of the plane are assumed not to occur. In three-dimensional pipe systems all basic equations given in section 3.1 can be coupled by the boundary conditions.

In the present study only one- and two-dimensional problems without torsion are considered. These can be described by the axial equations (3.59)-(3.62) and the lateral equations (3.90)-(3.93). The corresponding initial conditions are given by the expressions (3.111)-(3.114) and (3.121-3.124). Four boundary conditions, needed at each pipe end to constitute a proper *initial boundary value problem*, are obtained from a physical consideration of the specific situation at junction or end.

The cavitation-free boundary conditions used in the present work are given in the next subsections. Column separation, mostly encountered at junctions and ends, is discussed separately in the last subsection of this section.

3.3.1. *Reservoir*

The reservoir maintains a constant pressure P_{res}, and the connected pipes are assumed to be rigidly fixed (figure 3.7). The boundary values for the basic variables are

$$P = P_{res} \tag{3.133}$$

$$\overline{u_z} = \overline{u_y} = \overline{\dot{\theta}_x} = 0 \tag{3.134}$$

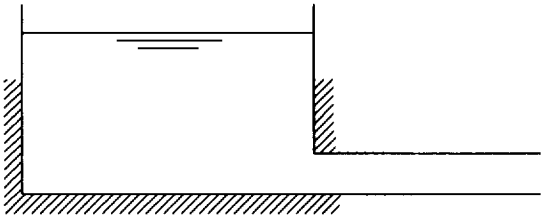

Figure 3.7. Definition sketch of reservoir.

3.3.2. *Valve*

The valve is an internal source of transients. The boundary conditions describing the instantaneous closure of a valve rigidly fixed to the ground are

$$V = 0 \tag{3.135}$$

$$\overline{u_z} = \overline{u_y} = \overline{\dot{\theta}_x} = 0 \tag{3.136}$$

so that at time $t = 0$ the initial liquid velocity $V(0,0)$ drops instantly to zero. Joukowsky's formula (2.1) gives the associated upstream pressure rise or downstream pressure drop.

If the valve can move in the axial direction, the boundary conditions become (figure 3.8)

$$V = \overline{u_z} \tag{3.137}$$

$$A_f \Delta P = A_t \Delta \overline{\sigma_z} \pm m \overline{\ddot{u}_z} \pm c \overline{\dot{u}_z} \pm k \overline{u_z} \tag{3.138}$$

$$\overline{u_y} = \overline{\theta_x} = 0 \tag{3.139}$$

where ΔP and $\Delta \overline{\sigma_z}$ are the pressure and axial-stress differences over the valve. The valve, of mass m, undergoes an acceleration $\overline{\ddot{u}_z}$. The damping coefficient c and the axial spring-stiffness k model the amount of axial restraint. Equation (3.137) is a mass balance defining the adherence of solid and liquid at the closed valve; equation (3.138) is a spring-mass-dashpot equation with fluid pressure and pipe stress as driving forces. Convective terms are neglected. Depending on the orientation of the pipe axis, the + or - signs in the right-hand side of (3.138) are valid. The initial liquid velocity $V(0,0)$ does not necessarily drop to zero now, but generally to a positive value, so that the initial change in pressure is less than predicted by the classical value of Joukowsky (2.1).

For non-instantaneous valve closures an orifice equation for steady flow replaces the equations (3.135) and (3.137),

$$\frac{V - \overline{u_z}}{(V - \overline{u_z})_0} = \pm \tau(t) \sqrt{\frac{|\Delta P|}{|\Delta P_0|}} \tag{3.140}$$

in which $(V - \overline{u_z})_0$ is the steady-state relative velocity through the valve, ΔP_0 is the steady-state pressure loss over the valve and $\tau(t)$ is a given function of time. The + or - sign depends on pipe orientation and flow direction. For points of time greater than the valve closure time T_c, $\tau(t) = 0$.

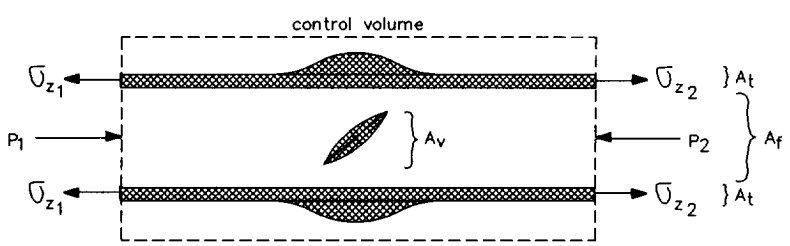

Figure 3.8. Definition sketch of valve; $\Delta P = P_1 - P_2$; $\Delta \sigma_z = (\sigma_z)_1 - (\sigma_z)_2$.

Many investigators, like Blade et al. [1962], D'Souza & Oldenburger [1964], Wilkinson [1978], Wiggert & Hatfield [1983] and Lavooij & Tijsseling [1988], let, in the force balance (3.138), the liquid pressure act on the cross-sectional *valve* area A_v, which varies in time between zero and A_f. However, a correct application of the force balance to a control volume over the valve (figure 3.8) leads to equation (3.138), which is consequently valid for a non-instantaneously closing valve as well.

3.3.3. *Closed end*

The boundary conditions for a closed end are essentially the same as those for a closed valve. These are (3.135)-(3.136) for an immovable end, and (3.137)-(3.139) for an axially unrestrained end, where in (3.138) the pressure and axial-stress differences are $\Delta P = P - P_{out}$ and $\Delta\sigma_z = \sigma_z + P_{out}$. For an entirely free end of mass m, subjected to a constant external pressure P_{out}, the boundary conditions are (figure 3.9)

$$V = \overline{u_z} \tag{3.141}$$

$$A_f(P - P_{out}) = A_t(\overline{\sigma_z} + P_{out}) \pm m\,\overline{\ddot{u}_z} \tag{3.142}$$

$$Q_y = M_x = 0 \tag{3.143}$$

The dimensions and the lateral and rotational inertia of the end piece are neglected.

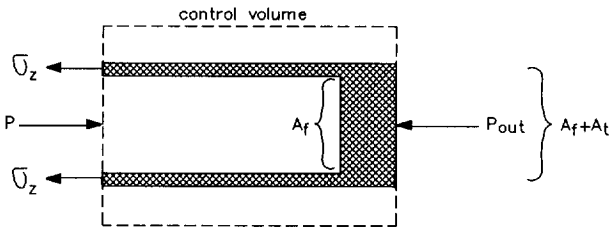

Figure 3.9. Definition sketch of closed end.

3.3.4. *Axial impact*

The axial impact of a freely movable closed end by a solid steel rod, as already sketched in figure 1.1, is an external source of transients, which is of less importance for practice, but was used in the experiments to be described in section 5.2. The impact is assumed to be

purely axial, so that lateral motion is not generated. The boundary conditions during the period that rod and pipe are in contact ($V_r = \overline{u_z}$), are (figure 3.10)

$$V = \overline{u_z} \tag{3.144}$$

$$A_f(P - P_{out}) + Y_r(\overline{u_z} - V_{0r}) = A_t(\overline{\sigma_z} + P_{out}) \pm m\overline{u_z} \tag{3.145}$$

$$Q_y = M_x = 0 \tag{3.146}$$

where V_{0r} is the velocity of the rod just before impact and m is the mass of the end piece. The *admittance* Y_r of the rod is

$$Y_r = A_r\sqrt{E_r\rho_r} \tag{3.147}$$

where the subscript r denotes the properties of the rod. The term $Y_r(\overline{u_z} - V_{0r})$ in (3.145), which is equal to $A_r(\sigma_z)_r$, is obtained from the axial-stress equivalent of Joukowsky's formula (2.1),

$$\Delta\overline{\sigma_z} = -\rho_t c_t \Delta\overline{u_z} \tag{3.148}$$

applied to the rod. Rod and pipe separate when the contact force becomes tensile. After separation the boundary conditions of a closed end, (3.141)-(3.143), remain.

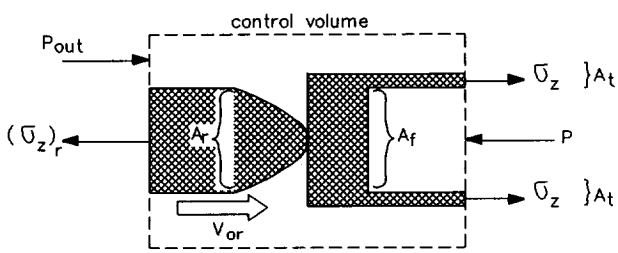

Figure 3.10. Definition sketch of axial impact.

3.3.5. *Straight junction*

The junction of two pipes in a direct line is described by eight coupling relations, since each of the connected pipes needs four boundary conditions. The eight relations, following from a consideration of continuity and equilibrium of forces, are (figure 3.11)

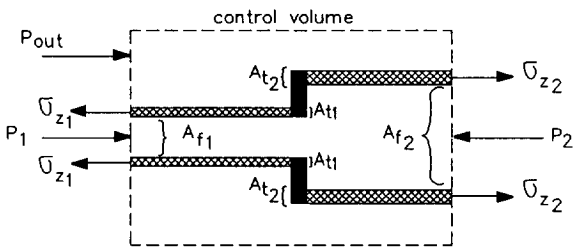

Figure 3.11. Definition sketch of straight junction.

$$\{ A_f(V-\overline{u_z}) \}_1 = \{ A_f(V-\overline{u_z}) \}_2 \tag{3.149}$$

$$\{ P \}_1 = \{ P \}_2 \tag{3.150}$$

$$\{ \overline{u_z} \}_1 = \{ \overline{u_z} \}_2 \tag{3.151}$$

$$\{ A_f(P-P_{out}) - A_t(\overline{\sigma_z}+P_{out}) \}_1 = \{ A_f(P-P_{out}) - A_t(\overline{\sigma_z}+P_{out}) \}_2 \tag{3.152}$$

$$\{ \overline{u_y} \}_1 = \{ \overline{u_y} \}_2 \tag{3.153}$$

$$\{ Q_y \}_1 = \{ Q_y \}_2 \tag{3.154}$$

$$\{ \overline{\theta_x} \}_1 = \{ \overline{\theta_x} \}_2 \tag{3.155}$$

$$\{ M_x \}_1 = \{ M_x \}_2 \tag{3.156}$$

where the indices 1 and 2 refer to either side of the pipe junction. The mass and dimensions of the junction are neglected, just as the forces due to change in liquid momentum, which is consistent with the acoustic approximation. The above relations allow for a discontinuity in the liquid velocity and in the axial pipe stress.

3.3.6. *Elbow junction*

The junction of two pipes perpendicular to each other is described by the next eight relations,

$$\{ A_f(V - \overline{u_z}) \}_1 = \{ A_f(V - \overline{u_z}) \}_2 \tag{3.157}$$

$$\{ P \}_1 = \{ P \}_2 \tag{3.158}$$

$$\{ \overline{u_z} \}_1 = \{ \overline{u_y} \}_2 \tag{3.159}$$

$$\{ A_f(P - P_{out}) - A_t(\overline{\sigma_z} + P_{out}) \}_1 = \{ Q_y \}_2 \tag{3.160}$$

$$\{ \overline{u_y} \}_1 = \{ -\overline{u_z} \}_2 \tag{3.161}$$

$$\{ -Q_y \}_1 = \{ A_f(P - P_{out}) - A_t(\overline{\sigma_z} + P_{out}) \}_2 \tag{3.162}$$

$$\{ \overline{\dot{\theta}_x} \}_1 = \{ \overline{\dot{\theta}_x} \}_2 \tag{3.163}$$

$$\{ M_x \}_1 = \{ M_x \}_2 \tag{3.164}$$

where the indices 1 and 2 refer to either side of the junction (figure 3.12). The mass and dimensions of the elbow junction are neglected, just as the forces due to change in liquid momentum, which is consistent with the acoustic approximation. This most simple model is valid if the length of the elbow is small compared to the lengths of the adjacent pipes. The angle between the pipes remains 90 degrees; elbow ovalization and the associated flexibility increase and stress intensification [Bantlin 1910; Von Kármán 1911; Hovgaard 1926] is ignored. However, these matters can be accounted for by flexibility and stress intensification factors [Vigness 1943; Clark & Reissner 1951; Dodge & Moore 1972]. Bathe & Almeida [1980, 1982ab] developed an accurate finite-element model of an elbow, which also includes the increased stiffness due to the internal pressure.

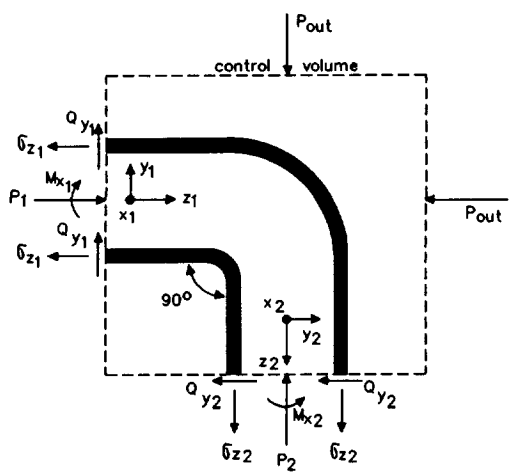

Figure 3.12. Definition sketch of elbow junction.

3.3.7. *Column separation*

The column separations, which are most important for the present study, generally occur at boundaries like valves, elbows, pumps and T-joints. The simple but adequate model of Bergeron [1950, pp. 89-95] and Streeter & Wylie [1967, p. 209] is used to simulate this phenomenon.

Closed end

Consider the closed end of a liquid-filled pipe which is allowed to move in the axial direction (figure 3.13). When the transient velocities of the closed end and the liquid next to it diverge, the local pressure decreases. At the instant that this pressure reaches the vapour pressure P_v, the velocities may still diverge and a vapour cavity is being formed, the growth of which follows the continuity equation

$$\frac{\partial \mathcal{V}}{\partial t} = \pm A_f (V - \overline{u_z}) \tag{3.165}$$

where $\mathcal{V}$ is the volume of the cavity, and V and $\overline{u_z}$ are the liquid and pipe velocities at the closed end. The + and - signs, again, depend on the orientation of the pipe axis. The influence of the radial motion of the pipe wall on the cavity volume is neglected. When, later on, V and $\overline{u_z}$ converge, the cavity becomes smaller until it finally collapses. This rejoining of liquid column and pipe end is usually accompanied with an instantaneous pressure rise. In the absence of gas, the absolute pressure equals the vapour pressure as long as the cavity exists,

$$P = P_v \tag{3.166}$$

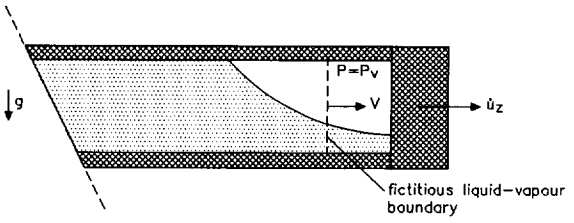

Figure 3.13. Definition sketch of column separation at closed end.

The boundary conditions in case of column separation at a closed end are (3.166), (3.145) and (3.146). So, equation (3.166) replaces equation (3.144) as long as the cavity exists. The duration of the column separation is inferred from the cavity volume governed by equation (3.165).

Elbow junction

When a column separation occurs at an elbow, the cavity volume follows from

$$\frac{\partial \mathcal{V}}{\partial t} = \mp \{ A_f(V - \overline{u_z}) \}_1 \pm \{ A_f(V - \overline{u_z}) \}_2 \qquad (3.167)$$

where the indices 1 and 2 refer to either side of the elbow (figure 3.14). The mass balance (3.157) in the elbow boundary conditions (3.157)-(3.164) is not valid during column separation; it is then replaced by the constant-pressure condition (3.166).

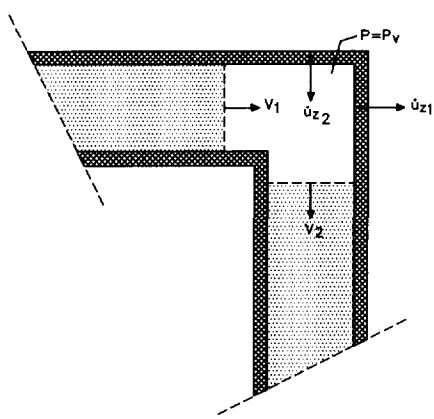

Figure 3.14. Definition sketch of column separation model at elbow.

Note

The liquid column may also break at any point along the pipe whenever two low pressure waves meet, leading to an intermediate boundary condition.

3.4. Review and conclusions

A thorough derivation of all (axial, radial, lateral and torsional) equations governing the transient motion of liquid-filled pipes is presented. One-dimensional basic equations were obtained after the cross-sectional integration of general three-dimensional equations for fluid dynamics and structural linear elasticity. Fluid-structure interaction has been taken into account. One-dimensional two-phase flow equations are given for regions of distributed cavitation. The steady-state situations in single pipes are used as initial conditions. Junction coupling and column separations are modelled as boundary conditions.

New elements in this chapter are: the four-equation model for *thick-walled* pipes (equations (3.59)-(3.62)), the liquid-pipe coupling through *radial* pipe stresses (equation (3.44)) and axial shear stresses (equation (3.43)), the *derivation* of the liquid-equation of radial motion (3.14), the omission of the rotatory inertia of the liquid in (3.90) of the basic equations for lateral motion, and, column separations ruled by both liquid and pipe variables (equations (3.165) and (3.167)).

4. NUMERICAL METHOD

The numerical solution of the initial boundary value problems posed in chapter 3 is described. The axial, lateral and torsional equations given in section 3.1 are dealt with in the same manner. The method of characteristics (MOC) is applied to obtain ordinary differential equations, which can be easily integrated. The initial and boundary conditions are treated in a straightforward way. Cavitation is simulated by the concentrated cavity model. The developed computer codes are shortly described. In illustration, significant results of numerical tests are presented in the last section of this chapter.

4.1. Introduction

The governing equations for fluid-structure interaction (FSI) problems can be solved in many different ways. Belytschko [1980] surveys the available computational methods for *general* FSI-problems. For FSI in liquid-filled pipe systems the literature review in the subsections 2.3.5 and 2.3.6 gives an indication of possible solution techniques. In this report the approach of Wiggert et al. [1987a] is adopted: the basic equations are solved by the MOC.

The term *method of characteristics* is attributed to Monge [1789]. In principle, it is not a numerical but an analytical solution method. However, some of the necessary integrations are generally done numerically.

The MOC-approach is chosen because it is based on the propagation of acoustic waves, which is the principal mechanism in the considered set of transient events. When the acoustic approximation is made, see subsection 3.1.1, the wave propagation speeds are constant. Then, the computational grids, which are based on wave paths in the distance-time plane, have constant mesh spacings. This is of great advantage; for some problems exact solutions may be found.

The axial, lateral and torsional equations in section 3.1 are deliberately formulated as first-order partial differential equations, which is the appropriate form for the present MOC-approach.

Although not necessary, the customary assumption has been made that the pipes are thin-walled. Wylie & Streeter [1978a, p. 23] state the requirement that the ratio of pipe diameter

to wall thickness, D/e, is greater than 25 in that case.

4.2. Axial motion

The four-equation model (3.59)-(3.62) applied to thin-walled pipes is solved numerically.

4.2.1. *Basic equations*

The coupled propagation of pressure waves in the liquid and axial stress waves in the pipe wall is described by the four equations (3.59)-(3.62). These equations are valid for thick-walled pipes; pipe stresses and pipe velocities are averaged over the cross-sectional wall area. Now the assumption is made that the pipes are thin-walled: $e \ll R$. The radial stresses are then small compared to the hoop and axial stresses (state of plane stress). This may be clear from the equations (3.56) and (A.13):

$$\overline{\sigma_\phi} = \frac{R}{e} P \tag{4.1}$$

$$\overline{\sigma_r} = -\frac{3}{4} P \tag{4.2}$$

where $\overline{\sigma_\phi}$, $\overline{\sigma_r}$ and P are relative to the external pressure P_{out}; $\overline{\sigma_\phi} = (\overline{\sigma_\phi})_{abs} + P_{out}$, $\overline{\sigma_r} = (\overline{\sigma_r})_{abs} + P_{out}$ and $P = P_{abs} - P_{out}$ (abs = absolute). In the following all pressures and stresses are relative to the outer pressure P_{out}. Furthermore, overlines, indicating averaged values of the pipe variables, are omitted, since the variations with r are negligible in thin walls. With the shear stress τ_0 according to equation (3.63), and $e/R \ll 1$, the equations (3.59)-(3.62) become

Liquid

$$\frac{\partial V}{\partial t} + \frac{1}{\rho_f}\frac{\partial P}{\partial z} = -f\frac{V_{rel}|V_{rel}|}{4R} + g\sin\gamma \tag{4.3}$$

$$\frac{\partial V}{\partial z} + \left(\frac{1}{K} + \frac{2R}{Ee}\right)\frac{\partial P}{\partial t} - \frac{2\nu}{E}\frac{\partial \sigma_z}{\partial t} = 0 \tag{4.4}$$

Pipe

$$\frac{\partial \dot{u}_z}{\partial t} - \frac{1}{\rho_t}\frac{\partial \sigma_z}{\partial z} = f\frac{\rho_f}{\rho_t}\frac{V_{rel}\,|V_{rel}|}{8e} + g\sin\gamma \tag{4.5}$$

$$\frac{\partial \dot{u}_z}{\partial z} - \frac{1}{E}\frac{\partial \sigma_z}{\partial t} + \frac{\nu R}{Ee}\frac{\partial P}{\partial t} = 0 \tag{4.6}$$

These are the basic equations for thin-walled pipes. Schwarz [1978] gives a clear derivation of the equations (4.3)-(4.6) in a way different from that in subsection 3.1.2. His approach links up with the classical waterhammer theory.

The stress-displacement relations for thin-walled pipes follow from the equations (3.31), (3.32), (3.34) and (3.35) with σ_r neglected and $r \equiv R$,

$$\sigma_z = \frac{E}{1-\nu^2}\left(\frac{\partial u_z}{\partial z} + \nu\frac{u_r}{R}\right) \tag{4.7}$$

$$\sigma_\phi = \frac{E}{1-\nu^2}\left(\frac{u_r}{R} + \nu\frac{\partial u_z}{\partial z}\right) \tag{4.8}$$

With σ_ϕ from (4.1) and, again, σ_r neglected and $r \equiv R$, the radial displacement given by equation (3.52) is

$$u_r = \frac{R^2}{Ee}P - \frac{\nu R}{E}\sigma_z \tag{4.9}$$

The basic equations (4.3)-(4.6) can be written in many different forms. The specific form used in the present work, and in earlier publications, is given now. The σ_z-term in equation (4.4) is replaced by a $\dot{u}_z$-term with aid of equation (4.6); the pressure P is replaced by the pressure head H defined by

$$H = \frac{P}{\rho_f g} - z\sin\gamma + h_0 \tag{4.10}$$

where h_0 is an arbitrary datum. With the ratio of discharge-area to wall-area, A_f/A_t, approximated by $R/(2e)$, the equations (4.3)-(4.6) become

Liquid

$$\frac{\partial V}{\partial t} + g\frac{\partial H}{\partial z} = -f\frac{V_{rel}|V_{rel}|}{4R} \tag{4.11}$$

$$\frac{\partial V}{\partial z} + \frac{g}{c_F^2}\frac{\partial H}{\partial t} = 2\nu\frac{\partial \dot{u}_z}{\partial z} \tag{4.12}$$

Pipe

$$\frac{\partial \dot{u}_z}{\partial t} - \frac{1}{\rho_t}\frac{\partial \sigma_z}{\partial z} = f\frac{\rho_f A_f}{\rho_t A_t}\frac{V_{rel}|V_{rel}|}{4R} + g\sin\gamma \tag{4.13}$$

$$\frac{\partial \dot{u}_z}{\partial z} - \frac{1}{\rho_t c_t^2}\frac{\partial \sigma_z}{\partial t} = -\rho_f g\frac{\nu R}{Ee}\frac{\partial H}{\partial t} \tag{4.14}$$

in which

$$c_F^2 = \left\{\rho_f\left[\frac{1}{K} + (1-\nu^2)\frac{2R}{Ee}\right]\right\}^{-1} \tag{4.15}$$

and

$$c_t^2 = \frac{E}{\rho_t} \tag{4.16}$$

correspond to the classical wave propagation speeds (2.5) and (2.10). See also subsections 2.3.1 and 2.3.3. The definitions (4.15) and (4.16) are rather arbitrary; they depend on the specific form in which the basic equations are written.

4.2.2. *MOC-transformation*[1]

The basic set of equations (4.11)-(4.14) looks particularly simple in matrix notation

$$\mathbf{A}\frac{\partial \mathbf{y}}{\partial t} + \mathbf{B}\frac{\partial \mathbf{y}}{\partial z} = \mathbf{r} \tag{4.17}$$

---

[1] This subsection is based on the theory given by Forsythe and Wasow [1964]

in which **y** is the vector of unknowns, **A** and **B** are the matrices of coefficients, and **r** is the right-hand-side vector:

$$\mathbf{y} = \begin{bmatrix} V \\ H \\ \dot{u}_z \\ \sigma_z \end{bmatrix} \tag{4.18}$$

$$\mathbf{A} = \begin{bmatrix} 1 & 0 & 0 & 0 \\ 0 & g/c_F^2 & 0 & 0 \\ 0 & 0 & 1 & 0 \\ 0 & \rho_f g \frac{\nu}{E}\frac{R}{e} & 0 & \frac{-1}{\rho_t c_t^2} \end{bmatrix} \tag{4.19}$$

$$\mathbf{B} = \begin{bmatrix} 0 & g & 0 & 0 \\ 1 & 0 & -2\nu & 0 \\ 0 & 0 & 0 & -1/\rho_t \\ 0 & 0 & 1 & 0 \end{bmatrix} \tag{4.20}$$

$$\mathbf{r} = \begin{bmatrix} -f\frac{V_{rel}\,|V_{rel}|}{4R} \\ 0 \\ f\frac{\rho_f A_f}{\rho_t A_t}\frac{V_{rel}\,|V_{rel}|}{4R} + g\sin\gamma \\ 0 \end{bmatrix} \tag{4.21}$$

The matrices **A** and **B** are regular. For $\mathbf{r} = \mathbf{0}$ the system (4.17) is linear with constant coefficients, whereas for $\mathbf{r} \neq \mathbf{0}$ the friction terms in (4.21) make the system non-linear. In appendix B it is shown that the *characteristic equation* $|\,\mathbf{B} - \lambda\,\mathbf{A}\,| = 0$ has four distinct

real roots, which is equivalent to the statement that the matrix $\mathbf{A}^{-1}\mathbf{B}$ has four distinct real eigenvalues. The four *characteristic roots* or *eigenvalues* λ_i are

$$\lambda_1 = +\tilde{c}_F\,, \quad \lambda_2 = -\tilde{c}_F\,, \quad \lambda_3 = +\tilde{c}_t\,, \quad \lambda_4 = -\tilde{c}_t \tag{4.22}$$

with $\tilde{c}_F \approx c_F$ and $\tilde{c}_t \approx c_t$ (see next subsection) and $\tilde{c}_F \neq \tilde{c}_t$. Because the values of λ_i are distinct and real, the system (4.17) is called *hyperbolic*. In that case it can be transformed into a more convenient form through multiplication by a regular matrix $\mathbf{T}$

$$\mathbf{TA}\frac{\partial \mathbf{y}}{\partial t} + \mathbf{TB}\frac{\partial \mathbf{y}}{\partial z} = \mathbf{Tr} \tag{4.23}$$

From the theory of linear algebra it is known that for every square matrix with distinct real eigenvalues, here $\mathbf{A}^{-1}\mathbf{B}$, there exists a matrix $\mathbf{S}$ such that

$$\mathbf{S}^{-1}\mathbf{A}^{-1}\mathbf{B}\,\mathbf{S} = \mathbf{\Lambda} \tag{4.24}$$

where $\mathbf{\Lambda}$ is diagonal:

$$\mathbf{\Lambda} = \begin{bmatrix} \lambda_1 & 0 & 0 & 0 \\ 0 & \lambda_2 & 0 & 0 \\ 0 & 0 & \lambda_3 & 0 \\ 0 & 0 & 0 & \lambda_4 \end{bmatrix} \tag{4.25}$$

The matrix $\mathbf{T}$ is now chosen as follows:

$$\mathbf{T} = \mathbf{S}^{-1}\mathbf{A}^{-1} \tag{4.26}$$

Substitution of (4.26) into (4.24) leads to the next condition for $\mathbf{T}$:

$$\mathbf{TB} = \mathbf{\Lambda TA} \tag{4.27}$$

The transformation matrix $\mathbf{T}$, which satisfies condition (4.27) for the specific matrices $\mathbf{A}$ and $\mathbf{B}$ given by (4.19) and (4.20), is determined in appendix C. With condition (4.27), equation (4.23) becomes

$$\mathbf{TA}\frac{\partial \mathbf{y}}{\partial t} + \mathbf{\Lambda TA}\frac{\partial \mathbf{y}}{\partial z} = \mathbf{Tr} \tag{4.28}$$

System (4.28) is called the *normal form* of system (4.17). Introducing the vector

$$\mathbf{v} = \mathbf{T}\mathbf{A}\,\mathbf{y} \tag{4.29}$$

(4.28) becomes

$$\frac{\partial \mathbf{v}}{\partial t} + \mathbf{\Lambda}\frac{\partial \mathbf{v}}{\partial z} = \mathbf{T}\mathbf{r} \tag{4.30}$$

since **TA** is independent of z and t. Obviously the basic system (4.17) is equivalent to a set of four uncoupled equations

$$\frac{\partial v_i}{\partial t} + \lambda_i \frac{\partial v_i}{\partial z} = (\mathbf{T}\mathbf{r})_i \quad , \quad i = 1,2,3,4 \tag{4.31}$$

Each of the equations (4.31) transforms into an ordinary differential equation

$$\frac{\mathrm{d}v_i}{\mathrm{d}t} = (\mathbf{T}\mathbf{r})_i \quad , \quad i = 1,2,3,4 \tag{4.32}$$

when it is considered along a line in the z-t plane having the *characteristic direction*

$$\frac{\mathrm{d}z}{\mathrm{d}t} = \lambda_i \quad , \quad i = 1,2,3,4 \tag{4.33}$$

The equations (4.32) are known as the *compatibility equations* along the *characteristic lines* with slopes λ_i^{-1} in the z-t plane.

For the simplified case in which $\mathbf{r} = \mathbf{0}$, the equations (4.32) and (4.33) state that v_i is constant along a characteristic line:

$$(v_i)_P = (v_i)_{A_i} \quad , \quad i = 1,2,3,4 \tag{4.34}$$

where P and A_i are points in the z-t plane such as shown in figure 4.1. According to definition (4.29) v_i is a linear combination of the four unknowns y_j (j = 1, 2, 3, 4). The relations (4.34) provide four equations for the four unknowns y_j, once $(v_i)_{A_i}$ is given for i = 1, 2, 3, 4. Using (4.29) and (4.34), the unknown vector $\mathbf{y}_P$ can be expressed in vectors $\mathbf{y}_{A_i}$ at previous times as follows

$$\mathbf{y}_P = \sum_{i=1}^{4} (\mathbf{T}\mathbf{A})^{-1}\,\mathbf{R}_i\,(\mathbf{T}\mathbf{A})\,\mathbf{y}_{A_i} \tag{4.35}$$

in which $(\mathbf{R}_i)_{kl} = 1$ if $k = l = i$ and $(\mathbf{R}_i)_{kl} = 0$ otherwise. In the matrix $\mathbf{R}_i$ the i^{th} element on the diagonal is 1, all other elements are 0.

Calculating forward in time, expression (4.35) gives the exact solution of the homogeneous (i.e. for $\mathbf{r} = \mathbf{0}$) system (4.17).

4.2.3. *Wave propagation speeds*

The four eigenvalues (4.22) of system (4.17) represent the propagation speeds of axial waves in a liquid-filled pipe. Their magnitudes are obtained from a bi-quadratic equation in appendix B. Gromeka [1883], Lamb [1898] and Lin & Morgan [1956b] find similar bi-quadratic equations as a result of wave-train analyses. In fact, the bi-quadratic equation (B.1) combined with (B.3) is a long-wavelength dispersion equation. It states that the two lowest propagation modes travel without dispersion. See also the subsections 2.3.1 and 2.3.2.

In addition to subsection 2.3.3, it is remarked that, within the present extended waterhammer theory, $\tilde{c}_F$ is the correct and unique pressure wave speed for the support conditions 1) and 3), whereas c_F remains valid for support condition 2). The wave speed $\tilde{c}_t$ corresponds to axial stress wave propagation in beams. In water-filled steel pipes, the values of $\tilde{c}_F$ and $\tilde{c}_t$ differ just slightly from those of c_F and c_t, respectively. The influence of the temperature on the wave propagation speeds may be more significant, just as the presence of free gas in the liquid.

The differences between, on the one hand, $\tilde{c}_F$ and $\tilde{c}_t$, which are theoretically correct for the basic equations (4.11)-(4.14), and, on the other hand, the classical values c_F and c_t, are caused by Poisson coupling. Junction coupling may have an even stronger effect on the wave speeds. Fluid-structure interaction in general, and junction coupling in particular, leads to a change of the eigenfrequencies of a system [Hatfield et al. 1982a; Kuiken 1988]. A shift in the main waterhammer frequency corresponds to a change in the virtual pressure wave speed. Kruisbrink and Heinsbroek [1992ab] show, both by measurement and simulation, that this change can be quite substantial.

4.2.4. *Compatibility equations*

The four compatibility equations (4.32) belonging to system (4.17), with $\mathbf{v}$, $\mathbf{T}$, $\mathbf{A}$ and $\mathbf{r}$ according to (4.29), (C.14), (4.19) and (4.21), respectively, can be written as

Liquid

$$\left[\frac{dV}{dt}\right]_1 + \frac{g}{c_F}\left\{\left[\frac{\tilde{c}_F}{c_F}\right] + 2\nu^2 \frac{R}{e}\frac{\rho_f}{\rho_t}\frac{(c_F\tilde{c}_F)/c_t^2}{1-(\tilde{c}_F/c_t)^2}\right\}\left[\frac{dH}{dt}\right]_1 +$$

$$+ 2\nu\frac{(\tilde{c}_F/c_t)^2}{1-(\tilde{c}_F/c_t)^2}\left[\frac{d\dot{u}_z}{dt}\right]_1 - \frac{2\nu}{\rho_t\tilde{c}_F}\frac{(\tilde{c}_F/c_t)^2}{1-(\tilde{c}_F/c_t)^2}\left[\frac{d\sigma_z}{dt}\right]_1 = \tag{4.36}$$

$$= -\frac{f}{4R}V_{rel}|V_{rel}| + 2\nu\frac{(\tilde{c}_F/c_t)^2}{1-(\tilde{c}_F/c_t)^2}\left[\frac{\rho_f A_f}{\rho_t A_t}\frac{f}{4R}V_{rel}|V_{rel}| + g\sin\gamma\right]$$

$$\left[\frac{dV}{dt}\right]_2 - \frac{g}{c_F}\left\{\left[\frac{\tilde{c}_F}{c_F}\right] + 2\nu^2 \frac{R}{e}\frac{\rho_f}{\rho_t}\frac{(c_F\tilde{c}_F)/c_t^2}{1-(\tilde{c}_F/c_t)^2}\right\}\left[\frac{dH}{dt}\right]_2 +$$

$$+ 2\nu\frac{(\tilde{c}_F/c_t)^2}{1-(\tilde{c}_F/c_t)^2}\left[\frac{d\dot{u}_z}{dt}\right]_2 + \frac{2\nu}{\rho_t\tilde{c}_F}\frac{(\tilde{c}_F/c_t)^2}{1-(\tilde{c}_F/c_t)^2}\left[\frac{d\sigma_z}{dt}\right]_2 = \tag{4.37}$$

$$= -\frac{f}{4R}V_{rel}|V_{rel}| + 2\nu\frac{(\tilde{c}_F/c_t)^2}{1-(\tilde{c}_F/c_t)^2}\left[\frac{\rho_f A_f}{\rho_t A_t}\frac{f}{4R}V_{rel}|V_{rel}| + g\sin\gamma\right]$$

Pipe

$$
\begin{aligned}
&-\nu\frac{R}{e}\frac{\rho_f}{\rho_t}\frac{(c_F/c_t)^2}{1-(c_F/\tilde{c}_t)^2}\left[\frac{dV}{dt}\right]_3-\nu\frac{R}{e}\frac{\rho_f}{\rho_t}\frac{g}{c_t}\left(\frac{\tilde{c}_t}{c_t}\right)\frac{(c_F/\tilde{c}_t)^2}{1-(c_F/\tilde{c}_t)^2}\left[\frac{dH}{dt}\right]_3+\\
&+\left[1+2\nu^2\frac{R}{e}\frac{\rho_f}{\rho_t}\frac{(c_F/c_t)^2}{1-(c_F/\tilde{c}_t)^2}\right]\left[\frac{d\dot{u}_z}{dt}\right]_3-\frac{1}{\rho_t c_t}\left(\frac{\tilde{c}_t}{c_t}\right)\left[\frac{d\sigma_z}{dt}\right]_3=\\
&=\left[1+2\nu^2\frac{R}{e}\frac{\rho_f}{\rho_t}\frac{(c_F/c_t)^2}{1-(c_F/\tilde{c}_t)^2}\right]\left[\frac{\rho_f A_f}{\rho_t A_t}\frac{f}{4R}V_{rel}|V_{rel}|+g\sin\gamma\right]+\\
&+\nu\frac{R}{e}\frac{\rho_f}{\rho_t}\frac{(c_F/c_t)^2}{1-(c_F/\tilde{c}_t)^2}\frac{f}{4R}V_{rel}|V_{rel}|
\end{aligned}
\tag{4.38}
$$

$$
\begin{aligned}
&-\nu\frac{R}{e}\frac{\rho_f}{\rho_t}\frac{(c_F/c_t)^2}{1-(c_F/\tilde{c}_t)^2}\left[\frac{dV}{dt}\right]_4+\nu\frac{R}{e}\frac{\rho_f}{\rho_t}\frac{g}{c_t}\left(\frac{\tilde{c}_t}{c_t}\right)\frac{(c_F/\tilde{c}_t)^2}{1-(c_F/\tilde{c}_t)^2}\left[\frac{dH}{dt}\right]_4+\\
&+\left[1+2\nu^2\frac{R}{e}\frac{\rho_f}{\rho_t}\frac{(c_F/c_t)^2}{1-(c_F/\tilde{c}_t)^2}\right]\left[\frac{d\dot{u}_z}{dt}\right]_4+\frac{1}{\rho_t c_t}\left(\frac{\tilde{c}_t}{c_t}\right)\left[\frac{d\sigma_z}{dt}\right]_4=\\
&=\left[1+2\nu^2\frac{R}{e}\frac{\rho_f}{\rho_t}\frac{(c_F/c_t)^2}{1-(c_F/\tilde{c}_t)^2}\right]\left[\frac{\rho_f A_f}{\rho_t A_t}\frac{f}{4R}V_{rel}|V_{rel}|+g\sin\gamma\right]+\\
&+\nu\frac{R}{e}\frac{\rho_f}{\rho_t}\frac{(c_F/c_t)^2}{1-(c_F/\tilde{c}_t)^2}\frac{f}{4R}V_{rel}|V_{rel}|
\end{aligned}
\tag{4.39}
$$

where $\left[\frac{dy_j}{dt}\right]_i$ is the directional derivative of the variable y_j in the z-t plane, along the

characteristic line with slope $1/\lambda_i$. It is convenient to summarize the compatibility equations (4.36)-(4.37) and (4.38)-(4.39) by the following equations

$$\alpha_f \left[\frac{\mathrm{d}V}{\mathrm{d}t} \right]_{1,2} \pm \beta_f \left[\frac{\mathrm{d}H}{\mathrm{d}t} \right]_{1,2} + \nu\gamma_f \left[\frac{\mathrm{d}\dot{u}_z}{\mathrm{d}t} \right]_{1,2} \pm \nu\delta_f \left[\frac{\mathrm{d}\sigma_z}{\mathrm{d}t} \right]_{1,2} = q_f(\dot{u}_z, V) \tag{4.40}$$

$$\nu\alpha_t \left[\frac{\mathrm{d}V}{\mathrm{d}t} \right]_{3,4} \pm \nu\beta_t \left[\frac{\mathrm{d}H}{\mathrm{d}t} \right]_{3,4} + \gamma_t \left[\frac{\mathrm{d}\dot{u}_z}{\mathrm{d}t} \right]_{3,4} \pm \delta_t \left[\frac{\mathrm{d}\sigma_z}{\mathrm{d}t} \right]_{3,4} = q_t(\dot{u}_z, V) \tag{4.41}$$

respectively, in which the coefficients α_f, β_f, γ_f, δ_f and α_t, β_t, γ_t, δ_t represent the corresponding coefficients in the equations (4.36)-(4.37) and (4.38)-(4.39), respectively. The functions q_f and q_t represent the right-hand sides in (4.36)-(4.37) and (4.38)-(4.39), respectively. Integration of (4.40)-(4.41) along the relevant characteristic lines yields

$$\alpha_f\{V_P - V_{A_1}\} + \beta_f\{H_P - H_{A_1}\} + \nu\gamma_f\{(\dot{u}_z)_P - (\dot{u}_z)_{A_1}\} + \nu\delta_f\{(\sigma_z)_P - (\sigma_z)_{A_1}\} = \int_{A_1}^{P} q_f \,\mathrm{d}t \tag{4.42}$$

$$\alpha_f\{V_P - V_{A_2}\} - \beta_f\{H_P - H_{A_2}\} + \nu\gamma_f\{(\dot{u}_z)_P - (\dot{u}_z)_{A_2}\} - \nu\delta_f\{(\sigma_z)_P - (\sigma_z)_{A_2}\} = \int_{A_2}^{P} q_f \,\mathrm{d}t \tag{4.43}$$

$$\nu\alpha_t\{V_P - V_{A_3}\} + \nu\beta_t\{H_P - H_{A_3}\} + \gamma_t\{(\dot{u}_z)_P - (\dot{u}_z)_{A_3}\} + \delta_t\{(\sigma_z)_P - (\sigma_z)_{A_3}\} = \int_{A_3}^{P} q_t \,\mathrm{d}t \tag{4.44}$$

$$\nu\alpha_t\{V_P - V_{A_4}\} - \nu\beta_t\{H_P - H_{A_4}\} + \gamma_t\{(\dot{u}_z)_P - (\dot{u}_z)_{A_4}\} - \delta_t\{(\sigma_z)_P - (\sigma_z)_{A_4}\} = \int_{A_4}^{P} q_t \,\mathrm{d}t \tag{4.45}$$

where P and A_i are points in the *z-t* plane as shown in figure 4.1. From the *integrated compatibility equations* (4.42)-(4.45) it can be seen that, for point P not on a boundary, the unknowns V, H, $\dot{u}_z$ and σ_z in P are fully determined by their values in the "upstream" points A_i. Hence, if the boundaries are left out of consideration, the solution of system (4.17) in any point P can be obtained from the equations (4.42)-(4.45), once initial values for V, H, $\dot{u}_z$ and σ_z are known. The integrals in (4.42)-(4.45) are treated numerically in the next subsection. Boundaries are considered in section 4.7.

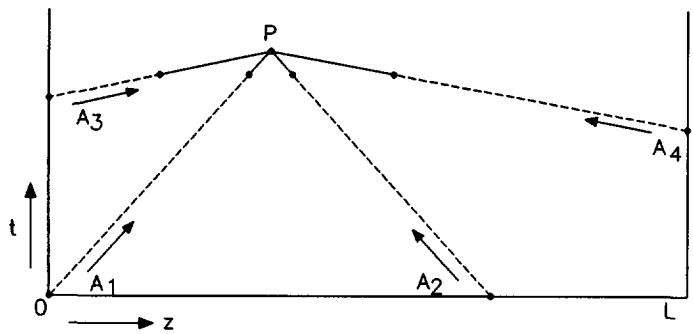

Figure 4.1. Characteristic lines through point P in the *z-t* plane.
Point A_i can be arbitrarily chosen along the characteristic line with slope $1/\lambda_i$.

Discontinuities

Discontinuities or *jumps* in the basic variables are disturbances which travel without dispersion along the characteristic lines. Steep wave fronts are generally considered as discontinuities. Pressure wave fronts in the liquid are accompanied with stress changes in the pipe wall, whereas stress wave fronts in the pipe wall are accompanied with pressure changes in the liquid (precursor waves). The relation between the discontinuities in pressure and axial stress at wave fronts is determined now.

Discontinuities across the characteristic line with slope $1/\tilde{c}_F$ in the *z-t* plane are examined first. In a point P on this line, designated as characteristic line 1 in figure 4.2, the other three characteristic lines intersect. Let the points A_i and B_i (i = 2, 3, 4) be situated on these three

characteristic lines on either side of characteristic line 1, as shown in figure 4.2. When the points A_i and B_i approach each other, from the integrated compatibility equations (4.43)-(4.45) it follows that, in the limit,

$$\alpha_f(\Delta V)_f - \beta_f(\Delta H)_f + \nu\gamma_f(\Delta \dot{u}_z)_f - \nu\delta_f(\Delta\sigma_z)_f = 0 \tag{4.46}$$

$$-\nu\alpha_t(\Delta V)_f - \nu\beta_t(\Delta H)_f - \gamma_t(\Delta \dot{u}_z)_f - \delta_t(\Delta\sigma_z)_f = 0 \tag{4.47}$$

$$\nu\alpha_t(\Delta V)_f - \nu\beta_t(\Delta H)_f + \gamma_t(\Delta \dot{u}_z)_f - \delta_t(\Delta\sigma_z)_f = 0 \tag{4.48}$$

in which Δ designates a discontinuity. These are three independent equations for four variable discontinuities. When one discontinuity is known, for example from a boundary condition, the other three are determined. Addition of (4.47) and (4.48) gives the desired relation between pressure and axial stress

$$-2\nu\beta_t(\Delta H)_f - 2\delta_t(\Delta\sigma_z)_f = 0 \tag{4.49}$$

so that

$$\frac{(\Delta\sigma_z)_f}{(\Delta H)_f} = -\frac{\nu\beta_t}{\delta_t} = -\nu\frac{R}{e}\rho_f g\{(\frac{\tilde{c}_t}{c_F})^2 - 1\}^{-1} \tag{4.50}$$

in which the subscript *f* indicates that a pressure wave is concerned. Equation (4.50), which is also valid for discontinuities across the characteristic line with slope $-1/\tilde{c}_F$ in the *z-t* plane, gives the ratio between a pressure jump travelling at velocity $\tilde{c}_F$ and its associated change in axial stress. Wilkinson and Curtis [1980, p. 232] find a slightly different expression.

Equation (4.46) gives, for $\nu = 0$ (no Poisson-coupling), the Joukowsky formula (2.1).

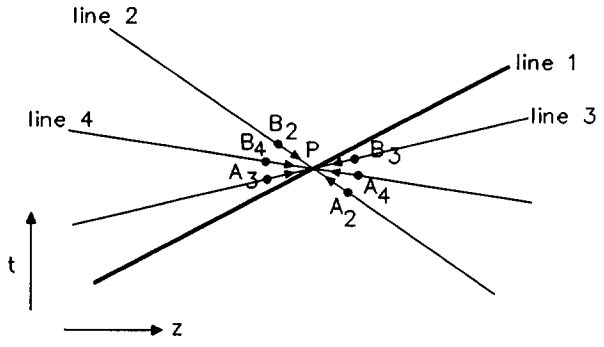

Figure 4.2. Characteristic lines in the *z-t* plane with assumed discontinuity across line 1.

For discontinuities across the characteristic line with slope $1/\bar{c}_t$ in the z-t plane, a similar approach leads via the integrated compatibility equations (4.42), (4.43) and (4.45) to

$$\alpha_f(\Delta V)_t + \beta_f(\Delta H)_t + \nu\gamma_f(\Delta \dot{u}_z)_t + \nu\delta_f(\Delta \sigma_z)_t = 0 \tag{4.51}$$

$$\alpha_f(\Delta V)_t - \beta_f(\Delta H)_t + \nu\gamma_f(\Delta \dot{u}_z)_t - \nu\delta_f(\Delta \sigma_z)_t = 0 \tag{4.52}$$

$$\nu\alpha_t(\Delta V)_t - \nu\beta_t(\Delta H)_t + \gamma_t(\Delta \dot{u}_z)_t - \delta_t(\Delta \sigma_z)_t = 0 \tag{4.53}$$

Subtracting (4.52) from (4.51) gives

$$2\beta_f(\Delta H)_t + 2\nu\delta_f(\Delta \sigma_z)_t = 0 \tag{4.54}$$

so that, with use of the relations (B.1) combined with (B.3) for $\lambda^2 = \bar{c}_F^{\,2}$ from appendix B,

$$\frac{(\Delta H)_t}{(\Delta \sigma_z)_t} = -\frac{\nu\delta_f}{\beta_f} = 2\nu\,\frac{1}{\rho_t g}\left\{\left(\frac{c_t}{\bar{c}_F}\right)^2 - 1\right\}^{-1} \tag{4.55}$$

in which the subscript t indicates that a stress wave is concerned. Equation (4.55), which is also valid for discontinuities across the characteristic line with slope $-1/\bar{c}_t$ in the z-t plane, gives the ratio between an axial stress jump travelling at velocity $\bar{c}_t$ and its associated change in pressure (precursor wave).

Equation (4.53) gives, for $\nu = 0$ (no Poisson-coupling), relation (3.148).

Simplified compatibility equations

By neglecting second-order Poisson-terms (ν^2-terms), friction terms ($f = 0$) and gravity terms ($\gamma = 0$), the following compatibility equations are obtained from (4.10) and (4.36)-(4.39),

Liquid

$$\frac{\mathrm{d}P}{\mathrm{d}t} \pm \rho_f c_f \frac{\mathrm{d}V}{\mathrm{d}t} + G_f\left\{\frac{\mathrm{d}\sigma_z}{\mathrm{d}t} \mp \rho_t c_f \frac{\mathrm{d}\dot{u}_z}{\mathrm{d}t}\right\} = 0 \tag{4.56}$$

Pipe

$$\frac{\mathrm{d}\sigma_z}{\mathrm{d}t} \mp \rho_t c_t \frac{\mathrm{d}\dot{u}_z}{\mathrm{d}t} + G_t\left\{\frac{\mathrm{d}P}{\mathrm{d}t} \pm \rho_f c_t \frac{\mathrm{d}V}{\mathrm{d}t}\right\} = 0 \tag{4.57}$$

where the Poisson coupling factors G_f and G_t are defined by

$$G_f = -2\nu \frac{\rho_f}{\rho_t} \{ (\frac{c_t}{c_f})^2 - 1 \}^{-1} \tag{4.58}$$

$$G_t = \nu \frac{R}{e} \{ (\frac{c_t}{c_f})^2 - 1 \}^{-1} \tag{4.59}$$

and

$$c_f = \left\{ \rho_f \left[\frac{1}{K} + \frac{2R}{Ee} \right] \right\}^{-\frac{1}{2}} \tag{4.60}$$

The equations (4.56)-(4.57) nicely exhibit the analogy between the liquid and pipe equations.

4.2.5. *Numerical integration*

The integrals in the final system of equations (4.42)-(4.45) have the following form

$$I = k_1 f \int_A^P V_{rel} \mid V_{rel} \mid \mathrm{d}t + k_2 g \int_A^P \sin\gamma \, \mathrm{d}t \tag{4.61}$$

where k_1 and k_2 are constants.

The second integral, which results from the gravity force, can be calculated exactly, since γ is assumed to be constant

$$\int_A^P \sin\gamma \, \mathrm{d}t = (t_P - t_A) \sin\gamma \tag{4.62}$$

The first integral, which results from the friction force, will be approximated by means of a rule of integration. Three obvious possibilities are

$$\int_A^P V_{rel} \mid V_{rel} \mid \mathrm{d}t = (V_{rel})_A \mid (V_{rel})_A \mid (t_P - t_A) \tag{4.63}$$

$$\int_A^P V_{rel} \mid V_{rel} \mid \mathrm{d}t = (V_{rel})_P \mid (V_{rel})_A \mid (t_P - t_A) \tag{4.64}$$

$$\int_{A}^{P} V_{rel} \, | V_{rel} | \, dt = \frac{1}{2} \left\{ (V_{rel})_A \, | (V_{rel})_A | + (V_{rel})_P \, | (V_{rel})_P | \right\} (t_P - t_A) \qquad (4.65)$$

The first two approximations are preferred, because they lead to a linear system of equations. Of them, the second one is the most accurate [Wylie 1983], but it leads to a time-dependent matrix of coefficients. The third approximation maintains the non-linearity and consequently gives rise to a more laborious solution procedure. In the present study the first, and most simple, approximation is used. Another integral has to be calculated to obtain the value of the axial displacement u_z

$$u_z = \int_{Q}^{P} \dot{u}_z \, dt \qquad (4.66)$$

in which $P = (z_P, t_P)$ and $Q = (z_P, t_Q)$. This integral is approximated by the trapezoidal rule

$$(u_z)_P = (u_z)_Q + \frac{1}{2} \left\{ (\dot{u}_z)_Q + (\dot{u}_z)_P \right\} (t_P - t_Q) \qquad (4.67)$$

The quantity u_z can also be approximated from axial stresses σ_z and pressures P with the aid of a stress-displacement relation. Then a numerical integration with respect to distance, instead of time, has to be carried out:

$$(u_z)_P = (u_z)_R + \frac{1}{2} \left\{ (\varepsilon_z)_R + (\varepsilon_z)_P \right\} (z_P - z_R) \qquad (4.67a)$$

in which $R = (z_R, t_P)$ and $\varepsilon_z = \frac{\partial u_z}{\partial z} = (\sigma_z - \nu \frac{R}{e} P) / E$ according to (4.6), or (4.7) and (4.9). It is thought that (4.67a) involves a smaller accumulation of integration errors than (4.67) [Heinsbroek et al. 1991], since the number of spatial steps (elements) is mostly smaller than the number of time steps.

4.2.6. *Computational grids*

In the integrated compatibility equations (4.42)-(4.45) the points P and A_i can be arbitrarily chosen in the z-t plane, whenever A_i lies "upstream" on the characteristic line with slope

$1/\lambda_i$ intersecting P. Although, theoretically, in every point P the four unknowns $V, H, \dot{u}_z$ and σ_z can be solved, a choice has to be made for the points in which this really will be done. Usually the points P are chosen at equal distances Δz and Δt in the z-t plane, where Δt is fixed and $\Delta z = L/N$ with N an integer number of elements and L the pipe length. (In pipe systems a common value of Δt is generally used for the computational grids of the individual pipes. Hence Δt is fixed and equal for each pipe of the system. For a system consisting of one pipe this is not necessarily the case.)

In figure 4.3 the points A_i are chosen one time step Δt earlier with respect to point P; if P = (z_P, t_P) then $A_i = (z_P - \lambda_i \Delta t, t_P - \Delta t)$. It is seen that, in general, interpolations are necessary to obtain the values of the unknowns in the points A_i, since these values are known only in grid points. However, it is well-known that interpolations cause numerical damping, especially when steep wave fronts are involved [Wiggert et al. 1986, p. 3]. Therefore the use of interpolations is avoided by adjusting the wave speeds λ_i in such a way that all A_i are points of the computational grid (see figure 4.4). The error in the calculated solution, introduced by adjusting the values of λ_i, is proportional to the magnitudes of the adjustments. Since these magnitudes decrease when the grid is refined, the introduced error will decrease too. The "pressure-wave" grid ($\Delta z / \Delta t = \tilde{c}_F$) in figure 4.4 has the disadvantage that interpolations are still necessary in the vicinity of a boundary (see figure 4.5). This disadvantage disappears when a "stress-wave" grid ($\Delta z / \Delta t = \tilde{c}_t$), as shown in figure 4.6, is used. In this grid, to avoid interpolations, the points A_1 and A_2 are located more than one time step earlier with respect to point P.

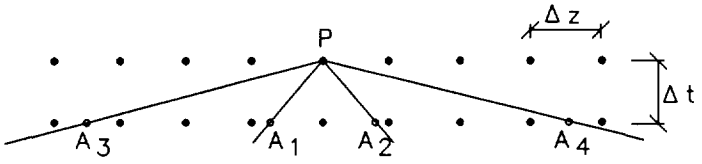

Figure 4.3. Computational grid and characteristic lines.

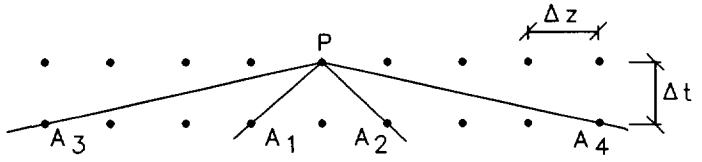

Figure 4.4. Computational grid and characteristic lines after adjustment of the wave speeds λ_i.

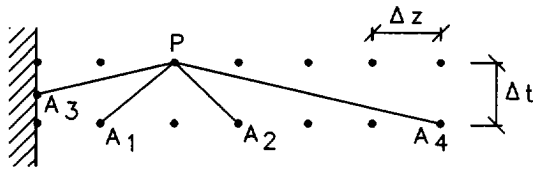

Figure 4.5. Computational grid and characteristic lines near to a boundary.

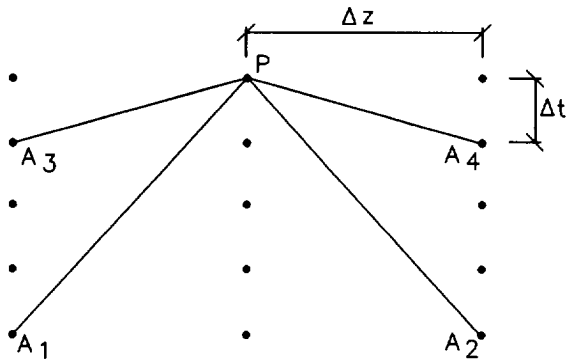

Figure 4.6. Alternative computational grid and characteristic lines.

There are many other computational grids, that is choices of P and A_i, that can be used to solve the equations (4.42)-(4.45). To minimize the errors introduced by adjusting the wave speeds, the following two alternative computational grids are used in the present study. Both grids permit the ratio of wave speeds, $\tilde{c}_t/\tilde{c}_F$, to be a rational number. The "pressure-wave" grid in figure 4.7 is obtained from that of figure 4.4 by a spatial grid refinement, whereas the "stress-wave" grid in figure 4.8 follows from that of figure 4.6 after a refinement of the time mesh. The grid in figure 4.7 still has the disadvantage that interpolations are needed for near-boundary points. To partly obviate this deficiency, the time mesh is refined at the boundaries only [Vardy 1976, Tijsseling & Lavooij 1989].

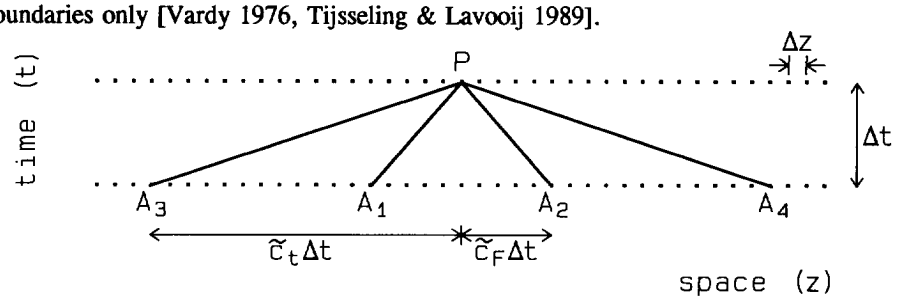

Figure 4.7. "Pressure-wave" grid ($\tilde{c}_t/\tilde{c}_F$ = 17/5).

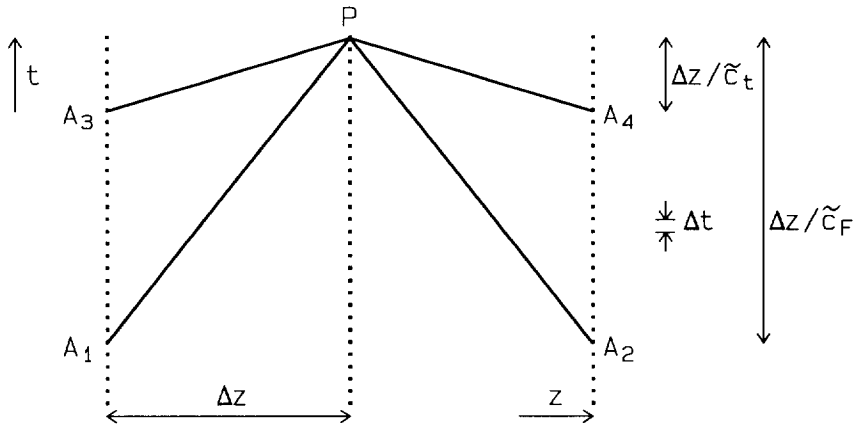

Figure 4.8. "Stress-wave" grid ($\tilde{c}_t/\tilde{c}_F$ = 25/6).

4.2.7. *Adjustment of wave speeds*

The computational grids in the previous subsection are based on adjusted wave speeds. Since the wave speeds are functions of K, ρ_f, E, ρ_t, R, e and ν, the only correct manner of adjusting them is by changing these physical and geometrical data. Here the mass densities ρ_f and ρ_t are changed to obtain the desired wave speeds $\tilde{c}_F^*$ and $\tilde{c}_t^*$, the superscript * indicates changed values. The wave speeds $\lambda_1 = \tilde{c}_F^*$ and $\lambda_3 = \tilde{c}_t^*$ are the roots of the characteristic equation (B.1) combined with (B.3) in appendix B:

$$\{\rho_f \rho_t\}\,\lambda^4 - \{(k_2 + k_1 k_3)\rho_f + k_1 \rho_t\}\,\lambda^2 + \{k_1 k_2\} = 0 \qquad (4.68)$$

with $k_1 = \rho_f c_F^2 = \{\frac{1}{K} + (1-\nu^2)\frac{2R}{Ee}\}^{-1}$, $k_2 = \rho_t c_t^2 = E$ and $k_3 = 2\nu^2\frac{R}{e}$. To obtain the desired wave speeds $\tilde{c}_F^*$ and $\tilde{c}_t^*$, the mass densities must fulfil the next two conditions

$$\{\rho_f^*\,\rho_t^*\}\,\tilde{c}_F^{*4} - \{(k_2 + k_1 k_3)\rho_f^* + k_1 \rho_t^*\}\,\tilde{c}_F^{*2} + \{k_1 k_2\} = 0 \qquad (4.69)$$

$$\{\rho_f^*\,\rho_t^*\}\,\tilde{c}_t^{*4} - \{(k_2 + k_1 k_3)\rho_f^* + k_1 \rho_t^*\}\,\tilde{c}_t^{*2} + \{k_1 k_2\} = 0 \qquad (4.70)$$

which is equivalent with

$$\rho_f^* = k_1 \frac{(\bar{c}_F^{*2} + \bar{c}_t^{*2}) + \{ (\bar{c}_F^{*2} + \bar{c}_t^{*2})^2 - 4(1 + k_1 k_3/k_2)\, \bar{c}_F^{*2} \bar{c}_t^{*2} \}^{\frac{1}{2}}}{2(1 + k_1 k_3/k_2)\, \bar{c}_F^{*2} \bar{c}_t^{*2}} \qquad (4.71)$$

$$\rho_t^* = k_2 \frac{(\bar{c}_F^{*2} + \bar{c}_t^{*2}) - \{ (\bar{c}_F^{*2} + \bar{c}_t^{*2})^2 - 4(1 + k_1 k_3/k_2)\, \bar{c}_F^{*2} \bar{c}_t^{*2} \}^{\frac{1}{2}}}{2\bar{c}_F^{*2} \bar{c}_t^{*2}} \qquad (4.72)$$

The computational grids in the figures 4.7 and 4.8 require that the ratio $\bar{c}_t^* / \bar{c}_F^*$ is rational. The ratio $\bar{c}_t^* / \bar{c}_F^*$ can then be chosen as close as desired to the actual ratio $\bar{c}_t / \bar{c}_F$, so that only slight changes in the physical data are necessary. In fact, ρ_f^* and ρ_t^* can be chosen within the range of measurement accuracy of ρ_f and ρ_t.

Liou [1983] presents an original method to correct for the adjusted wave speeds. Unfortunately his method introduces some numerical damping (opinion of present author).

4.3. Lateral motion

The four equations (3.90)-(3.93), describing the flexural behaviour of a liquid-filled Timoshenko-type pipe, are solved numerically also by the method of characteristics (MOC). The MOC is an unconventional approach in the area of structural dynamics. It is used here, because it leads to a unified approach: the axial and lateral equations are mathematically treated in the same manner. Another benefit of the MOC is in its connection with physical wave propagations. Furthermore it is thought that for impact loads, and hence steep wave fronts, the method is more accurate than the numerical methods conventionally applied.

In section 2.3, this is the FSI literature review, most attention is paid to axial (longitudinal) pipe motion. Here some important literature dealing with the lateral (flexural) motion of Timoshenko beams is summarized.

Literature

The Timoshenko [1921, 1922] beam theory is credited to Bresse [1859] by Schmidt [1987, pp. 4.2-4.3]. In his standard work on stress waves in solids, Kolsky [1953] shows that the

one-dimensional Timoshenko [1921,1922] theory for flexural waves in cylindrical beams is a very good approximation of the three-dimensional theory of Pochhammer [1876] and Chree [1889]. Flügge [1942] clearly explains the propagation of waves and discontinuities in beams. In [Flügge & Zajac 1959] an analytical solution is given of the wave propagation in a semi-infinite Timoshenko beam subjected to a step moment. Leonard & Budiansky [1954] solve the Timoshenko beam equations with the MOC. MOC, modal and analytical solutions are compared for the simplified, physically unrealistic case that shear and bending waves travel at the same speed. The analytical solutions concern a simply supported beam subjected to a step moment and a ramp-platform moment. Plass [1958] shows MOC-results for the case that shear and bending waves travel at different speeds. Semi-infinite beams are subjected to half-sine impact loads. The numerical results are validated against one analytical solution, and against measurements of Ripperger [1955]. Chou & Mortimer [1967] give a thorough mathematical treatment of the MOC applied to hyperbolic systems of second-order partial differential equations. Al-Mousawi [1984] uses the MOC when he investigates wave reflections at discontinuities of cross section in Timoshenko beams. Experimental results are presented in [Al-Mousawi & Harrison 1987]. Schmidt [1987] studies dispersion in hyperbolic systems and applies his findings to Timoshenko beams. Vardy & Alsarraj [1989] analyse the vibrations of free masses supported by single structural members using the MOC. Vardy & Fan [1989] compare experimental and MOC results on flexural waves in empty and liquid-filled pipes.

4.3.1. *Basic equations*

The lateral equations (3.90)-(3.93) are applied to thin-walled pipes. The overlines on $\dot{\theta}_x$ and $\dot{u}_y$ are then omitted and expression (3.89) is used for the shear coefficient κ^2. The basic equations read

Shear

$$\frac{\partial \dot{u}_y}{\partial t} + \frac{c_s^{\,2}}{\kappa^2 G A_t} \frac{\partial Q_y}{\partial z} = -g\cos\gamma \tag{4.73}$$

$$\frac{\partial \dot{u}_y}{\partial z} + \frac{1}{\kappa^2 G A_t} \frac{\partial Q_y}{\partial t} = -\dot{\theta}_x \tag{4.74}$$

Bending

$$\frac{\partial \dot{\theta}_x}{\partial t} + \frac{c_b^2}{E I_t} \frac{\partial M_x}{\partial z} = \frac{1}{\rho_t I_t} Q_y \tag{4.75}$$

$$\frac{\partial \dot{\theta}_x}{\partial z} + \frac{1}{E I_t} \frac{\partial M_x}{\partial t} = 0 \tag{4.76}$$

in which

$$c_s^2 = \frac{\kappa^2 G A_t}{\rho_t A_t + \rho_f A_f} \tag{4.77}$$

and

$$c_b^2 = \frac{E}{\rho_t} \tag{4.78}$$

are the shear and bending wave speeds [Flügge 1942], respectively. For all practical situations $c_s < c_b$.

Where shear deformation and rotatory inertia are neglected in the axial basic equations, these matters are included here to obtain a hyperbolic system of partial differential equations. The second term in (4.74) represents shear deformation, the first term in (4.75) rotatory inertia. When these terms are omitted, the Bernoulli-Euler beam equations remain. At first sight it may look inconsistent to incorporate shear deformation and rotatory inertia in the lateral, but not in the axial equations, where, in addition, radial inertia is neglected as well. However, shear deformation and rotatory inertia are needed to get finite wave propagation speeds, just as in the axial theory the propagation speeds are finite. The Bernoulli-Euler beam theory leads to waves travelling at infinite speed, which is physically unrealistic [Flügge 1942]. Nevertheless, Bernoulli-Euler theory is valid for low-frequency, long-wavelength phenomena in slender beams; the shear deformation and rotatory inertia terms in the basic equations (4.73)-(4.76) generally are small. Shear deformation is of importance for short

beams, rotatory inertia for high-frequency vibrations.

4.3.2. *MOC-transformation*

In the next subsections reference is frequently made to the previous section 4.2, since the lateral and axial basic equations are mathematically treated in the same way.

In matrix notation the system of lateral equations (4.73)-(4.76) reads

$$\mathbf{A}\frac{\partial \mathbf{y}}{\partial t} + \mathbf{B}\frac{\partial \mathbf{y}}{\partial z} = \mathbf{r} \tag{4.79}$$

in which $\mathbf{y}$ is the vector of unknowns, $\mathbf{A}$ and $\mathbf{B}$ are the matrices of coefficients, and $\mathbf{r}$ is the right-hand-side vector:

$$\mathbf{y} = \begin{bmatrix} \dot{u}_y \\ Q_y \\ \dot{\theta}_x \\ M_x \end{bmatrix} \tag{4.80}$$

$$\mathbf{A} = \begin{bmatrix} 1 & 0 & 0 & 0 \\ 0 & \dfrac{1}{\kappa^2 G A_t} & 0 & 0 \\ 0 & 0 & 1 & 0 \\ 0 & 0 & 0 & \dfrac{1}{EI_t} \end{bmatrix} \tag{4.81}$$

$$\mathbf{B} = \begin{bmatrix} 0 & \dfrac{c_s^{\,2}}{\kappa^2 G A_t} & 0 & 0 \\ 1 & 0 & 0 & 0 \\ 0 & 0 & 0 & \dfrac{c_b^{\,2}}{EI_t} \\ 0 & 0 & 1 & 0 \end{bmatrix} \tag{4.82}$$

$$\mathbf{r} = \begin{bmatrix} -g\cos\gamma \\ -\dot{\theta}_x \\ \dfrac{1}{\rho_t I_t} Q_y \\ 0 \end{bmatrix} \tag{4.83}$$

System (4.79) is a linear system with constant coefficients. The matrices **A** and **B** are decoupled with respect to shear and bending; the shear (4.73-4.74) and bending (4.75-4.76) equations are coupled via the right-hand-side vector (4.83). Because **A** and **B** are decoupled, they can be viewed as two $2 * 2$-matrices instead of one $4 * 4$-matrix, so that the MOC-transformation is simplified. From the characteristic equation $| \mathbf{B} - \lambda \mathbf{A} | = 0$, or

$$\left[\frac{\lambda^2}{\kappa^2 G A_t} - \frac{c_s^{\,2}}{\kappa^2 G A_t} \right] \left[\frac{\lambda^2}{E I_t} - \frac{c_b^{\,2}}{E I_t} \right] = 0 \tag{4.84}$$

it follows that the characteristic roots or eigenvalues of system (4.79) are

$$\lambda_1 = +c_s \,, \quad \lambda_2 = -c_s \,, \quad \lambda_3 = +c_b \,, \quad \lambda_4 = -c_b \tag{4.85}$$

The transformation matrix **T** is readily found,

$$\mathbf{T} = \begin{bmatrix} 1 & c_s & 0 & 0 \\ 1 & -c_s & 0 & 0 \\ 0 & 0 & 1 & c_b \\ 0 & 0 & 1 & -c_b \end{bmatrix} \tag{4.86}$$

See further subsection 4.2.2.

4.3.3. *Wave propagation speeds*

From the characteristic equation (4.84) it follows that the shear and bending waves travel at the constant speeds c_s and c_b. It is important to be more specific at this point. Discontinuities

in the shear force Q_y travel without attenuation at speed c_s, whereas discontinuities in the bending moment M_x travel without attenuation at speed c_b [Flügge 1942; Flügge & Zajac 1959]; see also next subsection. Behind these discontinuities at the fronts, the waves are highly dispersive. The dispersion is caused by the strong interaction between shear and bending waves. In the mathematical model this interaction takes place through the right-hand side (4.83). As the characteristic equation $| \mathbf{B} - \lambda \mathbf{A} | = 0$ does not depend on the right-hand side $\mathbf{r}$, dispersion is not predicted through its roots c_s and c_b; the wave speeds are not frequency-dependent. Schmidt [1987] takes the right-hand sides (in the present model) into account in a wave-train analysis. On page 5.8 of his work he derives a bi-quadratic equation, which is the dispersion relation for wave propagation in Timoshenko beams. He considers both phase and group velocities and clearly explains the two possible modes of deformation and their frequency-dependence. The highest mode occurs only beyond a certain cut-off frequency, the lowest mode is considered by Kolsky [1963].

For long wavelengths the phase velocity c_l of sinusoidal flexural waves is [Kolsky 1963, pp. 51, 85]

$$c_l = \frac{2\pi}{\lambda} \sqrt{\frac{EI_t}{\rho_t A_t + \rho_f A_f}} \tag{4.87}$$

where λ is the wavelength. The group velocity has a maximum for λ equal to about $R/0.3$ in case of a cylindrical bar [Kolsky 1963, pp. 72-73]. This implies that waves with a length of about $3R$ appear at the head of a travelling pulse.

It is noted that one must proceed with caution when results of wave-train analyses are applied to travelling discontinuities or step-pulses.

The influence of boundary conditions on wave propagation is disregarded in most literature. Timoshenko & Young [1955, pp. 324-357] study the *free vibrations* of beams. For a Bernoulli-Euler beam with hinged ends, they find, on page 332, formula (4.87) for the lowest mode of vibration, and, on page 334, for a Timoshenko beam, Schmidt's [1987, p. 5.8] dispersion relation.

4.3.4. *Compatibility equations*

The four compatibility equations (4.32) belonging to system (4.79), with $\mathbf{v}$, $\mathbf{A}$, $\mathbf{r}$ and $\mathbf{T}$

according to (4.29), (4.81), (4.83) and (4.86), respectively, can be written as

Shear

$$\left[\frac{\mathrm{d}\dot{u}_y}{\mathrm{d}t}\right]_1 + \frac{c_s}{\kappa^2 GA_t}\left[\frac{\mathrm{d}Q_y}{\mathrm{d}t}\right]_1 = -c_s\dot{\theta}_x - g\cos\gamma \tag{4.88}$$

$$\left[\frac{\mathrm{d}\dot{u}_y}{\mathrm{d}t}\right]_2 - \frac{c_s}{\kappa^2 GA_t}\left[\frac{\mathrm{d}Q_y}{\mathrm{d}t}\right]_2 = +c_s\dot{\theta}_x - g\cos\gamma \tag{4.89}$$

Bending

$$\left[\frac{\mathrm{d}\dot{\theta}_x}{\mathrm{d}t}\right]_3 + \frac{c_b}{EI_t}\left[\frac{\mathrm{d}M_x}{\mathrm{d}t}\right]_3 = \frac{1}{\rho_t I_t}Q_y \tag{4.90}$$

$$\left[\frac{\mathrm{d}\dot{\theta}_x}{\mathrm{d}t}\right]_4 - \frac{c_b}{EI_t}\left[\frac{\mathrm{d}M_x}{\mathrm{d}t}\right]_4 = \frac{1}{\rho_t I_t}Q_y \tag{4.91}$$

where $\left[\frac{\mathrm{d}y_j}{\mathrm{d}t}\right]_i$ is the directional derivative of the variable y_j in the z-t plane along the characteristic line with slope $1/\lambda_i$. Integration of the compatibility equations (4.88)-(4.91) yields

$$\{(\dot{u}_y)_P - (\dot{u}_y)_{A_1}\} + \frac{c_s}{\kappa^2 GA_t}\{(Q_y)_P - (Q_y)_{A_1}\} = -c_s\int_{A_1}^{P}\{\dot{\theta}_x + g\cos\gamma\}\,\mathrm{d}t \tag{4.92}$$

$$\{(\dot{u}_y)_P - (\dot{u}_y)_{A_2}\} - \frac{c_s}{\kappa^2 GA_t}\{(Q_y)_P - (Q_y)_{A_2}\} = +c_s\int_{A_2}^{P}\{\dot{\theta}_x - g\cos\gamma\}\,\mathrm{d}t \tag{4.93}$$

$$\{ (\dot{\theta}_x)_P - (\dot{\theta}_x)_{A_3} \} + \frac{c_b}{EI_t} \{ (M_x)_P - (M_x)_{A_3} \} = \frac{1}{\rho_t I_t} \int_{A_3}^{P} Q_y \, dt \tag{4.94}$$

$$\{ (\dot{\theta}_x)_P - (\dot{\theta}_x)_{A_4} \} - \frac{c_b}{EI_t} \{ (M_x)_P - (M_x)_{A_4} \} = \frac{1}{\rho_t I_t} \int_{A_4}^{P} Q_y \, dt \tag{4.95}$$

where P and A_i are points in the z-t plane as shown in figure 4.1.

Discontinuities

Flügge [1942] and Leonard & Budiansky [1954] show that discontinuities travel without attenuation along the characteristic lines in the z-t plane provided that the wave speeds c_s and c_b are not equal. Discontinuities in the shear force Q_y travel at speed c_s, whereas discontinuities in the bending moment M_x travel at speed c_b. The Joukowsky-type relations between Q_y and $\dot{u}_y$, and M_x and $\dot{\theta}_x$, are found to be

$$\Delta Q_y = \pm (\rho_t A_t + \rho_f A_f) \, c_s \, \Delta \dot{u}_y \tag{4.96}$$

$$\Delta M_x = \pm \rho_t I_t \, c_b \, \Delta \dot{\theta}_x \tag{4.97}$$

These relations are obtained from a consideration similar to that in subsection 4.2.4, thereby using (4.92)-(4.95) and (4.77)-(4.78).

4.3.5. *Numerical integration*

The numerical integration of the right-hand sides of the compatibility equations (4.88)-(4.91) is the weak spot in applying the MOC to the Timoshenko beam equations. The strong interaction between shear and bending waves, which is the dominant phenomenon, takes place via the right-hand sides, and these should therefore be calculated accurately.

The integrated right-hand sides in the final system of equations (4.92)-(4.95) have the form

$$I = k_1 \int_A^P y_j \, dt + k_2 g \int_A^P \cos\gamma \, dt \tag{4.98}$$

where k_1 and k_2 are constants and y_j is either $\dot{\theta}_x$ or Q_y.
The second integral, which results from the gravity force, can be calculated exactly, since γ is assumed to be constant

$$\int_A^P \cos\gamma \, dt = (t_P - t_A) \cos\gamma \tag{4.99}$$

The first integral will be approximated according to the most simple numerical integration scheme

$$\int_A^P y_j \, dt = \left\{ (1-\theta)(y_j)_A + \theta (y_j)_P \right\} (t_P - t_A) \tag{4.100}$$

where θ generally has the values 0, 1/2 or 1.

The lateral displacement u_y and the bending rotation θ_x are obtained from the respective velocities $\dot{u}_y$ and $\dot{\theta}_x$

$$(u_y)_P = (u_y)_Q + \frac{1}{2} \left\{ (\dot{u}_y)_Q + (\dot{u}_y)_P \right\} (t_P - t_Q) \tag{4.101}$$

$$(\theta_x)_P = (\theta_x)_Q + \frac{1}{2} \left\{ (\dot{\theta}_x)_Q + (\dot{\theta}_x)_P \right\} (t_P - t_Q) \tag{4.102}$$

in which $P = (z_P, t_P)$ and $Q = (z_P, t_Q)$.

The quantities u_y and θ_x can also be approximated from the stress-displacement relations (3.85)-(3.87). Then a numerical integration with respect to distance, instead of time, has to be carried out.

4.3.6. *Computational grids*

The applied computational grids are those of the figures 4.7 and 4.8, with characteristic directions according to (4.85).

4.3.7. *Adjustment of wave speeds*

To avoid the use of interpolations the wave speeds c_s and c_b are slightly adjusted by changing the mass densities ρ_f and ρ_t. From the definitions (4.77)-(4.78) it follows with $G = \frac{1}{2}E/(1+\nu)$ that

$$\rho_f^* = \frac{A_t}{A_f}\left\{\frac{\kappa^2}{2(1+\nu)} - \left[\frac{c_s^*}{c_b^*}\right]^2\right\}\frac{E}{c_s^{*2}} \tag{4.103}$$

$$\rho_t^* = \frac{E}{c_b^{*2}} \tag{4.104}$$

where c_s^* and c_b^* are the desired wave speeds, and ρ_f^* and ρ_t^* are the adjusted mass densities.

4.4. Torsional motion

The equations for torsional motion (3.98)-(3.99) can easily be solved by the method of characteristics. For two equations the procedure is simple and therefore not given in detail. Compatibility equations

$$\left[\frac{\mathrm{d}\dot{\theta}_z}{\mathrm{d}t}\right]_1 - \frac{c_{tor}}{GJ_t}\left[\frac{\mathrm{d}M_z}{\mathrm{d}t}\right]_1 = 0 \tag{4.105}$$

$$\left[\frac{\mathrm{d}\dot{\theta}_z}{\mathrm{d}t}\right]_2 + \frac{c_{tor}}{GJ_t}\left[\frac{\mathrm{d}M_z}{\mathrm{d}t}\right]_2 = 0 \tag{4.106}$$

can be derived which are valid along the characteristic directions $1/c_{tor}$ and $-1/c_{tor}$ in the z-t plane. The torsional wave propagation speed c_{tor} is

$$c_{tor} = \sqrt{\frac{G}{\rho_t}} \tag{4.107}$$

Torsional waves are non-dispersive as long as each cross section rotates as a whole about its centre [Clark 1956; Kolsky 1963].

The torsional equations are not used in the present work.

4.5. Cavitation

The numerical treatment of developing and collapsing vapour bubbles is described. The underlying assumptions and the limitations of the method are discussed in the last subsection.

4.5.1. *Concentrated cavity model*

The *concentrated cavity model*, see section 2.2, is used to simulate *vaporous cavitation*. Cavities are allowed to form at the *grid points* (*nodal points* or *computational sections*) whenever the absolute pressure drops to the vapour pressure. Between the grid points pure liquid is assumed to exist (see figure 4.9). A single cavity disappears when its volume is calculated to be equal or less than zero. The present model handles *distributed cavitation regions* and *column separations* numerically in the same manner. In distributed cavitation regions small cavity volumes are calculated for a series of grid points, whereas column separations are identified by large cavity volumes calculated for a single grid point.

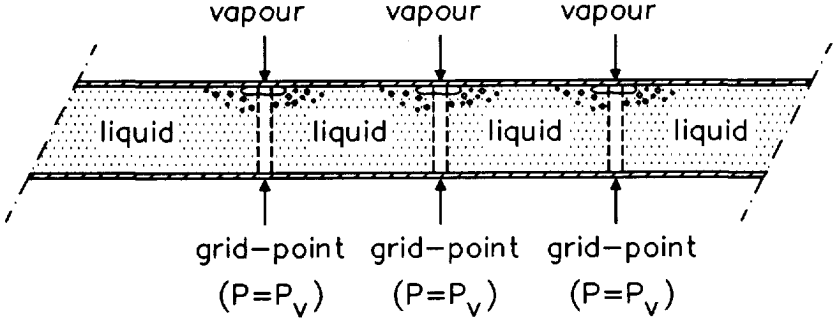

Figure 4.9. Definition sketch of concentrated cavity model.

4.5.2. *Numerical procedure*

In the numerical procedure of section 4.2 the absolute pressure P_{abs} is not allowed to drop below the vapour pressure P_v. When, at a grid point, P_{abs} is calculated to be less than P_v, P_{abs} is simply set equal to P_v,

$$P_{abs} = P_v \tag{4.108}$$

which is equivalent with

$$H = H_v \tag{4.109}$$

where

$$H_v = h_0 - z\sin\gamma - \frac{P_{out}}{\rho_f g} + \frac{P_v}{\rho_f g} \tag{4.110}$$

is the relative vapour head. Condition (4.109) and the integrated compatibility equations (4.42)-(4.45) constitute an undetermined system of five equations for the four unknowns V, H, $\dot{u}_z$ and σ_z. Instead of introducing the void fraction α as the fifth unknown[1], to obviate this problem, the liquid velocity V is assumed to be discontinuous at a grid point (z,t); V_1 and V_2 are the values of V at (z^-, t) and (z^+, t), respectively. A cavity is now formed, the volume $\mathcal{V}$ of which is governed by

$$\frac{\partial \mathcal{V}}{\partial t} = -A_f(V_1 - V_2) \tag{4.111}$$

or, when numerically integrated,

$$\mathcal{V}(t) = \mathcal{V}(t - \Delta t) + A_f\{V_2(t) - V_1(t)\}\Delta t \tag{4.112}$$

The cavity disappears when its volume is calculated to be negative. Then, to satisfy the mass balance, the last positive cavity volume is filled with liquid, according to

$$V_1(t) - V_2(t) = \frac{\mathcal{V}(t - \Delta t)}{A_f \Delta t} \tag{4.113}$$

which is equation (4.112) with $\mathcal{V}(t) = 0$.

[1] see subsection 3.1.5

4.5.3. *Assumptions and limitations*

When the absolute pressure reaches the vapour pressure, cavities, or bubbles, will develop in the liquid. In the present model these cavities are concentrated, or lumped, at the grid points. Between the grid points pure liquid is assumed for which the basic equations (4.11-4.14) or (4.42-4.45) of section 4.2 remain valid. This means that the pressure wave speed c_F is maintained between grid points in distributed cavitation regions. However, in bubble flows the pressure wave speed is very low and pressure-dependent. These matters are implicit in the model. Pressure waves do not propagate through an established distributed cavitation region, since this is at an assumed constant vapour pressure. The nullification of a distributed cavitation region by a pressure wave causes a delay in propagation which must be regarded as a reduction of the wave speed.

The basic equations (4.42)-(4.45) are only valid if there is pure liquid between the grid points. In the computational grid of figure 4.8 this is the case. In the grid of figure 4.7, however, the characteristic lines span more than one grid length. For the stress-wave characteristic lines, which concern the pipe wall, this may be of less significance, but for the pressure-wave characteristic lines this is not correct. The computational grid in figure 4.7 must therefore be viewed as ten (in figure 4.7) separate "pressure-wave" grids, coupled through the cavity volume equation (4.112), the stress-wave characteristic lines and the numerical treatment at the boundaries.

The cavities, concentrated at grid points, do not move. This is consistent with the acoustic approximation: since the overall time scale is acoustic, the convective displacements of a vapour bubble are small. Vreugdenhil [1964] takes into account, within the concentrated cavity model, the motion of liquid-vapour boundaries.

The maximum length, $L_{cav} = \mathcal{V}/A_f$, of a cavity must be small compared to the grid length. Simpson and Bergant [1991b] recommend

$$\frac{L_{cav}}{\Delta z} < 0.1 \tag{4.114}$$

For distributed cavitation regions, condition (4.114) is generally fulfilled. If not, the present model is not valid and the application of models for two-phase plug flow, slug flow or open-channel flow should be considered.

For column separations, condition (4.114) may sometimes be violated, which is acceptable (opinion of present author), since column separation is a local phenomenon, and only a few

grid points are concerned. However, care should be taken when $L_{cav}/\Delta z$ becomes greater than 1. In that case liquid-vapour boundaries moving from grid point to grid point should be explicitly modelled.

The mass of vapour is neglected, just as the influence of radial pipe displacements on the cavity volume.

From a physical "microscopic" point of view the "macroscopic" concentrated cavity model is not correct; a two-phase flow [Wallis 1969] approach would be better. However, $P_{abs} = P_v$ (4.108) is physically a strong condition, if there is no free gas or gas release involved. Furthermore, the continuity equation, that is the mass balance, is satisfied through (4.113).

The concentrated cavity model is a relatively simple model, which is able to cover the essential phenomena in transient cavitation. It fits in with the standard MOC-approach, so that it can be used in general waterhammer computer codes. Its main deficiency is in the numerical oscillations and unrealistic spikes appearing in the calculated pressure histories, when regions of distributed cavitation occur [De Vries 1972]. One way of partly suppressing the oscillations and spikes is by assuming small amounts of initial free gas in the grid points [De Vries 1973; Provoost 1976; Wylie 1984; Zielke & Perko 1985; Simpson 1986; Barbero & Ciaponi 1991]. Condition (4.108) is then replaced by

$$(P_{abs} - P_v)\, \forall = constant \tag{4.115}$$

where the free gas is assumed to behave isothermally. The used free gas void fractions are of the order of 10^{-7}. The numerical integration of equation (4.111) may also affect the amount of oscillations and spikes [Provoost & Wylie 1981; Simpson & Wylie 1985; Simpson & Bergant 1991b]. The application of a numerical filter may be considered [Vliegenthart 1970; Kranenburg 1974a]. Simpson & Bergant [1991b], who performed a systematic study of the numerical oscillations and non-physical spikes, come to the conclusion that the concentrated cavity model does not converge and, consequently, the number of grid points should be limited.

The opinion of the present author is the following. Numerical oscillations and spikes are due to multi-cavity collapse during the nullification of a cavitation region. In fact, the concentrated cavity model assumes small column separations in every grid point in such a region. Upon collapse of a single column separation a pressure rise or spike occurs, which, once generated, does not disappear. The spike travels in a cavitation-free region to and from

the boundaries and when two of these spikes meet a higher spike is the result. However, the one-dimensional long-wavelength waterhammer theory is not valid for these short-duration pressure spikes. (Note that the duration of the spikes decreases when the computational grid is refined.) Dispersion should be introduced in the model, so that spikes travel with attenuation and more realistic results are obtained. On the other hand, high-frequency oscillations are to a certain extent observed in cavitation measurements as well: they are unstable and physically not repeatable. This instability, reflected in the unstable numerical oscillations of the concentrated cavity model, is part of the cavitation phenomenon.

It is acceptable to smooth the grid-dependent highest frequencies by means of a numerical filter.

The overall conclusion is: the concentrated cavity model is adequate, but improvements concerning the numerical oscillations are welcome.

4.6. Initial conditions

Steady-state conditions form the starting-point of the transient analysis.

4.6.1. *Single pipe*

The initial values of the variables in the grid points are obtained from the steady-state solutions given in subsection 3.2.1. The liquid velocity is constant and the pressure head decreases linearly in downstream direction. The initial generalized forces are constant, linear or quadratic in z.

4.6.2. *Multi-pipe system*

Fluid-structure interaction is a dynamic phenomenon. It does not occur in liquid-filled pipe systems under stationary conditions, where the liquid exerts a static load on the pipe system. Therefore it is customary to determine first of all the steady-state of the hydraulic system. This can be quite complicated in multi-pipe systems and networks, since a, mostly large, set of non-linear algebraic equations must be solved. Several numerical procedures are available,

of which the *Hardy Cross method* is the oldest and probably most well-known [Cross 1936]. Other standard techniques are those of Shamir & Howard [1968], Epp & Fowler [1970] and Wood & Charles [1972]. Wood & Rayes [1981] and Walski [1985] give surveys. It is also possible to find the steady-state with a time-marching approach using the method of characteristics (MOC) [Fox & Keech 1975; Vardy & Chan 1983; Shimada 1988]. Once the hydraulic steady-state is found, the deformation of the pipe system can be determined with standard pipe-stress computer codes, which are generally based on the finite element method (FEM).

In the present work the axial, lateral and torsional equations describing the structure are coupled at junctions. To obtain the static deformation of the pipe system the constants of integration of each individual pipe must be known, see section 3.2. Since, in general, these constants depend on each other (they are coupled at junctions), a linear system of equations has to be solved. Alternatively, the MOC may be used to find the steady-state, so that a unified, that is for steady and unsteady situations, approach is obtained.

4.7. Boundary conditions

The boundary conditions of section 3.3, expressed in relative pressure heads H and relative axial stresses σ_z, are numerically treated.

4.7.1. *Introduction*

Ends

The terminal points of a pipe system are called *ends*.

When a grid point P in the z-t plane is an end point, as shown in figure 4.10 for an exemplary computational grid, there are only two characteristic lines meeting in P. Hence, there are only two compatibility equations available for the four unknowns y_j defined by either (4.18) or (4.80). Two additional equations are provided by two boundary conditions of the type

$$\varphi(y_1, y_2, y_3, y_4, t) = 0 \tag{4.116}$$

where φ is an arbitrary function of five arguments. It is assumed that the *end* conditions for

the axial and lateral equations are independent, so that the axial problem of section 4.2 requires two boundary conditions of the type

$$\varphi (V, H, \dot{u}_z, \sigma_z, t) = 0 \tag{4.117}$$

and the lateral problem of section 4.3 two of the type

$$\varphi (\dot{u}_y, Q_y, \dot{\theta}_x, M_x, t) = 0 \tag{4.118}$$

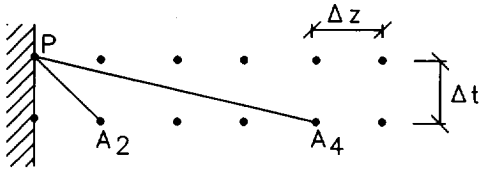

Figure 4.10. Point P at an end.

Junctions

The connection points of the single pipes in a pipe system are called *junctions*.

When a grid point P in the *z-t* plane lies on the *straight junction* of two single pipes, as shown in figure 4.11 for exemplary computational grids, the vectors of unknowns $\mathbf{y}_{P_1}$ and $\mathbf{y}_{P_2}$ at either side of the junction are generally different, since discontinuities may occur, for instance at a diameter-change. There are eight unknowns to be determined, for which four compatibility equations are available. The remaining four equations come from the junction coupling condition

$$\mathbf{M}_{jc}^{(1)} \, \mathbf{y}_{P_1} = \mathbf{M}_{jc}^{(2)} \, \mathbf{y}_{P_2} \tag{4.119}$$

which is derived, for both the axial and the lateral equations, from mass and momentum balances (see subsection 3.3.5).

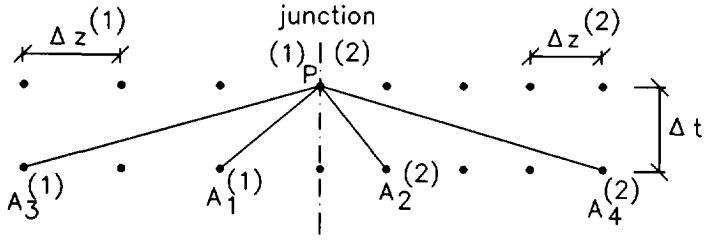

Figure 4.11. Point P at a junction.

For a *straight junction* the axial and lateral motions are assumed to be decoupled, so that two $4 * 4$ coupling matrices $\mathbf{M}_{jc}^{(k)}$ exist for both $k = 1$ and $k = 2$ (see subsection 4.7.6).

For an *elbow junction* the coupling between axial and lateral pipe motion leads to one $8 * 8$ matrix $\mathbf{M}_{jc}^{(k)}$ for both $k = 1$ and $k = 2$ (see subsection 4.7.7).

4.7.2. *Reservoir*

At a reservoir the following conditions are imposed (see subsection 3.3.1)

$$H = H_{res} \qquad \text{and} \qquad \dot{u}_z = 0 \tag{4.120}$$

$$\dot{u}_y = 0 \qquad \text{and} \qquad \dot{\theta}_x = 0 \tag{4.121}$$

where H_{res} is the reservoir's constant pressure head.

4.7.3. *Valve*

The instantaneous closure of a an immovable valve is modelled by (see subsection 3.3.2)

$$V = 0 \qquad \text{and} \qquad \dot{u}_z = 0 \tag{4.122}$$

$$\dot{u}_y = 0 \qquad \text{and} \qquad \dot{\theta}_x = 0 \tag{4.123}$$

The instantaneous closure of an axially unrestrained valve is modelled by (see subsection 3.3.2)

$$V = \dot{u}_z \qquad \text{and} \qquad \rho_f g A_f \Delta H = A_t \Delta \sigma_z \pm m \ddot{u}_z \pm c \dot{u}_z \pm k u_z \tag{4.124}$$

$$\dot{u}_y = 0 \qquad \text{and} \qquad \dot{\theta}_x = 0 \tag{4.125}$$

where ΔH is the pressure-head difference over the valve. Because the quantities $\ddot{u}_z$ and u_z in (4.124) are not basic variables, they have to be approximated. The acceleration $\ddot{u}_z$ and the displacement u_z are obtained from the velocity $\dot{u}_z$ by numerical differentiation and integration, respectively. The differentiation is with a backward finite-difference scheme, the integration with the trapezoidal rule. Then

$$(\ddot{u}_z)_P = \frac{(\dot{u}_z)_P - (\dot{u}_z)_Q}{\Delta t} \tag{4.126}$$

$$(u_z)_P = (u_z)_Q + \frac{1}{2}\{(\dot{u}_z)_Q + (\dot{u}_z)_P\}\,\Delta t \tag{4.127}$$

where $P = (z_P, t_P)$, $Q = (z_P, t_Q)$ and $\Delta t = t_P - t_Q$. Substitution of (4.126) and (4.127) in the second equation of (4.124) gives

$$\rho_f g A_f (\Delta H)_P - A_t (\Delta \sigma_z)_P \mp \{\frac{m}{\Delta t} + c + \frac{k\Delta t}{2}\}(\dot{u}_z)_P = \mp\{\frac{m}{\Delta t} - \frac{k\Delta t}{2}\}(\dot{u}_z)_Q \pm k(u_z)_Q \tag{4.128}$$

Alternative, and probably more accurate, ways of integrating the second equation in (4.124) are provided by the *average-acceleration method* or *Newmark-β =1/4 method* [Craig 1981, pp. 41-43, 146-150] and the method of Vardy & Alsarraj [1989]. Otwell [1984] uses the average-acceleration method, but calls it a trapezoidal rule [Wiggert, private communication with Lavooij, 1987].

Non-instantaneous valve closures are modelled by replacing the first equations in (4.122) and (4.124) by the non-linear equation (see subsection 3.3.2)

$$\frac{V - \dot{u}_z}{(V - \dot{u}_z)_0} = \pm \tau(t) \sqrt{\frac{|\Delta H|}{|\Delta H_0|}} \tag{4.129}$$

where ΔH_0 is the steady-state head-loss over the valve. The specific function $\tau(t)$ used in the present investigation is

$$\tau(t) = \begin{cases} (1 - t/T_c)^{3.53} & \text{for } 0 \le t \le 0.4T_c \\ 0.394\,(1 - t/T_c)^{1.70} & \text{for } 0.4T_c \le t \le T_c \\ 0 & \text{for } T_c \le t \end{cases} \tag{4.130}$$

in which T_c is the valve closure time. This function, which is based on empirically obtained ball-valve discharge coefficients, see [Lavooij & Tijsseling 1988, Vol. 1, App. A], was provided by Wiggert to Delft Hydraulics in 1987. More information on ball-valve discharge characteristics can be found in [Van Rij 1970; Schedelberger 1975].

The squared, and hence quadratic, equation (4.129) is solved simultaneously with three linear equations (two integrated compatibility equations and one boundary condition). This is done exactly [Lavooij & Tijsseling 1988, Vol. 2, App. E].

4.7.4. *Closed end*

The boundary conditions used for a freely moving closed end are (see subsection 3.3.3)

$$V = \dot{u}_z \qquad \text{and} \qquad \rho_f g A_f H = A_t \sigma_z \pm m \ddot{u}_z \tag{4.131}$$

$$Q_y = 0 \qquad \text{and} \qquad M_x = 0 \tag{4.132}$$

The second equation in (4.131) is numerically treated in the same manner as the second equation in (4.124).

4.7.5. *Axial impact*

The boundary conditions describing the axial impact of a solid rod with a closed pipe end are (see subsection 3.3.4)

$$V = \dot{u}_z \qquad \text{and} \qquad \rho_f g A_f H + Y_r(\dot{u}_z - V_{0r}) = A_t \sigma_z \pm m \ddot{u}_z \tag{4.133}$$

$$Q_y = 0 \qquad \text{and} \qquad M_x = 0 \tag{4.134}$$

4.7.6. *Straight junction*

The 4 * 4 matrices $\mathbf{M}_{jc,z}^{(k)}$ that couple the vectors of axial variables, $\mathbf{y}_1 = (V, H, \dot{u}_z, \sigma_z)_1^T$ and $\mathbf{y}_2 = (V, H, \dot{u}_z, \sigma_z)_2^T$, at either side ($k$) of a straight junction, are (see subsection 3.3.5)

$$\mathbf{M}_{jc,z}^{(k)} = \begin{bmatrix} A_f^{(k)} & 0 & -A_f^{(k)} & 0 \\ 0 & 1 & 0 & 0 \\ 0 & 0 & 1 & 0 \\ 0 & \rho_f g A_f^{(k)} & 0 & -A_t^{(k)} \end{bmatrix} \tag{4.135}$$

The 4 * 4 matrices $\mathbf{M}_{jc,y}^{(k)}$ that couple the vectors of lateral variables, $\mathbf{y}_1 = (\dot{u}_y, Q_y, \dot{\theta}_x, M_x)_1^T$ and $\mathbf{y}_2 = (\dot{u}_y, Q_y, \dot{\theta}_x, M_x)_2^T$, at either side ($k$) of a straight junction, are

$$\mathbf{M}_{\mathrm{jc,y}}{}^{(k)} = \begin{bmatrix} 1 & 0 & 0 & 0 \\ 0 & 1 & 0 & 0 \\ 0 & 0 & 1 & 0 \\ 0 & 0 & 0 & 1 \end{bmatrix} \tag{4.136}$$

4.7.7. *Elbow junction*

The $8 * 8$ matrices $\mathbf{M}_{\mathrm{jc,elbow}}{}^{(k)}$ that couple the vectors of axial and lateral variables $\mathbf{y}_k = (V, H, \dot{u}_z, \sigma_z, \dot{u}_y, Q_y, \dot{\theta}_x, M_x)_k^{\mathrm{T}}$ at either side (k) of an elbow, are (see subsection 3.3.6)

$$\mathbf{M}_{\mathrm{jc,elbow}}{}^{(1)} = \begin{bmatrix} A_f^{(1)} & 0 & -A_f^{(1)} & 0 & 0 & 0 & 0 & 0 \\ 0 & 1 & 0 & 0 & 0 & 0 & 0 & 0 \\ 0 & 0 & 1 & 0 & 0 & 0 & 0 & 0 \\ 0 & \rho_f g A_f^{(1)} & 0 & -A_t^{(1)} & 0 & 0 & 0 & 0 \\ 0 & 0 & 0 & 0 & 1 & 0 & 0 & 0 \\ 0 & 0 & 0 & 0 & 0 & -1 & 0 & 0 \\ 0 & 0 & 0 & 0 & 0 & 0 & 1 & 0 \\ 0 & 0 & 0 & 0 & 0 & 0 & 0 & 1 \end{bmatrix} \tag{4.137}$$

$$\mathbf{M}_{\mathrm{jc,elbow}}{}^{(2)} = \begin{bmatrix} A_f^{(2)} & 0 & -A_f^{(2)} & 0 & 0 & 0 & 0 & 0 \\ 0 & 1 & 0 & 0 & 0 & 0 & 0 & 0 \\ 0 & 0 & 0 & 0 & 1 & 0 & 0 & 0 \\ 0 & 0 & 0 & 0 & 0 & 1 & 0 & 0 \\ 0 & 0 & -1 & 0 & 0 & 0 & 0 & 0 \\ 0 & \rho_f g A_f^{(2)} & 0 & -A_t^{(2)} & 0 & 0 & 0 & 0 \\ 0 & 0 & 0 & 0 & 0 & 0 & 1 & 0 \\ 0 & 0 & 0 & 0 & 0 & 0 & 0 & 1 \end{bmatrix} \tag{4.138}$$

4.7.8. *Column separation*

Column separation is simulated when the pressure head H, at end or junction, is calculated to be less than the vapour head H_v defined in (4.110). The pressure head is then held constant

$$H = H_v \tag{4.139}$$

and a cavity is allowed to form. Condition (4.139) replaces the $V = 0$, the $V = \dot{u}_z$ and the $\{A_f(V - \dot{u}_z)\}_1 = \{A_f(V - \dot{u}_z)\}_2$ conditions in the foregoing subsections, since these are not valid any more, when a cavity exists. The volume $\forall$ of the cavity follows from the numerically forward integrated equations (3.165) or (3.167). These are

$$\forall(t) = \forall(t - \Delta t) \pm A_f\{V(t) - \dot{u}_z(t)\}\Delta t \tag{4.140}$$

for a closed end, and

$$\forall(t) = \forall(t - \Delta t) \mp \left[A_f\{V(t) - \dot{u}_z(t)\}\Delta t\right]_1 \pm \left[A_f\{V(t) - \dot{u}_z(t)\}\Delta t\right]_2 \tag{4.141}$$

for a straight junction or an elbow junction; the indices 1 and 2 refer to either side of the junction. The column separation collapses when its volume is calculated to be less than zero. To satisfy the overall mass balance, the last positive cavity volume is exactly filled up with liquid, according to

$$V(t) - \dot{u}_z(t) = \mp \frac{\forall(t - \Delta t)}{A_f \Delta t} \tag{4.142}$$

for a closed end, and

$$\pm \left[A_f\{V(t) - \dot{u}_z(t)\}\right]_1 \mp \left[A_f\{V(t) - \dot{u}_z(t)\}\right]_2 = \frac{\forall(t - \Delta t)}{\Delta t} \tag{4.143}$$

for a straight junction or an elbow junction.

The motion of the liquid-vapour interface is disregarded; column separation is modelled

as a non-moving boundary condition. However, care should be taken when

$$\frac{L_{cs}}{\Delta z} > 0.5 \tag{4.144}$$

where $L_{cs} = \forall / A_f$ is the length of the column separation. See further subsection 4.5.3.

4.8. Multi-pipe systems

In multi-pipe systems each individual pipe has its own computational grids: one for axial and one for lateral wave propagation. Torsional waves are not considered here. The "axial" and "lateral" grids are independent, so that the adjustment of wave propagation speeds (see subsections 4.2.7 and 4.3.7) may lead to different values of ρ_f and ρ_t in one and the same pipe. This is physically inconsistent. However, the differences may be brought within the measurement accuracy range of the mass densities.

A common numerical time step Δt is used for all computational grids, so that they can easily be coupled at junctions.

The stress-wave grid of figure 4.8 is preferred over the pressure-wave grid of figure 4.7. The latter grid leads to interpolations, which not only give numerical damping but also a more complicated computer code. Furthermore, the pressure-wave grid is not entirely correct when cavitation occurs, as explained in subsection 4.5.3. The pressure-wave grid has more elements than the stress-wave grid, so that condition (4.144) is more easily violated. It is noted that very fine computational grids are required to simulate the highly dispersive lateral wave propagations [Heinsbroek et al. 1991]. Then, because of the common numerical time step, the axial grids are very fine as well (small Δz), and possibly too fine with respect to condition (4.144).

4.9. Computer codes

The developed computer codes are called SINGLECS, SINGALT, BEND, BENDALT and DOUBLE. They are based on the numerical method(s) described in this chapter. SINGLECS and SINGALT simulate the *axial* motion of a single pipe, BEND and BENDALT the *lateral* motion. SINGLECS and BEND are based on the computational grid of figure 4.7, SINGALT and BENDALT on that of figure 4.8. The SINGLECS code uses linear interpolations at and

near to boundaries. In the codes the ratio λ_3/λ_1 of wave speeds is a rational number, except in BEND, where this ratio is an integer. Except for the non-linear valve closure in SINGLECS and SINGALT, the boundary conditions (4.117) and (4.118) are taken as linear combinations of the basic variables, in which the coefficients and the right-hand sides may be either constant or a function of t.

The program DOUBLE is a combination of SINGALT and BENDALT. Two pipes in the horizontal plane are connected by one junction. The coupling matrices representing a diameter-change and a 90-degrees elbow are given by (4.135)-(4.136) and (4.137)-(4.138), respectively.

4.10. Numerical tests

The developed computer codes, and hence the underlying mathematical model and numerical method, have been extensively tested. Numerical tests were performed on the Delft Hydraulics *benchmark problems* A-B-C-D, which are based on an inventory of field cases and defined in consultation with Wiggert [Lavooij & Tijsseling 1988, Vol. 1, pp. 20-27]. Verification and validation tests were carried out by comparing computed results with 1) results of other codes, 2) analytical solutions and 3) experimental data known from literature.

A selection of the tests performed is shortly discussed in this section.

4.10.1. *Axial motion*

The present MOC-approach gives exact solutions of a slightly changed physical problem if interpolations and numerical integrations are *not* part of the procedure. This is the case when the stress-wave grid of figure 4.8 is used, the relatively unimportant dynamic friction is neglected and numerical integration of boundary conditions is not necessary. Convergence is then trivial. With the pressure-wave grid of figure 4.7 almost identical results were obtained, so that it can be concluded that the influence of interpolations at and near to boundaries is small.

The numerical integration of the boundary conditions, such as described in subsection 4.7.3, may ask for a small time step to attain convergence, whereas the numerical integration scheme itself is also important.

The applied change of physical data in subsection 4.2.7 can be made so small, by choosing finer computational grids, that it is within the measurement accuracy range of the changed data.

The Delft Hydraulics benchmark problems A, B and C concern a simple reservoir-pipe-valve system. The solutions of these problems, computed with the codes for axial motion, were compared with MOC results of Wiggert [Wiggert, private communication with Lavooij, 1987] and with MOC-FEM results of the Delft Hydraulics FLUSTRIN-code [Lavooij & Tijsseling 1988 (Vol. 2), 1989, 1991; Heinsbroek et al. 1991]. The compared results were almost identical, although the MOC-FEM results exhibited numerical oscillations in case of instantaneous valve closures.

The experiment of Wilkinson & Curtis [1980] was simulated in [Tijsseling & Lavooij 1989], the experiments of Vardy & Fan [1986] and [1989] in [Tijsseling & Lavooij 1990] and [Lavooij & Tijsseling 1991], respectively. Favourable results were obtained.

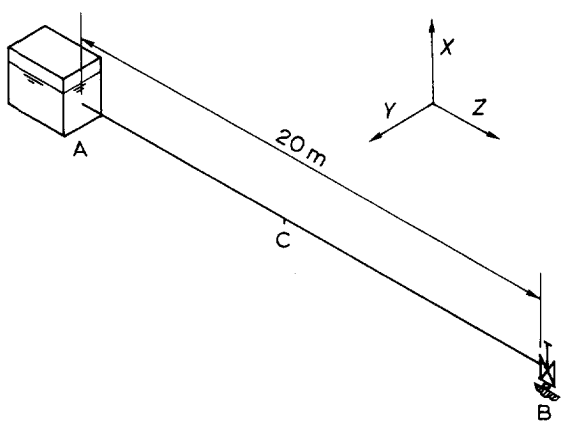

Schematic representation of reservoir-pipe-valve system. The pipe and valve are allowed to move freely in the axial (z) direction. Length = 20 m, inner radius = 0.3985 m, wall thickness = 0.008 m, Young's modulus = 210 GPa, Poisson's ratio = 0.3, shear coefficient = 0.5, mass density of pipe wall material = 7900 kg/m^3, mass density of liquid = 1000 kg/m^3, bulk modulus = 2.1 GPa, Darcy-Weisbach friction coefficient = 0.02, initial liquid velocity = 1 m/s, pressure behind valve = 0 Pa, valve closure time = 0 s.

Figure 4.12. Benchmark problem A.

The aforementioned tests before mentioned are not repeated here. Emphasis is laid upon the effects of interpolations, since a new element of the present numerical method is the avoidance of interpolations. Solutions of benchmark problem A, defined in figure 4.12, obtained with and without interpolations are shown in figure 4.13. A small time-shift is introduced to make the differences between both solutions better visible. The present method modifies the ratio $\tilde{c}_t/\tilde{c}_F$ of wave speeds from 5.153 to the rational number 67/13 by changing the mass densities into ρ_f^* = 1000.3 kg/m^3 and ρ_t^* = 7900.0 kg/m^3. The numerical time step used is 0.29 ms and the number of elements is just **1**. The results obtained with time-line interpolations [Goldberg & Wylie 1983] were provided by Fan [private communication 1992]. He used 8, 16 and 256 elements in his calculations and the corresponding time steps were 0.47 ms, 0.24 ms and 0.015 ms. The overall agreement between the present and Fan's results is excellent. It is seen that interpolations smooth the wave fronts and that details appear in the solution only when very fine grids are used. The advantage of the present method is that, with approximately the same time step such as in the middle graph of figure 4.13, 1 element, instead of 16 elements, is sufficient.

4.10.2. *Lateral motion*

The application of the MOC to problems on bending waves in beams is not common. One reason is that Bernoulli-Euler beam theory is not suitable for the MOC, since this theory does *not* lead to a *hyperbolic* system of partial differential equations. Timoshenko beam theory has to be used instead. A second reason is that the MOC requires very fine computational grids, as will be explained next.

The refinements of Timoshenko beam theory, being *shear deformation* and *rotatory inertia*, make the basic system of equations (4.73)-(4.76) or (4.79) hyperbolic. However, the terms in question in the equations (4.74) and (4.75) are very small with respect to the other terms and, in particular, with respect to the right-hand sides. Very fine grids are needed to take effectively into account the small terms inducing hyperbolic behaviour of the system. The experience of the author is that the element length Δz must be of the order of the radius of gyration R_g ($R_g = \sqrt{\frac{I_t}{A_t}} \approx \frac{R}{\sqrt{2}}$ for empty thin-walled cylindrical pipes of circular cross-section).

The major numerical error made in the MOC procedure is in the integration of the right-hand sides as described in subsection 4.3.5. In the equations (4.73)-(4.76) the right-hand

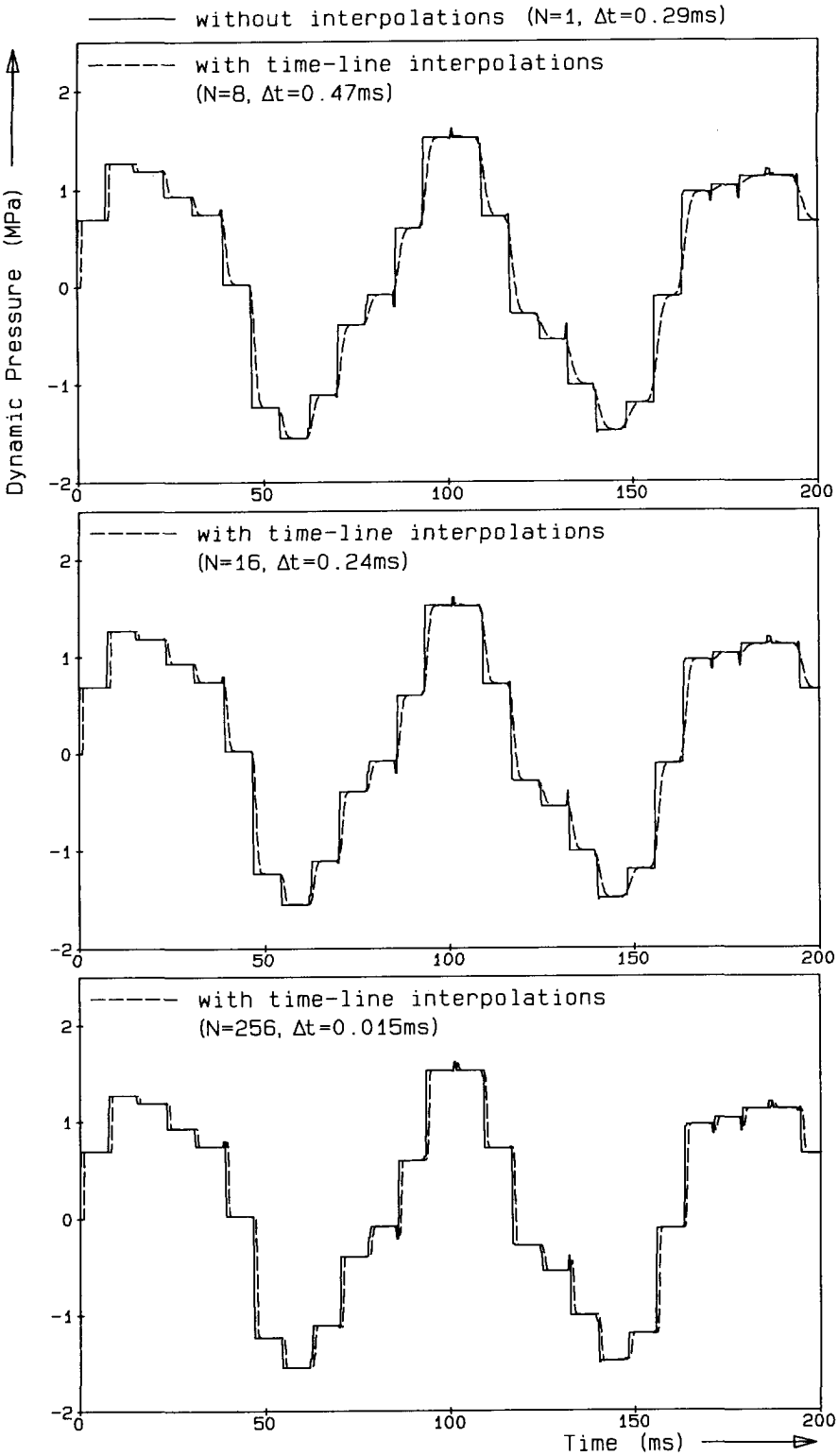

Figure 4.13. Effect of interpolations. Pressure history at valve for benchmark problem A.

sides are dominant. They couple the shear (4.73-4.74) and bending (4.75-4.76) wave equations and cause the strong physical dispersion already discussed in subsection 4.3.3. In the numerical solution, the right-hand sides in the integrated compatibility equations (4.92)-(4.95) dominate the shear deformation and rotatory inertia terms, unless the numerical time step is small (see equation (4.100)). Only for a small time step Δt, and hence small element length Δz, all the elements in the matrix of coefficients (**TA** in equation (4.28)) become important, thereby enhancing the hyperbolic character of the system and the performance of the MOC.

Summarizing one can say that the dominating right-hand sides impair the hyperbolic character of the basic system of equations, so that the MOC becomes less attractive. Nevertheless, the MOC is used in the present work because of its simplicity and the desired unified approach.

From numerical tests it became clear that the *trapezoidal rule* is the best way of integrating the right-hand sides. Hence θ is taken equal to 1/2 in equation (4.100). Other integration schemes produced too little or too much damping, or were too complicated [Lavooij & Tijsseling 1988, Vol. 2].

The free lateral vibrations of a simply-supported (hinged ends) liquid-filled pipe, with the dimensions and properties of the pipe in figure 4.12, were simulated with the codes for lateral motion in [Lavooij & Tijsseling 1988, Vol. 2]. The numerical results were compared with analytical solutions. Convergence was found, but relatively fine computational grids had to be used.

The analytical solution of Leonard & Budiansky [1954], concerning a simply-supported beam with a step-moment applied at one of the ends, was used for verification of the BEND-code [Lavooij & Tijsseling 1988, Vol. 2]. The analytical solution, in which the ratio of wave speeds c_b/c_s equals 1, could be reproduced.

In [Heinsbroek et al. 1991; Heinsbroek & Tijsseling 1993] MOC results and FEM results with respect to pulse and impact loads in a single liquid-filled pipe were shown to be in good agreement. It was concluded that the MOC needs fine computational grids when compared to the FEM.

One test case of [Lavooij & Tijsseling 1988, Vol. 2] is shown here. It concerns the response of the pipe in benchmark problem A (figure 4.12) to an impact load at one of the ends. The pipe is assumed to have one fixed and one free end and the ratio c_b/c_s of bending wave speed to shear wave speed is for simplicity taken as 5 ($\rho_f^* = 1220$ kg/m^3, $\rho_t^* = 7900$

kg/m^3). The number of elements used is 2049. The free end is subjected to a step moment of 200 kNm. Calculated responses at the instants $t_1 = \frac{1}{3}L/c_b$, $t_2 = \frac{2}{3}L/c_b$ and $t_3 = L/c_b$ are shown together in figure 4.14. The present results were calculated with the "bending-wave" grid of figure 4.8, those in [Lavooij & Tijsseling 1988, Vol. 2, Fig. 41] with the "shear-wave" grid of figure 4.7. The main reason for showing figure 4.14 is to demonstrate the propagation of discontinuities, discussed in subsection 4.3.4, and the physical dispersion, discussed in subsection 4.3.3. The instantaneous application of a moment on the right end (z = 20 m) generates a bending wave, the front of which travels with a velocity c_b = 5156 m/s to the left. The jump in the moment decreases when the front travels from right to left (figure 4.14 top). This is due to numerical error, since the jump remains theoretically equal to the initial value (200 kNm) [Flügge 1942; Leonard & Budiansky 1954]. Behind the wave front dispersion is nicely exhibited by shorter waves travelling the fastest. This is most evident at t_3 when the bending wave front reaches the fixed end (z = 0 m). The shear wave front is identified in figure 4.14 (bottom) by a peak in the shear force travelling at speed c_s = 1031 m/s to the left.

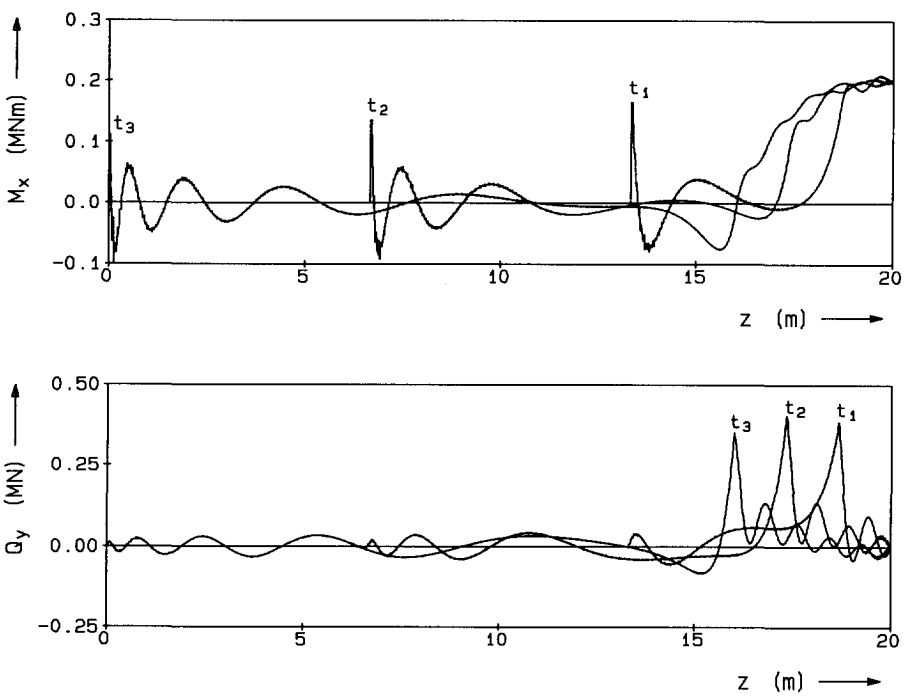

Figure 4.14. Propagation of discontinuity in bending moment M_x and associated shear force Q_y along pipe (benchmark problem A).

4.10.3. *Combined axial and lateral motion*

Delft Hydraulics benchmark problem D, defined in figure 4.15, is used to verify the code DOUBLE, in which axial and lateral pipe motions are combined through the elbow junction coupling. The present results are compared with results of the FLUSTRIN code [Lavooij & Tijsseling 1989; Heinsbroek & Tijsseling 1993] (see subsection 1.2.3), which solves the fluid equations with the MOC and the structural equations with the FEM. Pressures calculated at the valve and displacements at the elbow are shown in figure 4.16. The agreement between the present MOC (with $\check{c}_t/\check{c}_F$ = 35/8 and c_b/c_s = 24/8) and the FLUSTRIN MOC-FEM predictions is excellent.

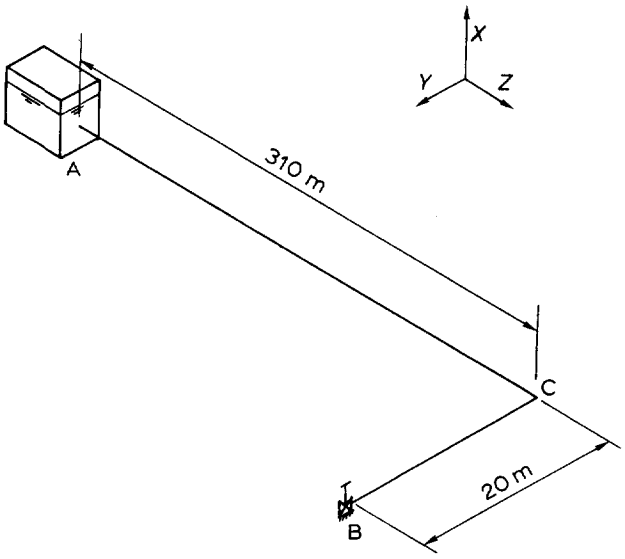

Schematic representation of reservoir-pipe-valve system with one elbow. The pipes and elbow are allowed to move freely in the horizontal (y-z) plane; the valve is rigidly fixed to the ground. Length of long pipe = 310 m, length of short pipe = 20 m, inner radius = 0.1032 m, wall thickness = 0.00635 m, Young's modulus = 210 GPa, Poisson's ratio = 0.3, shear coefficient = 0.53, mass density of pipe wall material = 7900 kg/m^3, mass density of liquid = 880 kg/m^3, bulk modulus = 1.55 GPa, Darcy-Weisbach friction coefficient = 0, initial liquid velocity = 4 m/s, pressure behind valve = 0 Pa, valve closure time = 0.5 s.

Figure 4.15. Benchmark problem D.

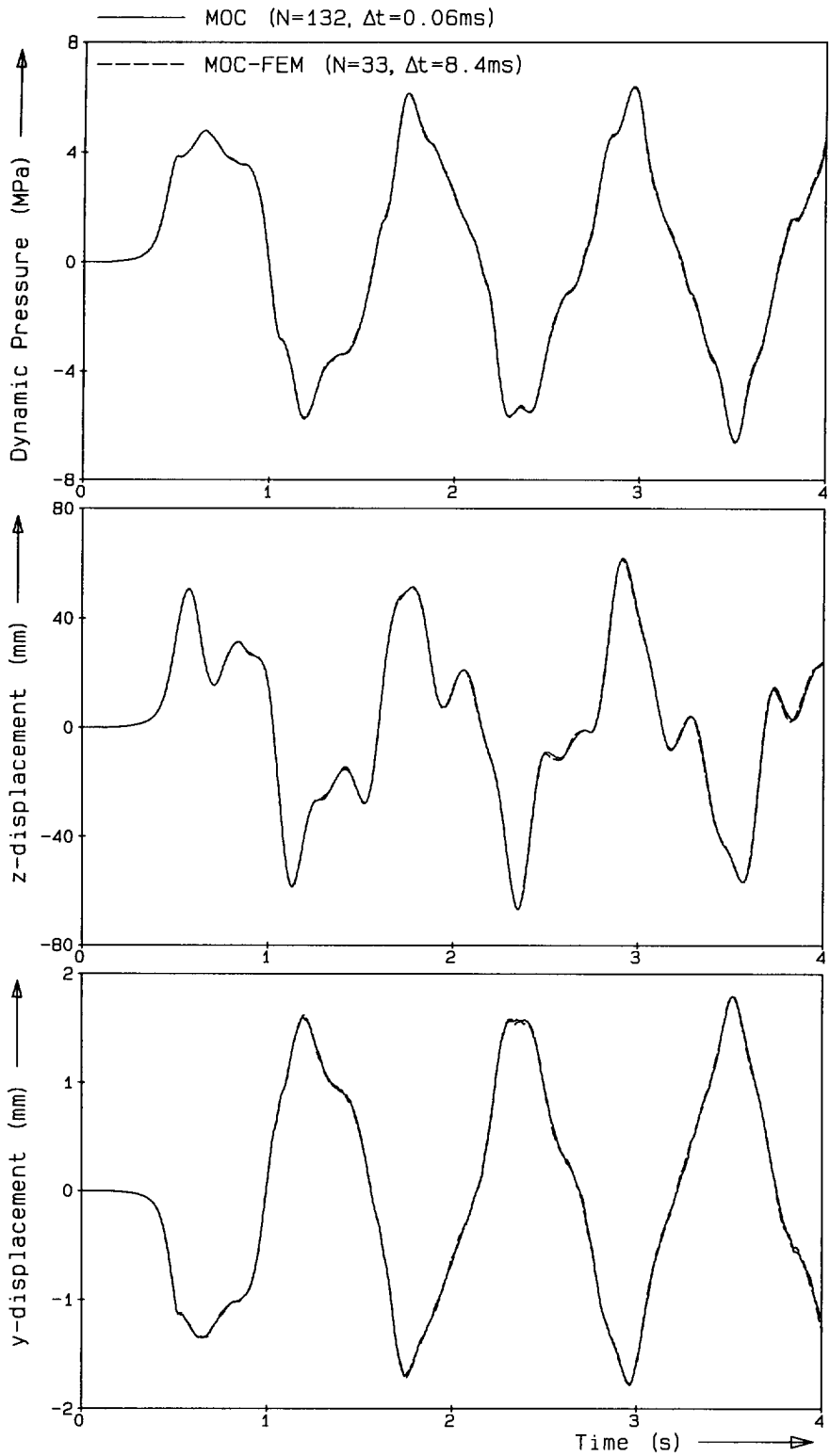

Figure 4.16. Comparison of MOC and MOC-FEM results for benchmark problem D. Pressure at valve and displacements at elbow.

4.10.4. *Cavitation and column separation*

The numerical models for cavitation and column separation were tested on simple reservoir-pipe-valve systems. Results obtained with column separation at the valve only were validated against the experiments of Martin [1983] in [Tijsseling & Lavooij 1989]. Results obtained with cavitation along the entire pipe in benchmark problem A were verified against predictions of the Delft Hydraulics waterhammer code WILMA, which also uses the concentrated cavity model. Except for the high-frequency numerical oscillations and unrealistic pressure spikes, see subsection 4.5.3, the results obtained (not shown here) were the same. The concentrated cavity model is validated against the experimental data of Simpson [1986] in section 6.1.

One thing to be reported here is the grid-dependency of the present model, when regions of distributed cavitation occur. Benchmark problem A (figure 4.12) is the test case. The ratio of wave speeds c_t^* / c_F^* is for simplicity taken equal to 5 by modifying the mass densities into $\rho_f^* = 1008$ kg/m^3, $\rho_t^* = 8463$ kg/m^3. The pressure head is not allowed to drop below -10 m: $H_v = -10$ m. Results obtained with the grids of the figures 4.7 and 4.8 are compared in figure 4.17. The upper two graphs show pressure-head histories at the valve as calculated with the grid of figure 4.7. The lower two graphs result from calculations with the grid of figure 4.8 with plotted values every fifth time step. The middle two graphs were obtained with the finest grids (40 elements), whereas the top and bottom graphs were obtained with coarser grids (8 elements). The predicted durations of the two column separations shown are slightly different for all four grids, but the magnitudes of the pressure peaks following their collapse are nearly the same. The shapes of the pressure peaks caused by cavity collapse show large differences due to the grid-dependent numerical oscillations of high frequency.

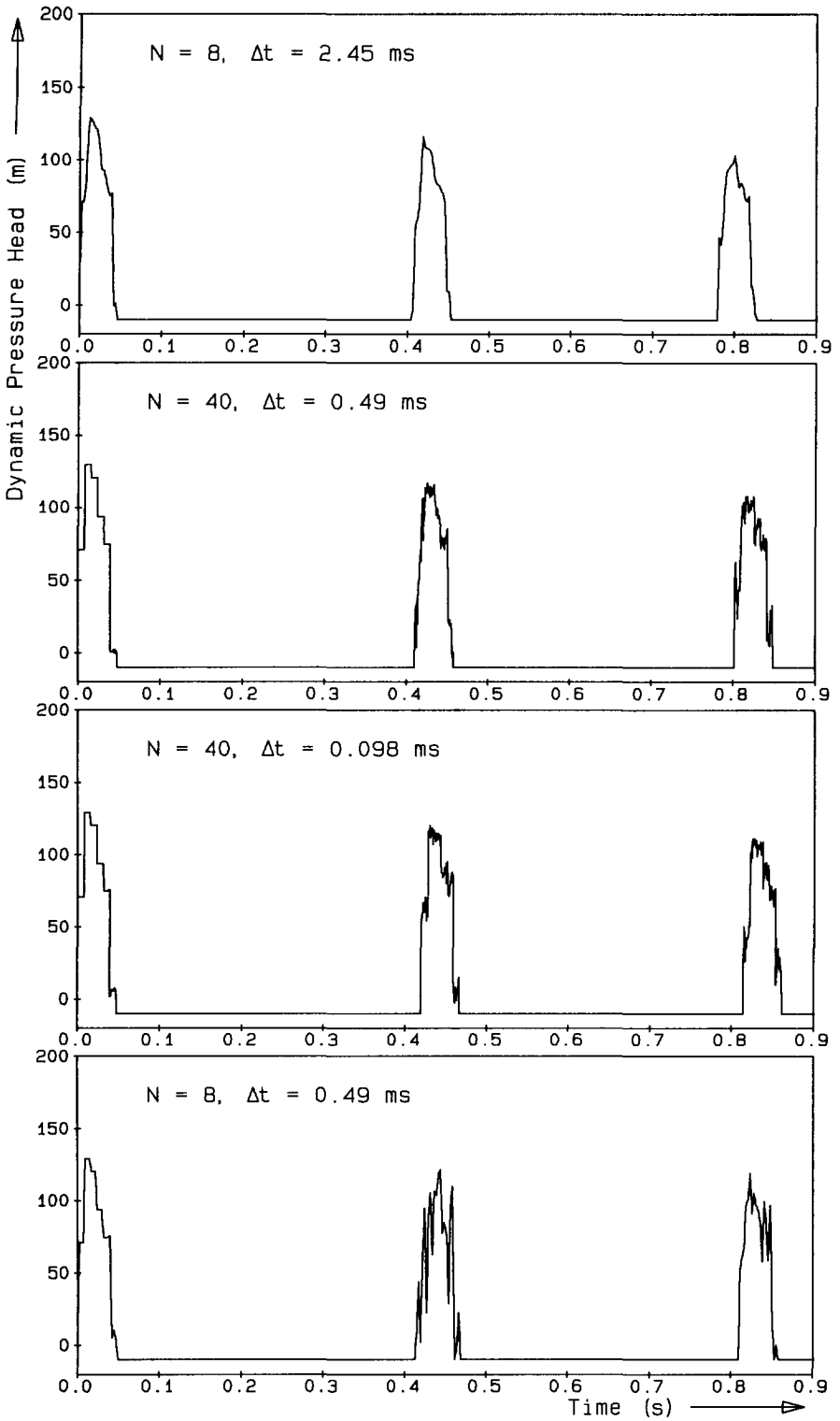

Figure 4.17. Grid-dependency of results. Benchmark problem A with cavitation. Dynamic pressure heads at valve.

4.11. Review and conclusions

The method of characteristics (MOC) is applied in the numerical solution of the basic equations derived in chapter 3. Although not strictly necessary, the assumption has been made that the pipes are thin-walled. The numerical procedure is worked out in detail. Compatibility equations, these are ordinary differential equations which are valid along the characteristic lines in the distance-time plane, are obtained for which the special case $\nu = 0$ (no Poisson coupling) does not require a separate treatment, such as in [Otwell 1984; Budny 1988]. Simplified compatibility equations for axial motion, resembling those of Wiggert et al. [1987a], are given. Discontinuity relations are derived for both axial and lateral motion. The validity of the calculated axial wave propagation speeds is discussed, just as the dispersive propagation of lateral waves and discontinuities. A short literature review is given on the MOC-application in Timoshenko beam theory.

New are the computational grids in the figures 4.7 and 4.8, which permit the ratios of wave speeds $\tilde{c}_t/\tilde{c}_F$ and c_b/c_s to be rational numbers. Interpolations, which cause numerical damping, can then be avoided by just a slight modification of the actual wave speeds. This is done through an adjustment of the mass densities ρ_t and ρ_f ; explicit formulae are given.

New is the incorporation of the concentrated cavity model within the FSI four-equation model of subsection 3.1.2. The underlying assumptions and associated limitations are discussed.

The calculation of the steady-state situation in liquid-filled pipe systems is shortly reviewed. The numerical treatise of the boundary conditions representing pipe ends and pipe junctions is described. The performed numerical tests are summarized and a few important results are presented.

5. EXPERIMENTS

Experimental results obtained in three different pipe systems are used to validate the cavitation and fluid-structure interaction (FSI) models of the chapters 3 and 4. The test rigs and the experiments performed are described in this chapter, the obtained results in chapter 6.

The experiment of Simpson [1986] is used to validate the cavitation model without the influence of FSI, whereas two experiments of Vardy and Fan [1989, 1993] are used to validate the FSI model without the influence of cavitation. New are the experiments with both FSI and cavitation. These were performed in Vardy and Fan's test rig by Fan and the present author.

5.1. Cavitation

Simpson [1986] studied short-duration pressure pulses due to cavity collapse. An experimental pipeline apparatus was designed and constructed in the G.G. Brown Hydraulics Laboratory at the University of Michigan (USA), in which measurements were done for eight levels of cavitation severity. Experimental results obtained for three levels of cavitation severity are compared with predictions by the concentrated cavity model in the next chapter. The laboratory set-up is shortly described here. A more detailed description is given by Simpson [1986, pp. 92-108].

The test rig, sketched in figure 5.1, consists of a 36 m long copper pipeline with an inner diameter of 19 mm and a wall thickness of 1.6 mm. The pipeline connects two reservoirs and is upward sloping. The difference in elevation between the downstream end and the upstream end is 1 m, so that the elevation angle γ = -0.028 rad. The pipeline is rigidly supported every 2.5 m by brackets affixed to a wall. The elbow in the pipeline is also rigidly fixed, by two brackets, so that FSI effects are insignificant. Pressure waves are generated by the manual closure of a downstream ball-valve. Ordinary tap water has been used in the experiments.

Dynamic pressures were measured at three locations along the pipe: at the valve, at the downstream one-quarter point and at the upstream one-quarter point. The used piezoelectric

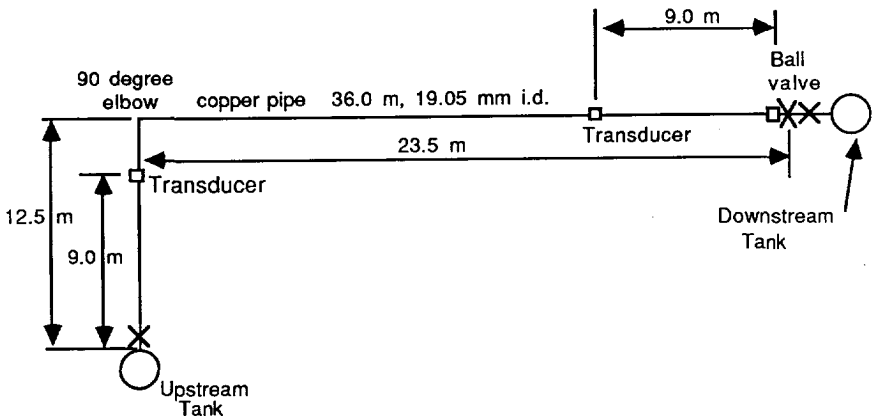

PLAN VIEW

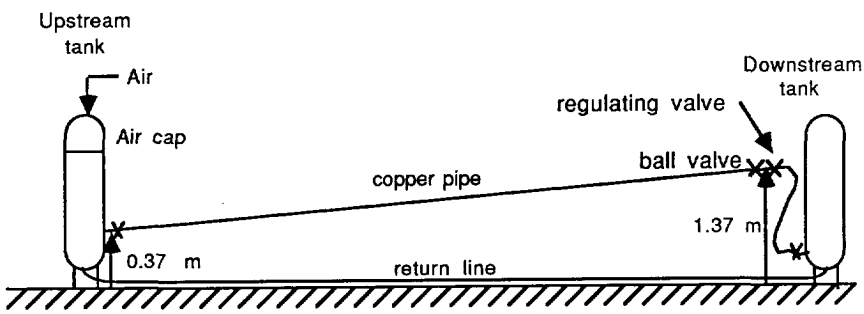

SIDE VIEW (not to scale)

Figure 5.1. Schematic representation of Simpson's [1986] experimental apparatus.

pressure transducers (PCB Piezotronics Inc., Series S111A26) have a rise time of 2 μs and a natural frequency of 400 kHz. The frequency of sampling was 1 kHz.

The data used in the simulations of chapter 6 are given in table 5.1. Note that the vapour head H_v depends on the barometric pressure.

<table>
<tr><td colspan="2">Water-filled pipe

L = 36.0 m
R = 9.525 mm
e = 1.588 mm
γ = -0.027781 rad
K = 1.9534 GPa (so that c_f = 1280 m/s)
ρ_f = 996.8 kg/m^3
E = 119.5 GPa
ρ_t = 8900 kg/m^3 (not used)
ν = 0 (no Poisson coupling)
g = 9.813 m/s^2</td><td colspan="2">Position of instrumentation

z (PT1) = 9.0 m
z (PT2) = 27.0 m
z (PT3) = 36.0 m</td></tr>
<tr><td>Level 0
(no cavitation)</td><td>Level 2</td><td>Level 5</td><td>Level 7</td></tr>
<tr><td>f = 0.0325
V_0 = 0.239 m/s
H_0 (z=L) = 24.12 m
H_v = -9.83 m
T_c = 65 ms</td><td>f = 0.029
V_0 = 0.401 m/s
H_0 (z=L) = 22.93 m
H_v = -9.86 m
T_c = 65 ms</td><td>f = 0.027
V_0 = 0.596 m/s
H_0 (z=L) = 22.32 m
H_v = -9.83 m
T_c = 65 ms</td><td>f = 0.024
V_0 = 0.938 m/s
H_0 (z=L) = 20.51 m
H_v = -9.83 m
T_c = 65 ms</td></tr>
</table>

Table 5.1. Simpson's [1986] experiment; input data for simulations.

5.2. Fluid-structure interaction

Vardy and Fan [1986, 1989, 1993] studied, without cavitation, fluid-structure interaction in liquid-filled pipe systems. An extensive series of high-quality measurements was carried out on four different pipe systems in a test rig built in the Hydraulics Laboratory at the University of Dundee (UK). Two of these pipe systems are considered here: a straight pipe and a system with one elbow. The two systems are described in the next subsections, experimental results are shown in chapter 6.

5.2.1. *Straight pipe*

The first FSI experiments in Dundee started in 1984 with bouncing a water-filled pipe onto a concrete block (see figure 5.2a). Besides the occurrence of cavitation, there was the problem of the experimenter getting wet. Both problems were solved by closing the pipe (figure 5.2b). Results of this experiment were presented at the 5th Conference on Pressure Surges [Vardy & Fan 1986]. Two problems exist in the experiment: 1) the system is accelerating, 2) the adhesive between concrete block and steel impact plate causes too much damping, in the opinion of Vardy and Fan. Therefore a third configuration, sketched in figure 5.3, was adopted.

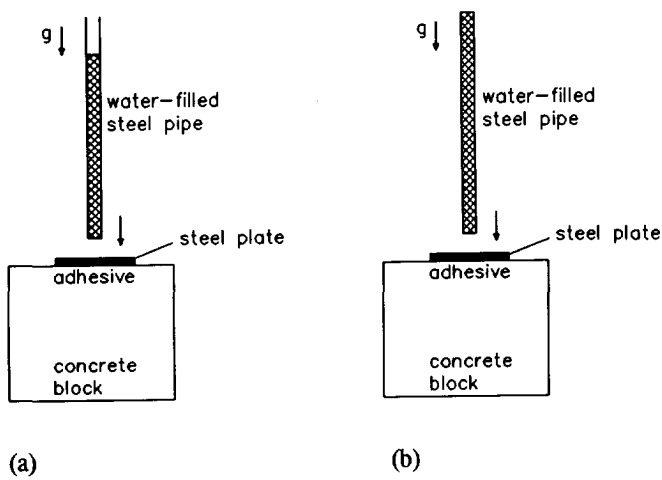

Figure 5.2. (a) Falling pipe with open end,
(b) Falling pipe with closed end.

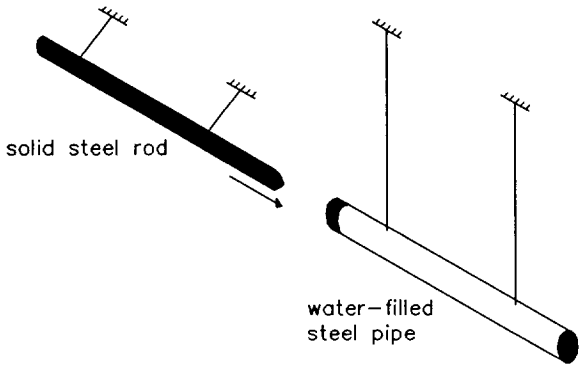

Figure 5.3. Straight-pipe experimental apparatus.

The principal part of the ultimate system (figure 5.3) is a 4.5 m long stainless steel pipe with an inner diameter of 52 mm and a wall thickness of 3.9 mm. The pipe is closed at both ends and filled with pressurized tap water. It is suspended by two long (about 3.3 m) thin, vertical steel wires from the ceiling, so that it can move freely in a nearly horizontal plane. The measured static deflection of the pipe caused by its weight is less than 0.2 mm relative to the suspension points, which are situated about 0.95 m from the pipe ends. Transients are generated by the impact of a solid steel rod onto one of the pipe ends. The used rod is 5 m long and suspended on a movable frame by short steel wires.

This apparatus is less complicated than the conventional reservoir-pipe-valve system, since 1) an initial steady-state pressure gradient is absent, 2) valve-closure characteristics are not needed and 3) the influence of pipe supports is negligible. Friction and gravity effects are unimportant due to the time scale (milliseconds) of the experiment. The experiment isolates the effects of fluid-structure interaction in case of axial wave propagations. Cavitation is avoided by taking a sufficiently high static pressure of the water, usually 2-7 MPa.

The pipe is extensively instrumented. Piezoelectric pressure transducers (Kistler 7031, 701A) are mounted (with their diaphragms flush with the inner wall of the pipe) near to the impact end, at the remote end and at three intermediate points, as indicated in figure 5.4. The transducers have an observed rise time of 0.15 ms [Fan 1989, p. 20], or 0.2 ms/MPa, and a natural frequency of 80 kHz. The connected amplifiers (Flyde FE428CA) have a cut-

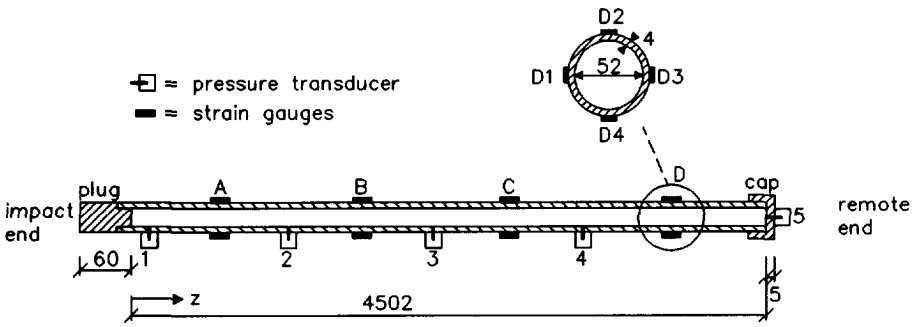

Figure 5.4. Water-filled straight pipe. (Measures in mm.)
Pressure transducers at sections 1 through 5.
Strain gauges at sections A through D.
Axial pipe-wall velocity measured near to section 1.

off frequency of 50 kHz. Strain gauges (TML-FRA-1-11) are attached to the pipe wall at four locations along the pipe. At each location four three-way (axial, hoop, shear) strain gauges are equidistantly placed around the pipe circumference, see figure 5.4. The connected amplifiers (Flyde FE458AC) have a cut-off frequency of 70 kHz. A laser Doppler vibrometer (DISA 55X) is used for non-contact measurements of one-directional pipe wall velocities at one selected location. Furthermore it is used to determine the impact velocity of the rod. The connected amplifier (DISA 55N21, 55N11) has a cut-off frequency of 26 kHz. A high-speed video camera (Kodak Ektapro 1000) was used to film the impact of the rod and the subsequent response of the pipe. The maximum sampling rate of the camera is 6000 frames per second. This is, unfortunately, too small with respect to the time scale of the present experiment (milliseconds). Nevertheless, pipe vibrations on a larger time scale can nicely be recorded. Furthermore, the impact velocity of the rod can be determined from the successive frames prior to impact.

The results presented in chapter 6 were obtained with a sampling frequency of 125 kHz, although a few 1 MHz (cavitation) measurements have also been performed. More details on the instrumentation and its performance can be found in [Fan 1989, pp. 17-26].

The procedure preceding each test or series of tests is described in subsection 5.3.1, where the cavitation experiments carried out by the present author, after instruction by Fan, are discussed. Vardy and Fan performed only non-cavitation tests. They investigated axial and lateral wave propagation in both empty and water-filled pipes. In the present work only the axial motion of the water-filled straight pipe is studied; the lateral motion of a straight pipe is less interesting, because it does not involve significant FSI effects. Lateral motion is considered in the one-elbow system of the next subsection.

The physical dimensions and material properties of pipe, water and rod, such as used in the simulations of chapter 6, are given in table 5.2, together with the measuring positions of the pressure transducers (PT), strain gauges (SG) and laser Doppler vibrometer (LDV). The method of measurement and the accuracy of the values in table 5.2 are given in [Fan 1989, p. 28; Fan & Tijsseling 1992]. The masses m_1 and m_2 of the end plug and end cap, respectively, which close the pipe, are incorporated in the simulations. The dimensions of the end pieces and the mass of the attached instrumentation, given by Fan [1989, p. 29 and p. 16, respectively], are neglected. The influence of the inertia of the end pieces, which can be assessed from the empty-pipe measurements of Fan [1989, pp. 41-42], is neither negligible nor dominating the phenomena. The relatively unimportant friction factor f in table 5.2 is four times smaller than the one assumed by Fan [1989, p. 28]. The gravitational acceleration g is taken as 9.813 m/s^2.

If cavitation does not occur, the underlying theory in chapter 3 is almost linear (see subsection 3.1.1). The pressures, velocities and strains are then linearly proportional to the impact velocity of the rod, so that measurements for one particular impact velocity are considered to be sufficient.

Water-filled pipe	Position of instrumentation	Solid steel rod
L = 4.502 m	z (PT1) = 0.0195 m	L_r = 5.006 m
R = 26.01 mm	z (PT2) = 1.1265 m	R_r = 25.37 mm
e = 3.945 mm	z (PT3) = 2.2510 m	E_r = 200 GPa
γ = 0	z (PT4) = 3.3760 m	ρ_r = 7848 kg/m^3
K = 2.14 GPa	z (PT5) = 4.5020 m	V_{0r} = 0.739 m/s
ρ_f = 999 kg/m^3	z (SGA) = 0.5740 m	
E = 168 GPa	z (SGB) = 1.6880 m	
ρ_t = 7985 kg/m^3	z (SGC) = 2.8140 m	
ν = 0.29	z (SGD) = 3.9440 m	
f = 0.01	z (LDV) = 0.0465 m	
m_1 = 1.2866 kg		
m_2 = 0.2925 kg		
H_v = −1000 m		
(no cavitation)		

Table 5.2. Vardy and Fan's straight-pipe experiment; input data for simulations.

5.2.2. *One-elbow pipe system*

In the one-elbow pipe system the 4.5 m long straight pipe of the previous subsection is connected to a second pipe of length 1.3 m by a rigid 90-degrees elbow, as sketched in figure 5.5. The system is suspended by three wires now. The experiments, performed by Fan and the present author, concern the axial impact of a water-filled system. After impact at the long pipe's end, lateral motion is induced at the elbow by reflecting/transmitting axial stress and pressure waves.

The data used in the simulations of chapter 6 are given in table 5.3. The elbow is assumed to be entirely rigid; the 90-degrees angle between the two pipes does not change. The mass of the elbow, 0.8807 kg, is not explicitly modelled; it is partly incorporated in the pipe lengths. The masses of the end pieces are taken into account with regard to their motion in

axial direction, which is the direction of the important junction coupling. The lateral inertia forces acting on the end pieces are neglected. The value of the relatively unimportant Darcy-Weisbach friction factor f is four times smaller than Fan's [1989, p. 28] skin friction factor. The value of the shear modulus $G = E/(2(1+\nu))$ is 65.1 GPa and the value of the shear coefficient $\kappa^2 = 2(1+\nu)/(4+3\nu)$ is 0.53. The value of g is again 9.813 m/s^2.

The data in table 5.3 (provided by Fan) correspond to the data in table 5.2, except for the length of the long pipe, the mass of the end plug and the impact velocity of the rod.

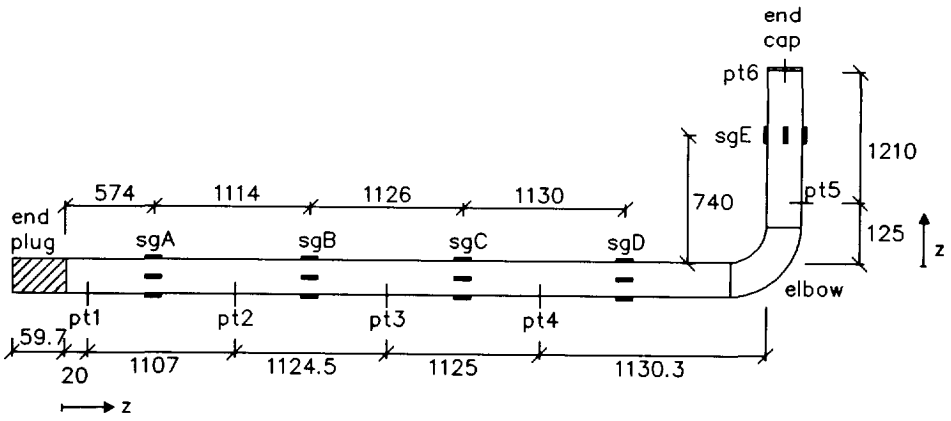

Figure 5.5. Water-filled one-elbow pipe system. (Measures in mm.)

Long pipe	Short pipe	Liquid	Solid rod
L = 4.51 m	L = 1.34 m	K = 2.14 GPa	L_r = 5.006 m
R = 26.01 mm	R = 26.01 mm	ρ_f = 999 kg/m^3	R_r = 25.37 mm
e = 3.945 mm	e = 3.945 mm	H_v = -1000 m	E_r = 200 GPa
γ = 0	γ = 0	(no cavitation)	ρ_r = 7848 kg/m^3
E = 168 GPa	E = 168 GPa		V_{0r} = 0.809 m/s
ρ_t = 7985 kg/m^3	ρ_t = 7985 kg/m^3		
ν = 0.29	ν = 0.29		
f = 0.01	f = 0.01		
m_1 = 1.312 kg	m_2 = 0.3258 kg		
z (PT1) = 0.0195 m	z (PT5) = 0.13 m		
z (PT2) = 1.1265 m	z (PT6) = 1.34 m		
z (PT3) = 2.2510 m	z (SGE) = 0.74 m		
z (PT4) = 3.3760 m	z (LDV) = 1.34 m		
z (SGA) = 0.5740 m			
z (SGB) = 1.6880 m			
z (SGC) = 2.8140 m			
z (SGD) = 3.9440 m			
z (LDV) = 0.0465 m			

Table 5.3. Vardy and Fan's one-elbow pipe system experiment; input data for simulations.

5.3. Fluid-structure interaction and cavitation

For the sake of the present investigation, experiments with both fluid-structure interaction and cavitation were performed in Vardy and Fan's straight-pipe and one-elbow systems described in the previous section. The experimental results are used, in chapter 6, to validate the combined FSI-cavitation model developed in the present work. As far as the author knows, the present experiments are the only well-documented experiments in which FSI and

cavitation occur simultaneously and are both significant[1].

5.3.1. *Straight pipe*

The cavitation experiments in Vardy and Fan's straight-pipe apparatus, see subsection 5.2.1, were performed in September 1989. If the static pressure of the water is not too high, the rod-pipe impact will lead to dynamic pressures which cause transient cavitation and column separation. The advantage of the present apparatus is that the (ordinary tap) water is stored under pressure in a closed container, so that the amount of free gas is negligible. The release of dissolved gas is negligible as well due to the time scale of the experiment (milliseconds) [Zielke et al. 1989]. The experiment isolates *vaporous* cavitation in combination with fluid-structure interaction. The way of generating transients leads to very steep wave fronts (pressure rises in microseconds) and the vapour-liquid interfaces at column separations are, in contrast to figure 3.13, believed to be nearly perpendicular to the pipe axis. Furthermore, it is noted that the column separations in closed pipe systems are small.

The amount of cavitation depends on the initial pressure of the water. Cavitation experiments were performed for five different initial pressures, and hence five levels of cavitation severity. Furthermore, the impact velocity of the rod, 0.739 m/s, has been increased to 1.122 m/s in one special experiment, in which, for the first time, Poisson coupling induced cavitation has been observed. *Poisson coupling induced cavitation* is cavitation caused by the radial expansion of the pipe wall such as associated with a compressive stress wave, or, in other words, cavitation induced by a precursor wave.

Although, in theory, the cavitation phenomena are non-linear, all but one series of tests were done with the same impact velocity of the rod (0.739 m/s).

Prior to all tests the pipe is filled with water. This is done with a garden hose connected to the municipal water supply system and the pipe finally placed in a nearly vertical position. When filled, the pipe is closed by fastening the end cap to its top. The water is slightly pressurized with the aid of a hand pump connected by a rubber hose to a small ball-valve in the end plug. A mallet is used to tap the pipe to encourage gas bubbles, possibly attached to the pipe wall, to rise to the top of the pipe. Then the water is highly pressurized and the

[1] see section 2.4

bleed screw in the end cap is carefully opened to let the free gas, accumulated at the top end, out. The procedure of tapping with a mallet at low pressure and opening the bleed screw at high pressure is repeated several times, until just water comes out of the opened bleed screw. The water is highly pressurized before the pipe is placed in its horizontal position in the suspension wires, which are attached to the ceiling in such a way that the released rod almost touches the pipe. The vertical line of each suspension wire is checked with the aid of a theodolite, and, if necessary, adjusted by changing the position of the suspension points at the ceiling. The initial pressure is obtained by depressurizing the water to the desired value. This is done through the hand pump and a calibrated (with a dead-weight tester) manometer. The valve is closed and the rubber hose of the hand pump is disconnected. The cables of the instrumentation are connected. The horizontal position ($\gamma = 0$) of the pipe is checked and adjusted, by shortening or lengthening the suspension wires, with the aid of a surveying level and a staff. The impact of the rod must be exactly in the centre of the pipe cross-section to avoid the generation of flexural waves. Therefore the difference in vertical position between the top of the pipe's impact end and the top of the released rod's end, which theoretically should be $R + e - R_r = 4.6$ mm, is checked with a dial gauge and adjusted, if necessary, by changing the pipe's vertical position via the lengths of the suspension wires. When the pipe has finally got the right horizontal and vertical position, rod and pipe must be brought in a direct line to ensure axial impact and hence to avoid, again, the occurrence of flexural waves. This is done with the aid of a theodolite and small remote-controlled magnets which bring and maintain the pipe in the right position. Rod and pipe are brought in one line prior to each test run, whereas the pipe's horizontal and vertical position are checked prior to a each series of test runs. The rod is finally raised to a fixed position, the constant height of which ensures one and the same impact velocity for all tests. The release of the rod is remote-controlled and data acquisition is triggered just before impact by the signal from an accelerometer (PCB305A05) attached to the rod. The recorded signals are directly transmitted from the data acquisition system (Microlink) to a personal computer, where they are plotted on the screen. Then it must be decided which part of the recorded signal will be stored on hard disk. For most tests the first 20 to 30 ms after impact were stored.

In the cavitation experiments pressures were measured at all five locations along the pipe. Axial strains were measured at all four locations along the pipe, at the top of the pipe cross-section. At location B (figure 5.4) the axial strains were also measured at the bottom and at

the sides of the pipe. Hoop and shear strains, which are not important if one is interested in the axial and hoop stresses only, have not been measured. The axial stress and the hoop stress are related to the pressure and the axial strain by

$$\sigma_z = E\,\varepsilon_z + \nu\,\frac{R}{e}\,P \tag{5.1}$$

$$\sigma_\phi = \frac{R}{e}\,P \tag{5.2}$$

The axial pipe-wall velocity was measured close to the impact end with the laser beam focused on a small PVC block bolted to the pipe.

Difficulties

The static pressure of the water appeared to be highly dependent on the temperature. Due to the daily changes of the temperature in the laboratory it was difficult to get test results for one and the same static pressure. Three test runs were usually performed within ten minutes of time, so that the three initial pressures were nearly the same (the ten minutes change of the laboratory temperature is sufficiently small). The time elapsed between (de)pressurizing the water and doing a next series of test runs was usually larger than ten minutes. The static pressure, as measured with the manometer on the hand pump, is therefore not valid any more. An accurate value for the initial pressure of the water is inferred from the dynamic pressure measured at the remote end (PT5), knowing that the pressure remains at the vapour pressure, which has at room temperature an almost constant value of 2 kPa (absolute, see figure 3.6), as long as a column separation exists.

The signals recorded by the pressure transducer near to the impact end (PT1 in figure 5.4) showed unrealistic pressure spikes and spurious oscillations. Signals of the other pressure transducers did not show this behaviour. Replacing PT1 by an other pressure transducer led to the same results. The violent signals recorded by PT1 are thought to be due to its location very close to the edge of the column separation occurring at the impact end. The numerous exploding and imploding cavitation bubbles in this particular area may lead to pressure signals with a frequency spectrum up to 1 MHz [Oldenziel & Teijema 1976, p. 14]. The pressure transducer's natural frequency of 80 kHz (manufacturer's value) is then too low.

Graze and Horlacher [1983] and Simpson and Bergant [1991a] reported unrealistic pressure spikes and oscillations for inductive and strain-gauge type pressure transducers and attributed these to the fact that the natural frequency of the transducer was too low. Sayir and Hausler [1991], who performed cavitation experiments in a 20 m long, 0.11 m diameter, closed tube of transparent PVC, had also problems with a too low natural frequency of piezoelectric transducers. Le Quang et al. [1989, p. 3] developed their own special transducers with a natural frequency of 1.7 MHz to overcome this problem. In the present work all signals recorded by PT1 in the cavitation experiments were filtered by a Shuman filter [Vliegenthart 1970], which smooths oscillations of the (sample-rate dependent) highest frequency. The filtered signals are believed to represent reliably the low-frequency phenomena.

Another matter to be remarked in this context is that several pressure transducers got damaged during the tests. One of them even got a hole in its diaphragm. Apparently the local, nearby explosion and implosion of small cavitation bubbles is a too severe load for the transducers [Chen & Israelachvili 1991].

5.3.2. *One-elbow pipe system*

The cavitation experiments in Vardy and Fan's one-elbow system, see subsection 5.2.2, were performed in April-May 1990. Now a needle-valve is mounted at the end plug, which explains the different masses m_1 in the tables 5.2 and 5.3. Pressures were measured at all six locations along the pipe. Axial strains were measured at all four positions around the pipe cross-section at the locations A, D and E (see figure 5.5). The bending moment is related to the axial strains by

$$M = \frac{E I_t}{2(R+e)} \{ \varepsilon_z^{(1)} - \varepsilon_z^{(3)} \} \tag{5.3}$$

where $\varepsilon_z^{(1)}$ and $\varepsilon_z^{(3)}$ are axial strains measured at opposite positions of the pipe circumference as indicated in figure 5.4. The shear force cannot be inferred from the measured axial strains. Axial pipe-wall velocities were measured near to the impact end, and, via a mirror, at the remote end.

Of the recorded signals 30 to 40 ms was stored on hard disk.

5.4. Review and conclusions

The laboratory set-ups and the measurements performed in three different pipe systems are described. The upward sloping pipe system of Simpson [1986] is used for cavitation experiments. Two closed pipe systems, a straight pipe and a system with one elbow, of Vardy and Fan [1989, 1993] are used for fluid-structure interaction (FSI) experiments. These pipe systems are also used for experiments in which the simultaneous occurrence of FSI and cavitation is evident. The latter experiments, which are described in section 5.3, form a major new element in the present study.

Experimental results were not shown in this chapter. They will be presented in the next chapter together with predictions of the various models. The input data for the calculations underlying the predictions are given in the tables 5.1, 5.2 and 5.3.

Three illustrative photographs are shown next.

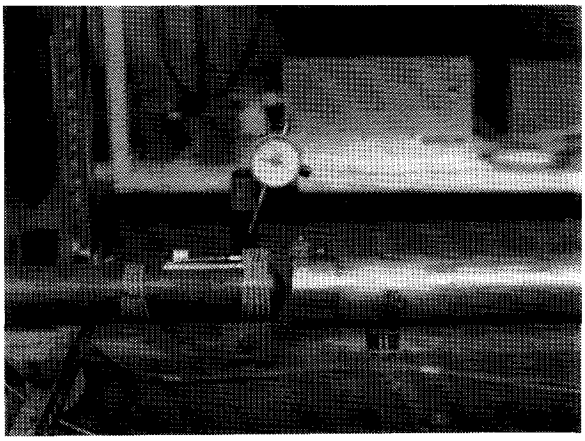

Photo 5.1. Rod (left) and pipe (right) prior to impact.

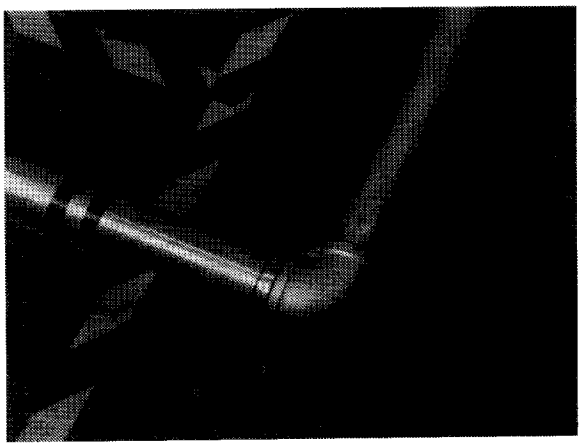

Photo 5.2. Detail of pipe, with from right to left: pressure transducer (PT2), suspension wire, remote-controlled magnets and strain gauges (SGA).

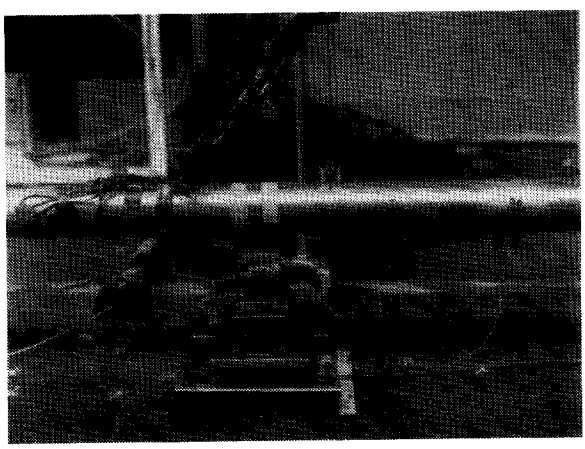

Photo 5.3. Rigid 90-degrees elbow.

6. EXPERIMENTAL AND THEORETICAL RESULTS

Experimental results obtained in the test rigs described in chapter 5 are compared with predictions from the numerical models of the chapters 3 and 4. The object of the comparison is 1) a validation of the theory underlying the predictions, and 2) a better understanding of the physical phenomena involved. A novel aspect of the experiments is the inclusion of both fluid-structure interaction (FSI) and cavitation. In particular the prediction and observation of Poisson-coupling induced cavitation is a highlight of the present work.

6.1. Cavitation

The experiment of Simpson [1986] is used to validate the concentrated cavity model of section 4.5 without the effects of FSI. It is important to know what can and what cannot be expected of the concentrated cavity model, before it is incorporated in a more complex FSI model.

Simpson's test rig, a reservoir-pipe-valve system, is described in section 5.1. Simpson performed experiments for eight different levels (1-8) of cavitation severity. Martin [1983] infers the severity of cavitation from the duration, T_{cs}, of the first, mostly largest, column separation at the valve. He introduces the cavitation severity index $S = T_{cs} c_f/(2L)$, where c_f is the pressure wave speed and L is the pipe length. Carmona et al. [1987] and Anderson et al. [1991a] propose a somewhat different index. Numerical values for the cavitation severity have not been used in the present work. Simpson increased the cavitation severity by taking higher initial velocities of the liquid, see table 5.1.

Results, viz. gauge pressure-heads at the valve, for three cavitation severity levels (2, 5 and 7) are presented in figure 6.1 as function of time, together with calculated results. Non-cavitation results, representing the case of classical waterhammer, are shown in the upper graph of figure 6.1; the results of measurement and calculation are in phase because the measured wave speed of 1280 m/s has been taken as input to the calculations. The calculated cavitation results were obtained on a conventional computational grid, not staggered, with fixed mesh-spacings Δz = 0.56 m and Δt = 0.44 ms, so that the number of elements N is 64. The decreasing amplitudes in the non-cavitation results measured give an idea of the

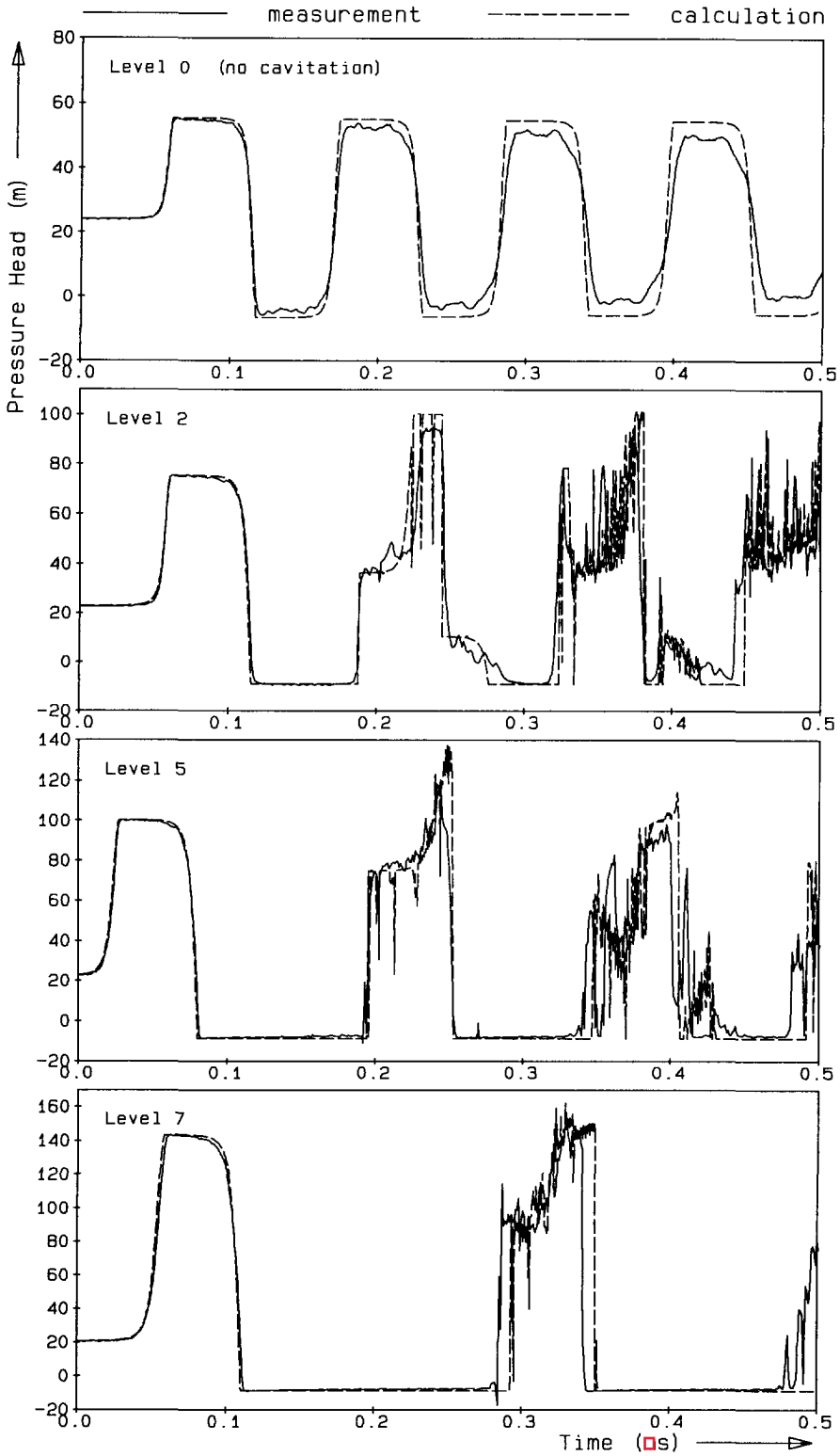

Figure 6.1. Validation of the concentrated cavity model against experimental results of Simpson [1986]. Gauge pressure-heads at valve for four different steady-state situations (table 5.1).

amount of damping in the system; FSI seems to be of less importance, since only small disturbing oscillations are observed in the recorded pressure traces.

The level 2 and level 5 graphs in figure 6.1 are typical for the concentrated cavity model; the researchers mentioned in section 2.2 show similar graphs for other pipe systems. The durations of the column separations and the magnitudes of the pressures following their collapse are predicted reasonably accurate. The amplitudes are slightly over-predicted, but this is also the case with the non-cavitation results. The calculated oscillations, already discussed in subsection 4.5.3 and inherent in the concentrated cavity model, do not occur in the measurements. The most severe case of cavitation, level 7 in the lower graph, shows a too long existence of the computed column separation. The maximum pressure is predicted accurately. Simpson [1986], who compared level 1, 3 and 8 measurements with predictions from both the concentrated cavity model and his own interface model, gives a more detailed analysis.

In conclusion it can be stated that the concentrated cavity model gives reasonable estimates of the extreme pressures, considering its simplicity. The timing of the events becomes less accurate when the cavitation becomes more severe. Non-physical oscillations of high, grid-dependent frequency, disturb the calculated results, but the low-frequency results remain valid.

6.2. Fluid-structure interaction (no cavitation)

Vardy and Fan [1989, 1993] have already shown that the present mathematical model for FSI, in combination with a numerical method based on the MOC, leads to excellent predictions of the transient behaviour of the pipe systems described in section 5.2 if cavitation does *not* occur. Their results are not reproduced in this section; in section 6.3 non-cavitation results are presented as a reference for the cavitation results. The physical phenomena in the straight-pipe system are explained in terms of axial waves travelling up and down the pipe. The individual wave fronts are clearly visible in the measured and calculated pressure histories. The situation in the one-elbow system is more complex due to the dispersive lateral waves.

6.2.1. *Straight pipe*

Krause et al. [1977] and Barez et al. [1979] hit a closed liquid-filled straight pipe with a steel sphere and use the axial strains measured near to the point of impact as input to their calculations. Strong point of Vardy and Fan's [1989] work is that, beside the geometrical and material properties, the impact velocity of the rod is the only measured input to their calculations. In fact, this is not necessary either, since the impact velocity is theoretically equal to $\sqrt{2gh_r}$, where h_r is the elevation of the rod in raised position. However, a slight deviation was observed [Fan 1989, p. 24] in practice.

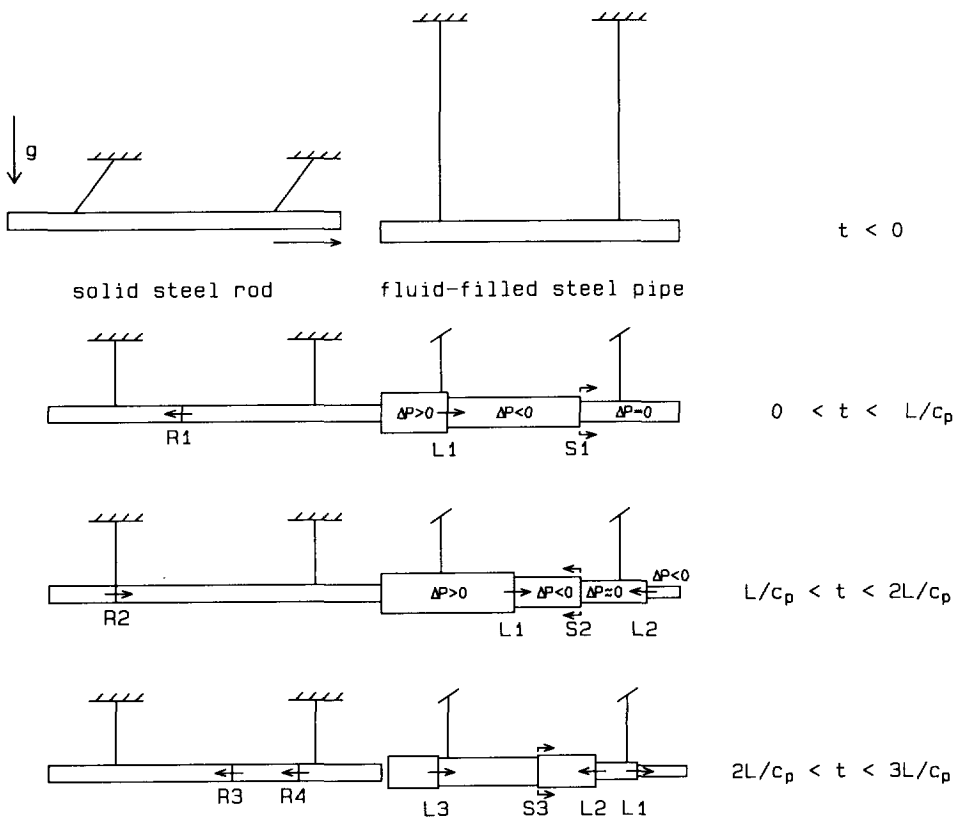

Figure 6.2. Sequence of events in straight-pipe experiment ($c_p = c_t$).

Figure 6.2 shows the sequence of events following the impact of the solid rod onto the water-filled steel pipe. The radial expansion/contraction of the pipe is portrayed in an exaggerated way. The impact generates two axial waves in the pipe: a pressure wave (L1) in the liquid and a compressive stress wave (S1) in the pipe wall. One stress wave (R1) propagates in the rod. When the stress wave, which travels 3.4 times faster than the pressure wave, reaches the remote end of the pipe, the end cap is pushed away from the liquid so that the pressure drops and a new pressure wave (L2) is generated. The reflected stress wave (S2) arrives at the impact end before its counterpart (R2) in the rod does, since the length L_r of the rod is deliberately chosen such that $L_r/c_r > L/\tilde{c}_t$. Pipe and rod separate and a third pressure wave (L3) is generated. The stress waves S3 and R3 stem from the separation, R4 is the reflection of R2.

The characteristic time scale of the experiment, $L/\tilde{c}_t$, is about 1 ms. Computed (with present numerical model) and observed (repeat of Vardy and Fan's measurements) pressures for the first 10 ms after impact are shown in figure 6.3. These pressures can best be understood from the calculated wave paths in the distance-time diagram of figure 6.4. Each wave front is associated with a jump in the pressure. The arrivals of the wave fronts in the diagram are easily recognized in the pressure traces of figure 6.3. The first pressure drop recorded at the middle of the pipe is caused by a stress wave (S1) in the pipe wall. It travels in front of the main pressure wave arriving at t = 1.7 ms and is therefore called a *precursor wave*. From the wave paths diagram it is seen that each incident wave leads to two reflected waves: one in the pipe wall and one in the liquid. This is a general rule when fluid-structure interaction is taking place at a pipe boundary.

6.2.2. *One-elbow pipe system*

Vardy and Fan [1993] conducted *non*-cavitation experiments in the one-elbow system of subsection 5.2.2. The interactions between axial and lateral waves at the elbow make, in combination with the dispersive character of the lateral waves, the situation significantly more complex than in the straight-pipe experiment. An explanation of the physical phenomena, such as in the previous subsection, has therefore not been attempted. Non-cavitation results (repeat of Vardy and Fan's measurements) are used as a reference for the cavitation results in subsection 6.3.2.

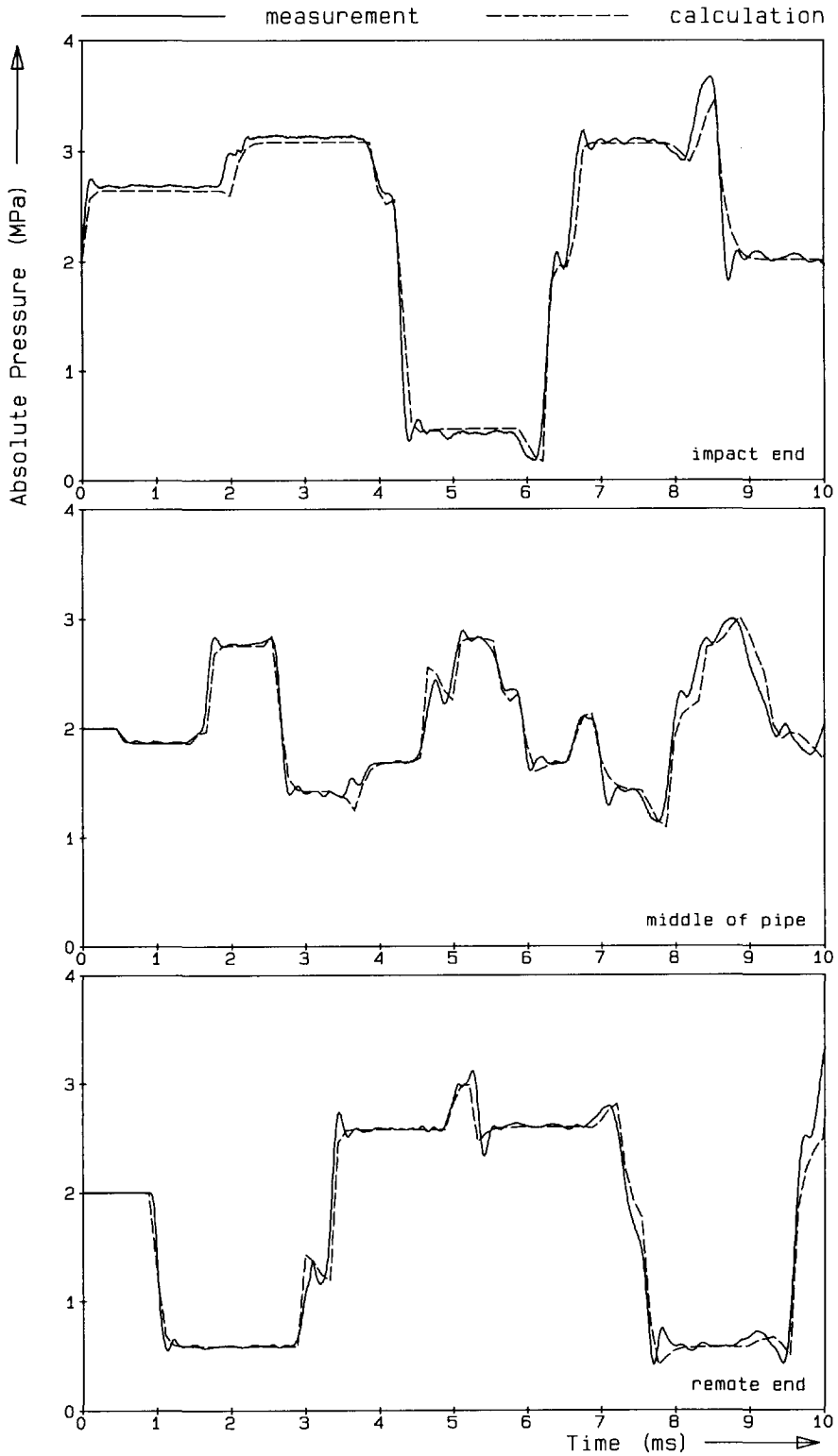

Figure 6.3. Calculated and measured pressures in straight-pipe experiment.

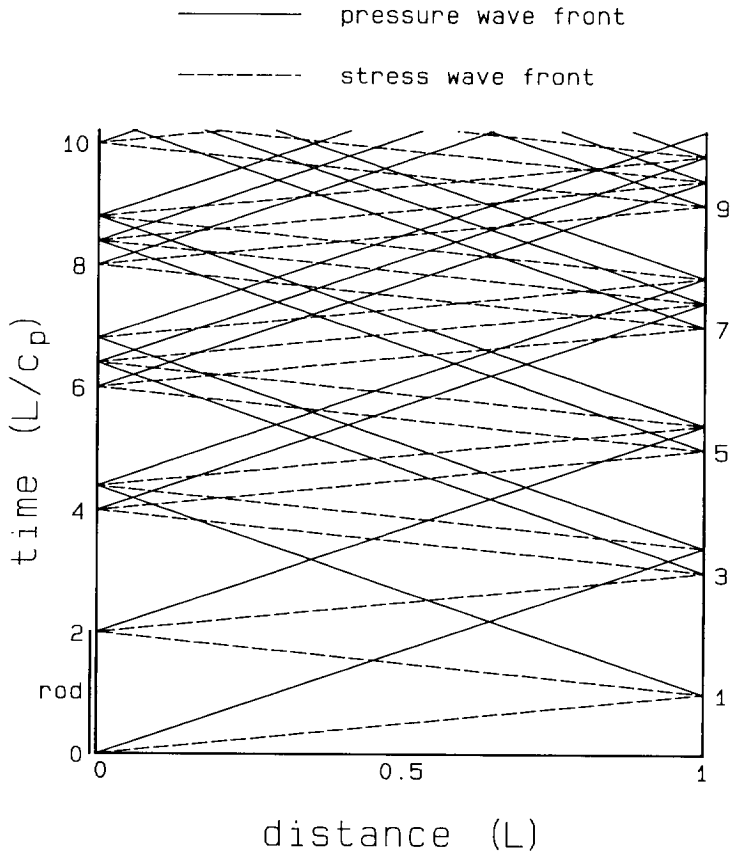

Figure 6.4. Wave paths in distance-time diagram ($c_p = \tilde{c}_t$).

6.3. Fluid-structure interaction and cavitation

Results of the cavitation experiments in Vardy and Fan's FSI test rig are compared with output from the computer codes developed by the present author. The experiments are described in the sections 5.2 and 5.3, the computer codes in section 4.9. Pressures, velocities and strains, measured at various locations along the pipe(s) for several levels of cavitation severity, are compared with calculated values. Non-cavitation results are given as a reference.

The results presented in this section form a significant selection out of the large number of experimental data obtained in about 160 successful test runs.

6.3.1. *Straight pipe*

Kot and Youngdahl [1978ab] used an apparatus similar to the present straight pipe to study transient cavitation. However, FSI was not fully included in their numerical model and measured pipe velocities were input to their calculations. In the calculations presented in this section the only measured input data are the impact velocity of the rod and the initial pressure of the liquid. Both impact velocity and initial pressure can be adjusted by the experimenter; together they define the cavitation severity. A numerical index for cavitation severity, such as given in [Fan & Tijsseling 1992], may be useful but has not been applied here.

The reproducibility of the experiments is good as regards the time of occurrence and the amplitudes of the highest pressure peaks [Fan & Tijsseling 1992]. High-frequency oscillations due to collapsing vapour bubbles are not reproducible.

The numerical results shown in this subsection were obtained with the SINGLECS-code, which is based on the computational grid of figure 4.7. The number of elements used is 150, so that Δz = 0.03 m and Δt = 0.11 ms. The ratio of wave speeds $\bar{c}_t/\bar{c}_F$ is taken exactly equal to 17/5 through an adjustment of the mass densities of liquid and pipe wall (subsection 4.2.7). The input data are given in table 5.2. The densities ρ_f and ρ_t were changed into ρ_f^* = 999 kg/m^3 and ρ_t^* = 8039 kg/m^3 leading to a pressure wave speed $\bar{c}_F^* \approx$ 1354 m/s and an axial stress wave speed $\bar{c}_t^* \approx$ 4602 m/s in the simulations. The characteristic time scales are $L/\bar{c}_t^* \approx$ 1 ms and $L/\bar{c}_F^* \approx$ 3.4 ms.

Measured and calculated pressure histories for five different levels of cavitation severity are shown in the figures 6.5, 6.6 and 6.7. Non-cavitation results are shown in the upper frames. The cavitation severity increases, when the static pressure in the pipe, given in the bottom right corner of each frame, decreases. The lowest static pressure in the experiments performed is close to the atmospheric pressure of 0.1 MPa. The vapour pressure of water, which is about 0.002 MPa at room temperature, is negligible with respect to the dynamic pressures. In the following, cavitation at the pipe ends will be referred to as column separation.

In figure 6.5 pressures near to the impact end are presented. A static pressure of 2 MPa is sufficiently high to prevent cavitation; the dynamic pressures remain above the zero-line, which is the bottom level for the calculated absolute pressures. The agreement between

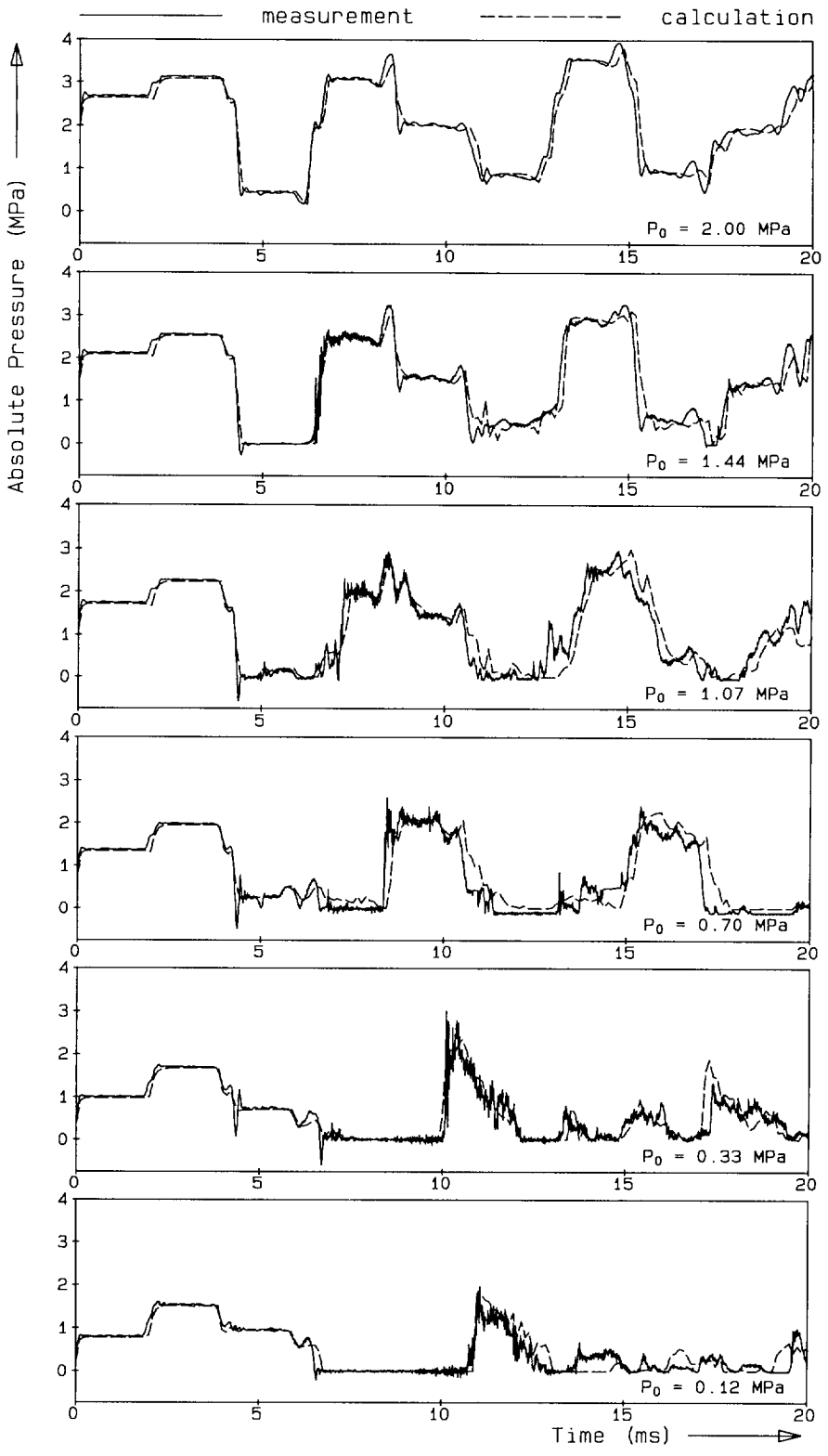

Figure 6.5. Measured and calculated pressures near to impact end in straight-pipe experiment.

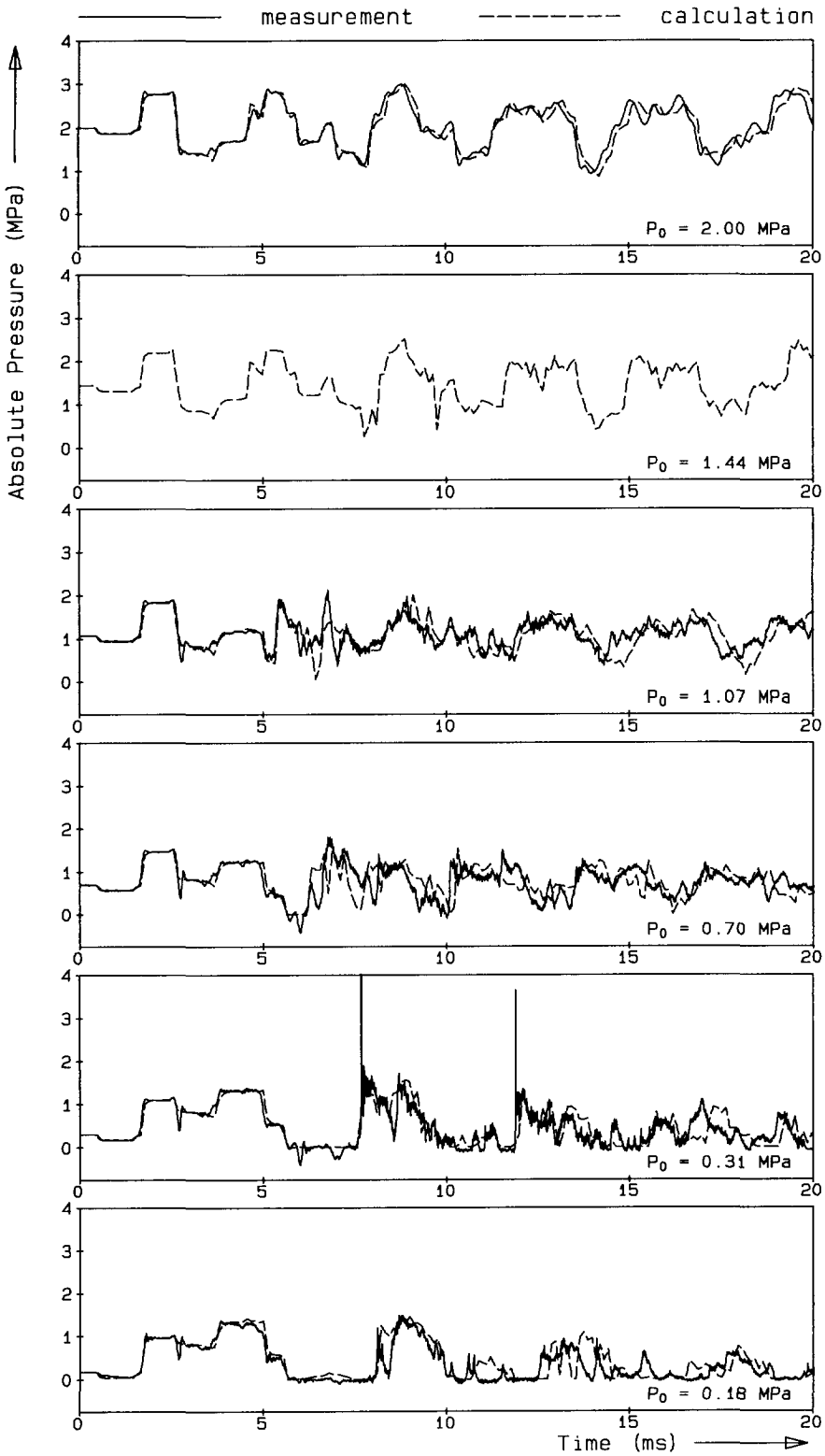

Figure 6.6. Measured and calculated pressures at pipe middle in straight-pipe experiment.

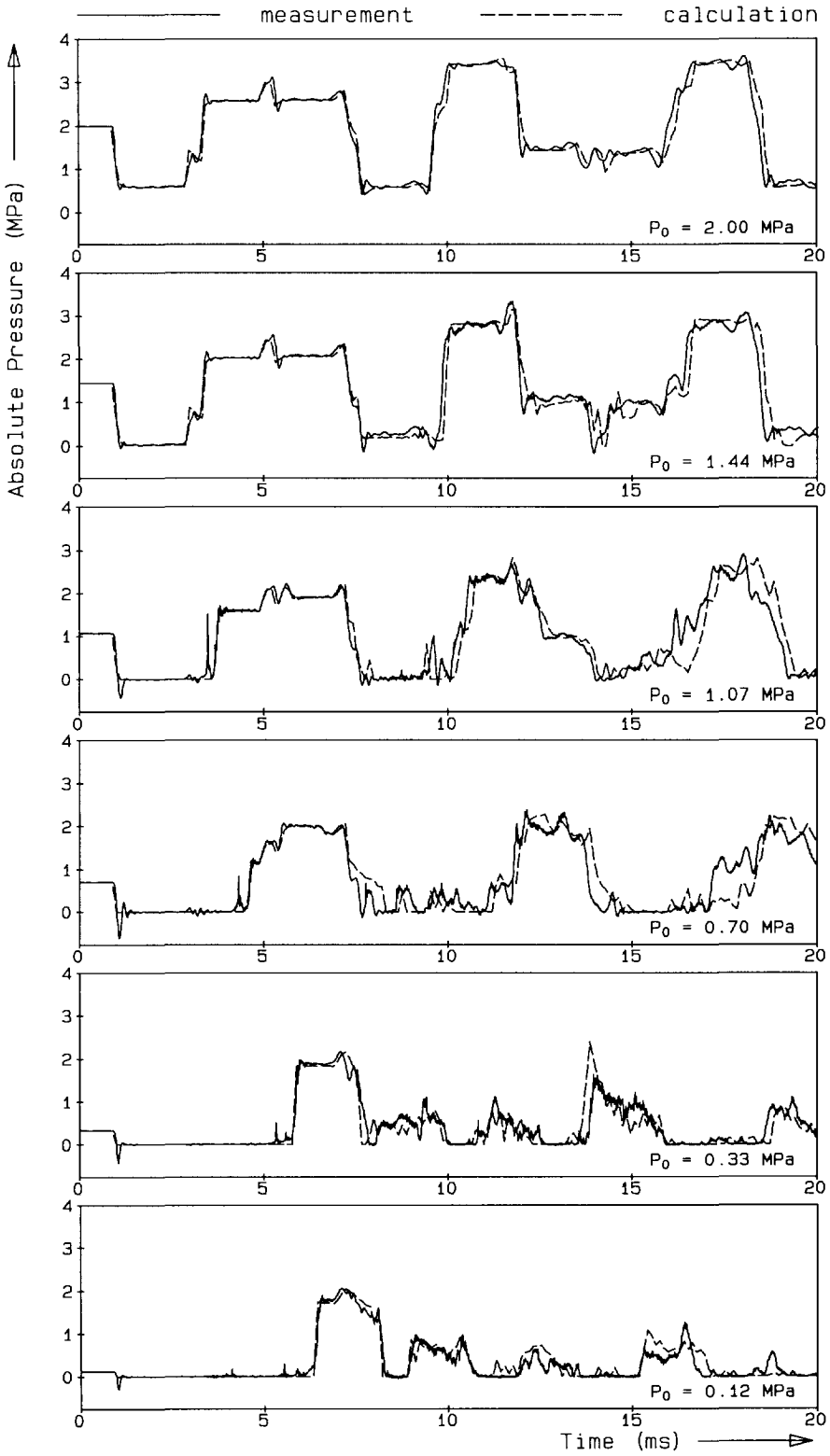

Figure 6.7. Measured and calculated pressures at remote end in straight-pipe experiment.

measurement and calculation is excellent, see also subsection 6.2.1. An initial pressure of 1.44 MPa, in combination with a rod impact velocity of 0.739 m/s, is too low to prevent cavitation. From a comparison with the non-cavitation results in the upper frame, it is seen that column separation occurs about 4.5 ms after impact. The pressure remains at the zero-line until, about 6 ms after impact, the cavity collapses. High-frequency small-amplitude oscillations are then observed in the measured signal, possibly due to local vapour bubbles collapsing under the high pressure (see also section 5.3). Note that the time scale is milliseconds and that the events are strongly dynamic. Since there is only a small amount of cavitation, the P_0 = 1.44 MPa results resemble the non-cavitation results. The agreement between measurement and calculation is still excellent. When the initial pressure is 1.07 MPa, the occurrence of cavitation is more evident. Nevertheless, the agreement between numerical simulation and physical experiment is very good. In the P_0 = 0.70 MPa results the recorded pressure traces have small negative values, when the calculation predicts column separations. This must be a measuring error. A loose contact in the connection of the cables to the pressure transducers is the most likely cause; these had to be checked regularly. Simpson and Bergant [1991a] report a drift in the measured signals when moisture affected their electrical equipment. The two bottom frames give the most severe cases of cavitation. The agreement between measurement and calculation is amazingly good considering the complexity of the phenomena and the simplicity of the cavitation model.

The pressures at the middle of the pipe are shown in figure 6.6. Due to a damaged pressure transducer, $P_0 \approx$ 1.44 MPa measurements are not available. For the same reason the lower two graphs have different initial pressures from the corresponding graphs in the figures 6.5 and 6.7. The two pressure spikes in the P_0 = 0.31 MPa results are unrealistic and can be attributed, again, to a loose contact. The impact of the solid steel rod is an extremely heavy load for the attached instrumentation. The agreement between experiment and simulation goes from excellent for the non-cavitation case to satisfactory in the most severe cavitation cases.

The pressures measured and calculated at the remote end (figure 6.7) are the most interesting ones, since this is the place where the largest column separations occur. The non-cavitation results are explained in subsection 6.2.1. For P_0 = 1.44 MPa the first pressure drop, after about 1 ms, is too small to cause a column separation at the remote end; for this case the first column separation occurs at the impact end. For the other four cases (i.e.

P_0 = 1.07 MPa and lower) the first column separation is at the remote end. Their durations increase with decreasing initial pressures. The pressure rises after the collapse of the first column separations are predicted accurately by the present numerical model, because the early events are dominated by the column separations at the pipe ends. Later on, when distributed cavitation occurs in the interior of the pipe, the predictions become less accurate. For example, in the P_0 = 0.33 MPa case a too high pressure peak is predicted about 14 ms after impact. The most severe cavitation case in the lowest frame shows one high pressure peak, all subsequent peaks are substantially lower. After 20 ms high peaks did not occur either.

The overall agreement between the measured and calculated pressures is very good. Numerical oscillations as observed in the simulation of Simpson's experiment (figure 6.1) are absent. This is thought to be due to the relatively large numerical time step of 0.11 ms used in the calculations. Results obtained with the SINGALT-code, which is based on the computational grid of figure 4.8, exhibited more high-frequency oscillations.

Tensile stresses

Davies et al. [1956] used an apparatus resembling the present one to determine the tensile strength of water; transient pressures were generated by firing a bullet at a closed pipe's end. They included junction coupling effects in their analysis. Tensile stresses in liquids, already described by Huygens [Rouse & Ince 1963, p. 80], are identified here as short-duration negative pressures tearing the liquid before it separates from the solid end pieces. For example, in the P_0 = 1.07 MPa case of figure 6.7 the pressure drop after 1 ms is initially of the same magnitude as in the non-cavitation case. The absolute pressure then becomes negative, so that a tensile stress exists in the liquid. The liquid sustains this tensile stress for a short period of time, about 0.15 ms, before it begins to cavitate and the pressure becomes equal to the vapour pressure. Large tensile stresses, up to 0.7 MPa, are observed only preceding the first occurrence of cavitation and, in particular, of a column separation. Later on the cavitation susceptibility [Oldenziel 1982a] is sufficiently high to prevent large tensile stresses. Oldenziel [1982a], who performed quasi-static tests, finds for ordinary tap water a tensile strength of 0.12 MPa. It should be remarked that column separation in the present experiment can be compared to the breaking of a solid rod (this analogy was already

described by Galilei [Rouse & Ince 1963, p. 57]). A more thorough treatise of the tensile strength of liquids is given by Plesset [1969], Overton et al. [1984] and Trevena [1984].

Axial pipe wall velocities, measured and calculated near to the impact end, are shown in figure 6.8. If the dynamic pressure at the impact end is above the vapour pressure, liquid and end plug are in contact, so that the local liquid velocity is equal to the velocity of the plug. Hence, the axial pipe wall velocities measured close to the end plug give an indirect indication of the convective velocities in the liquid. From theory and experiment [Fan 1989, p. 42; Vardy & Fan 1989] it is known that the response of an empty (air-filled) pipe to axial rod impact consists of two rises in the velocity, one at $t = 0$ ms and one at $t = 2L/\bar{c}_t \approx$ 2 ms. After the second rise the pipe maintains a constant velocity. Here the velocity response of the pipe is more whimsical due to the interaction with the pressure waves in the liquid. The amount of cavitation affects the response of the pipe. Roughly one can say that the frequency of the major oscillations tends to increase with the cavitation severity. The magnitude of the second velocity rise, at $t \approx 2$ ms, increases with a decreasing initial pressure, because a smaller pressure drop at the remote end (figure 6.7), at $t \approx 1$ ms, makes it easier for the end cap to move away from the liquid (see stress wave S1 and its reflection S2 in figure 6.2). A higher second rise in velocity results also in a higher second rise in pressure as can be seen in figure 6.5. The agreement between measurement and calculation is of the same degree as in the pressure histories of the figures 6.5, 6.6 and 6.7.

The axial strain histories in the figures 6.9 and 6.10 demonstrate that the rod impact is the most severe load for the pipe wall. A strong compressive stress wave (S1) travels up and down the pipe as sketched in figure 6.2. When pipe and rod separate after about 2 ms, the pipe has two free ends. In an empty (air-filled) pipe the strain then remains zero [Fan 1989, p. 42], since the pipe ends are stress-free. In a liquid-filled pipe pressure waves and collapsing column separations excite the pipe wall. The dynamic strains in the figures 6.9 and 6.10, which were measured at about 0.57 m from the impact end and the remote end respectively, oscillate around the zero level. The magnitude of the first and largest strain drop in figure 6.10 is, both in experiment and calculation, smaller than the corresponding drop in figure 6.9. Except for the first positive strain peaks, the agreement between measurements and calculations is good.

One observation to be mentioned concerns audible sound. The sound generated by the rod impact is less dull when the amount of cavitation is larger.

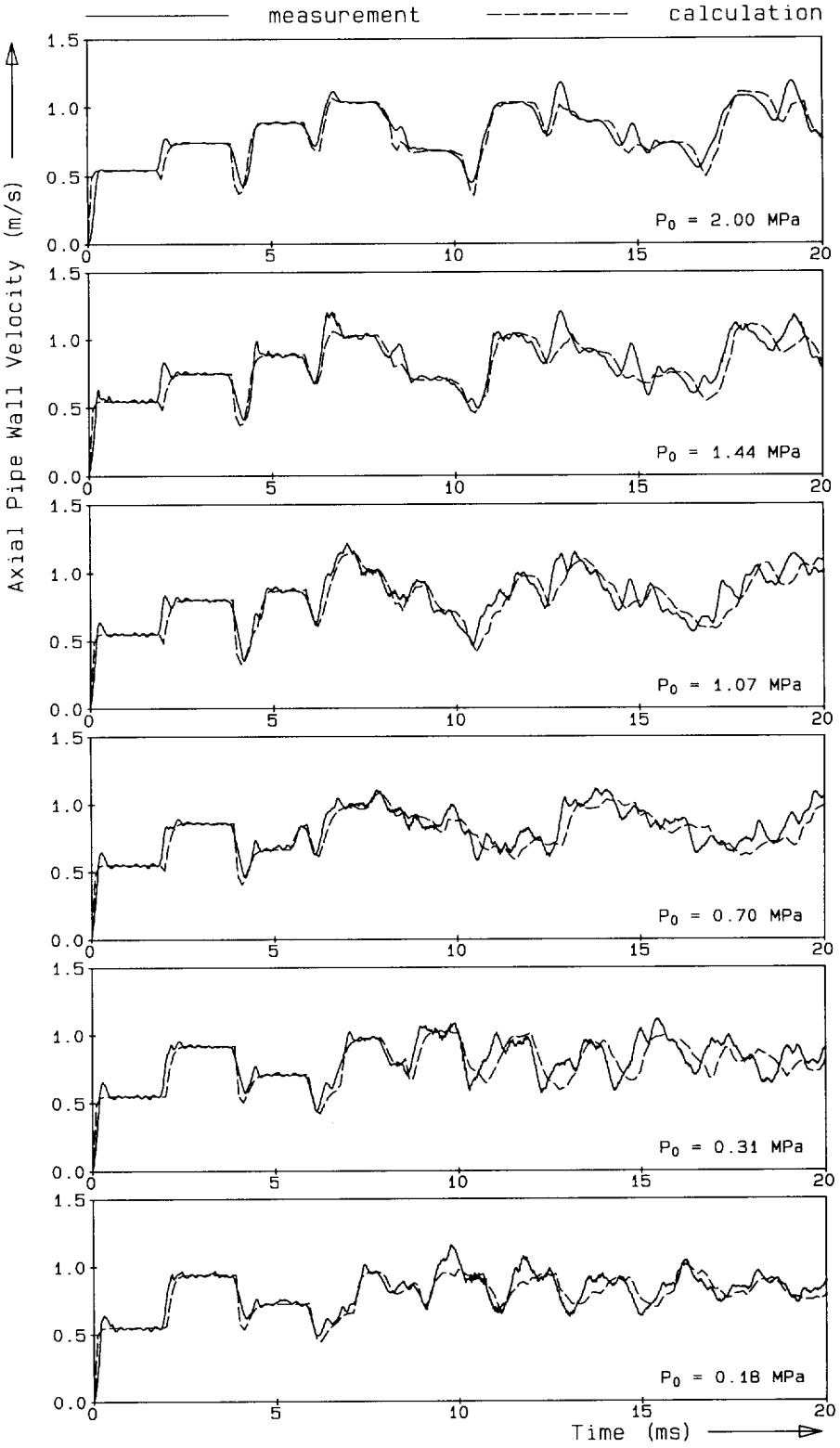

Figure 6.8. Measured and calculated axial pipe-wall velocities near to impact end in straight-pipe experiment.

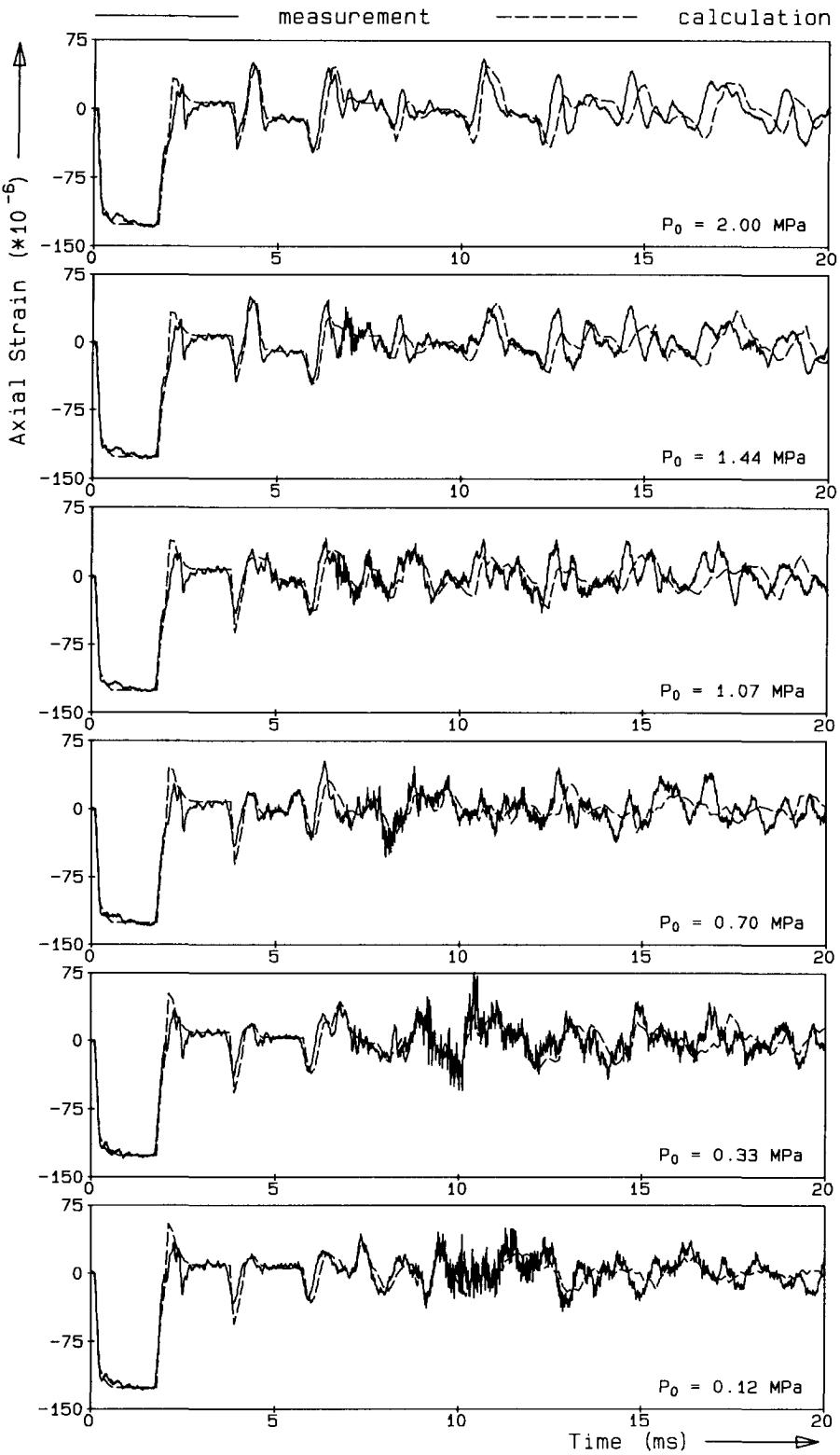

Figure 6.9. Measured and calculated axial strains at 0.57 m from impact end in straight-pipe experiment.

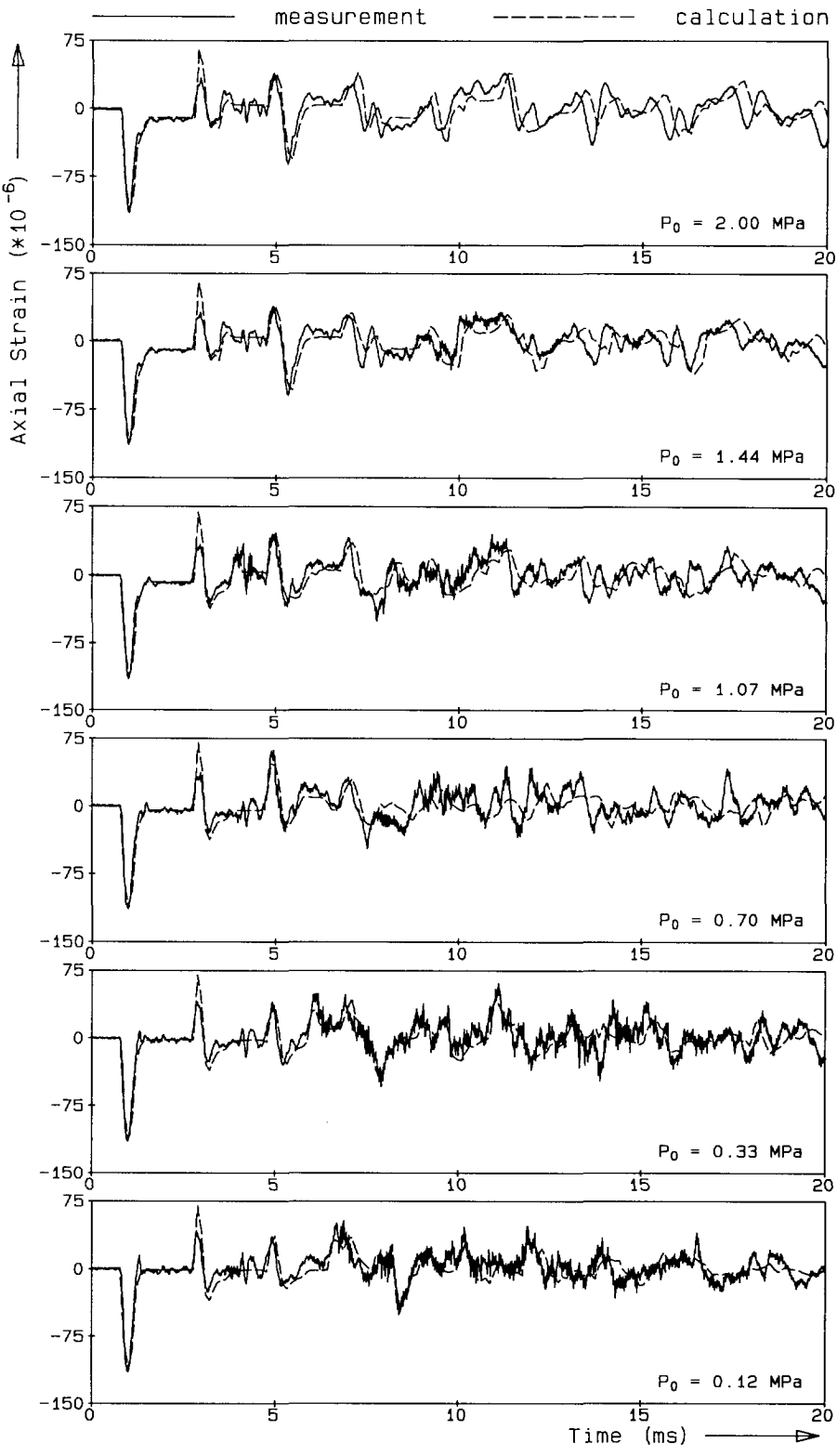

Figure 6.10. Measured and calculated axial strains at 0.57 m from remote end in straight-pipe experiment.

Poisson-coupling induced cavitation

The compressive stress wave S1 in figure 6.2 is accompanied with a pressure drop in the fluid due to the pipe wall's radial expansion. Since the pressure drop travels with the speed of the stress wave, it is called a *precursor wave*. See also subsection 1.1.4. The precursor wave arrives at the middle of the pipe 0.5 ms after impact, as can be seen from figure 6.6; the associated drop in pressure lasts for about 1 ms.

When a precursor wave causes cavitation, it is referred to as *Poisson-coupling induced cavitation*. In the experiment considered sofar, the precursor wave causes a pressure drop of 0.14 MPa. This drop is too small to induce cavitation in the cases shown in figure 6.6. The cases in the lowest graphs of the figures 6.5 and 6.7 correspond to an initial pressure of 0.12 MPa, or more accurately 0.125 MPa, so that, in theory, Poisson-coupling induced cavitation should occur. However, there is no experimental evidence that it actually does. Possibly the precursor pressure-drop is still too small to surmount the threshold of cavitation inception.

To obtain a significant amount of Poisson-coupling induced cavitation the impact velocity of the rod has been increased to 1.122 m/s, which is about 1.5 times the previous value. The precursor-wave pressure-drop is then about 0.21 MPa. With a static initial pressure of 0.11 MPa, this pressure drop is sufficiently high to cause the desired cavitation by radial pipe motion. Figure 6.11, where measured and calculated pressures at four locations along the pipe are presented, is, to the author's knowledge, the first record of Poisson-coupling induced cavitation. In the upper graph the oscillations of the pressure during the first two milliseconds indicate that there is cavitation right from the beginning, both in experiment and calculation. The pressure wave L1 in figure 6.2 is entering a distributed cavitation zone which has been generated by the precursor wave. This can be inferred from the middle two graphs where the first pressure drop, which would have been 0.21 MPa in the non-cavitation case, generates vapour bubbles either in the liquid or at the solid-liquid interface of the pipe wall.

The collapse of the column separation at the remote end gives now a high pressure rise of 3 MPa. The pressure histories at the impact end and at the remote end are similar to the P_0 = 0.12 MPa case in the figures 6.5 and 6.7, respectively. As opposed to the non-linear cavitation model, the experimental results seem to exhibit linearity with here a multiplication factor 1.5. It is remarked that the first 8 ms the phenomena are dominated by column separations at the pipe ends [Tijsseling & Fan 1992], so that distributed cavitation is of minor importance. The agreement between experiment and simulation is, again, amazingly good.

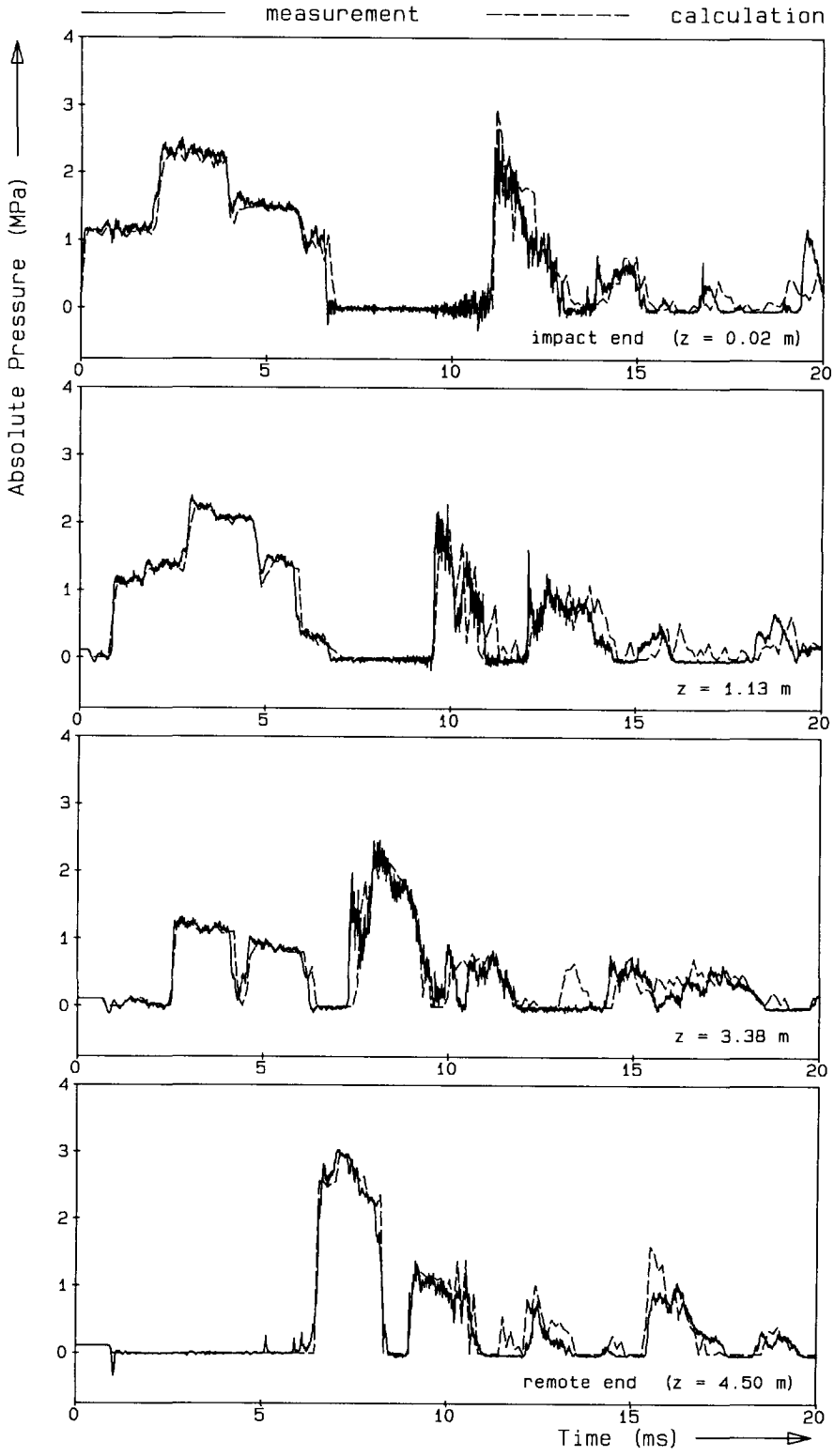

Figure 6.11. Measured and calculated pressures in straight-pipe experiment with increased rod-pipe impact velocity. (Poisson-coupling induced cavitation.)

Poisson-coupling induced cavitation is predicted and observed, but its effects seem to be of less importance.

6.3.2. *One-elbow pipe system*

The one-elbow system and the experiments performed are described in the subsections 5.2.2 and 5.3.2. The main difference with the straight-pipe system is in the occurrence of lateral waves. These are generated at the elbow. The dispersive character of the lateral waves, the interactions between axial and lateral waves at the elbow, and the formation of column separations at the elbow, make the situation significantly more complex than in the straight-pipe experiment. Consequently, the computations are more complex. Lateral wave propagation is, with the present numerical model, more difficult to calculate than axial wave propagation, as discussed in subsection 4.10.2. Furthermore, the simple elbow plus column-separation model of the subsections 4.7.7 and 4.7.8 is new and has to be validated.

The numerical results presented in this subsection were obtained with the DOUBLE-code, which is based on the computational grid of figure 4.8. Four independent grids, two for each pipe (one for axial motion and one for lateral motion), are used in the calculations. The grids are coupled at the elbow. The grid properties and ρ-adjustments, to avoid interpolations, are given in table 6.1.

	N	Δz (m)	Δt (μs)	$\tilde{c}_t^* / \tilde{c}_F^*$ (-)	c_b^* / c_s^* (-)	ρ_f^* ρ_t^* (kg/m^3)	$\Delta\rho_f/\rho_f$ $\Delta\rho_t/\rho_t$ (%)	i_{OUT}
axial motion of long pipe	138	0.033	7.1/5	17/5	-	999 8036	-0.0 +0.6	40
axial motion of short pipe	41	0.033	7.1/5	17/5	-	998 8035	-0.1 +0.6	40
lateral motion of long pipe	138	0.033	7.1/5	-	13/5	1006 7929	+0.7 -0.7	40
lateral motion of short pipe	41	0.033	7.1/5	-	13/5	1006 7929	+0.7 -0.7	40

Table 6.1. Properties of the four independent grids.

The number of elements ratio N_1/N_2 = 138/41 corresponds to the pipe-length ratio L_1/L_2 = 3.366. The adjustments in the mass densities are then less than 1%. The small numerical time step, 1.42 μs, leads, with a simulation time of 20 ms, to huge output files. For practical reasons, computed results were written to an output file every 40 (i_{OUT}) time steps.

The geometrical and material properties of the elbow system are given in table 5.3. The changed mass densities in table 6.1 lead to the following propagation speeds for the pressure, the axial stress, the shear and the bending waves, respectively: $\bar{c}_F^*$ = 1354 (1354) m/s, $\bar{c}_t^*$ = 4603 (4618) m/s, c_s^* = 1770 (1768) m/s and c_b^* = 4603 (4587) m/s, where the numbers in brackets are the original values. The shear and bending waves are highly dispersive; the c_s^* and c_b^* values represent the speeds of their leading edges. See also the subsections 4.3.3 and 4.3.4. The main time-scales for the axial waves are: T_1 = $(L_1 + L_2)/\bar{c}_F \approx$ 4.3 ms, T_2 = $L_1/\bar{c}_F \approx$ 3.4 ms, T_3 = $(L_1 + L_2)/\bar{c}_t \approx$ 1.3 ms, T_4 = $L_2/\bar{c}_F \approx$ 1 ms, T_5 = $L_1/\bar{c}_t \approx$ 1 ms and T_6 = $L_2/\bar{c}_t \approx$ 0.3 ms. The mass of the elbow (see subsection 5.2.2) is neglected, the masses of the end pieces are maintained in the calculations of the axial motions.

The reproducibility of the experiments is examined in figure 6.12. Dynamic pressures measured at the remote end in two successive experimental runs, the second run about five minutes later than the first run, are compared. The non-cavitation experiment in the upper graph shows excellent reproducibility. In the cavitation experiments for P_0 = 1.24 MPa and P_0 = 0.87 MPa the reproducibility is less. This is due to a slightly increased static pressure in the second run resulting from a small change in the laboratory temperature (see subsection 5.3.1). In the P_0 = 0.30 MPa experiment in the bottom graph, the initial static pressure in the two runs is practically the same. The time of occurrence and the magnitude of the first and highest pressure peak are highly reproducible. The subsequent pressure peaks are less reproducible, possibly due to the large amount of cavitation. For the purpose of the present work the level of reproducibility is considered to be sufficient.

The impact velocity of the rod in the elbow-system experiment is about 10% higher than in the straight-pipe experiment. Accordingly, the initial jumps in pressure, velocity and strain at the impact end are about 10% higher as well.

Measured and calculated pressures near to the impact end (PT1), close to the elbow (PT5) and at the remote end (PT6) are shown in the figures 6.13, 6.14 and 6.15, respectively. The non-cavitation results in the upper graphs are considered first. The second pressure rise at the impact end (figure 6.13) is, when compared to the straight-pipe experiment (figure 6.5),

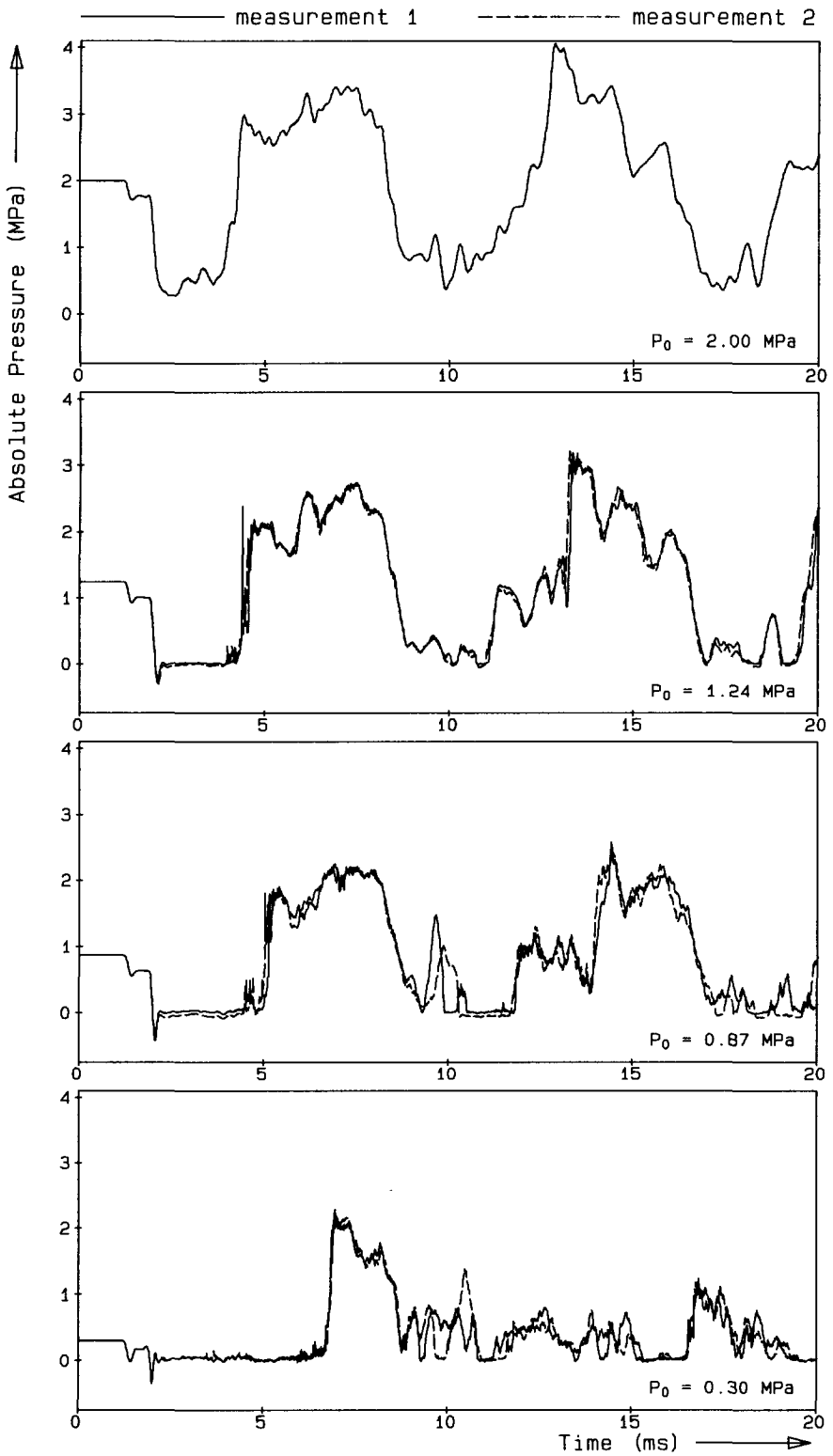

Figure 6.12. Reproducibility of one-elbow pipe-system experiments; pressures at remote end.

more rounded, because the axial motion of the long pipe is retarded at the elbow by the lateral inertia forces in the short pipe. The pressure history close to the elbow (figure 6.14) is the most interesting one, since the interactions between axial and lateral waves take place here. It is difficult to make a correct wave paths diagram in the distance-time plane, because of the dispersive character, and hence non-constant propagation speeds, of the lateral waves. Therefore only a few early-time main effects are explained next.

The arrival of the compressive stress wave (S1) at the elbow, about 1 ms after impact, causes a pressure drop of 0.7 MPa (figure 6.14, top frame) which is substantially lower than in the straight-pipe experiment (figure 6.7). The pressure drop leads to an unbalanced force in the short pipe, which makes the remote end move away from the liquid. This happens about 1.3 ms after impact, as can be inferred from the first pressure drop in figure 6.15. The low-pressure wave generated at the elbow arrives and reflects at the remote end 2.0 ms after impact, giving a total pressure drop of about 1.7 MPa relative to the initial pressure (figure 6.15, top frame). It is this pressure drop that causes the first column separation when the initial pressure is 1.24 MPa and 0.87 MPa. In the P_0 = 0.30 MPa case, the first column separation occurs at the elbow. After 3.4 ms the initial pressure wave (L1) generated by the rod impact reaches the elbow. The pressure rise at the elbow causes a large unbalanced force in the short pipe which makes, 3.7 ms after impact, the end cap move in the direction of the fluid thereby increasing the pressure (figure 6.15, top frame). The original pressure wave (L1), as transmitted at the elbow, arrives at t = 4.4 ms at the remote end, thereby raising the pressure over the initial value of 2 MPa (figure 6.15, top frame).

The agreement between experiment and numerical simulation is, in view of the complexity of the phenomena, good in the non-cavitation case. The first 12 to 15 milliseconds in the cavitation experiments are predicted rather accurately. Later on, the agreement between experiment and prediction becomes much less. In particular, the P_0 = 0.30 MPa simulation shows cavitation (P = 0 MPa) where the experiment does not. A possible reason is a too simple model for column separation at the elbow. Another plausible reason is in the generation of distributed cavitation by lateral pipe accelerations, which cannot be simulated with the present one-dimensional model.

Axial pipe-wall velocities measured and calculated near to the impact end are shown in figure 6.16. The shape of the velocity traces during the first four milliseconds corresponds to the shape of the pressure traces in figure 6.13. This confirms the junction coupling phenomenon: the axial motion of the pipe end generates pressure waves in the liquid. The overall agreement between measurement and calculation is good, even for the cavitation

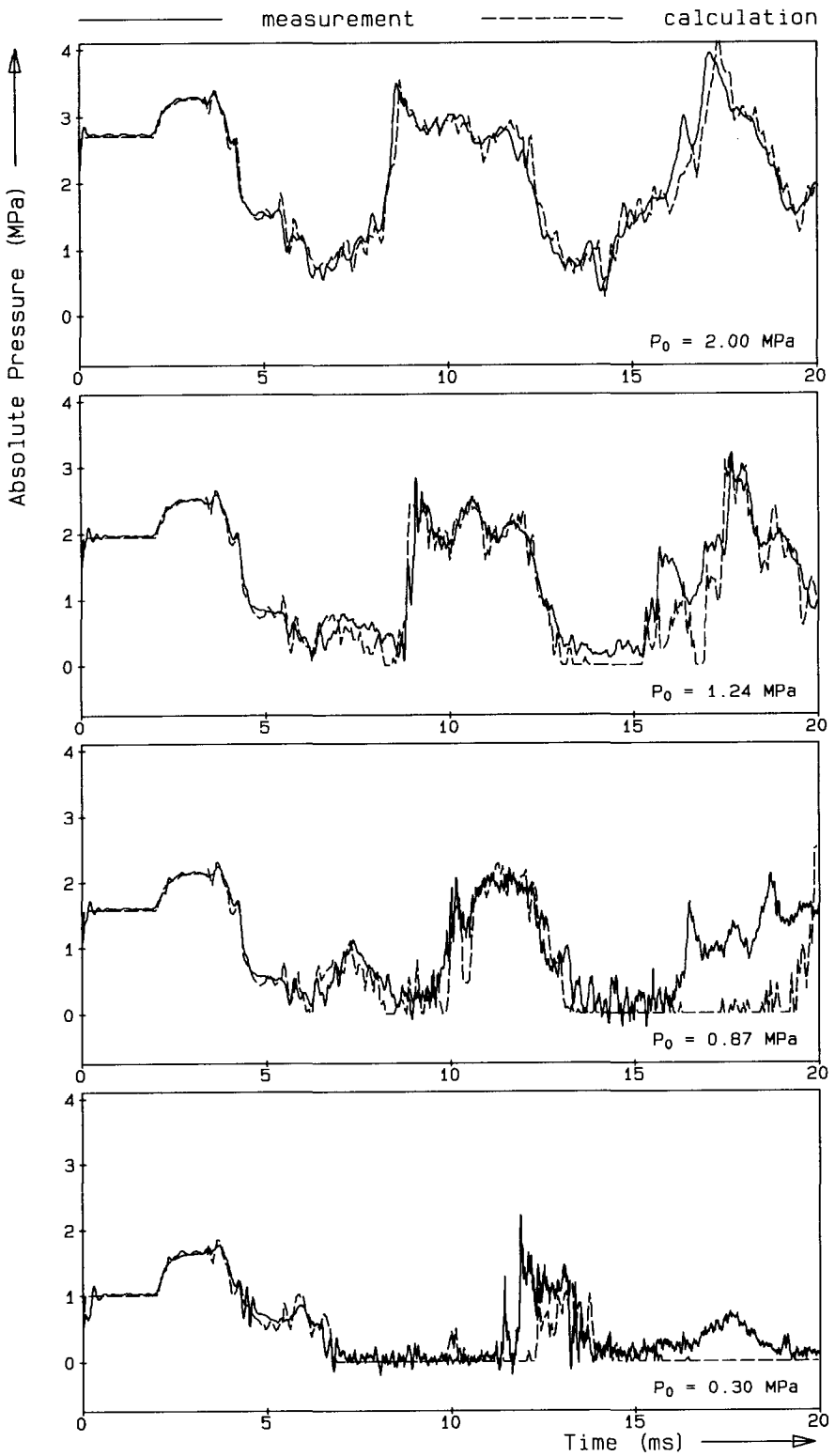

Figure 6.13. Measured and calculated pressures near to impact end in one-elbow pipe-system experiment.

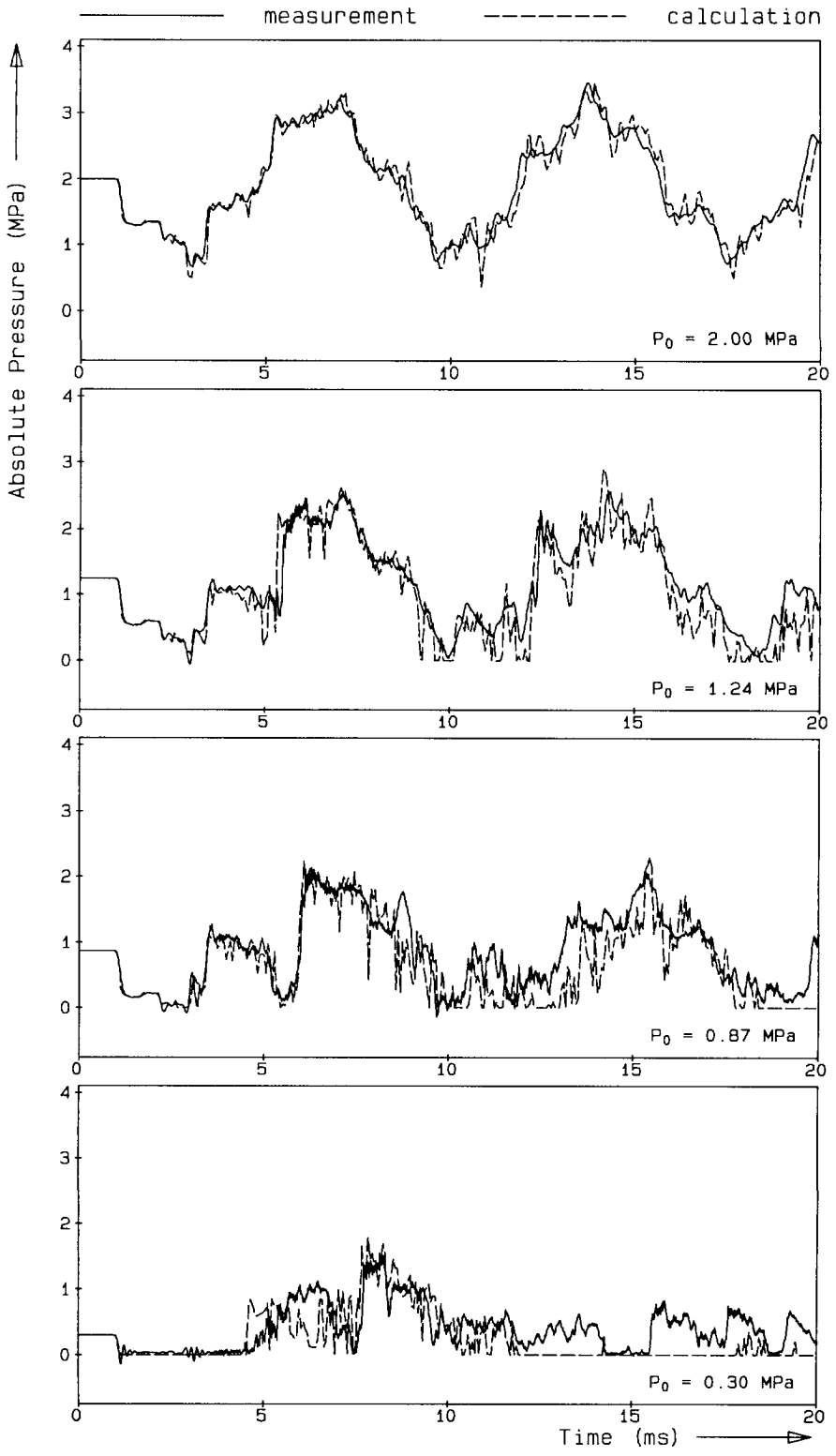

Figure 6.14. Measured and calculated pressures close to elbow in one-elbow pipe-system experiment.

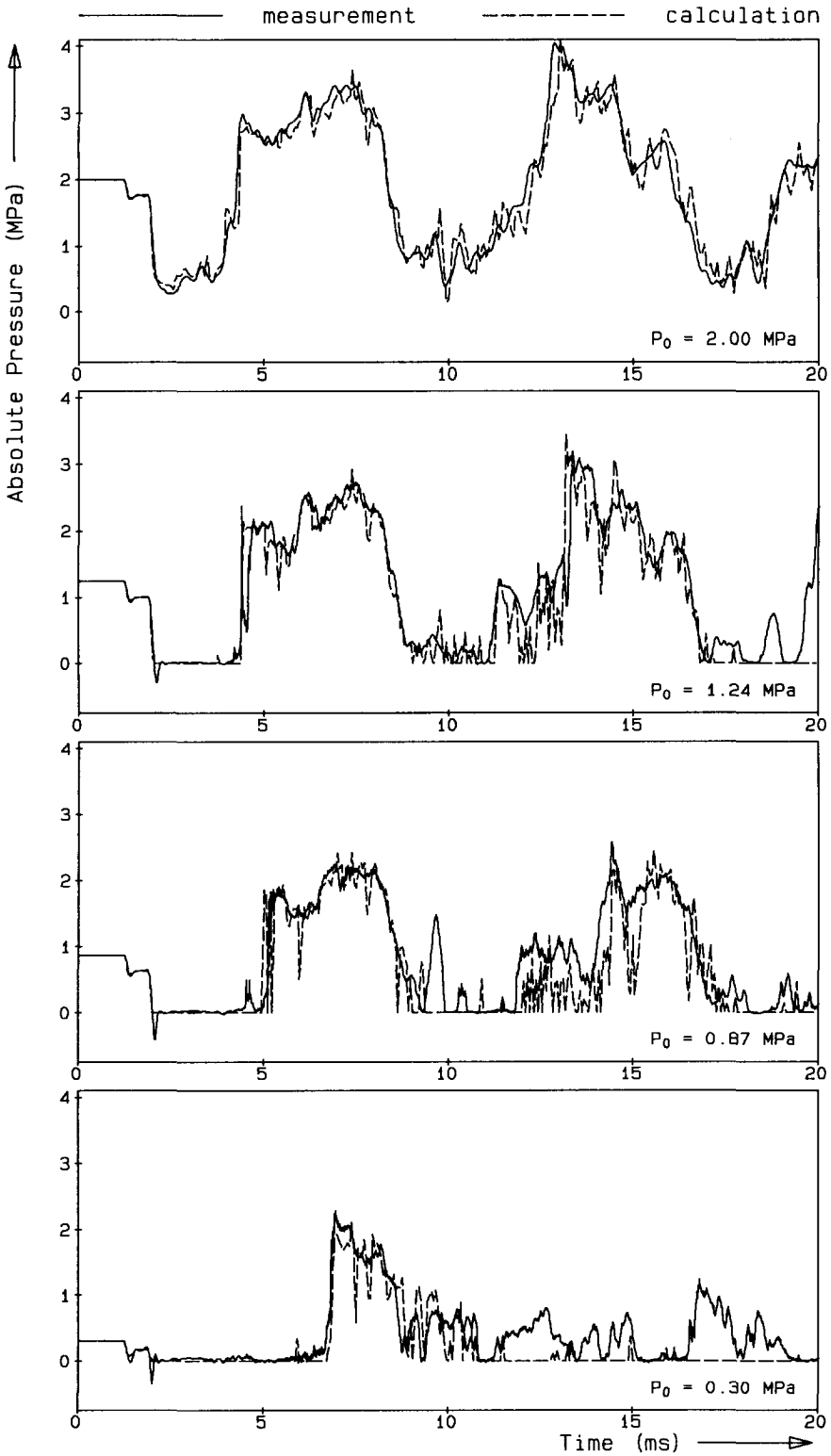

Figure 6.15. Measured and calculated pressures at remote end in one-elbow pipe-system experiment.

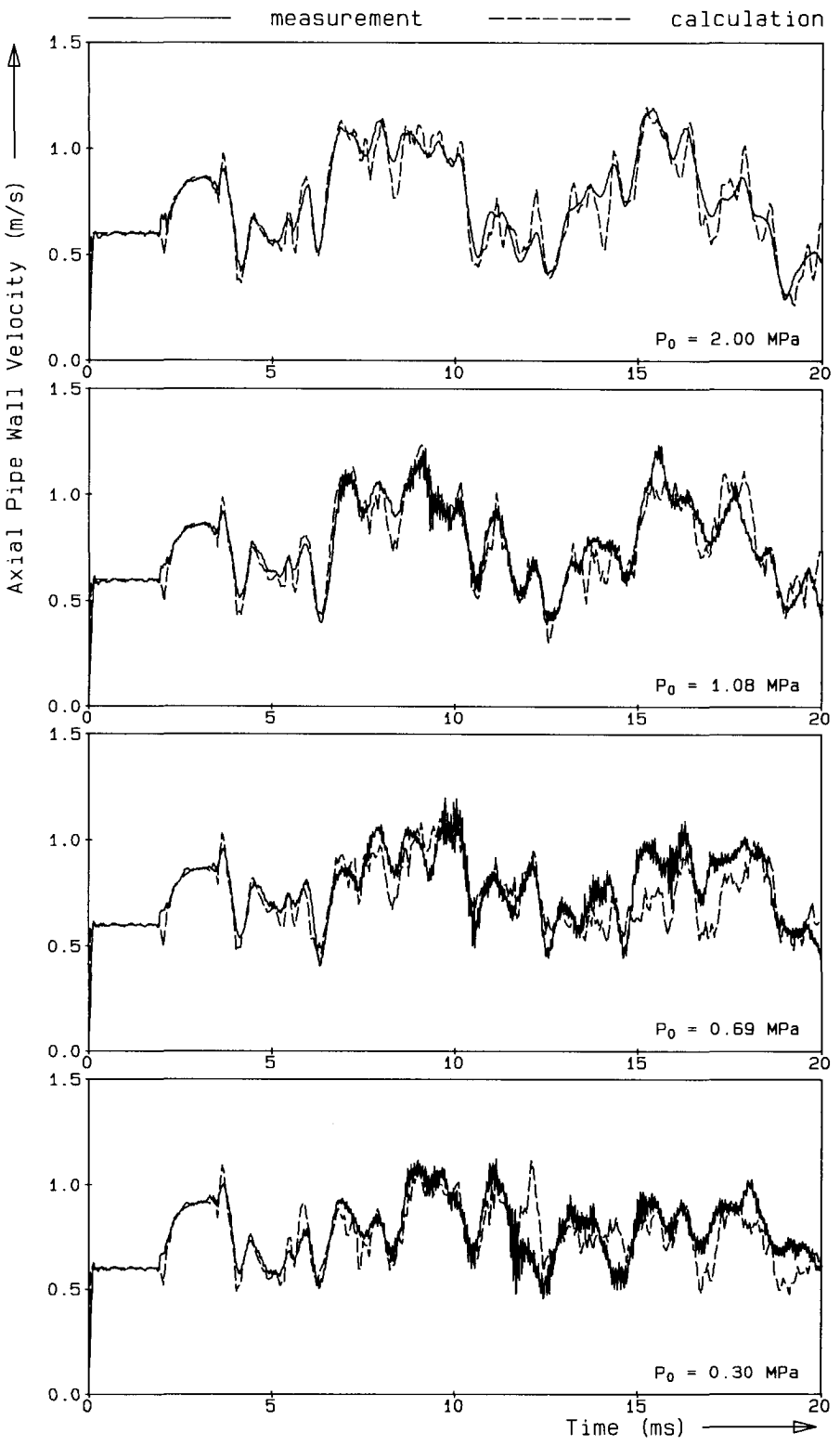

Figure 6.16. Measured and calculated axial pipe-wall velocities near to impact end in one-elbow pipe-system experiment.

experiments. The calculated, but not observed, peak after 12 ms in the P_0 = 0.30 MPa experiment corresponds to the mismatch in time of occurrence and magnitude of the pressure rise caused by the collapse of the first column separation at the impact end in figure 6.13.

Axial strains, measured and calculated at position A on the long pipe and at position E on the short pipe (figure 5.5), are shown in the figures 6.17 and 6.18, respectively. The calculated axial strains in the long pipe, figure 6.17, exhibit, in contrast to the axial strain results in the straight-pipe experiment of figure 6.9, too large amplitudes. This is supposed to have to do something with the lateral waves; the use of finer computational grids might give some improvement. The frequency of the strain oscillations is calculated accurately, for all levels of cavitation severity. The axial strains in the short pipe, figure 6.18, are, as can be expected, of a higher frequency. The first drop, after 1.15 ms, is a consequence of the first pressure drop at the elbow (figure 6.14), which makes the short pipe move in the direction of the remote end through a compressive axial stress wave. The observed, but surprisingly not calculated, highest strain peak in the bottom graph corresponds to the collapse of the first column separation at the remote end (figure 6.15).

Calculated bending moments, according to formula (5.3), are validated against measurements in the figures 6.19 and 6.20. The bending moments at position A on the long pipe show to some extent the dispersive character of the lateral waves; small oscillations of relatively high frequency are recorded before the arrival of the larger oscillations. Although there is a qualitative agreement between predictions and observations, the calculated moments are obviously too high. This is, again, attributed to a too coarse computational grid for the lateral wave propagation. The number of elements in the present grid, see table 6.1, has been taken of the same order of magnitude as in the straight-pipe simulation in order to get a similar number of concentrated cavities in both numerical calculations. The bending moments in the short pipe, figure 6.20, show a considerably better agreement between experiment and calculation than those in the long pipe. A plausible explanation for this fact has not yet been found. The axial impact of the rod onto the long pipe leads to a lateral impact of the short pipe. The extreme bending moments in the short pipe are therefore larger, about a factor 2, than in the long pipe. The arrival of the calculated bending moments is somewhat too early in both the short and long pipe.

Due to the large number of waves, axial and lateral, travelling up and down the two pipes, and due to the occurrence of cavitation at various locations in the system, a detailed analysis and interpretation of the recorded signals has not been attempted.

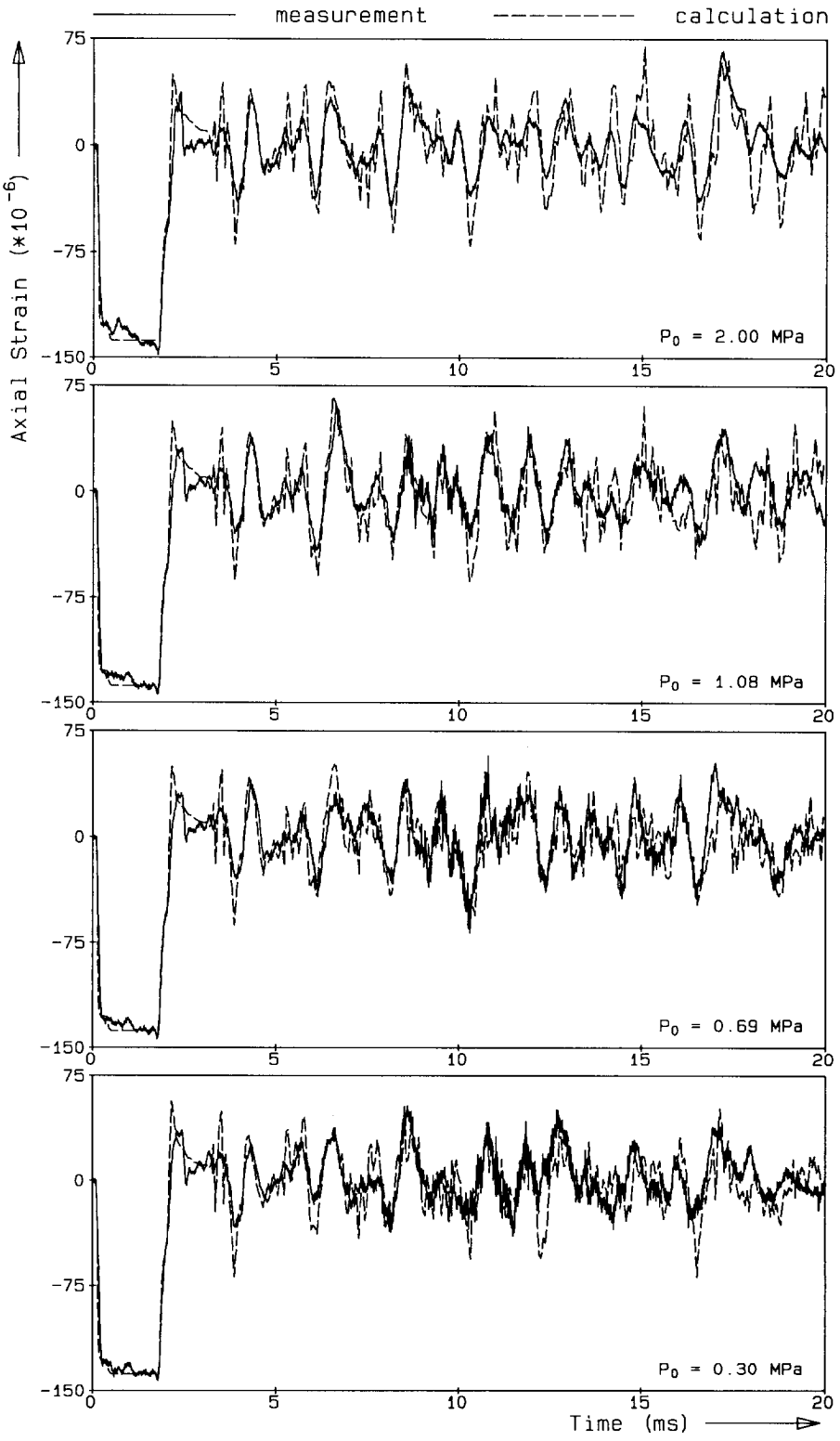

Figure 6.17. Measured and calculated axial strains in long pipe at 0.57 m from impact end in one-elbow pipe-system experiment.

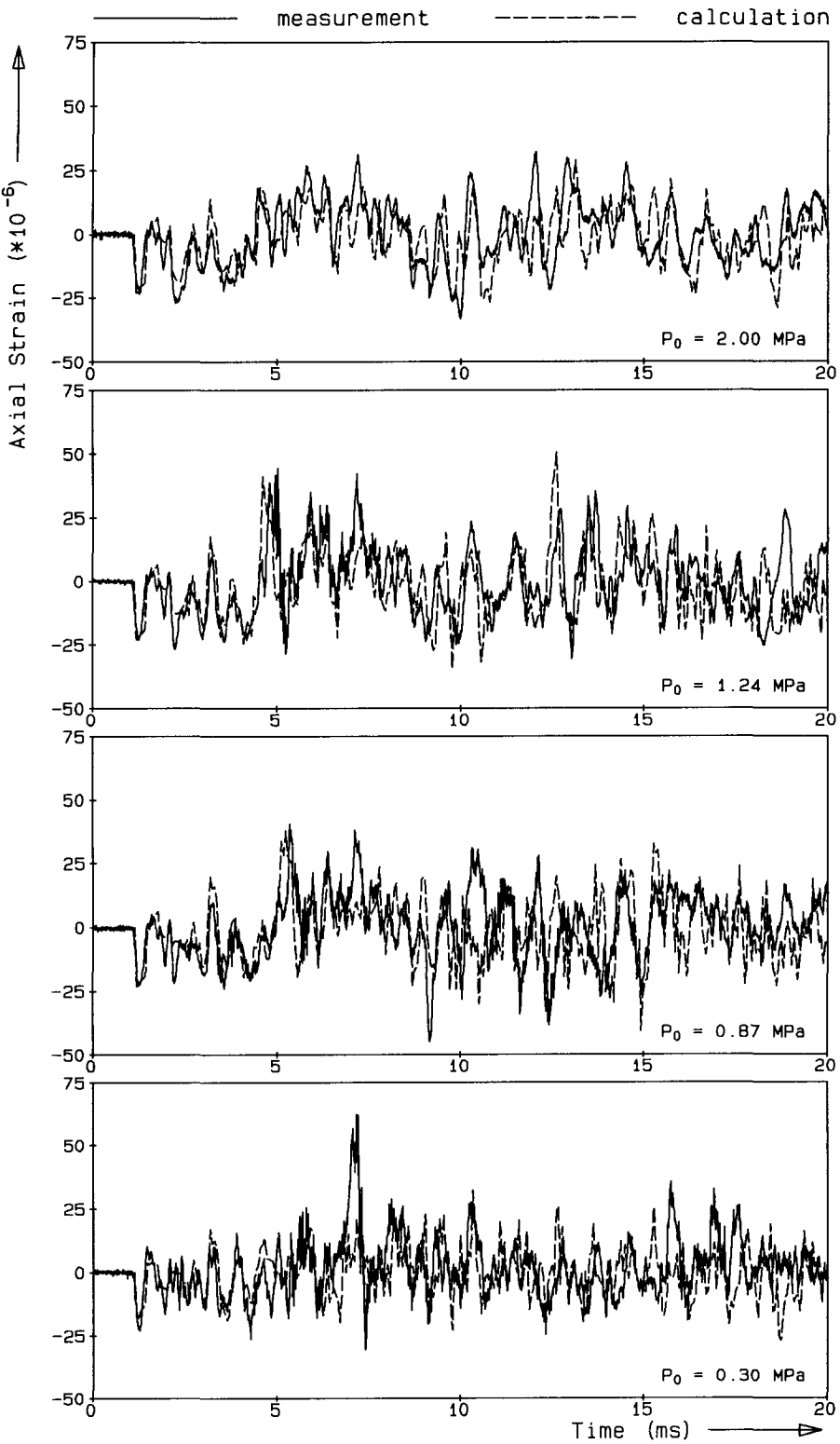

Figure 6.18. Measured and calculated axial strains close to middle of short pipe in one-elbow pipe-system experiment.

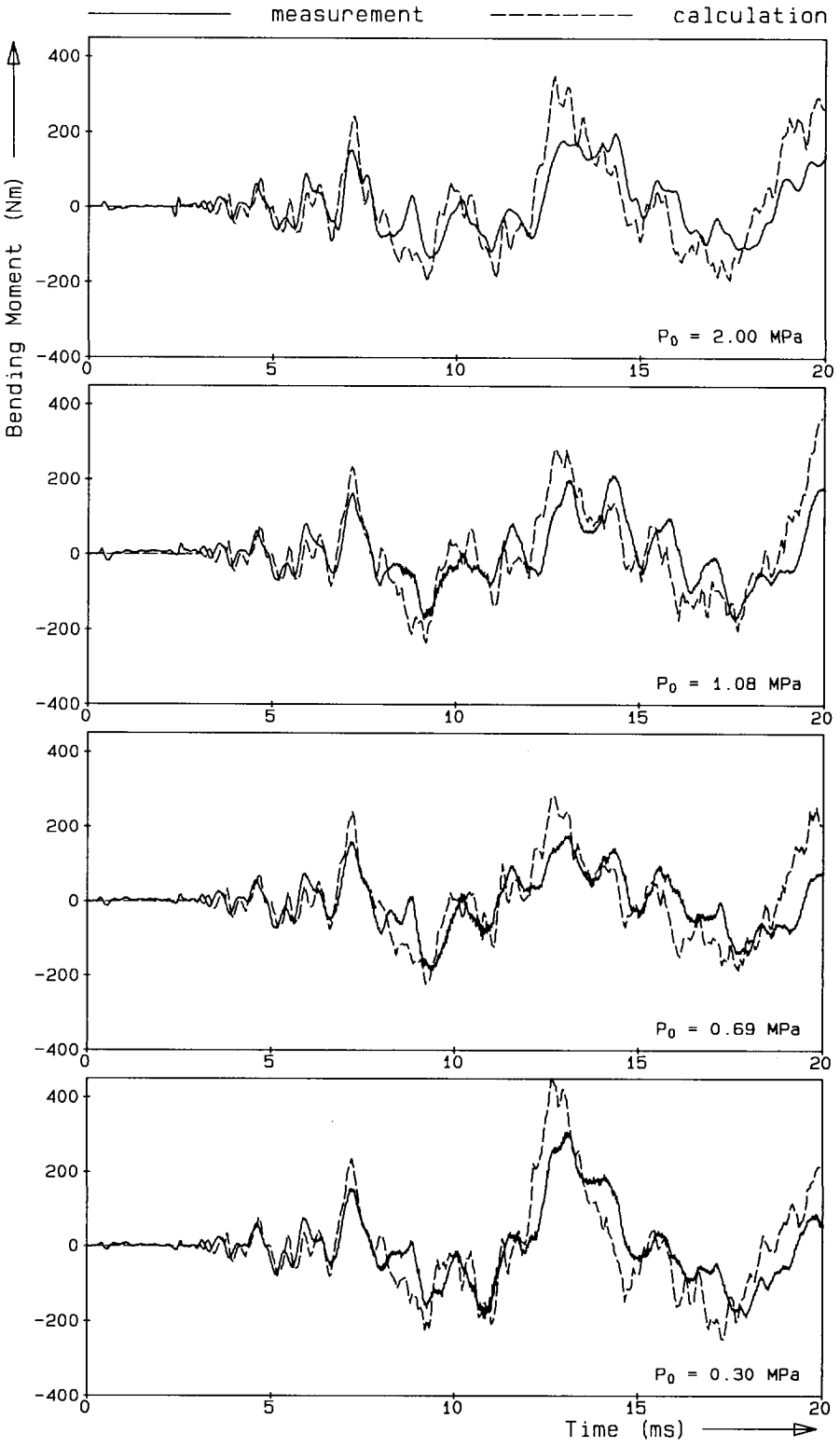

Figure 6.19. Measured and calculated bending moments in long pipe at 0.57 m from impact end in one-elbow pipe-system experiment.

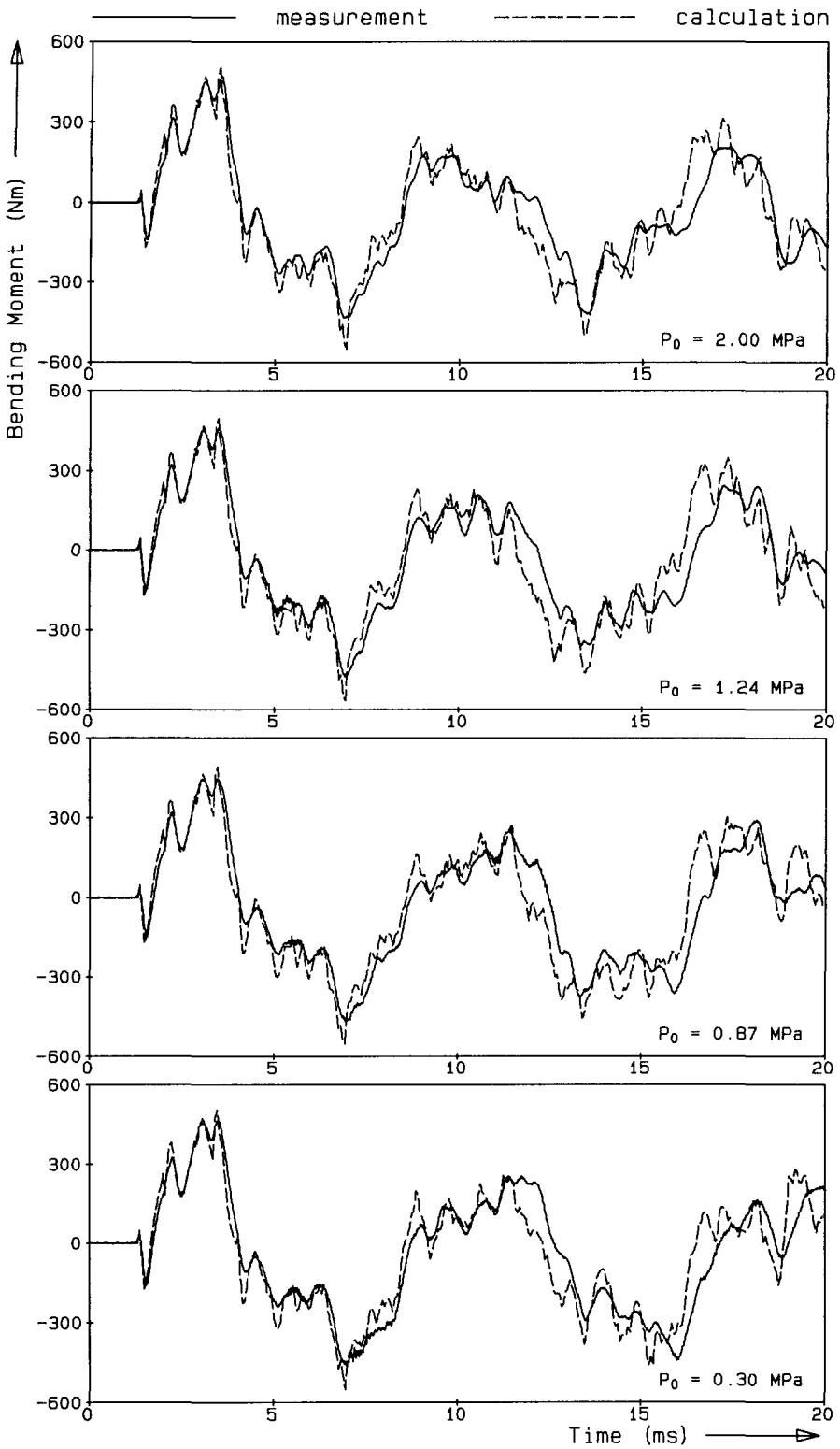

Figure 6.20. Measured and calculated bending moments close to middle of short pipe in one-elbow pipe-system experiment.

6.4. Review and conclusions

Experimental and theoretical results are compared in this chapter.

The concentrated cavity model of section 4.5 is validated against the experiments of Simpson [1986] in which FSI effects are of minor importance. The agreement between experiment and numerical simulation for three different levels of cavitation severity is typical for the concentrated cavity model. The durations of the first column separations and the magnitudes of the pressures following their collapse are predicted reasonably well. High-frequency oscillations, not observed in the measurements, appear in the calculated results. For practical purposes the validity of the model is sufficient. It is noted that in the experiment considered free gas and gas release did not play a role.

The straight-pipe FSI experiment of Vardy and Fan [1989] is explained by means of an illustrative sketch of the sequence of events in the apparatus. Measured and calculated pressures are understood from a wave paths diagram in the distance-time plane.

The cavitation measurements and corresponding numerical simulations in Vardy and Fan's straight-pipe and one-elbow experimental apparatus are new. The reproducibility of the experiments is sufficient for the present purpose. Measured and calculated pressures, velocities and strains are presented for five different levels of cavitation severity in the straight-pipe experiment and for three levels in the one-elbow pipe system experiment. Non-cavitation results are given as a reference. The agreement between experiment and simulation is good for all levels of cavitation severity in the straight-pipe experiment, whereas the agreement is somewhat less satisfactory in the one-elbow pipe system experiment for the more severe cavitation cases. In view of the complexity of the phenomena and the simplicity of, in particular, the cavitation model, the theoretical results obtained are amazingly good. In this respect it has to be remarked that Vardy and Fan's apparatus is of high quality; it has been designed and constructed carefully and accurately.

Poisson-coupling induced cavitation, that is cavitation generated by the radial expansion of the pipe wall, was predicted and observed, for the first time, in one special experiment.

7. REVIEW AND CONCLUSIONS

The transient behaviour of liquid-filled pipe systems is studied, including the effects of cavitation and fluid-structure interaction (FSI). An extensive review of literature on the subject reveals that a thorough theoretical and experimental investigation into the occurrence of cavitation combined with FSI does not exist.

One-dimensional governing equations are derived from the cross-sectional integration of general three-dimensional equations for fluid dynamics and structural linear elasticity. The FSI-mechanisms junction-, Poisson- and friction-coupling are taken into account. The equations derived are valid for phenomena with long wavelength and hence low frequency. Low-frequency dynamic behaviour is characterized by pipes which respond only in their beam (rather than radial) modes and by fluid wavelengths which are large compared to the pipe diameter. The equations for the liquid are extended waterhammer equations. The equations for the axial motion of the pipe wall are extended beam equations; these are membrane equations in which the radial inertia of pipe-wall and liquid (added mass) is neglected. In radial direction a quasi-static relation between the fluid pressure and the hoop stress has been assumed. The equations for the lateral motion of the pipe correspond to the Timoshenko beam theory in which the liquid mass is incorporated. The relatively simple equations for torsional motion are not used in this study, since pipe systems moving in one plane only are considered. One-dimensional two-phase flow equations are given for regions of distributed cavitation.

The basic equations, which are valid for thick-walled pipes, are formulated as a hyperbolic set of fourteen first-order partial differential equations. These are solved by the method of characteristics (MOC). The MOC is probably the best solution method for hyperbolic problems with constant eigenvalues, that is for systems in which disturbances propagate with constant speeds. This is the case for the coupled axial motion of liquid and pipe-wall. Almost exact solutions can be found if friction is neglected and cavitation is absent. The dispersive character of the lateral wave propagations make the MOC less suitable to solve the equations for lateral motion. Very fine computational grids are required to get satisfying results. Computational grids are introduced by which the use of interpolations can be avoided, so that the inherent numerical damping does not occur. Cavitation is simulated by the concentrated

cavity model, which - and that is new - is incorporated in the four-equation model describing the coupled axial motion of liquid and pipe wall. The model used is valid for transient vaporous cavitation; free gas and gas-release effects are not included. Column separations, governed by both liquid and pipe motion, are modelled as boundary conditions.

The concentrated cavity model is validated against experiments of Simpson [1986]. The results shown are typical for the concentrated cavity model: the duration of the first, mostly largest, column separation and the maximum pressure following its collapse are predicted accurately. The durations of subsequent column separations are predicted less accurately and numerical oscillations, not existing in the measurements, appear in the calculated pressure histories. Nevertheless, the accuracy of the model, which has been adopted for its simplicity and its general applicability within standard waterhammer computer codes, is sufficient for practical purposes.

The FSI-model, applied to thin-walled pipes, can be attributed to Wiggert et al. [1987a]. It has been extensively validated by Vardy and Fan [1989, 1993] for the case that cavitation does not occur. However, Vardy and Fan's FSI test rig is also suitable for cavitation tests. These tests have been performed by Fan and the present author on a straight-pipe system and on a system consisting of two straight pipes connected by a rigid 90-degrees elbow, for several levels of cavitation severity. A representative selection of results obtained in about 160 successful test runs is presented in this report. In 135 test runs the combination of FSI and cavitation was evident.

The predictions of the numerical model developed are in good agreement with the observations for the straight-pipe experiment, whereas the agreement becomes less in the one-elbow-system experiment for the more severe cases of cavitation. The lesser agreement may be attributed to a too simple model for column separation at an elbow and to ignoring distributed cavitation induced by lateral pipe motions.

Poisson-coupling induced cavitation, that is cavitation generated by the radial expansion of the pipe wall, was predicted and observed, for the first time, in one special experiment.

It is noted that the pipes in the FSI experiments were relatively thick, $R/e = 6.6$, and that, on the contrary, the numerical simulation was based on the assumption of thin-walled pipes. Regarding the good results, it can be concluded that thin-walled FSI-theory may also be applied to fairly thick pipes.

The good agreement between numerical simulation and measurement allows to explain the

physical phenomena in the relatively simple experiments with the help of computer output. The program developed is not (yet) suitable to predict dynamic pressures and stresses in practical systems, because it is restricted to two straight pipes connected by either a straight junction or an elbow junction. But many lessons can be learned from it. It makes clear what is happening, when cavitation and pipe motion due to waterhammer occur simultaneously.

In conclusion it can be stated that the numerical model developed gives accurate predictions of the physical phenomena in the two pipe systems considered. The simplicity of the model and the satisfying validation tests may lead to more general applications.

References

Adachi T., Ujihashi S. & Matsumoto H. 1991 *Impulsive responses of a circular cylindrical shell subjected to waterhammer waves.* ASME Journal of Pressure Vessel Technology, Vol. 113, No. 4, pp. 517-523. [2.3.5]

Aga J., Karterud T.J. & Nielsen T.K. 1980 *Testing of transient flow and column separation in crude oil pipelines.* Proc. of the 3rd Int. Conf. on Pressure Surges, BHRA, Canterbury, UK, March 1980, pp. 113-126. [2.2]

Allievi L. 1903 *Teoria generale del moto perturbato dell'acqua nei tubi in pressione.* (General theory of perturbed flow of water in pressure conduits.) Annali della Societa degli Ingegneri ed Architetti italiani, Milan, Italy (in Italian). (French translation by Allievi himself, in Revue de Mécanique, Paris, 1904; German translation by R. Dubs and V. Bataillard, Berlin: Springer, 1909) [2.1]

Allievi L. 1913 *Teoria del colpo d'ariete.* (The theory of water hammer.) Atti del Collegio degli Ingegneri ed Architetti, Milan, Italy (in Italian). (French translation by D. Gaden, 1921, Paris: Dunod; English translation by E.E. Halmos, New York: ASME, 1925, Rome: Riccardo Garoni) [2.1]

Almeida A.B. de 1987 *Some contributions to the transient macrocavitation's knowledge and modelling (1978-1987).* Proc. of the 8th Int. Round Table on Hydraulic Transients in Power Stations, IAHR, Madeira, Portugal, Paper D1. [2.2]

Almeida A.B. de & Koelle E. 1992 *Fluid transients in pipe networks.* Southampton, UK, Boston, USA: Computational Mechanics Publications; London, New York: Elsevier Applied Science. [2.1, 2.3.5]

Al-Mousawi M.M. 1984 *Transient response of Timoshenko beams with discontinuities of cross-section.* Int. Journal of Mechanical Sciences, Vol. 26, No. 4, pp. 277-292. [4.3]

Al-Mousawi M.M. & Harrison H.R. 1987 *Experimental investigation of transient flexural waves in beams with discontinuities of cross section.* Experimental Mechanics, Vol. 27, No. 4, pp. 404-413. [4.3]

A-Moneim M.T. & Chang Y.W. 1978 *Comparison of ICEPEL code predictions with straight flexible pipe experiments.* Nuclear Engineering and Design, Vol. 49, July, pp. 187-196. [2.3.6, 2.4]

A-Moneim M.T. & Chang Y.W. 1979 *Comparison of ICEPEL predictions with single-elbow flexible piping system experiment.* ASME Journal of Pressure Vessel Technology, Vol. 101, May, pp. 142-148. [2.3.6, 2.4]

Anderson A. 1976 *Menabrea's note on waterhammer: 1858.* ASCE Journal of the Hydraulics Division, Vol. 102, No. HY1, pp. 29-39. [2.1]

Anderson A., Sandoval-Pena R. & Arfaie M. 1991a *Column separation behaviour modes in a simple test rig.* Proc. of the Int. Meeting on Hydraulic Transients with Water Column Separation, 9th Round Table of the IAHR Group, Valencia, Spain, September 1991, pp. 33-50. [2.2, 6.1]

Anderson A. & Arfaie M. 1991b *Variable waterhammer wavespeed in column separation.* Proc. of the Int. Meeting on Hydraulic Transients with Water Column Separation, 9th Round Table of the IAHR Group, Valencia, Spain, September 1991, pp. 183-199. [2.2]

Angus R.W. 1935 *Simple graphical solution for pressure rise in pipes and discharge lines.* Journal of the Engineering Institute of Canada, Vol. 18, No. 2, pp. 72-81, 264-273. [2.2]

Angus R.W. 1937a *Water hammer in pipes, including those supplied by centrifugal pumps: graphical treatment.* Proc. of the Institution of Mechanical Engineers, Vol. 136, pp. 245-331. Also: Bulletin No. 152, University of Toronto, Canada, 1938. [2.2]

Angus R.W. 1937b *Air chambers and valves in relation to water hammer.* Trans. of the ASME, Vol. 59, pp. 661-668. [2.2]

Arndt R.E.A. 1981 *Cavitation in fluid machinery and hydraulic structures.* Annual Review of Fluid Mechanics, Vol. 13, pp. 273-328. [2.2]

Axisa F. & Gibert R.J. 1982 *Non-linear analysis of fluid-structure coupled transients in piping systems using finite elements.* ASME - PVP, Vol. 63, Flow-induced vibration of circular cylindrical structures, pp. 151-165. [2.3.6, 2.4]

Bach P. & Spangenberg S. 1990 *A numerical method for simulation of liquid and gas flow in pipeline networks.* 3R international, Vol. 29, No. 4, pp. 185-190. [2.3.6]

Baltzer R.A. 1967 *Column separation accompanying liquid transients in pipes.* ASME Journal of Basic Engineering, Series D, Vol. 89, No. 4, pp. 837-846. [2.2]

Bantlin A. 1910 *Formänderung und Beanspruchung federnder Ausgleichröhren.* (Deformation and loading of elastic expansion pipes.) Zeitschrift des Vereines deutscher Ingenieure, Vol. 54, No. 2, pp. 43-49 (in German). [3.3.6]

Barbero G. & Ciaponi C. 1991 *Experimental validation of a discrete free gas model for*

numerical simulation of hydraulic transients with cavitation. Proc. of the Int. Meeting on Hydraulic Transients with Water Column Separation, 9th Round Table of the IAHR Group, Valencia, Spain, September 1991, pp. 51-69. [2.2, 4.5.3]

Barez F., Goldsmith W. & Sackman J.L. 1979 *Longitudinal waves in liquid-filled tubes - I. Theory, II. Experiments.* Int. Journal of Mechanical Sciences, Vol. 21, No. 4, pp. 213-221, 223-236. [2.3.5, 3.2.1, 6.2.1]

Bathe K.J. & Almeida C.A. 1980 *A simple and effective pipe elbow element - linear analysis.* ASME Journal of Applied Mechanics, Vol. 47, March, pp. 93-100. [3.3.6]

Bathe K.J. & Almeida C.A. 1982a *A simple and effective pipe elbow element - interaction effects.* ASME Journal of Applied Mechanics, Vol. 49, March, pp. 165-171. [3.3.6]

Bathe K.J. & Almeida C.A. 1982b *A simple and effective pipe elbow element - pressure stiffening effects.* ASME Journal of Applied Mechanics, Vol. 49, December, pp. 914-916. [3.3.6]

Belytschko T. 1980 *Fluid-structure interaction.* Computers & Structures, Vol. 12, No. 4, pp. 459-469. [4.1]

Belytschko T., Karabin M. & Lin J.I. 1986 *Fluid-structure interaction in waterhammer response of flexible piping.* ASME Journal of Pressure Vessel Technology, Vol. 108, No. 3, pp. 249-255. [2.3.6]

Bergant A.& Simpson A.R. 1992 *Interface model for transient cavitating flow in pipelines.* Proc. of the Int. Conf. on Unsteady Flow and Fluid Transients, HR Wallingford, IAHR, Durham, UK, September-October 1992, pp. 333-342. [2.2, 3.1.5]

Bergeron L. 1935 *Etude des variations de régime dans les conduites d'eau. Solution graphique générale.* (Study on the steady-state variations in water-filled conduits. General graphical solution.) Revue générale de l'Hydraulique, Vol. 1, No. 1, pp. 12-25 (in French). [2.1]

Bergeron L. 1939 *Discussion of "Experiments and calculations on the resurge phase of water hammer" by J.N. LeConte and discussion of "Air chambers for discharge lines" by L. Allievi.* Trans. of the ASME, Vol. 61, pp. 441-445. [2.2]

Bergeron L. 1950 *Du coup de bélier en hydraulique - Au coup de foudre en électricité.* (Waterhammer in hydraulics and wave surges in electricity.) Paris: Dunod (in French). (English translation by ASME committee, New York: John Wiley & Sons, 1961) [2.1, 2.2, 3.3.7]

Bettinali F., Molinaro P., Ciccotelli M. & Micelotta A. 1991 *Transient analysis in piping networks including fluid-structure interaction and cavitation effects.* Trans. of SMiRT11, Tokyo, Japan, August 1991, Paper K35/5, pp. 565-570. [2.3.5, 2.4]

Bietenbeck F., Petruschke W. & Wünnenberg H. 1985 *Piping response due to blowdown - Significant parameters for a comparison of experimental and analytical results.* Trans. of SMiRT8, Brussels, Belgium, August 1985, Division F1 3/7, pp. 103-108. [2.3.6]

Billings A.W.K., Dodkin O.K., Knapp F. & Santos A. 1933 *High head penstock design.* ASME Water Hammer Symposium, Chicago, USA, pp. 29-61. [2.2]

Bird R.B., Stewart W.E. & Lightfoot E.N. 1960 *Transport phenomena.* New York: John Wiley & Sons. [3.1.2]

Blade R.J., Lewis W. & Goodykoontz J.H. 1962 *Study of a sinusoidally perturbed flow in a line including a 90 degrees elbow with flexible supports.* National Aeronautics & Space Administration, Technical Note D-1216. [2.3.4, 2.3.5, 3.3.2]

Boulanger A. 1913 *Etude sur la propagation des ondes liquides dans les tuyaux élastiques.* (Study on the propagation of liquid waves in elastic tubes.) Travaux et Mémoires de l'Université de Lille, Nouvelle Serie, II. Médecine-Sciences, Vol. 8, Lille: Tallandier, Paris: Gauthier-Villars (in French). [2.3.1]

Bresse J.A.C. 1859 *Cours de mécanique appliquée.* (Course on applied mechanics.) Paris: Mallet-Bachelier, 1859; Gauthier-Villars, 1866 (in French). [3.1.3, 4.3]

Brown R.J. 1968 *Water-column separation at two pumping plants.* ASME Journal of Basic Engineering, Vol. 90, No. 4, pp. 521-531. [2.2]

Budny D.D. 1988 *The influence of structural damping on the internal fluid pressure during a fluid transient pipe flow.* Dissertation, Michigan State University, Dep. of Civil Engineering, East Lansing, USA. [2.3.5, 3.1.1, 3.1.2, 4.11]

Budny D.D., Wiggert D.C. & Hatfield F.J. 1989 *Energy dissipation in the axially-coupled model for transient flow.* Proc. of the 6th Int. Conf. on Pressure Surges, BHRA, Cambridge, UK, October 1989, pp. 15-26. [2.3.5]

Budny D.D., Hatfield F.J. & Wiggert D.C. 1990 *An experimental study on the influence of structural damping on internal fluid pressure during a transient flow.* ASME Journal of Pressure Vessel Technology, Vol. 112, No. 3, pp. 284-290. [2.3.5]

Budny D.D., Wiggert D.C. & Hatfield F.J. 1991 *The influence of structural damping on internal pressure during a transient flow.* ASME Journal of Fluids Engineering, Vol. 113,

No. 3, pp. 424-429. [2.3.5]

Bühl G. 1987 *Zur rechnerischen Simulation des Turbinenschnellschlusses in konventionellen Kraftwerken.* (The computer simulation of turbine trip events in conventional power plants.) 3R international, Vol. 26, No. 7, pp. 438-445 (in German). [2.3.6]

Bürmann W. 1974a *Druckstöße in koaxialen Rohrsystemen.* (Water hammer in coaxial pipe systems.) Dissertation, Universität Karlsruhe, Karlsruhe, Germany: O. Berenz (in German). [2.3.5]

Bürmann W. 1974b *Druckstöße in koaxialen Rohrsystemen.* (Water hammer in coaxial pipe systems.) 3R international, Vol. 13, No. 3, pp. 155-163 (in German). [2.3.5]

Bürmann W. 1975 *Water hammer in coaxial pipe systems.* ASCE Journal of the Hydraulics Division, Vol. 101, No. HY6, pp. 699-715. [2.3.5, 3.1.2]

Bürmann W., Janson H. & Thielen H. 1979 *Eine Druckstoßtheorie für nicht axialsymmetrisch verformte Rohre.* (Water hammer theory for non-axisymmetrically deformed pipes.) Universität Karlsruhe, Institut für Hydromechanik, Bericht Nr. 614, May 1979, Karlsruhe, Germany (in German). [2.3.5]

Bürmann W. 1979 *Druckstoßmessungen in koaxialen Rohren.* (Water hammer measurements in coaxial pipes.) 3R international, Vol. 18, No. 10, pp. 624-628 (in German). [2.3.5]

Bürmann W. 1980a *Längsbewegung frei verlegter Rohrleitungen durch Druckstöße.* (Longitudinal motion of pipelines laid in the open due to water hammer.) 3R international, Vol. 19, No. 1/2, pp. 84-91 (in German). [2.3.5, 3.1.2]

Bürmann W. 1980b *Längsbewegung koaxialer Rohre durch Druckstöße.* (Longitudinal motion of coaxial pipes due to water hammer.) 3R international, Vol. 19, No. 7/8, pp. 398-404 (in German). [2.3.5]

Bürmann W., Janson H. & Thielen H. 1980 *Rohrleitungsbewegung durch Druckstöße.* (Pipeline motion due to water hammer.) Universität Karlsruhe, Institut für Hydromechanik, Bericht Nr. 618, December 1980, Karlsruhe, Germany (in German). [2.3.5]

Bürmann W., Janson H. & Thielen H. 1983 *Eine Druckstoßtheorie für nicht axialsymmetrisch verformte Rohre. Bericht über die Messungen.* (Water hammer theory for non-axisymmetrically deformed pipes. Report on measurements.) Universität Karlsruhe, Institut für Hydromechanik, Bericht Nr. 616, August 1983, Karlsruhe, Germany (in German). [2.3.5]

Bürmann W. 1983 *Beanspruchung der Rohrwandung infolge von Druckstößen.* (Strain on pipe walls resulting from water hammer.) 3R international, Vol. 22, No. 9, pp. 426-431 (in German). [2.3.5]

Bürmann W., Feser G., Janson H. & Thielen H. 1985 *Mathematische Simulation der Dynamik frei verlegter Rohrleitungen bei instationärer Durchströmung. Bericht über die Messungen und rechnerische Simulation der Messungen an der Neckarbrücke.* (Mathematical simulation of the dynamics of pipelines laid in the open in case of unsteady flows. Report on the measurements and numerical simulation of the measurements on the Neckar bridge.) Universität Karlsruhe, Institut für Hydromechanik, Bericht Nr. 623, July 1985, Karlsruhe, Germany (in German). [2.3.5]

Bürmann W., Feser G., Janson H. & Thielen H. 1986a *Mathematische Simulation der Dynamik frei verlegter Rohrleitungen bei instationärer Durchströmung. Bericht über die Messungen und rechnerische Simulation der Messungen an der Umschlaganlage Jade.* (Mathematical simulation of the dynamics of pipelines laid in the open in case of unsteady flows. Report on the measurements and numerical simulation of the measurements on the Jade transhipment station.) Universität Karlsruhe, Institut für Hydromechanik, Bericht Nr. 622, January 1986, Karlsruhe, Germany (in German). [2.3.5]

Bürmann W., Feser G., Janson H. & Thielen H. 1986b *Mathematische Simulation der Dynamik frei verlegter Rohrleitungen bei instationärer Durchströmung. Bericht über die zweiten Messungen und rechnerische Simulation der zweiten Messungen an der Neckarbrücke.* (Mathematical simulation of the dynamics of pipelines laid in the open in case of unsteady flows. Report on the second measurements and numerical simulation of the second measurements on the Neckar bridge.) Universität Karlsruhe, Institut für Hydromechanik, Bericht Nr. 640, July 1986, Karlsruhe, Germany (in German). [2.3.5]

Bürmann W., Feser G., Janson H. & Thielen H. 1987a *Druck- und Beschleunigungsmessungen an der Rohrbrücke einer Fernwasserleitung zur Untersuchung der Rohrleitungsdynamik bei instationärer Durchströmung.* (Pressure and acceleration measurements on the pipe bridge of a long-distance water main to study the piping dynamics in case of unsteady flow.) 3R international, Vol. 26, No. 9, pp. 638-646 (in German). [2.3.5]

Bürmann W., Feser G., Janson H. & Thielen H. 1987b *Mathematische Simulation der Dynamik frei verlegter Rohrleitungen bei instationärer Durchströmung. Bericht über die*

zweiten Messungen und rechnerische Simulation der zweiten Messungen an der Umschlaganlage Jade. (Mathematical simulation of the dynamics of pipelines laid in the open in case of unsteady flows. Report on the second measurements and numerical simulation of the second measurements on the Jade transhipment station.) Universität Karlsruhe, Institut für Hydromechanik, Bericht Nr. 656, December 1987, Karlsruhe, Germany (in German). [2.3.5]

Bürmann W., Feser G., Janson H. & Thielen H. 1987c *Eine Druckstoßtheorie für nicht axialsymmetrisch verformte Rohre. Bericht über die rechnerische Simulation der Messungen.* (Water hammer theory for non-axisymmetrically deformed pipes. Report on the numerical simulation of the measurements.) Universität Karlsruhe, Institut für Hydromechanik, Bericht Nr. 657, 1987, Karlsruhe, Germany (in German). [2.3.5]

Bürmann W. & Thielen H. 1988 *Untersuchung der Bewegung des Befüllstrangs einer Salzkaverne.* (Study on the motion of the filling string of a saline cavern.) 3R international, Vol. 27, No. 4, pp. 275-281 (in German). [2.3.5]

Carmona R., Sanchez A. & Sanchez J.L. 1987 *Experimental relation between the highest transient pressure and the severity of water column separation.* Proc. of the 8th Int. Round Table on Hydraulic Transients in Power Stations, IAHR, Madeira, Portugal, Paper D2. [2.2, 6.1]

Chaudhry M.H. 1979 *Applied hydraulic transients.* New York: Van Nostrand Reinhold. (1st edition 1979, 2nd edition 1987) [2.1]

Chaudhry M.H. & Yevjevich V. (Editors) 1981 *Closed-conduit flow.* Littleton, USA: Water Resources Publications. [2.1]

Chen Y.L. & Israelachvili J. 1991 *New mechanism of cavitation damage.* Science, Vol. 252, May, Reports, pp. 1157-1160. [5.3.1]

Chou P.C. & Mortimer R.W. 1967 *Solution of one-dimensional elastic wave problems by the method of characteristics.* ASME Journal of Applied Mechanics, Vol. 34, September, pp. 745-750. [4.3]

Chree C. 1889 *The equations of an isotropic elastic solid in polar and cylinder coordinates, their solution and application.* Trans. of the Cambridge Philosophical Society, Vol. 14, pp. 250-369. [4.3]

Clark R.A. & Reissner E. 1951 *Bending of curved tubes.* Advances in Applied Mechanics, Vol. 2, pp. 93-122. [3.3.6]

Clark S.K. 1956 *Torsional wave propagation in hollow cylindrical bars.* Journal of the Acoustical Society of America, Vol. 28, No. 6, pp. 1163-1165. [4.4]

Clough R.W. & Penzien J. 1975 *Dynamics of structures.* Singapore: McGraw-Hill. [3.1.3]

Cowper G.R. 1966 *The shear coefficient in Timoshenko's beam theory.* ASME Journal of Applied Mechanics, Vol. 33, June, pp. 335-340. [3.1.3]

Craig R.R., Jr. 1981 *Structural dynamics.* New York: John Wiley & Sons. [4.7.3]

Cross H. 1936 *Analysis of flow in networks of conduits or conductors.* University of Illinois, Engineering Experimental Station, Bulletin No. 286, November 1936, Urbana, USA. [4.6.2]

Darcy H.P.G. 1857 *Recherches expérimentales relatives au mouvement de l'eau dans les tuyaux.* (Experimental investigation with respect to the motion of water in tubes.) Paris: Mallet-Bachelier (in French). [3.1.2]

Davidson L.C. & Smith J.E. 1969 *Liquid-structure coupling in curved pipes.* The Shock and Vibration Bulletin, No. 40, Part 4, pp. 197-207. [2.3.4, 2.3.5, 2.3.6]

Davidson L.C. & Samsury D.R. 1972 *Liquid-structure coupling in curved pipes - II.* The Shock and Vibration Bulletin, No. 42, Part 1, pp. 123-136. [2.3.4, 2.3.5]

Davies R.M., Trevena D.H., Rees N.J.M. & Lewis G.M. 1956 *The tensile strength of liquids under dynamic stressing.* Proc. of the 1955 NPL (National Physical Laboratory) Symp. on Cavitation in Hydrodynamics, Paper 5, 20 pp. [6.3.1]

DeArmond R.P. & Rouleau W.T. 1972 *Wave propagation in viscous, compressible liquids confined in elastic tubes.* ASME Journal of Basic Engineering, Vol. 94, December, pp. 811-817. [2.3.2]

Dieterman H.A. 1988 *Dynamics of towers: liquid-structure-foundation interaction.* Dissertation, Delft University of Technology, Dep. of Civil Engineering, Delft, The Netherlands. [1.2.3]

Dijkman H.K.M. 1968 *Cavitatieverschijnselen in een horizontale leiding met water waarin gas is opgelost.* (Cavitation phenomena in a horizontal conduit filled with water in which gas is dissolved.) Delft Hydraulics Laboratory, Report S 103-III, March 1968, Delft, The Netherlands (in Dutch). [1.2.2]

Dijkman H.K.M. & Vreugdenhil C.B. 1969 *The effect of dissolved gas on cavitation in horizontal pipe-lines.* IAHR Journal of Hydraulic Research, Vol. 7, No. 2, pp. 301-314. Also: Delft Hydraulics Laboratory, Publication No. 70, November 1969. [1.2.2]

Dodge W.G. & Moore S.E. 1972 *Stress indices and flexibility factors for moment loadings on elbows and curved pipe.* Welding Research Council Bulletin 179, December 1972, pp. 1-16. [3.3.6]

D'Souza A.F. & Oldenburger R. 1964 *Dynamic response of fluid lines.* ASME Journal of Basic Engineering, Vol. 86, No. 3, pp. 589-598. [2.3.4, 2.3.5, 3.1.2, 3.3.2]

Edwards N.A. & Please C.P. 1988 *An assessment of the moving point method for numerical calculation of fluid-structure interaction in water hammer.* Central Electricity Generating Board (CEGB) Research Report TPRD/L/3258/R88 (Obtainable from National Power PLC, Library and Information Services, Senator House, London EC4V 4DP). [2.3.5]

Eichinger P. & Lein G. 1992 *The influence of friction on unsteady pipe flow.* Proc. of the Int. Conf. on Unsteady Flow and Fluid Transients, HR Wallingford, IAHR, Durham, UK, September-October 1992, pp. 41-50. [3.1.2]

Ellis J. 1980 *A study of pipe-liquid interaction following pump-trip and check-valve closure in a pumping station.* Proc. of the 3rd Int. Conf. on Pressure Surges, BHRA, Canterbury, UK, March 1980, pp. 203-220. [2.3.4, 2.3.5]

Enever K.J. 1972 *Surge pressures in a gas-liquid mixture with low gas content.* Proc. of the 1st Int. Conf. on Pressure Surges, BHRA, Canterbury, UK, September 1972, Paper C1, pp. 1-11. [2.2]

Epp R. & Fowler A.G. 1970 *Efficient code for steady-state flows in networks.* ASCE Journal of the Hydraulics Division, Vol. 96, No. HY1, pp. 43-56. [4.6.2]

EUREKA 1988 *Wetenschap en industrie weten elkaar te vinden.* (Science and industry meet each other.) Eureka Bulletin, Vol. 2, No. 4, pp. 7-9 (in Dutch). [1.2.3]

Evans E.P. & Sage P.V. 1983 *Surge analysis of a large gravity pipeline.* Proc. of the 4th Int. Conf. on Pressure Surges, BHRA, Bath, UK, September 1983, pp. 447-460. [2.2]

Everstine G.C. 1984 *Dynamic analysis of fluid-filled piping systems using finite element techniques.* ASME - PVP, Vol. 78, Advances in fluid-structure interaction, pp. 125- 139. [2.3.6]

Ewing D.J.F. 1980 *Allowing for free air in waterhammer analysis.* Proc. of the 3rd Int. Conf. on Pressure Surges, BHRA, Canterbury, UK, March 1980, pp. 127-146. [2.2]

Fan D. 1989 *Fluid-structure interactions in internal flows.* Dissertation, The University of Dundee, Dep. of Civil Engineering, Dundee, UK. [2.3.5, 5.2.1, 5.2.2, 6.2.1, 6.3.1]

Fan D. & Tijsseling A. 1992 *Fluid-structure interaction with cavitation in transient pipe flows.* ASME Journal of Fluids Engineering, Vol. 114, No. 2, pp. 268-274. [1.2.4, 5.2.1, 6.3.1]

Firnhaber M. & Müller W. Ch. 1987 *Evaluation of a German Standard Problem on the statics and dynamics of a large pipe.* Trans. of SMiRT9, Lausanne, Switzerland, August 1987, Vol. F, pp. 225-230. [2.3.6]

Flügge W. 1942 *Die Ausbreitung von Biegungswellen in Stäben.* (The propagation of flexural waves in bars.) Zeitschrift für angewandte Mathematik und Mechanik, Vol. 22, No. 6, pp. 312-318 (in German). [4.3, 4.3.1, 4.3.3, 4.3.4, 4.10.2]

Flügge W. & Zajac E.E. 1959 *Bending impact waves in beams.* Ingenieur-Archiv, Vol. 28, pp. 59-70. [4.3, 4.3.3]

FLUSTRIN 1986 Proc. of Seminar on Fluid-Structure Interaction, Delft Hydraulics, Delft, The Netherlands, October 1986, Report J0113. [1.2.3]

FLUSTRIN 1990 Manual, version 1. Vol. 1: *Theory, Global design, Tests.* Vol. 2: *User manual, components.* March 1990, Delft Hydraulics, Delft, The Netherlands. [1.2.3]

Forsythe G.E. & Wasow W.R. 1964 *Finite-difference methods for partial differential equations.* New York: John Wiley & Sons. [4.2.2]

Fox J.A. & Keech A.E. 1975 *Pipe network analysis - a novel steady state technique.* Journal of the Institution of Water Engineers and Scientists, Vol. 29, pp. 183-194. [4.6.2]

Fox J.A. 1977 *Hydraulic analysis of unsteady flow in pipe networks.* London: MacMillan Press Ltd. [2.1]

Fox J.A. 1989 *Transient flow in pipes, open channels and sewers.* Chichester, UK: Ellis Horwood. [2.1]

Frizell J.P. 1898 *Pressures resulting from changes of velocity of water in pipes.* Trans. of the ASCE, Vol. 39, Paper No. 819, June 1898, pp. 1-18. [2.1]

Gandenberger W. 1950 *Druckschwankungen in Wasserversorgungsleitungen.* (Pressure surges in water supply conduits.) Munich, Germany: R. Oldenbourg (in German). [2.1]

Gibert R.J., Axisa F. & Villard B. 1978 *Flow induced vibrations of piping system. (Vibration sources - Mechanical response of the pipes).* Proc. BNES Int. Conf. on Vibration in Nuclear Plant, Keswick, UK, May 1978, Paper 6.2, pp. 617-631. [2.3.6]

Giesecke H.D. 1981 *Calculation of piping response to fluid transients including effects of fluid/structure interaction.* Trans. of SMiRT6, Paris, France, August 1981, Paper B4/4.

[2.3.6, 2.4]

Goldberg D.E. & Wylie E.B. 1983 *Characteristics method using time-line interpolations.* ASCE Journal of Hydraulic Engineering, Vol. 109, No. 5, pp. 670-683. [4.10.1]

Golia U.M. & Greco M. 1990 *Cavitation during water-hammer: quick closure of a downstream valve.* Proc. of the 3rd Int. Conf. on Hydraulic Engineering Software, Hydrosoft '90, Boston, USA, April 1990, pp. 121-129. [2.2]

Gottlieb L., Larnæs G. & Vasehus J. 1981 *Transient cavitation in pipelines - Laboratory tests and numerical calculations.* Proc. of the 5th Int. Symp. on Water Column Separation, IAHR, Obernach, Germany, September 1981, pp. 487-508. [2.2]

Graze H.R. & Horlacher H.B. 1983 *Pressure transients following the collapse of vapour cavities.* Proc. of the 6th Int. Symp. on Hydraulic Transients in Power Stations, IAHR, Gloucester, UK, September 1983. [2.2, 5.3.1]

Gregory R.W. & Païdoussis M.P. 1966 *Unstable oscillations of tubular cantilevers conveying fluids:* I. *Theory,* II. *Experiments.* Proc. of the Royal Society, London, Series A, Vol. 293, pp. 512-527, 528-542. [2.3.7]

Grillenberger T. 1985 *Simulation von Druckwellen im Kühlsystem von Druckwasserreaktoren mit einem Netzwerk eindimensionaler Strömungskanäle unter Berücksichtigung der Strukturflexibilität.* (Simulation of pressure waves in the cooling system of pressurized-water reactors by a network of one-dimensional flow-reaches taking into account the structural flexibility.) Dissertation, Technische Universität München, Fakultät für Maschinenwesen, May 1985, Munich, Germany. Also: Gesellschaft für Reaktorsicherheit, GRS-60, November 1985, Cologne, Germany, ISBN 3-923875-08-8 (in German). [2.3.6]

Gromeka I.S. 1883 *О скорости распространенія волнообразнаго движенія жидкостей въ упругихъ трубкахъ.* (On the velocity of propagation of wave-like motion of fluids in elastic tubes.) Physical-Mathematical Section of the Scientific Society of the Imperial University of Kazan, Kazan, Russia, May 1883, pp. 1-19 (in Russian). [2.3.1, 4.2.3]

Halliwell A.R. 1963 *Velocity of a water-hammer wave in an elastic pipe.* ASCE Journal of the Hydraulics Division, Vol. 89, No. HY4, pp. 1-21. (Discussed by V.L. Streeter in No. HY6, pp. 295-296.) [2.3.3]

Hammitt F.G. 1980 *Cavitation and multiphase flow phenomena.* New York: McGraw-Hill.

[2.2]

Hankinson R.F. & Van Duyne D.A. 1987 *Dynamic analysis of fluid transients utilizing the force time-history modal-superposition method.* Advances in piping analysis and life assessment for pressure vessels and piping, ASME - PVP, Vol. 129, pp. 109-113. [2.3.6]

Hatfield F.J., Wiggert D.C. & Otwell R.S. 1982a *Fluid structure interaction in piping by component synthesis.* ASME Journal of Fluids Engineering, Vol. 104, No. 3, pp. 318-325. [2.3.5, 4.2.3]

Hatfield F.J., Davidson L.C. & Wiggert D.C. 1982b *Acoustic analysis of liquid-filled piping by component synthesis: experimental validation and examination of assumptions.* ASME - PVP, Vol. 64, Fluid transients and fluid-structure interaction, pp. 106-115. [2.3.5]

Hatfield F.J., Wiggert D.C. & Davidson L.C. 1983 *Experimental validation of the component synthesis method for predicting vibration of liquid-filled piping.* The Shock and Vibration Bulletin, No. 53, Part 2, pp. 1-10. [2.3.5]

Hatfield F.J. & Wiggert D.C. 1983 *Harmonic analysis of coupled fluid and piping.* Proc. of the ASCE Engineering Mechanics Specialty Conf., May 1983, pp. 180-192. [2.3.5]

Hatfield F.J. & Wiggert D.C. 1987 *Response of pipelines to seismic motion in the axial direction.* ASME Pressure Vessels and Piping Conference, Symp. on Recent Advances in Design, Analysis, Testing and Qualification Methods, San Diego, USA, July 1987. [2.3.5]

Hatfield F.J., Wiggert D.C. & Zielke W. 1987 *Strömung-Struktur-Wechselwirkung in Rohrleitungssystemen.* (FSI in liquid-filled piping.) Hochschulkurs, Institut für Strömungsmechanik und Elektronisches Rechnen im Bauwesen, Universität Hannover, Hanover, Germany, November-December 1987 (partly in German). [1.2.4]

Hatfield F.J. & Wiggert D.C. 1990 *Seismic pressure surges in liquid-filled pipelines.* ASME Journal of Pressure Vessel Technology, Vol. 112, No. 3, pp. 279-283. [2.3.5]

Heinsbroek A.G.T.J., Lavooij C.S.W. & Tijsseling A.S. 1991 *Fluid-structure interaction in non-rigid piping - a numerical investigation* -. Trans. of SMiRT11, Tokyo, Japan, August 1991, Paper B12/1*, pp. 309-314. [1.2.3, 4.2.5, 4.8, 4.10.1, 4.10.2]

Heinsbroek A.G.T.J. & Kruisbrink A.C.H. 1991 *FLUSTRIN Phase 3 - Validation experiments and simulations.* Report J526, November 1991, Delft Hydraulics, Delft, The Netherlands. [1.2.3]

Heinsbroek A.G.T.J. 1993 *Fluid-structure interaction in non-rigid pipeline systems* -

comparative analyses. ASME/TWI 12th Int. Conf. on Offshore Mechanics and Arctic Engineering, Paper OMAE-93-1018, Glasgow, Scotland, June 1993. [1.2.3]

Heinsbroek A.G.T.J. & Kruisbrink A.C.H. 1993 *Fluid-structure interaction in non-rigid pipeline systems - large scale validation experiments* -. Trans. of SMiRT12, Stuttgart, Germany, August 1993, Paper J08/1. [1.2.3]

Heinsbroek A.G.T.J. & Tijsseling A.S. 1993 *Fluid-structure interaction in non-rigid pipeline systems - a numerical investigation II* -. Trans. of SMiRT12, Stuttgart, Germany, August 1993, Paper J08/2. [1.2.3, 4.10.2, 4.10.3]

Helmholtz H.L.F. von 1848 In: Die Fortschritte der Physik, dargestellt von der physikalischen Gesellschaft in Berlin, Vol. 4, pp. 101-118. Also: *Bericht über die theoretische Akustik betreffenden Arbeiten vom Jahre 1848 und 1849.* (Report on theoretical acoustics with regard to works of the years 1848 and 1849.) Gesammelte wissenschaftliche Abhandlungen, 1882, Vol. 1, Paper 13, pp. 233-255, in particular p. 246, Leipzig, Germany: J.A. Barth (in German). [2.3.1]

Herrmann G. & Mirsky I. 1956 *Three-dimensional and shell-theory analysis of axially symmetric motions of cilinders.* ASME Journal of Applied Mechanics, Vol. 23, No. 4, pp. 563-568. [2.3.2, 2.3.5]

Hogg T.H. & Traill J.J. 1926 *Discussion of "Speed changes of hydraulic turbines for sudden changes of load" by E.B. Strowger & S.L. Kerr.* Trans. of the ASME, Vol. 48, pp. 252-257. [2.2]

Holmboe E.L. & Rouleau W.T. 1967 *The effect of viscous shear on transients in liquid lines.* ASME Journal of Basic Engineering, Vol. 89, March, pp. 174-180. [2.3.4]

Housner G.W. 1952 *Bending vibrations of a pipe line containing flowing fluid.* ASME Journal of Applied Mechanics, Vol. 19, June, pp. 205-208. [2.3.7]

Hovgaard W. 1926 *The elastic deformation of pipe-bends.* Journal of Mathematics and Physics, Massachusetts Institute of Technology, Vol. 6, pp. 69-118. [3.3.6]

Howlett J.T. 1971 *Applications of NASTRAN to coupled structural and hydrodynamic responses in aircraft hydraulic systems.* NASTRAN: Users' experiences, NASA TM X-2378, National Aeronautics and Space Administration, Washington DC, USA, pp. 407-419. [2.3.6]

Hutchinson J.R. & El-Azhari S.A. 1986 *Vibrations of free hollow circular cylinders.* ASME Journal of Applied Mechanics, Vol. 53, September, pp. 641-646. [3.1.3]

Idelchik I.E. 1986 *Handbook of hydraulic resistance* (2nd edition). Washington: Hemisphere, Berlin: Springer. [3.2.2]

Jaeger C. 1977 *Fluid transients (in hydro-electric engineering practice).* Glasgow, UK: Blackie & Son. [2.1]

Jelev I. 1989 *The damping of flow and pressure oscillations in water hammer analysis.* IAHR Journal of Hydraulic Research, Vol. 27, No. 1, pp. 91-114. [2.3.5]

Jendrzejczyk J.A. & Chen S.S. 1984 *Experiments on tubes conveying fluid.* ASME - PVP, Vol. 78, Advances in fluid-structure interaction, pp. 145-162. [2.3.7]

Jendrzejczyk J.A. & Chen S.S. 1985 *Experiments on tubes conveying fluid.* Thin-Walled Structures, Vol. 3, pp. 109-134. [2.3.7]

Jones S.E. & Wood D.J. 1972 *The effect of axial boundary motion on pressure surge generation.* ASME Journal of Basic Engineering, Vol. 94, No. 2, pp. 441-446. [2.3.4]

Joukowsky N. 1898 *Über den hydraulischen Stoss in Wasserleitungsröhren.* (On the hydraulic hammer in water supply pipes.) Mémoires de l'Académie Impériale des Sciences de St.-Pétersbourg, 1900, Series 8, Vol. 9, No. 5 (in German). (English translation, partly, by O. Simin: Water hammer. Proc. of the American Water Works Association, Vol. 24, pp. 341-424, 1904) [p. ii, 2.1, 2.3.1]

Kalkwijk J.P.Th. & Kranenburg C. 1971 *Cavitation in horizontal pipelines due to water hammer.* ASCE Journal of the Hydraulics Division, Vol. 97, No. HY10, pp. 1585-1605. (Discussed by C.B. Vreugdenhil and A.H. de Vries in Vol. 98, No. HY9, pp. 1723-1725.) Also part of: Delft University of Technology, Dep. of Civil Engineering, Laboratory of Fluid Mechanics, Report No. B/71/3. [1.2.2, 2.2, 3.1.5]

Kalkwijk J.P.Th., Kranenburg C., Vreugdenhil C.B. & Vries A.H. de 1972 *Cavitation caused by water hammer in horizontal pipelines.* Delft Hydraulics Laboratory, Publication No. 97, March 1972, Delft, The Netherlands. [1.2.2]

Kalkwijk J.P.Th. & Kranenburg C. 1973 *Closure to "Cavitation in horizontal pipelines due to water hammer".* ASCE Journal of the Hydraulics Division, Vol. 99, No. HY3, pp. 529-530. [1.2.2, 2.2]

Kármán Th. von 1911 *Ueber die Formänderung dünnwandiger Rohre, insbesondere federnder Ausgleichrohre.* (On the deformation of thin-walled pipes, in particular elastic expansion pipes.) Zeitschrift des Vereines deutscher Ingenieure, Vol. 55, No. 45, pp. 1889-1895 (in German). [3.3.6]

Karney B.W. 1990 *Energy relations in transient closed-conduit flow.* ASCE Journal of Hydraulic Engineering, Vol. 116, No. 10, pp. 1180-1196.

Kellner A. & Schönfelder C. 1982 *Die Bedeutung der Fluid/Struktur-Wechselwirkung für die Druckstoßbelastung von Rohrleitungen.* (The effect of fluid/structure-interaction on pressure pulse loads on pipes.) 3R international, Vol. 21, No. 8, pp. 443-449 (in German). [2.3.6]

Kellner A., Voss J. & Schönfelder C. 1983 *Fluid/structure-interaction in piping systems: theory and experiment.* Trans. of SMiRT7, Chicago, USA, August 1983. [2.3.6]

King W.W. & Frederick D. 1968 *Transient elastic waves in a fluid-filled cylinder.* ASCE Journal of the Sanitary Engineering Mechanics Division, Vol. 94, No. EM5, pp. 1215-1230. [2.3.2]

Kloosterman A.H., Kranenburg C., Vries A.H. de & Wijdieks J. 1973 *Niet-stationaire hydrodynamische verschijnselen in transportleidingen voor vloeistoffen.* (Non-stationary hydrodynamic phenomena in fluid-conveying conduits.) Bijdragen KIvI Symp., Delft, June 1972. Also: Delft Hydraulics Laboratory, Publication No. 109N, May 1973, Delft, The Netherlands (in Dutch). [1.2.2]

Knapp F. 1937a *Discussion of "Water hammer in pipes, including those supplied by centrifugal pumps: graphical treatment" by R.W. Angus.* Proc. of the Institution of Mechanical Engineers, Vol. 136, pp. 304-309. [2.2]

Knapp F. 1937b *Operation of emergency shutoff valves in pipelines.* Trans. of the ASME, Vol. 59, pp. 679-682. [2.2]

Knapp F. 1939 *Discussion of "Experiments and calculations on the resurge phase of water hammer" by J.N. LeConte.* Trans. of the ASME, Vol. 61, pp. 440-441. [2.2]

Knapp R.T., Daily J.W. & Hammitt F.G. 1970 *Cavitation.* New York: McGraw-Hill. [2.2]

Kojima E., Shinada M., Nishimuta S. & Murayama S. 1986 *The dynamic behaviour of a finite length straight pipe subject to waterhammer.* Trans. of the Japanese Society of Mechanical Engineers, Series B, Vol. 52, No. 474, pp. 777-784 (in Japanese). [2.3.5]

Kolsky H. 1953 *Stress waves in solids.* Oxford: Clarendon Press. (Reprint in 1963, New York: Dover Publications.) [3.1.2, 4.3, 4.3.3, 4.4]

Korteweg D.J. 1878 *Ueber die Fortpflanzungsgeschwindigkeit des Schalles in elastischen Röhren.* (On the velocity of propagation of sound in elastic pipes.) Annalen der Physik und Chemie, New Series, Vol. 5, No. 12, pp. 525-542 (in German). [2.1, 2.3.1, 2.3.3]

Kot C.A. & Youngdahl C.K. 1978a *Transient cavitation effects in fluid piping systems.* Nuclear Engineering and Design, Vol. 45, January, pp. 93-100. [2.2, 6.3.1]

Kot C.A. & Youngdahl C.K. 1978b *The analysis of fluid transients in piping systems, including the effects of cavitation.* Fluid Transients and Acoustics in the Power Industry, Winter Annual Meeting of the ASME, San Francisco, USA, December 1978, pp. 45-52. [2.2, 6.3.1]

Kot C.A., Hsieh B.J., Youngdahl C.K. & Valentin R.A. 1980 *Transient cavitation phenomena in fluid-structure interactions.* Proc. of the 3rd Int. Conf. on Pressure Surges, BHRA, Canterbury, UK, March 1980, pp. 165-184. [2.4]

Kot C.A., Hsieh B.J., Youngdahl C.K. & Valentin R.A. 1981 *Transient cavitation in fluid-structure interactions.* ASME Journal of Pressure Vessel Technology, Vol. 103, November, pp. 345-351. [2.4]

Kottmann A. 1989 *Vorgänge beim Abreißen einer Wassersäule.* (Phenomena during breakaway of a water column.) 3R international, Vol. 28, No. 2, pp. 106-110 (in German).

Kranenburg C. 1972 *The effect of free gas on cavitation in pipelines induced by water hammer.* Proc. of the 1st Int. Conf. on Pressure Surges, BHRA, Canterbury, UK, September 1972, Paper C4, pp. 41-52. [1.2.2, 3.1.5]

Kranenburg C. 1974a *Transient cavitation in pipelines.* Dissertation, Delft University of Technology, Dep. of Civil Engineering, Laboratory of Fluid Mechanics, February 1974, Delft, The Netherlands. Also: Communications on Hydraulics, Delft University of Technology, Dep. of Civil Engineering, Report No. 73-2, 1973. [1.2.2, 3.1.5, 4.5.3]

Kranenburg C. 1974b *The effect of gas release on column separation.* ASCE Journal of the Hydraulics Division, Vol. 100, No. HY10, pp. 1383-1398. Also part of: Communications on Hydraulics, Delft University of Technology, Dep. of Civil Engineering, Report No. 74-3, 1974. [1.2.2, 3.1.5]

Krause N., Goldsmith W. & Sackman J.L. 1977 *Transients in tubes containing liquids.* Int. Journal of Mechanical Sciences, Vol. 19, No. 1, pp. 53-68. [2.3.5, 6.2.1]

Kruisbrink A.C.H. 1990 *Modelling of safety and relief valves in waterhammer computer codes.* Proc. of the 3rd Int. Conf. on Developments in Valves and Actuators for Fluid Control, BHRA, Bournemouth, UK, March 1990, pp. 137-149. [2.3.5]

Kruisbrink A.C.H. & Heinsbroek A.G.T.J. 1992a *Fluid-structure interaction in non-rigid*

pipeline systems - large scale validation tests. Proc. of the Int. Conf. on Pipeline Systems, British Hydromechanics Research Group, Manchester, UK, March 1992, pp. 151-164, ISBN 0-7923-1668-1. [1.2.3, 2.3.5, 4.2.3]

Kruisbrink A.C.H. & Heinsbroek A.G.T.J. 1992b *Fluid-structure interaction in non-rigid pipeline systems - large scale validation tests.* Proc. of the Second National Mechanics Congress, Kerkrade, The Netherlands, November 1992; Dordrecht, The Netherlands: Kluwer Academic Publishers. [1.2.3, 4.2.3]

Kuiken G.D.C. 1984a *Wave propagation in initially stressed orthotropic compliant tubes containing a compressible, viscous and heat-conducting fluid.* Dissertation, Delft University of Technology, Dep. of Mechanical Engineering, WTHD 165, September 1984, Delft, The Netherlands. [1.2.3, 2.3.2]

Kuiken G.D.C. 1984b *Approximate dispersion equations for thin walled liquid-filled tubes.* Applied Scientific Research, Vol. 41, pp. 37-53. [1.2.3, 2.3.2]

Kuiken G.D.C. 1984c *Wave propagation in fluid lines.* Applied Scientific Research, Vol. 41, pp. 69-91. [1.2.3, 2.3.2]

Kuiken G.D.C. 1984d *Wave propagation in a thin-walled liquid-filled initially stressed tube.* Journal of Fluid Mechanics, Vol. 141, pp. 289-308. [1.2.3, 2.3.2]

Kuiken G.D.C. 1986 *Amplifications of pressure fluctuations due to fluid-structure interaction.* Proc. of Seminar on Fluid-Structure Interaction, Delft Hydraulics, Delft, The Netherlands, October 1986, Report J0113. [1.2.3, 3.1.2]

Kuiken G.D.C. 1988 *Amplification of pressure fluctuations due to fluid-structure interaction.* Journal of Fluids and Structures, Vol. 2, pp. 425-435. [1.2.3, 2.3.5, 4.2.3]

Kulak R.F. 1982 *Some aspects of fluid-structure coupling.* ASME - PVP, Vol. 64, Fluid transients and fluid-structure interaction, pp. 244-260. [2.3.6]

Kulak R.F. 1985 *Three-dimensional fluid-structure coupling in transient analysis.* Computers & Structures, Vol. 21, No. 3, pp. 529-542. [2.3.6]

Kussmaul K., Kerkhof K. & Herter K.-H. 1989 *System response of piping configurations under overload conditions.* Trans. of SMiRT10, Anaheim, USA, August 1989, Division T, pp. 93-104. [2.3.6]

Lamb H. 1898 *On the velocity of sound in a tube, as affected by the elasticity of the walls.* Memoirs of the Manchester Literary and Philosophical Society, Manchester, UK, Vol. 42, No. 9, pp. 1-16. [2.3.1, 2.3.2, 4.2.3]

Lamé G. 1852 *Leçons sur la théorie de l'élasticité.* (Lessons on the theory of elasticity.) Paris: Gauthier-Villars (in French). [App. A]

Langevin A. 1928 In: Bulletin de l'Union Technique du Bâtiment. (Reference in [Bergeron 1939, 1950]) (in French). [2.2]

Lavooij C.S.W. 1986 *Fluid transients in MDOF piping systems.* Proc. of Seminar on Fluid-Structure Interaction, Delft Hydraulics, Delft, The Netherlands, October 1986, Report J0113. [1.2.3, 3.1.3]

Lavooij C.S.W. & Tijsseling A.S. 1988 *FLUSTRIN Phase 1 - Fluid structure interaction in MDOF pipe systems.* Report J0252/J0284, Vol. 1: *Results*, May 1988, Vol. 2: *Theory*, June 1988, Delft Hydraulics, Delft, The Netherlands. [1.2.3, 3.3.2, 4.7.3, 4.10, 4.10.1, 4.10.2]

Lavooij C.S.W. & Tijsseling A.S. 1989 *Fluid-structure interaction in compliant piping systems.* Proc. of the 6th Int. Conf. on Pressure Surges, BHRA, Cambridge, UK, October 1989, pp. 85-100. [1.2.3, 2.3.5, 4.10.1, 4.10.3]

Lavooij C.S.W. 1990 *Fluid hammer and interaction.* PetroChem, Processen en Technieken, No. 6, pp. 11-15. [1.2.3]

Lavooij C.S.W. & Tijsseling A.S. 1991 *Fluid-structure interaction in liquid-filled piping systems.* Journal of Fluids and Structures, Vol. 5, pp. 573-595. [1.1.4, 1.2.3, 2.3.5, 4.10.1]

LeConte J.N. 1937 *Experiments and calculations on the resurge phase of water hammer.* Trans. of the ASME, Vol. 59, Paper HYD-59-12, pp. 691-694. [2.2]

Leonard R.W. & Budiansky B. 1954 *On traveling waves in beams.* Washington: National Advisory Committee for Aeronautics, Report 1173. [4.3, 4.3.4, 4.10.2]

Le Quang, Franc J.P. & Michel J.M. 1989 *Analyse expérimentale des pressions statique et dynamique dans la zone de fermeture des poches de cavitation partielle.* (Experimental analysis of static and dynamic pressures in the region of partially collapsing cavitation bubbles.) Journées de l'Hydraulique, Société Hydrotechnique de France, Machines Hydrauliques, conception et exploitation, Vol. 20, No. 1, pp. 1.15.1-9, Lyon, France (in French). [5.3.1]

Lesmez M.W. 1989 *Modal analysis of vibrations in liquid-filled piping systems.* Dissertation, Michigan State University, Dep. of Civil and Environmental Engineering, East Lansing, USA. [2.3.5]

Lesmez M.W., Wiggert D.C. & Hatfield F.J. 1990 *Modal analysis of vibrations in liquid-filled piping-systems.* ASME Journal of Fluids Engineering, Vol. 112, No. 3, pp. 311-318. [2.3.5]

Lide D.R. (Editor) 1991 CRC *Handbook of chemistry and physics,* 72nd edition 1991-1992. Boca Raton, USA: CRC Press. (CRC = Chemical Rubber Company) [3.1.5]

Lin T.C. & Morgan G.W. 1956a *A study of axisymmetric vibrations of cylindrical shells as affected by rotatory inertia and transverse shear.* ASME Journal of Applied Mechanics, Vol. 23, June, pp. 255-261. [2.3.2, 3.1.2]

Lin T.C. & Morgan G.W. 1956b *Wave propagation through fluid contained in a cylindrical, elastic shell.* Journal of the Acoustical Society of America, Vol. 28, No. 6, pp. 1165-1176. [2.3.2, 3.1.2, 4.2.3]

Liou C.P. 1983 *Calculations of transients in batched pipelines.* Proc. of the 4th Int. Conf. on Pressure Surges, BHRA, Bath, UK, September 1983, pp. 13-25. [4.2.7]

Malcher L. & Steinhilber H. 1991 *A review of 15 years full-scale seismic testing at the HDR.* Trans. of SMiRT11, Tokyo, Japan, August 1991, Paper K15/1*, pp. 397-408. [2.3.6]

Manuel A.R. 1968 *Waterslag in drukleidingen.* (Waterhammer in pressure conduits.) Land en Water, January/February, pp. 36-43 (in Dutch). Also: Delft Hydraulics Laboratory, Publication No. 54, January 1970. [1.2.1]

Manuel A.R., Vreugdenhil C.B. & Wijdieks J. 1968 *Waterslag.* (Waterhammer.) De Ingenieur, Vol. 80, No. 30, pp. 93-100. Also: Delft Hydraulics Laboratory, Publication No. 57N, July 1968 (in Dutch). [1.2.1]

Martin C.S. 1973 *Status of fluid transients in Western Europe and the United Kingdom. Report on laboratory visits by Freeman scholar.* ASME Journal of Fluids Engineering, Vol. 95, No. 2, pp. 301-318. [2.1]

Martin C.S. 1983 *Experimental investigation of column separation with rapid closure of downstream valve.* Proc. of the 4th Int. Conf. on Pressure Surges, BHRA, Bath, UK, September 1983, pp. 77-88. [2.2, 4.10.4, 6.1]

Mase G.E. 1970 *Continuum mechanics.* New York: McGraw-Hill. [3.1.2]

Meder G. & Nguyen-Tuong B. 1984 *Strukturdynamische Methoden der Druckstoßberechnung von Rohrleitungen.* (Structural-dynamics methods in waterhammer calculations of pipelines.) VGB Kraftwerkstechnik, Vol. 64, No. 2, pp. 119-132 (in German). [2.3.6]

Meißner E. 1978 *Einfluß der Massenträgheit einer Rohrwand auf instationäre*

Strömungsvorgänge in Druckleitungen. (Influence of the radial inertia of a pipe wall on non-stationary flow phenomena in pressurized conduits.) Technische Universität München, Hydraulik und Gewässerkunde, Mitteilungen, Heft 25, Munich, Germany, pp. 43-62 (in German). [3.1.2]

Ménabréa L.-F. 1858 *Note sur les effets du choc de l'eau dans les conduites.* (Note on effects of water shock in conduits.) Comptes Rendus Hebdomadaires des Séances de l'Académie des Sciences, Paris, Vol. 47, July-December, pp. 221-224 (in French). (English translation by A. Anderson [1976]) [2.1]

Ménabréa L.-F. 1862 *Note sur l'effet du choc de l'eau dans les conduites.* (Note on effects of water shock in conduits.) Annales du Genie Civil, Paris, Vol. I, pp. 269-275 (in French). [2.1]

Miller D.S. 1990 *Internal flow systems* (2nd edition). Cranfield, UK: BHRA (Information Services). [3.2.2]

Mirsky I. & Herrmann G. 1957 *Nonaxially symmetric motions of cylindrical shells.* The Journal of the Acoustical Society of America, Vol. 29, No. 10, pp. 1116-1123. [2.3.2]

Mirsky I. & Herrmann G. 1958 *Axially symmetric motions of thick cylindrical shells.* ASME Journal of Applied Mechanics, Vol. 25, March, pp. 97-102. [2.3.2]

Moens A.I. 1878 *Die Pulscurve.* (The pulsation.) Leyden, The Netherlands: E.J. Brill (in German). [2.3.1]

Monge G. 1789 *Graphical integration, etc.* Annales des Ingénieurs Sortis des Ecoles de Gand (in French). (Reference in Wood [1970]) [4.1]

Moody L.F. 1944 *Friction factors for pipe flow.* Trans. of the ASME, Vol. 66, November, pp. 97-107. [3.1.2]

Möser M., Heckl M. & Ginters K.-H. 1986 *Zur Schallausbreitung in flüssigkeitsgefüllten kreiszylindrischen Rohren.* (On wave propagation in fluid-filled circular cylindrical tubes.) Acustica, Vol. 60, pp. 34-44 (in German). [2.3.2]

Müller W.Ch. 1986 *Pre- and posttest calculations of the fluiddynamic and structural dynamic behaviour of a pipeline under blowdown conditions including valve dynamics.* Proc. of the 5th Int. Conf. on Pressure Surges, BHRA, Hanover, Germany, September 1986, pp. 223-227. [2.3.6, 2.4]

Müller W.Ch. 1987a *Piping analysis of large scale experiments with ADINA and DAPSY.* Computers & Structures, Vol. 26, No. 1/2, pp. 111-121. [2.3.6, 2.4]

Müller W.Ch. 1987b *Uncoupled and coupled analysis of a large HDR pipe.* Trans. of SMiRT9, Lausanne, Switzerland, August 1987, Vol. F, pp. 31-36. [2.3.6, 2.4]

Nuhoff H.A., Vreugdenhil C.B. & Wijdieks J. 1969 *Computing-technique for non-permanent flow in closed conduits.* Delft Hydraulics Laboratory, Publication No. 68, November 1969, Delft, The Netherlands. [1.2.1]

Obradović P. 1990a *Analysis of hydrodynamic loads on piping structures - F S I theory applied on pipe support design.* Int. Conf. on Engineering Design, ICED, Dubrovnik, Yugoslavia, August 1990. [2.3.5, 3.1.3]

Obradović P. 1990b *Fluid-structure interactions: an accident which has demonstrated the necessity for FSI analysis.* Trans. of the 15th IAHR Symp. on Hydraulic Machinery and Cavitation, Belgrade, Yugoslavia, September 1990, Paper J2. [1.1.4, 2.3.5, 3.1.3]

Obradović P. 1990c *Istraživanje dinamičkih naprezanja cevovoda usled prelaznih procesa.* (Investigation of dynamic loading in piping systems due to pressure surges.) Dissertation, University of Belgrade, Dep. of Mechanical Engineering, Belgrade, Yugoslavia (in Serbo-Croatian). [2.3.5, 3.1.3]

Oldenziel D.M. 1975 *Measurements on the cavitation susceptibility of water.* Proc. of the 5th IAHR Conf. on Fluid Machinery, Budapest, Hungary, September 1975, Vol. 2, pp. 737-748. Also: Delft Hydraulics Laboratory, Publication No. 153, November 1975. [1.2.2]

Oldenziel D.M. 1976 *Gas transport into a cavitation bubble during the explosion.* Proc. of the IAHR Symp. on Two Phase-Flow and Cavitation in Power Generation Systems, Grenoble, France, March-April 1976, pp. 77-88. Also: Delft Hydraulics Laboratory, Publication No. 168, November 1976. [1.2.2]

Oldenziel D.M. & Teijema J. 1976 *Cavitation on valves in correlation to liquid properties.* Proc. of the IAHR Symp. on Problems of Hydraulic Machine - Hydraulic Structure Interaction, Leningrad, USSR, September 1976, pp. 221-240. Also: Delft Hydraulics Laboratory, Publication No. 173, December 1976. [1.2.2, 5.3.1]

Oldenziel D.M. 1979 *Bubble cavitation in relation to liquid quality.* Dissertation, University of Twente, Dep. of Mechanical Engineering, May 1979, Enschede, The Netherlands. Also: Delft Hydraulics Laboratory, Publication No. 211. [1.2.2]

Oldenziel D.M. 1982a *A new instrument in cavitation research: the cavitation susceptibility meter.* ASME Journal of Fluids Engineering, Vol. 104, June, pp. 136-142. [1.2.2, 6.3.1]

Oldenziel D.M. 1982b *A set of instruments useful for liquid quality control during cavitation research.* ASME Journal of Fluids Engineering, Vol. 104, December, pp. 443-450. [1.2.2]

Otwell R.S. 1982 *The effect of elbow translations on pressure transient analysis of piping systems.* ASME - PVP, Vol. 64, Fluid transients and fluid-structure interaction, pp. 127-136. [2.3.5]

Otwell R.S. 1984 *The effect of elbow restraint on pressure transients.* Dissertation, Michigan State University, Dep. of Civil and Sanitary Engineering, East Lansing, USA. [2.3.5, 4.7.3, 4.11]

Overton G.D.N., Williams P.R. & Trevena D.H. 1984 *The influence of cavitation history and entrained gas on liquid tensile strength.* Journal of Physics, D: Applied Physics, Volume 17, No. 5, pp. 979-987. [6.3.1]

Païdoussis M.P. & Issid N.T. 1974 *Dynamic stability of pipes conveying fluid.* Journal of Sound and Vibration, Vol. 33, No. 3, pp. 267-294. [2.3.7]

Païdoussis M.P. & Laithier B.E. 1976 *Dynamics of Timoshenko beams conveying fluid.* Journal Mechanical Engineering Science, IMechE, Vol. 18, No. 4, pp. 210-220. [2.3.7, 3.1.3]

Parmakian J. 1955 *Waterhammer analysis.* New York: Prentice-Hall. (Reprint in 1963, New York: Dover Publications.) [2.1]

Paynter H.M. 1961 *Fluid transients in engineering systems.* Section 20 in Handbook of Fluid Dynamics by V.L. Streeter (Editor), New York: McGraw-Hill. [2.1]

Plass H.J., Jr. 1958 *Some solutions of the Timoshenko beam equation for short pulse-type loading.* ASME Journal of Applied Mechanics, Vol. 25, No. 3, Trans. of the ASME, Vol. 80, September 1958, pp. 379-385. [4.3]

Plesset M.S. 1969 *The tensile strength of liquids.* Cavitation State of Knowledge, ASME Fluids Engineering and Applied Mechanics Conference, Evanston, Illinois, USA, June 1969, pp. 15-25. [6.3.1]

Pochhammer L. 1876 *Beitrag zur Theorie der Biegung des Kreiscylinders.* (Contribution to the theory of bending of circular cylinders.) Journal für Mathematik, Vol. 81, No. 1, pp. 33-61 (in German). [4.3]

Provoost G.A. 1975 *Waterslagmeting aan de leiding Biesbosch-Berenplaat.* (Waterhammer measurements on the Biesbosch-Berenplaat pipeline.) Delft Hydraulics Laboratory, Report

R 1014, November 1975, Delft, The Netherlands (in Dutch). [1.2.2]

Provoost G.A. 1976 *Investigation into cavitation in a prototype pipeline caused by water hammer.* Proc. of the 2nd Int. Conf. on Pressure Surges, BHRA, London, UK, September 1976, Paper D2, pp. 13-29. Also: Delft Hydraulics Laboratory, Publication No. 170, November 1976. [1.2.2, 2.2, 4.5.3]

Provoost G.A. 1978 *Waterslag in PVC-transportleidingen.* (Waterhammer in PVC-transmission lines.) Delft Hydraulics Laboratory, Publication No. 196N, April - May 1978, pp. 91-111, Delft, The Netherlands (in Dutch). [1.2.1]

Provoost G.A. & Wylie E.B. 1981 *Discrete gas model to represent distributed free gas in liquids.* Proc. of the 5th Int. Symp. on Water Column Separation, IAHR, Obernach, Germany, September 1981, 8 pp. Also: Delft Hydraulics Laboratory, Publication No. 263, April 1982. [1.2.2, 2.2, 4.5.3]

Rankine W.J.M. 1870 *On the thermodynamic theory of waves of finite longitudinal disturbance.* Trans. of the Royal Society, London, Vol. 160, Paper 15, pp. 277-288. [2.1]

Regetz J.D., Jr. 1960 *An experimental determination of the dynamic response of a long hydraulic line.* National Aeronautics & Space Administration, Technical Note D-576, December 1960. [2.3.4]

Résal H. 1876 *Note sur les petits mouvements d'un fluide incompressible dans un tuyau élastique.* (Note on the small motions of incompressible fluids in an elastic tube.) Journal de Mathématiques Pures et Appliquées, Paris, 3rd series, Vol. 2, pp. 342-344 (in French). [2.3.1]

Rich G.R. 1951 *Hydraulic transients.* New York: McGraw-Hill. (Reprint in 1963, New York: Dover Publications.) [2.1]

Rij A.A. van 1970 *Standaard afsluiterkarakteristieken.* (Standard valve characteristics.) Delft Hydraulics Laboratory, Report V 195, October 1970, Delft, The Netherlands (in Dutch). [4.7.3]

Ripperger E.A. 1955 *Measurements of short bending wave pulses in steel bars.* Defense Research Laboratory, The University of Texas, Report DRL-367, CM-838. [4.3]

Romander C.M., Schwer L.E. & Cagliostro D.J. 1980 *Response of water-filled thin-walled pipes to pressure pulses: experiments and analysis.* ASME Journal of Pressure Vessel Technology, Vol. 102, No. 1, pp. 56-61. [2.3.6]

Rouse H. & Ince S. 1957 *History of hydraulics.* Iowa Institute of Hydraulic Research, University of Iowa, Ames, Iowa, USA. (Reprint in 1963, New York: Dover Publications.) [6.3.1]

Rubinow S.I. & Keller J.B. 1978 *Wave propagation in a viscoelastic tube containing a viscous fluid.* Journal of Fluid Mechanics, Vol. 88, Part 1, pp. 181-203. [2.3.2]

Safwat H.H. 1972a *On the elastic behavior of the pipe wall for water-hammer applications.* Nuclear Engineering and Design, Vol. 21, No. 1, pp. 85-94. [1.2.2]

Safwat H.H. 1972b *Photographic study of water column separation.* ASCE Journal of the Hydraulics Division, Vol. 98, No. HY4, pp. 739-746. [1.2.2]

Safwat H.H. 1972c *Transients in cooling water systems of thermal power plants.* Dissertation, Delft University of Technology, Dep. of Mechanical Engineering, April 1972, Delft, The Netherlands. Also: Delft Hydraulics Laboratory, Publication No. 101, April 1972. [1.2.2]

Safwat H.H. 1972d *Experimental study of pressure surges in condenser cooling water systems.* Proc. of the 1st Int. Conf. on Pressure Surges, BHRA, Canterbury, UK, September 1972, Paper D2, pp. 17-32. [1.2.2]

Safwat H.H. & Kluyver J.P. de 1972 *Digital computations for water hammer-column separation.* Proc. of the 1st Int. Conf. on Pressure Surges, BHRA, Canterbury, UK, September 1972, Paper C5, pp. 53-68. [1.2.2]

Safwat H.H. & Polder J. van den 1973a *Experimental and analytic data correlation study of water column separation.* ASME Journal of Fluids Engineering, Vol. 95, No. 1, pp. 91-97. [1.2.2]

Safwat H.H. & Polder J. van den 1973b *Frequency-dependent friction for oscillatory flows in circular pipes.* ASCE Journal of the Hydraulics Division, Vol. 99, pp. 1933-1945.

Sayir M. & Hausler K. 1991 *Cavitation and pipeline failure: a case study.* ASME - PVP, Vol. 219, Transient thermal-hydraulics and coupled vessel and piping system responses, pp. 47-50. [5.3.1]

Schedelberger J. 1975 *Schließkarakteristiken von Kugelhähnen.* (Closing characteristics of spherical valves.) 3R international, Vol. 14, No. 6, pp. 333-339 (in German). [4.7.3]

Schmidt J. 1987 *Entwurf von Reglern zur aktiven Schwingungsdämpfung an flexiblen mechanischen Strukturen.* (Design of control systems for active vibration damping of flexible mechanical structures.) Dissertation, Technische Hochschule Darmstadt,

Fachbereich Mechanik, D 17, Darmstadt, Germany (in German). [4.3, 4.3.3]

Schnyder O. 1929 *Druckstöße in Pumpensteigleitungen.* (Waterhammer in pump risers.) Schweizerische Bauzeitung, Vol. 94, No. 22, pp. 271-273, No. 23, pp. 283-286 (in German). [2.1]

Schwarz W. 1978 *Druckstoßberechnung unter Berücksichtigung der Radial- und Längsverschiebungen der Rohrwandung.* (Waterhammer calculations taking into account the radial and longitudinal displacements of the pipe wall.) Dissertation, Universität Stuttgart, Institut für Wasserbau, Mitteilungen, Heft 43, Stuttgart, Germany, ISSN 0343-1150 (in German). [2.3.3, 2.3.5, 3.1.2, 4.2.1]

Schwirian R.E. & Karabin M.E. 1981a *Use of spar elements to simulate fluid-solid interaction in the finite element analysis of piping system dynamics.* ASME Symp. on Fluid Transients and Structural Interactions in Piping Systems, Boulder, USA, June 1981, pp. 1-11. [2.3.6]

Schwirian R.E. & Karabin M.E. 1981b *Use of spar elements to simulate fluid acoustical effects and fluid-solid interaction in the finite element analysis of piping system dynamics.* Nuclear Engineering and Design, Vol. 66, No. 1, pp. 47-59. [2.3.6]

Schwirian R.E. 1982 *Methods for simulating fluid-structure interaction and cavitation with existing finite element formulations.* ASME - PVP, Vol. 64, Fluid transients and fluid-structure interaction, pp. 261-285. [2.3.6, 2.4]

Schwirian R.E. 1984 *On the use of structural finite element computer codes to perform fluid-dynamical and fluid-structure interactive analyses.* Proc. of the Int. Conf. on Numerical Methods for Transient and Coupled Problems, Venice, Italy, July 1984, pp. 186-197. [2.3.6, 2.4]

Shamir U. & Howard C.D.D. 1968 *Water distribution systems analysis.* ASCE Journal of the Hydraulics Division, Vol. 94, No. HY1, pp. 219-234. [4.6.2]

Sharp B.B. 1977 *A simple model for water column rupture.* Proc. of the 17th IAHR Congress, Baden-Baden, Germany, Vol. D, pp. 155-160. [2.2]

Shimada M. 1988 *Time-marching approach for pipe steady flows.* ASCE Journal of Hydraulic Engineering, Vol. 114, No. 11, pp. 1301-1320. (Discussed by J.A. Fox and A.E. Vardy in Vol. 116, No. 10, pp. 1295-1296.) [4.6.2]

Siemons J. 1966 *Cavitatieverschijnselen in een buisleiding.* (Cavitation phenomena in a conduit.) Delft Hydraulics Laboratory, Report S 103-I, September 1966, Delft, The

Netherlands (in Dutch). [1.2.2]

Siemons J. 1967 *The phenomenon of cavitation in a horizontal pipe-line due to a sudden pump-failure.* IAHR Journal of Hydraulic Research, Vol. 5, No. 2, pp. 135-152. Also: Delft Hydraulics Laboratory, Publication No. 53, February 1967. [1.2.2, 2.2]

Simpson A.R. & Wylie E.B. 1985 *Problems encountered in modeling vapor column separation.* Proc. Symp. on Fluid Transients in Fluid-Structure Interaction, ASME Winter Annual Meeting, Miami Beach, Florida, USA, November 1985, pp. 103-107. [2.2, 4.5.3]

Simpson A.R. 1986 *Large water hammer pressures due to column separation in sloping pipes.* Dissertation, The University of Michigan, Dep. of Civil Engineering, Ann Arbor, USA. [p. iii, 2.2, 3.1.5, 4.5.3, 4.10.4, 5, 5.1, 5.4, 6.1, 6.4, 7]

Simpson A.R. & Wylie E.B. 1989 *Towards an improved understanding of waterhammer column separation in pipelines.* Civil Engineering Transactions 1989, The Institution of Engineers, Australia, CE31 (3), pp. 113-120. [2.2]

Simpson A.R. & Wylie E.B. 1991 *Large water-hammer pressures for column separation in pipelines.* ASCE Journal of Hydraulic Engineering, Vol. 117, No. 10, pp. 1310-1316. (Discussed by M. Greco, B. Brunone and U.M. Golia in Vol. 119, No. 1, pp. 142-145.) [2.2]

Simpson A.R. & Bergant A. 1991a *Column separation research at the University of Adelaide, South Australia.* Proc. of the Int. Meeting on Hydraulic Transients with Water Column Separation, 9th Round Table of the IAHR Group, Valencia, Spain, September 1991, pp. 253-269. [5.3.1, 6.3.1]

Simpson A.R. & Bergant A. 1991b *The accuracy of a pipe column separation numerical model.* Submitted for publication to ASCE Journal of Hydraulic Engineering. [4.5.3]

Skalak R. 1956 *An extension of the theory of waterhammer.* Trans. of the ASME, Vol. 78, No. 1, pp. 105-116. [2.3.2, 2.3.5, 3.1.2]

Spillers W.R. 1965 *Wave propagation in a thin cylindrical shell.* ASME Journal of Applied Mechanics, Series E, Vol. 32, No. 2, pp. 346-350. [2.3.2]

Streeter V.L. & Wylie E.B. 1967 *Hydraulic transients.* New York: McGraw-Hill. [2.1, 2.2, 3.3.7]

Streeter V.L. 1969 *Water hammer analysis.* ASCE Journal of the Hydraulics Division, Vol. 95, No. HY6, pp. 1959-1972. [2.2]

Streeter V.L. 1983 *Transient cavitating pipe flow.* ASCE Journal of Hydraulic Engineering, Vol. 109, No. HY11, pp. 1408-1423. [2.2, 3.1.5]

Stuckenbruck S., Wiggert D.C. & Otwell R.S. 1985 *The influence of pipe motion on acoustic wave propagation.* ASME Journal of Fluids Engineering, Vol.107, No. 4, pp. 518-522. [2.3.3]

Stuckenbruck S. & Wiggert D.C. 1986 *Unsteady flow through flexible tubing with coupled axial wall motion.* Proc. of the 5th Int. Conf. on Pressure Surges, BHRA, Hanover, Germany, September 1986, pp. 11-17. [2.3.5]

Suda M. 1990 *Berechnung von Druckstößen in einer flüssigkeitsgefüllten Rohrleitung bei Kavitationsprozessen.* (Computersimulation of water hammer and cavitation process in a liquid pipeline.) 3R international, Vol. 29, No. 7/8, pp. 378-381 (in German). [2.2]

Swaffield J.A. 1968-1969 *The influence of bends on fluid transients propagated in incompressible pipe flow.* Proc. of the Institution of Mechanical Engineers, Vol. 183, Part 1, No. 29, pp. 603-614. [2.3.4, 2.3.6]

Tacke J.H.P.M. 1988 *Hydraulic rams - a comparative investigation.* Communications on Hydraulic and Geotechnical Engineering, Delft University of Technology, Faculty of Civil Engineering, Report 88-1, March 1988, ISSN 0169-6548. [1.2.1]

Tacke J.H.P.M. & Verspuy C. 1989 *Hydraulic rams.* World Pumps, July 1989, pp. 200-203. [1.2.1]

Tanahashi T. & Kasahara E. 1969 *Analysis of the waterhammer with water column separation.* Bulletin of the Japanese Society of Mechanical Engineers, Vol. 12, No. 50, pp. 206-214. [2.2]

Tang S.-C. 1965 *Dynamic response of a tube under moving pressure.* ASCE Journal of the Engineering Mechanics Division, Vol. 91, No. EM5, pp. 97-122. [2.3.2]

Thibessard G. 1961 *La simulation du coup de bélier sur calculateur numérique.* (The simulation of water hammer on a numerical calculator.) Proc. of the 9th IAHR Convention, Dubrovnik, Yugoslavia, September 1961, pp. 881-890 (in French). [2.2]

Thielen H. & Bürmann W. 1980 *Berechnung und Sicherung frei verlegter Rohrleitungen gegen unzulässige Innendrücke und Auflagerkräfte infolge von Druckstößen.* (Calculation and protection of pipe lines laid in the open against undue internal pressure and reactive forces resulting from water hammer.) 3R international, Vol. 19, No. 11, pp. 622-628 (in German). [2.3.5]

Thomas P. 1991 *Prise en compte des sources acoustiques dans les modèles de tuyauteries en mécanique.* (Sound sources in pipe mechanical models.) Electricité de France (E.D.F.) - Bulletin de la Direction des Etudes et Recherches - Série A, Nucléaire, Hydraulique, Thermique, No. 2, pp. 19-36 (in French). [2.3.6]

Thorley A.R.D. 1969 *Pressure transients in hydraulic pipelines.* ASME Journal of Basic Engineering, Vol. 91, September, pp. 453-461. [2.3.2]

Thorley A.R.D. 1976 *A survey of investigations into pressure surge phenomena.* Research Memorandum ML83, The City University, Dep. of Mechanical Engineering, London, UK, April 1976. [2.1, 2.2]

Tijsseling A.S. & Lavooij C.S.W. 1989 *Fluid-structure interaction and column separation in a straight elastic pipe.* Proc. of the 6th Int. Conf. on Pressure Surges, BHRA, Cambridge, UK, October 1989, pp. 27-41. [1.2.4, 4.2.6, 4.10.1, 4.10.4]

Tijsseling A.S. & Lavooij C.S.W. 1990 *Waterhammer with fluid-structure interaction.* Applied Scientific Research, Vol. 47, No. 3, pp. 273-285. [1.1.4, 1.2.3, 4.10.1]

Tijsseling A.S. & Fan D. 1991a *The response of liquid-filled pipes to vapour cavity collapse.* Trans. of SMiRT11, Tokyo, Japan, August 1991, Paper J10/2, pp. 183-188. [1.2.4]

Tijsseling A.S. & Fan D. 1991b *The concentrated cavity model validated by experiments in a closed tube.* Proc. of the Int. Meeting on Hydraulic Transients with Water Column Separation, 9th Round Table of the IAHR Group, Valencia, Spain, September 1991, pp. 145-155. [1.2.4]

Tijsseling A.S. & Fan D. 1992 *Fluid-structure interaction and column separation in a closed pipe.* Proc. of the Second National Mechanics Congress, Kerkrade, The Netherlands, November 1992; Dordrecht, The Netherlands: Kluwer Academic Publishers. [1.2.4, 6.3.1]

Timoshenko S.P. 1921 *On the correction for shear of the differential equation for transverse vibrations of prismatic bars.* Philosophical Magazine, Vol. 41, Paper 66, pp. 744-746. [3.1.3, 4.3]

Timoshenko S.P. 1922 *On the transverse vibrations of bars of uniform cross-section.* Philosophical Magazine, Vol. 43, Paper 10, pp. 125-131. [3.1.3, 4.3]

Timoshenko S.P. & Young D.H. 1955 *Vibration problems in engineering* (3rd edition). Princeton, New Jersey, USA: D. Van Nostrand Company. [4.3.3]

Timoshenko S.P. & Goodier J.N. 1970 *Theory of elasticity* (3rd edition). Singapore:

McGraw-Hill. [3.1.4, App. A]

Trevena D.H. 1984 *Cavitation and the generation of tension in liquids.* Journal of Physics, D: Applied Physics, Volume 17, No. 11, pp. 2139-2164. [6.3.1]

Trikha A.K. 1975 *An efficient method for simulating frequency-dependent friction in transient liquid flow.* ASME Journal of Fluids Engineering, Vol. 97, No. 1, pp. 97-105. [3.1.2]

Tullis J.P., Streeter V.L. & Wylie E.B. 1976 *Waterhammer analysis with air release.* Proc. of the 2nd Int. Conf. on Pressure Surges, BHRA, London, UK, September 1976, Paper C3, pp. 35-47. [2.2]

Tullis J.P. 1989 *Hydraulics of pipelines.* New York: John Wiley & Sons. [2.1]

Valentin R.A., Phillips J.W. & Walker J.S. 1979 *Reflection and transmission of fluid transients at an elbow.* Trans. of SMiRT5, Berlin, Germany, August 1979, Paper B 2/6. [2.3.5]

Vardy A.E. 1976 *On the use of the method of characteristics for the solution of unsteady flows in networks.* Proc. of the 2nd Int. Conf. on Pressure Surges, BHRA, London, UK, September 1976, Paper H2, pp. 15-30, X65-X71. [4.2.6]

Vardy A.E. & Chan L.I. 1983 *Rapidly attenuated water hammer and steel hammer.* Proc. of the 4th Int. Conf. on Pressure Surges, BHRA, Bath, UK, September 1983, pp. 1-12. [4.6.2]

Vardy A.E. & Fan D. 1986 *Water hammer in a closed tube.* Proc. of the 5th Int. Conf. on Pressure Surges, BHRA, Hanover, Germany, September 1986, pp. 123-137. [2.3.5, 4.10.1, 5.2, 5.2.1]

Vardy A.E. & Fan D. 1987 *Constitutive factors in transient internal flows.* Proc. of the NUMETA'87 Conf., Swansea, UK, Vol. 2, Paper T37. [2.3.5]

Vardy A.E. & Alsarraj A.T. 1989 *Method of characteristics analysis of one-dimensional members.* Journal of Sound and Vibration, Vol. 129, No. 3, pp. 477-487. [4.3, 4.7.3]

Vardy A.E. & Fan D. 1989 *Flexural waves in a closed tube.* Proc. of the 6th Int. Conf. on Pressure Surges, BHRA, Cambridge, UK, October 1989, pp. 43-57. [p. iii, 2.3.5, 3.1.3, 4.3, 4.10.1, 5, 5.2, 5.4, 6.2, 6.2.1, 6.3.1, 6.4, 7]

Vardy A.E. & Hwang K.-L. 1991 *A characteristics model of transient friction in pipes.* IAHR Journal of Hydraulic Research, Vol. 29, No. 5, pp. 669-684. [3.1.2]

Vardy A.E. & Fan D. 1993 *Measurements of fluid/structure interactions in pipes.* (to be

offered for publication) [p. iii, 2.3.5, 5, 5.2, 5.4, 6.2, 6.2.2, 7]

Vasconcellos M.M. 1991 *Fluid-pipe interaction analysis and modelling.* Research Report, IST/FCUC, Lisbon/Coimbra, Portugal (in Portuguese). [2.3.5]

Verspuy C. & Tijsseling A.S. 1993 *Hydraulic ram analysis.* IAHR Journal of Hydraulic Research, Vol. 31, No. 2, pp. 267-278. [1.2.1]

Vigness I. 1943 *Elastic properties of curved tubes.* Trans. of the ASME, Vol. 65, February, pp. 105-120. [3.3.6]

Vliegenthart A.C. 1970 *The Shuman filtering operator and the numerical computation of shock waves.* Journal of Engineering Mathematics, Vol. 4, No. 4, pp. 341-348. [4.5.3, 5.3.1]

Vreugdenhil C.B. 1964 *Digital computations of water-hammer.* Delft Hydraulics Laboratory, Report S 103-I, July 1964, Delft, The Netherlands. [1.2.1, 4.5.3]

Vreugdenhil C.B., Vries A.H. de, Kalkwijk J.P.Th. & Kranenburg C. 1972 *Investigation into cavitation in long horizontal pipelines caused by water hammer.* Trans. of the 6th IAHR Symp., Section for Hydraulic Machinery, Equipment and Cavitation, Rome, Italy, September 1972, Paper J3. Also: Kalkwijk et al., Delft Hydraulics Laboratory, Publication No. 115, February 1974. [1.2.2]

Vries A.H. de, Vreugdenhil C.B. & Kranenburg C. 1971 *Cavitatie door waterslag in horizontale leidingen.* (Cavitation due to waterhammer in horizontal pipelines.) Delft Hydraulics Laboratory, Report S 143, June 1971, Delft, The Netherlands (in Dutch). [1.2.2]

Vries A.H. de 1972 *Cavitatie door waterslag in horizontale leidingen.* (Cavitation due to waterhammer in horizontal pipelines.) Delft Hydraulics Laboratory, Report M 1116 (in Dutch). [1.2.2, 2.2, 4.5.3]

Vries A.H. de 1973 *Cavitatie door waterslag in horizontale leidingen met enige hoge punten.* (Cavitation due to waterhammer in horizontal pipelines with several high points.) Delft Hydraulics Laboratory, Report M 1152 (in Dutch). [1.2.2, 4.5.3]

Vries A.H. de 1974 *Hydraulic aspects of cooling water systems for thermal power plants.* Trans. of the 7th IAHR Symp., Section for Hydraulic Machinery, Equipment and Cavitation, Vienna, Austria, September-October 1974. Also: Delft Hydraulics Laboratory, Publication No. 136, November 1974. [1.2.2]

Vries A.H. de 1975 *Research on cavitation due to water hammer in the Netherlands.*

L'Energia Elettrica, No. 9, pp. 478-485. [1.2.2]

Walker J.S. & Phillips J.W. 1977 *Pulse propagation in fluid-filled tubes.* ASME Journal of Applied Mechanics, Vol. 44, March, pp. 31-35. [2.3.5]

Wallis G.B. 1969 *One-dimensional two-phase flow.* New York: McGraw-Hill. [2.2, 4.5.3]

Walski T.M. 1985 *State-of-the-art pipe network optimization.* Proc. of the ASCE Specialty Conf. on Computer Applications in Water Resources, Buffalo, USA, June 1985, pp. 559-568. [4.6.2]

Wang C.Y., Pizzica P.A., Gvildys J. & Spencer B.W. 1989 *Analysis of fluid-structure interaction and structural response of Chernobyl-4 reactor.* Trans. of SMiRT10, Anaheim, USA, August 1989, Division T, pp. 109-119. [1.1.4]

Wang J.S. & Locher F.A. 1991 *Verification of modelling water column separation.* Proc. of the Int. Meeting on Hydraulic Transients with Water Column Separation, 9th Round Table of the IAHR Group, Valencia, Spain, September 1991, pp. 343-354. [2.2]

Ware A.G. & Williamson R.L. 1982 *BLAZER - A RELAP5/MODI post processor to generate force-time history input data for structural computer codes.* ASME - PVP, Vol. 64, Fluid transients and fluid-structure interaction, pp. 183-198. [2.3.6]

Watters G.Z. 1979 *(Modern) Analysis and control of unsteady flow in pipelines.* Boston, USA: Butterworths, an Ann Arbor science book. (1st edition 1979, 2nd edition 1984) [2.1]

Weber W. 1866 *Theorie der durch Wasser oder andere incompressibele Flüssigkeiten in elastischen Rohren fortgepflanzten Wellen.* (Theory of waves propagating in water or other incompressible liquids contained in elastic pipes.) Berichte über die Verhandlungen der Königlichen Sachsischen Gesellschaft der Wissenschaften zu Leipzig, Leipzig, Germany, Mathematical-Physical Section, Vol. 18, pp. 353-357 (in German). [2.3.1]

Weijde P.J. van der 1984 *Ankerkrachten in leidingsystemen ten gevolge van instationaire stromingsverschijnselen (waterslag).* (Anchor forces in piping systems due to non-stationary flow phenomena (waterhammer).) Delft Hydraulics Laboratory, Report S0103, Voorjaar 1984, Delft, The Netherlands (in Dutch). [1.2.3]

Weijde P.J. van der 1985a *Ankerkrachten in leidingsystemen.* (Anchor forces in piping systems.) PT Procestechniek, Vol. 40, No. 4, 1-5 pp. (in Dutch). [1.2.3]

Weijde P.J. van der 1985b *Prediction of pressure surges and dynamic forces in pipeline systems, influence of system vibrations on pressures and dynamic forces (fluid structure*

interaction). Symp. on Pipelines, Utrecht, The Netherlands, November 1985, The Institution of Chemical Engineers, European Branch Symposium Series 4/1985, pp. 327-335. [1.2.3, 2.4]

Weijde P.J. van der 1986 *State of the art; waterhammer and dynamic forces, the FLUSTRIN project.* Proc. of Seminar on Fluid-Structure Interaction, Delft Hydraulics, Delft, The Netherlands, October 1986, Report J0113. [1.2.3]

Weisbach J. 1855 *Die Experimentalhydraulik.* (Experimental hydraulics.) Freiburg im Breisgau, Germany: J.G. Engelhardt (in German). [3.1.2]

Wiedermann A.H. 1982 *An elastic-plastic pipe response model for small thickness to diameter ratio pipes in water hammer analysis.* ASME - PVP, Vol. 64, Fluid transients and fluid-structure interaction, pp. 116-126. [2.3.6, 2.4]

Wiggert D.C. & Hatfield F.J. 1983 *Time domain analysis of fluid-structure interaction in multi-degree-of-freedom piping systems.* Proc. of the 4th Int. Conf. on Pressure Surges, BHRA, Bath, UK, September 1983, pp. 175-188. [2.3.5, 3.3.2]

Wiggert D.C., Hatfield F.J. & Otwell R.S. 1983 *Fluid-structure interaction in piping systems.* Proc. Druckstoßberechnung von Rohrleitungssystemen, Haus der Technik, Essen, Germany, December 1983. [2.3.5]

Wiggert D.C., Otwell R.S. & Hatfield F.J. 1985a *The effect of elbow restraint on pressure transients.* ASME Journal of Fluids Engineering, Vol. 107, No. 3, pp. 402-406. (Discussed by R.E. Schwirian and J.S. Walker in Vol. 108, No. 1, pp. 121-122.) [2.3.5]

Wiggert D.C., Hatfield F.J. & Stuckenbruck S. 1985b *Analysis of liquid and structural transients in piping by the method of characteristics.* ASME - FED, Vol. 30, pp. 97-102. [2.3.5]

Wiggert D.C. 1986 *Coupled transient flow and structural motion in liquid-filled piping systems: a survey.* Proc. of the ASME Pressure Vessels and Piping Conf., Chicago, USA, July 1986, Paper 86-PVP-4. [2.3.5]

Wiggert D.C., Hatfield F.J. & Lesmez M.W. 1986 *Coupled transient flow and structural motion in liquid-filled piping systems.* Proc. of the 5th Int. Conf. on Pressure Surges, BHRA, Hanover, Germany, September 1986, pp. 1-9. [2.3.5, 3.1.3, 4.2.6]

Wiggert D.C., Hatfield F.J. & Stuckenbruck S. 1987a *Analysis of liquid and structural transients by the method of characteristics.* ASME Journal of Fluids Engineering, Vol. 109, No. 2, pp. 161-165. [2.3.5, 3.1.3, 4.1, 4.11, 7]

Wiggert D.C., Lesmez M.L. & Hatfield F.J. 1987b *Modal analysis of vibrations in liquid-filled piping systems.* ASME - FED, Vol. 56, Fluid transients in fluid-structure interaction, pp. 107-113. [2.3.5, 3.1.3]

Wijdieks J. 1972 *Water hammer in large oil transmission lines.* 3R international, Vol. 11, April, pp. 34- . Also: Delft Hydraulics Laboratory, Publication No. 98, April 1972, Delft, The Netherlands. [1.2.1]

Wijdieks J. 1974 *Wrijvingsverliezen en waterslag bij watertransportleidingen.* (Friction losses and waterhammer in water transmission lines.) H_2O, Vol. 7, No. 25. Also: Delft Hydraulics Laboratory, Publication No. 142N, May 1975, Delft, The Netherlands (in Dutch). [1.2.1]

Wijdieks J. 1978 *Waterslagverschijnselen in vloeistoftransportleidingen.* (Waterhammer phenomena in fluid transmission lines.) Delft Hydraulics Laboratory, Publication No. 196N, April - May 1978, pp. 3-39, Delft, The Netherlands (in Dutch). [1.2.1]

Wijdieks J. 1983 *Waterhammer (practice - criteria - provisions - mathematical description - examples).* Delft Hydraulics Laboratory, Publication No. 310, June 1983, Delft, The Netherlands. [1.2.1]

Wilkinson D.H. 1978 *Acoustic and mechanical vibrations in liquid-filled pipework systems.* Proc. BNES Int. Conf. on Vibration in Nuclear Plant, Keswick, UK, May 1978, Paper 8.5, pp. 863-878. [2.3.5, 3.3.2]

Wilkinson D.H. 1980 *Dynamic response of pipework systems to water hammer.* Proc. of the 3rd Int. Conf. on Pressure Surges, BHRA, Canterbury, UK, March 1980, pp. 185-202. [2.3.4, 2.3.5]

Wilkinson D.H. & Curtis E.M. 1980 *Water hammer in a thin-walled pipe.* Proc. of the 3rd Int. Conf. on Pressure Surges, BHRA, Canterbury, UK, March 1980, pp. 221-240. [2.3.5, 4.2.4, 4.10.1]

Williams D.J. 1977 *Waterhammer in non-rigid pipes: precursor waves and mechanical damping.* Journal of Mechanical Engineering Science, Institution of Mechanical Engineers, Vol. 19, No. 6, pp. 237-242. [2.3.5]

Wood D.J. 1968 *A study of the response of coupled liquid flow-structural systems subjected to periodic disturbances.* ASME Journal of Basic Engineering, Vol. 90, December, pp. 532-540. [2.3.4]

Wood D.J. 1969 *Influence of line motion on waterhammer pressures.* ASCE Journal of the

Hydraulics Division, Vol. 95, May, pp. 941-959. [2.3.4]

Wood D.J. & Chao S.P. 1971 *Effect of pipeline junctions on water hammer surges.* ASCE Transportation Engineering Journal, Vol. 97, August, pp. 441-456. [2.3.4]

Wood D.J. & Charles C.O.A. 1972 *Hydraulic network analysis using linear theory.* ASCE Journal of the Hydraulics Division, Vol. 98, No. HY7, pp. 1157-1170. [4.6.2]

Wood D.J. & Rayes A.G. 1981 *Reliability of algorithms for pipe network analysis.* ASCE Journal of the Hydraulics Division, Vol. 107, No. HY10, pp. 1145-1161. [4.6.2]

Wood F.M. 1970 *History of waterhammer.* Report No. 65, Dep. of Civil Engineering, Queen's University at Kingston, Ontario, Canada, April 1970. [2.1]

Wylie E.B. & Streeter V.L. 1978a *Fluid transients.* New York: McGraw-Hill. (Republished with minor corrections by FEB Press, Ann Arbor, Michigan, USA, 1983) [2.1, 2.3.3, 3.1.2, 4.1]

Wylie E.B. & Streeter V.L. 1978b *Column separation in horizontal pipelines.* Proc. of the Joint Symp. on Design and Operation of Fluid Machinery, IAHR/ASME/ASCE, Colorado State University, Fort Collins, USA, June 1978, Vol. 1, pp. 3-13. [2.2, 3.1.5]

Wylie E.B. 1983 *Advances in the use of MOC in unsteady pipeline flow.* Proc. of the 4th Int. Conf. on Pressure Surges, BHRA, Bath, UK, September 1983, pp. 27-37. [4.2.5]

Wylie E.B. 1984 *Simulation of vaporous and gaseous cavitation.* ASME Journal of Fluids Engineering, Vol. 106, No. 3, pp. 307-311. [2.2, 4.5.3]

Wylie E.B. & Streeter V.L. 1993 *Fluid transients in systems.* Englewood Cliffs, New Jersey, USA: Prentice Hall. [2.1]

Young F.R. 1989 *Cavitation.* London: McGraw-Hill. [2.2]

Young T. 1808 *Hydraulic investigations, subservient to an intended Croonian lecture on the motion of the blood.* Philosophical Trans. of the Royal Society, London, Vol. 98, Part 2, Paper 13, pp. 164-186. [2.3.1]

Youngdahl C.K., Kot C.A. & Valentin R.A. 1980 *Pressure transient analysis in piping systems including the effects of plastic deformation and cavitation.* ASME Journal of Pressure Vessel Technology, Vol. 102, February, pp. 49-55. [2.3.6, 2.4]

Zielke W. 1968 *Frequency-dependent friction in transient pipe flow.* ASME Journal of Basic Engineering, Vol. 90, No. 1, pp. 109-115. [3.1.2]

Zielke W. (Editor) 1974 *Elektronische Berechnung von Rohr- und Gerinneströmungen.* (Electronic calculation of pipe and open-channel flows.) Munich, Germany: Erich Schmidt

Verlag (in German). [2.1]

Zielke W. & Perko H.-D. 1985 *Unterdruckerscheinungen und Druckstoßberechnung.* (Low pressure phenomena and water hammer analysis.) 3R international, Vol. 24, No. 7, pp. 348-355 (in German). [2.2, 4.5.3]

Zielke W., Perko H.-D. & Keller A. 1989 *Gas release in transient pipe flow.* Proc. of the 6th Int. Conf. on Pressure Surges, BHRA, Cambridge, UK, October 1989, pp. 3-13. [5.3.1]

Abbreviations

ASCE	American Society of Civil Engineers
ASME	American Society of Mechanical Engineers
BHRA	British Hydromechanics Research Association
BNES	British Nuclear Engineering Society
FED	Fluids Engineering Division
IAHR	International Association of Hydraulic Research
PVP	Pressure Vessels and Piping
3R	Rohre Rohrleitungsbau Rohrleitungstransport
SMiRT	Structural Mechanics in Reactor Technology

Conf.	Conference
Dep.	Department
Int.	International
Proc.	Proceedings
Symp.	Symposium
Trans.	Transactions

[1.2.3] The code in brackets after each literature entry refers to the number(s) of the (sub)section(s) where results of the relevant publication are cited, reviewed and/or applied.

Appendix A. Two-dimensional stress distribution in a pressurized ring

In the present investigation the radial inertia forces in both liquid and pipe wall are neglected. For the liquid this means that the pressure is uniform over the pipe cross-section, whereas for the pipe a quasi-static stress distribution across the thickness of the pipe wall is assumed. This particular stress distribution, given by Timoshenko & Goodier [1970, pp. 68-71] and attributed to Lamé [1852], is integrated here over the pipe wall cross-section.

Consider the two-dimensional axially symmetric stress problem of a circular ring subjected to an internal pressure P and an external pressure P_{out}. The ring, shown in figure A.1, has inner radius R and thickness e. The hoop and radial stresses have the form

$$\sigma_\phi = -\frac{A}{r^2} + 2C \tag{A.1}$$

$$\sigma_r = \frac{A}{r^2} + 2C \tag{A.2}$$

where the constants of integration, A and C, are determined from the boundary conditions

$$\sigma_r|_{r=R} = -P(z,t) \qquad \sigma_r|_{r=R+e} = -P_{out} \tag{A.3}$$

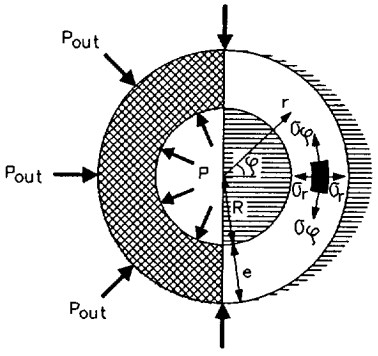

Figure A.1. Definition sketch of stress distribution in a pressurized ring.

It follows that

$$A = \frac{R^2 (R+e)^2 (P_{out} - P)}{2 (R + \frac{1}{2}e) e} \tag{A.4}$$

$$2C = \frac{R^2 P - (R+e)^2 P_{out}}{2 (R + \frac{1}{2}e) e} \tag{A.5}$$

The stress solutions σ_ϕ and σ_r are independent of Poisson's ratio ν, so that they are valid for both plane stress and plane strain situations. The sum $\sigma_\phi + \sigma_r$ equals $4C$ and is therefore independent of r.

The value of σ_ϕ at $r = R$ follows from (A.1), (A.4) and (A.5),

$$\sigma_\phi \big|_{r=R} = -\frac{A}{R^2} + 2C = \frac{R}{e} P - \frac{R+e}{e} P_{out} + \frac{1 + \frac{e}{R}}{2 + \frac{e}{R}} (P - P_{out}) \tag{A.6}$$

The averaged value of σ_ϕ, defined by equation (3.24) and calculated with (A.1), (A.4) and (A.5), is

$$\overline{\sigma_\phi} = \frac{1}{e} \int_R^{R+e} \sigma_\phi \, dr = -\frac{A}{R(R+e)} + 2C = \frac{R}{e} P - \frac{R+e}{e} P_{out} \tag{A.7}$$

The averaged value of σ_ϕ, defined by equation (3.41) and calculated with (A.1), (A.4) and (A.5), is

$$\overline{\overline{\sigma_\phi}} = \frac{1}{2\pi(R+\frac{1}{2}e)\,e}\int_R^{R+e} 2\pi r\,\sigma_\phi\,dr = -\frac{\ln(1+\frac{e}{R})}{(R+\frac{1}{2})\,e}A + 2C =$$

$$= \{\frac{R^2}{2e^2}\frac{(R+e)^2\ln(1+\frac{e}{R}) + (R+\frac{1}{2}e)\,e}{(R+\frac{1}{2}e)^2}\}P + \tag{A.8}$$

$$- \{\frac{R^2}{2e^2}\frac{(R+e)^2\ln(1+\frac{e}{R}) + (1+\frac{e}{R})^2(R+\frac{1}{2}e)\,e}{(R+\frac{1}{2}e)^2}\}P_{out}$$

The averaged value of σ_r, defined by equation (3.42) and calculated with (A.2), (A.4) and (A.5), is

$$\overline{\sigma_r} = \frac{1}{2\pi(R+\frac{1}{2}e)\,e}\int_R^{R+e} 2\pi r\,\sigma_r\,dr = \frac{\ln(1+\frac{e}{R})}{(R+\frac{1}{2})\,e}A + 2C =$$

$$= \{-\frac{R^2}{2e^2}\frac{(R+e)^2\ln(1+\frac{e}{R}) - (R+\frac{1}{2}e)\,e}{(R+\frac{1}{2}e)^2}\}P + \tag{A.9}$$

$$+ \{\frac{R^2}{2e^2}\frac{(R+e)^2\ln(1+\frac{e}{R}) - (1+\frac{e}{R})^2(R+\frac{1}{2}e)\,e}{(R+\frac{1}{2}e)^2}\}P_{out}$$

The sum of the averaged values of σ_ϕ and σ_r, defined by the equations (3.41) and (3.42), and calculated with (A.1), (A.2), (A.4) and (A.5), is

$$\overline{\overline{\sigma_\phi}} + \overline{\sigma_r} = \frac{1}{2\pi(R+\frac{1}{2}e)\,e}\int_R^{R+e} 2\pi r\,(\sigma_\phi+\sigma_r)\,dr = 4C = \frac{R}{e}\frac{1}{1+\frac{1}{2}\frac{e}{R}}P - \frac{R}{e}\frac{(1+\frac{e}{R})^2}{1+\frac{1}{2}\frac{e}{R}}P_{out} \tag{A.10}$$

For *thin-walled* pipes, $e << R$, the approximation $\ln(1 + e/R) \approx e/R$ is made. Terms of order e/R, and higher, are neglected with respect to unity. The averaged values of σ_ϕ and σ_r, given by the expressions (A.7), (A.8) and (A.9), then become

$$\overline{\sigma_\phi} = \frac{R}{e}(P - P_{out}) \tag{A.11}$$

$$\overline{\overline{\sigma_\phi}} = \frac{R}{e}(P - P_{out}) \tag{A.12}$$

$$\overline{\sigma_r} = -\frac{3}{4}P - \frac{1}{4}P_{out} \tag{A.13}$$

Appendix B. Solution of the characteristic equation belonging to system (4.17)

In this appendix the *characteristic equation* of system (4.17)

$$|\mathbf{B} - \lambda\mathbf{A}| = 0 \tag{B.1}$$

is solved. The matrices **A** and **B** are given by (4.19) and (4.20), so that

$$\mathbf{B} - \lambda\mathbf{A} = \begin{bmatrix} -\lambda & g & 0 & 0 \\ 1 & -\lambda g/c_F^2 & -2\nu & 0 \\ 0 & 0 & -\lambda & -1/\rho_t \\ 0 & -\lambda\rho_f g\dfrac{\nu}{E}\dfrac{R}{e} & 1 & \dfrac{\lambda}{\rho_t c_t^2} \end{bmatrix} \tag{B.2}$$

and

$$\begin{aligned} |\mathbf{B} - \lambda\mathbf{A}| &= -\frac{g}{\rho_t}\{1 - (\frac{\lambda}{c_F})^2\}\{1 - (\frac{\lambda}{c_t})^2\} + 2\lambda^2\frac{\rho_f g}{\rho_t}\frac{\nu^2}{E}\frac{R}{e} \\ &= -\frac{g}{\rho_t c_F^2 c_t^2}\{\lambda^4 - (c_F^2 + c_t^2 + 2\rho_f\frac{\nu^2}{E}\frac{R}{e}c_F^2 c_t^2)\lambda^2 + c_F^2 c_t^2\} \end{aligned} \tag{B.3}$$

For $\nu = 0$ the solution of the characteristic equation (B.1) is

$$\lambda_1 = c_F = c_f\,, \quad \lambda_2 = -c_F = -c_f\,, \quad \lambda_3 = c_t\,, \quad \lambda_4 = -c_t \tag{B.4}$$

with c_F, c_f and c_t defined by (4.15), (4.60) and (4.16), respectively, whereas for $\nu \neq 0$ the solution is

$$\begin{aligned} \lambda_1 &= +[\tfrac{1}{2}\{q^2 - (q^4 - 4c_F^2 c_t^2)^{\frac{1}{2}}\}]^{\frac{1}{2}} \\ \lambda_2 &= -[\tfrac{1}{2}\{q^2 - (q^4 - 4c_F^2 c_t^2)^{\frac{1}{2}}\}]^{\frac{1}{2}} \\ \lambda_3 &= +[\tfrac{1}{2}\{q^2 + (q^4 - 4c_F^2 c_t^2)^{\frac{1}{2}}\}]^{\frac{1}{2}} \\ \lambda_4 &= -[\tfrac{1}{2}\{q^2 + (q^4 - 4c_F^2 c_t^2)^{\frac{1}{2}}\}]^{\frac{1}{2}} \end{aligned} \tag{B.5}$$

with $q^2 = c_F^2 + c_t^2 + 2\nu^2\dfrac{\rho_f}{\rho_t}\dfrac{R}{e}c_F^2$.

If the second-order Poisson-term (ν^2-term) in q^2 and in c_F is neglected, the solutions (B.4) and (B.5) are equal.

Physically the characteristic roots λ_1 and λ_2 represent the speed of pressure waves in the

liquid, whilst the characteristic roots λ_3 and λ_4 represent the speed of stress waves in the pipe wall. For most practical situations the pressure wave speed is smaller than the stress wave speed: $0 < \lambda_1 < \lambda_3$.

For convenience the following notation is used for the four characteristic roots specified by the formulae (B.5):

$$\lambda_1 = \tilde{c}_F , \quad \lambda_2 = -\tilde{c}_F , \quad \lambda_3 = \tilde{c}_t , \quad \lambda_4 = -\tilde{c}_t \tag{B.6}$$

Appendix C. Determination of the transformation matrix T according to condition (4.27)

In this appendix a regular transformation matrix **T** is determined that satisfies the condition

$$\mathbf{T}\,\mathbf{B} = \mathbf{\Lambda}\,\mathbf{T}\,\mathbf{A} \tag{C.1}$$

with **A** and **B** given by (4.19) and (4.20) and **Λ** (diagonal) given by (4.25). Written out in full, condition (C.1) reads

$$\begin{bmatrix} t_{11} & t_{12} & t_{13} & t_{14} \\ t_{21} & t_{22} & t_{23} & t_{24} \\ t_{31} & t_{32} & t_{33} & t_{34} \\ t_{41} & t_{42} & t_{43} & t_{44} \end{bmatrix} \begin{bmatrix} 0 & g & 0 & 0 \\ 1 & 0 & -2\nu & 0 \\ 0 & 0 & 0 & -1/\rho_t \\ 0 & 0 & 1 & 0 \end{bmatrix} =$$

$$= \begin{bmatrix} \lambda_1 & 0 & 0 & 0 \\ 0 & \lambda_2 & 0 & 0 \\ 0 & 0 & \lambda_3 & 0 \\ 0 & 0 & 0 & \lambda_4 \end{bmatrix} \begin{bmatrix} t_{11} & t_{12} & t_{13} & t_{14} \\ t_{21} & t_{22} & t_{23} & t_{24} \\ t_{31} & t_{32} & t_{33} & t_{34} \\ t_{41} & t_{42} & t_{43} & t_{44} \end{bmatrix} \begin{bmatrix} 1 & 0 & 0 & 0 \\ 0 & g/c_F^{\,2} & 0 & 0 \\ 0 & 0 & 1 & 0 \\ 0 & \rho_f g \dfrac{\nu}{E}\dfrac{R}{e} & 0 & \dfrac{-1}{\rho_t c_t^{\,2}} \end{bmatrix} \tag{C.2}$$

which is equivalent with

$$\begin{bmatrix} t_{12} & g t_{11} & -2\nu t_{12} + t_{14} & -t_{13}/\rho_t \\ t_{22} & g t_{21} & -2\nu t_{22} + t_{24} & -t_{23}/\rho_t \\ t_{32} & g t_{31} & -2\nu t_{32} + t_{34} & -t_{33}/\rho_t \\ t_{42} & g t_{41} & -2\nu t_{42} + t_{44} & -t_{43}/\rho_t \end{bmatrix} = \begin{bmatrix} \lambda_1 t_{11} & \lambda_1 (\dfrac{g}{c_F^{\,2}} t_{12} + \rho_f g \dfrac{\nu}{E}\dfrac{R}{e} t_{14}) & \lambda_1 t_{13} & \dfrac{-\lambda_1}{\rho_t c_t^{\,2}} t_{14} \\ \lambda_2 t_{21} & \lambda_2 (\dfrac{g}{c_F^{\,2}} t_{22} + \rho_f g \dfrac{\nu}{E}\dfrac{R}{e} t_{24}) & \lambda_2 t_{23} & \dfrac{-\lambda_2}{\rho_t c_t^{\,2}} t_{24} \\ \lambda_3 t_{31} & \lambda_3 (\dfrac{g}{c_F^{\,2}} t_{32} + \rho_f g \dfrac{\nu}{E}\dfrac{R}{e} t_{34}) & \lambda_3 t_{33} & \dfrac{-\lambda_3}{\rho_t c_t^{\,2}} t_{34} \\ \lambda_4 t_{41} & \lambda_4 (\dfrac{g}{c_F^{\,2}} t_{42} + \rho_f g \dfrac{\nu}{E}\dfrac{R}{e} t_{44}) & \lambda_4 t_{43} & \dfrac{-\lambda_4}{\rho_t c_t^{\,2}} t_{44} \end{bmatrix} \tag{C.3}$$

These are sixteen equations for the sixteen unknowns t_{ij}. Consider row i :

$$
\begin{aligned}
t_{i2} &= \lambda_i t_{i1} \\
g\, t_{i1} &= \lambda_i \frac{g}{c_F^{\,2}} t_{i2} + \lambda_i \rho_f g \frac{\nu}{E} \frac{R}{e} t_{i4} \\
-2\nu t_{i2} + t_{i4} &= \lambda_i t_{i3} \\
-\frac{1}{\rho_t} t_{i3} &= -\lambda_i \frac{1}{\rho_t c_t^{\,2}} t_{i4}
\end{aligned}
\tag{C.4}
$$

or

$$
\begin{bmatrix}
-\lambda_i & 1 & 0 & 0 \\
g & -\lambda_i \frac{g}{c_F^{\,2}} & 0 & -\lambda_i \rho_f g \frac{\nu}{E} \frac{R}{e} \\
0 & -2\nu & -\lambda_i & 1 \\
0 & 0 & -\frac{1}{\rho_t} & \frac{\lambda_i}{\rho_t c_t^{\,2}}
\end{bmatrix}
\begin{bmatrix} t_{i1} \\ t_{i2} \\ t_{i3} \\ t_{i4} \end{bmatrix}
=
\begin{bmatrix} 0 \\ 0 \\ 0 \\ 0 \end{bmatrix}
\tag{C.5}
$$

With $\mathbf{t}_i = (t_{i1}, t_{i2}, t_{i3}, t_{i4})^{\mathrm{T}}$ system (C.5) can be written in matrix notation,

$$
(\mathbf{B} - \lambda_i \mathbf{A})^{\mathrm{T}} \mathbf{t}_i = \mathbf{0} \tag{C.6}
$$

If matrix $(\mathbf{B} - \lambda_i \mathbf{A})^{\mathrm{T}}$ is regular, equation (C.6) has only the trivial solution $\mathbf{t}_i = \mathbf{0}$, which leads to a singular matrix $\mathbf{T}$. To obtain a regular matrix $\mathbf{T}$, $(\mathbf{B} - \lambda_i \mathbf{A})^{\mathrm{T}}$ has to be singular. Hence

$$
|\, \mathbf{B} - \lambda_i \mathbf{A} \,| = 0 \tag{C.7}
$$

since $|\mathbf{M}| = |\mathbf{M}^{\mathrm{T}}|$ for every square matrix $\mathbf{M}$.

Choosing λ_i according to equation (4.22), that is (B.5)-(B.6), condition (C.7) is fulfilled. The equations in system (C.4) or (C.5) are now dependent, which means that for the determination of $\mathbf{t}_i$ one of them can be omitted. To avoid the trivial solution $0 = 0$ when $\nu = 0$, the second equation in (C.4) is omitted if $i = 1$ or $i = 2$. For the same reason the fourth equation is omitted if $i = 3$ or $i = 4$.

For $i = 1$ and $i = 2$ the (eigen)vector $\mathbf{t}_i$ is calculated as follows. From (C.4) or (C.5):

$$
\begin{aligned}
-\lambda_i t_{i1} + t_{i2} &= 0 \\
-2\nu t_{i2} - \lambda_i t_{i3} + t_{i4} &= 0 \\
-\frac{1}{\rho_t} t_{i3} + \lambda_i \frac{1}{\rho_t c_t^{\,2}} t_{i4} &= 0
\end{aligned}
\tag{C.8}
$$

which is equivalent with

$$\begin{aligned} t_{i1} &= \frac{1}{\lambda_i} t_{i2} \\ (1 - \frac{\lambda_i^2}{c_t^2}) t_{i4} &= 2\nu t_{i2} \\ t_{i3} &= \lambda_i \frac{1}{c_t^2} t_{i4} \end{aligned} \tag{C.9}$$

Take $t_{i2} = \lambda_i$, then:

$$\begin{aligned} t_{i1} &= 1 \\ t_{i2} &= \lambda_i \\ t_{i3} &= 2\nu\lambda_i^2/(c_t^2 - \lambda_i^2) \\ t_{i4} &= 2\nu\lambda_i c_t^2/(c_t^2 - \lambda_i^2) \end{aligned} \tag{C.10}$$

For $i = 3$ and $i = 4$ the (eigen)vector $\mathbf{t}_i$ is calculated as follows. From (C.4) or (C.5):

$$\begin{aligned} -\lambda_i t_{i1} + t_{i2} &= 0 \\ g t_{i1} - \lambda_i \frac{g}{c_F^2} t_{i2} - \lambda_i \rho_f g \frac{\nu}{E} \frac{R}{e} t_{i4} &= 0 \\ -2\nu t_{i2} - \lambda_i t_{i3} + t_{i4} &= 0 \end{aligned} \tag{C.11}$$

which is equivalent with

$$\begin{aligned} t_{i1} &= \frac{1}{\lambda_i} t_{i2} \\ (\frac{1}{\lambda_i^2} - \frac{1}{c_F^2}) t_{i2} &= \rho_f \frac{\nu}{E} \frac{R}{e} t_{i4} \\ t_{i3} &= \frac{1}{\lambda_i} (t_{i4} - 2\nu t_{i2}) \end{aligned} \tag{C.12}$$

Take $t_{i4} = \lambda_i$, then:

$$\begin{aligned} t_{i1} &= \rho_f \frac{\nu}{E} \frac{R}{e} \lambda_i^2 c_F^2/(c_F^2 - \lambda_i^2) \\ t_{i2} &= \rho_f \frac{\nu}{E} \frac{R}{e} \lambda_i^3 c_F^2/(c_F^2 - \lambda_i^2) \\ t_{i3} &= 1 - 2\rho_f \frac{\nu^2}{E} \frac{R}{e} \lambda_i^2 c_F^2/(c_F^2 - \lambda_i^2) \\ t_{i4} &= \lambda_i \end{aligned} \tag{C.13}$$

Substitution of the characteristic roots or eigenvalues λ_i from equation (4.22) in (C.10) for $i = 1, 2$ and in (C.13) for $i = 3, 4$ yields

$$
\begin{aligned}
t_{11} &= t_{21} = 1 \\
t_{12} &= -t_{22} = \tilde{c}_F \\
t_{13} &= t_{23} = 2\nu\left(\frac{\tilde{c}_F}{c_t}\right)^2\left\{1-\left(\frac{\tilde{c}_F}{c_t}\right)^2\right\}^{-1} \\
t_{14} &= -t_{24} = 2\nu\,\tilde{c}_F\left\{1-\left(\frac{\tilde{c}_F}{c_t}\right)^2\right\}^{-1} \\
t_{31} &= t_{41} = -\rho_f\frac{\nu}{E}\frac{R}{e}c_F^2\left\{1-\left(\frac{c_F}{\tilde{c}_t}\right)^2\right\}^{-1} \\
t_{32} &= -t_{42} = -\rho_f\frac{\nu}{E}\frac{R}{e}c_F^2\,\tilde{c}_t\left\{1-\left(\frac{c_F}{\tilde{c}_t}\right)^2\right\}^{-1} \\
t_{33} &= t_{43} = 1+2\rho_f\frac{\nu^2}{E}\frac{R}{e}c_F^2\left\{1-\left(\frac{c_F}{\tilde{c}_t}\right)^2\right\}^{-1} \\
t_{34} &= -t_{44} = \tilde{c}_t
\end{aligned}
\tag{C.14}
$$

The equations (C.14) give the components t_{ij} of a transformation matrix **T** that satisfies condition (C.1). Finally, the regularity of **T** is checked. From (C.14) it follows that $|\mathbf{T}|$ can be written as

$$
|\mathbf{T}| = \begin{vmatrix} t_{11} & t_{12} & t_{13} & t_{14} \\ t_{11} & -t_{12} & t_{13} & -t_{14} \\ t_{31} & t_{32} & t_{33} & t_{34} \\ t_{31} & -t_{32} & t_{33} & -t_{34} \end{vmatrix} \tag{C.15}
$$

Addition and subtraction of rows leads to

$$
\begin{aligned}
|\mathbf{T}| &= \begin{vmatrix} t_{11} & 0 & t_{13} & 0 \\ 0 & t_{12} & 0 & t_{14} \\ t_{31} & 0 & t_{33} & 0 \\ 0 & t_{32} & 0 & t_{34} \end{vmatrix} \\
&= t_{11}\left(t_{12}t_{33}t_{34} - t_{32}t_{33}t_{14}\right) + t_{31}\left(-t_{12}t_{13}t_{34} + t_{32}t_{13}t_{14}\right) \\
&= \left(t_{11}t_{33} - t_{13}t_{31}\right)\left(t_{12}t_{34} - t_{14}t_{32}\right)
\end{aligned}
\tag{C.16}
$$

For the sake of simplicity it is assumed that $\tilde{c}_F < c_t$ and $c_F < \tilde{c}_t$. With these assumptions it can easily be shown (substitution of (C.14) in (C.16)) that $|\mathbf{T}| > 0$. Hence **T** is regular.

Levensloop en opleiding

De schrijver van dit proefschrift werd op 18 augustus 1960 geboren te Bellingwolde. Hij bezocht lagere scholen in Bellingwolde en Rotterdam, en middelbare scholen in Rotterdam en Zeist. Het VWO-diploma werd behaald in 1978. In datzelfde jaar begon hij de studie Technische Wiskunde en Informatica aan de Technische Universiteit Delft (TUD). In 1986 studeert hij af bij prof. dr. ir. A.J. Hermans van de sectie Mathematische Fysica van de vakgroep Toegepaste Analyse. Het afstudeerwerk werd verricht bij het Nationaal Lucht- en Ruimtevaartlaboratorium (NLR), afdeling Wiskundige Methoden en Modellen, in de Noordoostpolder. Onder begeleiding van dr. ir. H. Schippers en ir. J. van der Vooren werd onderzoek verricht naar de toepassing van singuliere scheurtipelementen in de randelementenmethode.

In de periode 1986-1988 vervult de schrijver zijn vervangende dienstplicht bij de afdeling Industriële Hydrodynamica van het Waterloopkundig Laboratorium (WL) te Delft. Onder begeleiding van en in samenwerking met ir. C.S.W. Lavooij werkt hij aan de numerieke modellering van vloeistof-leiding interactie in volledig met vloeistof gevulde buizen.

In 1988 volgt een aanstelling als assistent in opleiding (AIO) aan de faculteit der Civiele Techniek van de TUD. Bij de sectie Vloeistofmechanica van de vakgroep Waterbouwkunde wordt vloeistof-leiding interactie onderzocht in combinatie met cavitatie. De onderzoeksresultaten zijn vastgelegd in dit proefschrift.

Vanaf 1 maart 1993 is de schrijver als post-doctoraal onderzoeker verbonden aan de Universiteit van Dundee (Schotland), alwaar hij het huidige onderzoek voortzet.

STELLINGEN *behorende bij het proefschrift "Fluid-structure interaction in case of waterhammer with cavitation" van A.S. Tijsseling, Delft, 29 juni 1993*

1) De snelheid waarmee de belangrijkste waterslaggolf zich voortplant kan wezenlijk worden beïnvloed door junctiekoppeling; Poissonkoppeling is hierbij van ondergeschikt belang.

2) De methode der karakteristieken vervalt tot een gewone eindige-differentie-methode als de roosterpunten buiten de karakteristieken vallen.

3) Het gascavitatiemodel van Kalkwijk en Kranenburg wordt instabiel bij grotere gasfracties. De instabiliteit zal verdwijnen als, naar het voorbeeld van Geurst in het geval van bellenmengsels, toegevoegde vloeistofmassa in rekening wordt gebracht.

   J.P.Th. Kalkwijk & C. Kranenburg, 1971, ASCE J. Hydr. Div., 97, 1585-1605.
   J.A. Geurst, 1985, Physica, 129A, 233-261.

4) Leidingsystemen voor drink- en rioolwater zijn in het algemeen beter op waterslag doorgerekend dan leidingsystemen in de chemische industrie.

5) Het opnemen van historische aspecten in vakcolleges leidt niet alleen tot een beter zicht op het betreffende vakgebied, maar verlevendigt bovendien het onderwijs.

6) Nut van lidwoord is minimaal.

7) Mede gezien het feit dat er nog steeds nieuwe diersoorten worden ontdekt, dient de wettelijk vastgestelde lijst van beschermde uitheemse diersoorten vervangen te worden door een lijst van onbeschermde diersoorten.

8) Het korten op de WAO is niet rechtvaardig: WAO'ers hebben al de pech lichamelijk niet volledig gezond te zijn; een financieel ongezonde situatie daar bovenop wordt teveel van het slechte.

9) Uit een vergelijking van de misdaadcijfers van Australië met die van andere landen blijkt niet dat crimineel gedrag erfelijk is.

10) De conditie van veel recreatievoetballers is zodanig dat op het veld de speelbal over de meeste lucht beschikt.

TU Delft

Technische Universiteit Delft

College van Dekanen

Technische Universiteit Delft

Postbus 5
2600 AA Delft

Julianalaan 134
2628 BL Delft
Telefoon (015) 78 91 11
Telex bhtud 38151

De heer ir. A.S. Tijsseling
Bierkade 3 H
's-Gravenhage

Uw kenmerk en datum	Ons kenmerk	Doorkiesnummer	Datum
	C/02.64/CW	(015)78 6456	10-03-1993

Onderwerp
Instelling promotiecommissie en vaststelling promotiedatum.

Onderdeel

Geachte heer Tijsseling,

Het College van Dekanen van de Technische Universiteit Delft zal bij uw promotie tot doctor vertegenwoordigd worden door een commissie, bestaande uit de Rector Magnificus (of diens vervanger) en de hierna genoemde commissieleden:

Prof.dr.ir. J.A. Battjes	Promotor
Prof.dr.ir. J.P.Th. Kalkwijk	Rijksinspectiekantoor in de Meern
Prof.dr.ir. A.A. van Steenhoven	Technische Universiteit Eindhoven
Prof. A.E. Vardy	University of Dundee, Groot Brittannië
Dr.ir. H.L. Fontijn	UHD-Technische Universiteit Delft
Dr.ir. G.D.C. Kuiken	UHD-Technische Universiteit Delft
Ir. C.S.W. Lavooij	Gast, N.V. Duinwaterbedrijf Zuid Holland
Prof.dr. R.V.A. Oliemans	Reservelid

De verdediging van uw proefschrift en de daarbij behorende stellingen is bepaald op **dinsdag 29 juni 1993** om 16.00 uur in de Senaatszaal van het Aulagebouw, Mekelweg 5 te Delft.

Nadere informatie zal U desgevraagd worden verstrekt door de medewerkster Protocollaire Zaken, toestel 6456.

Hoogachtend,
Het College van Dekanen,

Rector Magnificus.